EXPERIMENTAL STUDIES OF COLD ATOM GUIDING USING HOLLOW LIGHT BEAMS

Daniel Paul Rhodes

A Thesis Submitted for the Degree of PhD
at the
University of St Andrews

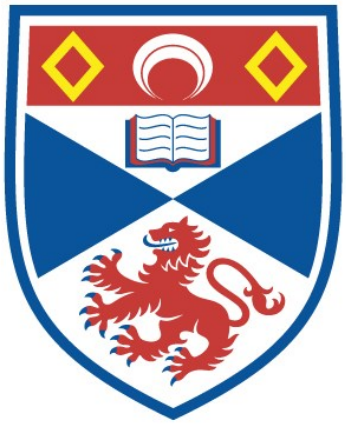

2005

Experimental Studies of Cold Atom Guiding Using Hollow Light Beams

A Thesis submitted to the
University of St Andrews in
application for the Degree of
Doctor of Philosophy

Daniel Paul Rhodes

February 2005

Declarations

I, Daniel Paul Rhodes, hereby certify that this thesis, which is approximately 50,000 words in length, has been written by me, that it is the record of work carried out by me and that it has not been submitted in any previous application for a higher degree.

date 28.2.05 signature of candidate. .....

I was admitted as a research student in September 2000 and as a candidate for the degree of Doctor of Philosophy in September 2001; the higher study for which this is a record was carried out in the University of St Andrews between 2000 and 2004.

date 28.2.05 signature of candidate.. .....

I hereby certify that the candidate has fulfilled the conditions of the Resolution and Regulations appropriate for the degree of Doctor of Philosophy in the University of St Andrews and that the candidate is qualified to submit this thesis in application for that degree.

date 28.2.05 signature of supervisor.....

In submitting this thesis to the University of St Andrews I understand that I am giving permission for it to be made available in accordance with the regulations of the University Library for the time being in force, subject to any copyright vested in the work not being affected thereby. I also understand that the title and abstract will be published, and that a copy of the work may be made and supplied to any bona fide library or research worker. I hereby certify that the candidate has fulfilled the conditions of the Resolution and Regulations appropriate for the degree of Doctor of Philosophy in the University of St Andrews and that the candidate is qualified to submit this thesis in application for that degree.

date 28.2.05 signature of candidate .....

Abstract

This thesis is concerned with the guiding of cold atoms using optical forces, which is of great importance in the field of atom optics. Atomic beams can be used for precision sensor equipment, building nano-scale structures, construction of quantum computers and to further the understanding of the properties of atoms.

Atoms are guided along light beams using the dipole force; there are two regimes under which this force works. Typically red-detuned guides are used (atoms are attracted towards the light) such guides, however, require large detuning and high powers. In this thesis we investigate the use of blue-detuned (atoms are repelled from the light) hollow light beams of moderate power (a few hundred mW) and confine atoms in the dark centre of the beams.

Several magneto-optical traps (MOTs) have been constructed to exploit different guiding geometries. Hollow beams have been generated using a variety of methods; in particular the use of a computer controlled spatial light modulator (SLM) has provided great versatility and simplicity to the experimental arrangements.

First, experiments were performed with a low-velocity intense source (LVIS) of atoms. A co-linear LG beam significantly enhances the observed flux, however, considerable difficulties are encountered loading atoms into oblique guides. Imaging a hole in the walls of the light tube was used to improve the

loading efficiency. Second, guiding a free-falling atom cloud is performed using a non-diffracting Bessel beam. It is found that while the potential of the Bessel beam is steeper than equivalent LG beams the power distribution across the beam severely limits its usefulness. The next study investigated higher-order LG guide beams generated with an SLM. High order modes have a narrower profile so confine the atoms with less interaction with the guide beam, leading to a more natural guide (as opposed to a pushing force). Finally the SLM was used to create non-trivial beam shapes for beam splitters and interferometers.

Acknowledgements

So, start with the obvious: my supervisor, Prof. Kishan Dholakia, for his encouragement and unlimited "crazy ideas" when all seemed to be working against us (my only concern was the unerring ability of his exclamations of delight in watching an experiment work to instantly cause the stabilisation electronics to lose lock).

Faces in a dark room: The original trap was inherited from Gavin Lancaster, he who taught me how the damn thing worked during my first year, I'm still not sure if I could have decoded the black arts of the locking electronics without his guidance. This has never been a solo experiment and my partner in crime during all this research has been John Livesey, a man who has always succeeded in making the lab experience interesting (though I really could have done without all the 80's music), and more recently David Gherardi has appeared on the scene on his way to build a BEC with Donatella Cassettari and David McGloin has also been on hand to offer advice, assistance and the occasional computer simulation.

Fritz Akerboom deserves special mention as our in-house glass blower and has been vital for producing the glass traps and manufacturing other vacuum components.

Faces in the light: The group also consists of a (frighteningly) large number of non-atom-trapping people who have helped keep me insane throughout, among the permanent fixtures and the passers by (as summer or project

students) have been (deep breath...): Mike, Lynn, Vene, Tat, Toni, Hannah, Klaus, Phil, Anjali, Michael, Helen, Paul, Gabe, Tim, Jacqueline, Jochen, Karen, Mark, Jill, Matt, Fabrice, Anne...(I'm sorry I can't name everybody, but be assured there is a list and it does go on)

To all of the above and any not mentioned who may have simply wandered though our offices to offer distractions that have led to a life outside the darkened room:

Cheers!

I would also like to acknowledge the Engineering and Physical Sciences Research Council who have provided financial support throughout these studies.

Publications

D. P. Rhodes, G. P. T. Lancaster, J. Livesey, J. Arlt and K. Dholakia, "*Atom guiding of a cold atomic beam along laguerre-gaussian light beams.*" Quantum Electronics and Photonics 15, Glasgow. Technical Digest, p.36 (2001)

D P Rhodes, J G Livesey, G P T Lancaster, J Arlt, and K Dholakia, "*All optical guiding and splitting of a cold atomic beam.*" Quantum Electronics and Laser Science, Long Beach. Conference Program, Poster QtuF25 (2002)

D. P. Rhodes, G. P. T. Lancaster, J. Livesey, D. McGloin, J. Arlt and K. Dholakia, "*Guiding a cold atomic beam along a co-propagating and oblique hollow light guide.*" Opt. Commun. **214** 247 (2002)

J.G. Livesey, D.P. Rhodes, D. McGloin and K. Dholakia, "*Transient response of a cold atomic beam in the presence of a far-off resonance light guide.*" J. Mod. Opt. **50** 1751 (2003)

D. P. Rhodes, J. G. Livesey, D. McGloin H. Melville, G. C. Spalding and K. Dholakia "*Tailored optical potentials for guiding cold atoms.*" 16th International Conference on Laser Spectroscopy, Palm Cove. Conference Program, Poster, p.147 (2003)

D.P. Rhodes, J. G. Livesey, D. McGloin, H. Melville, D.M. Gherardi, T Freegarde and K. Dholakia, "*Atom guiding along dynamically generated Laguerre-Gaussian light beams.*" UK Cold Atom Network, Poster (2004)

D.P. Rhodes, D.M. Gherardi, J. Livesey, D. McGloin, H. Melville, T Freegarde and K. Dholakia, "*Atom guiding along holographically generated high order Laguerre-Gaussian light beams.*" To be submitted

Glossary of Acronyms

Abbreviation	Meaning
AOM	Acousto-optic Modulator
BEC	Bose-Einstein Condensate
CCD	Charged Coupled Device
CW	Continuous Wave
HeNe	Helium-Neon Laser
ECDL	Extended Cavity Diode Laser
FLC	Ferroelectric Liquid Crystal
HG	Hermite Gaussian. Rectangularly symmetric laser mode, higher order beams have nodes in the horizontal and vertical axis
LCD	Liquid Crystal Display
LG	Laguerre-Gaussian. Circularly symmetric laser mode with a helical phase structure and phase singularity at its centre
LVIS	Low-velocity Intense Source (of atoms)
MOT	Magneto-optical Trap
ND	Neutral Density
PMT	Photomultiplier Tube
PSD	Phase Space Density
PZT	Piezoelectric Transducer
Rb	Rubidium

SLM	Spatial Light Modulator
TEM_{00}	Transverse Electro-magnetic mode with no nodes in the vertical and horizontal planes, the fundamental Gaussian mode.
UHV	Ultra High Vacuum
UV	Ultra Violet

Contents

List of Figures

Chapter 1: Introduction

Chapter 2: Interaction between Light and Matter

Chapter 3: Review of Guiding Experiments

Chapter 5: Hollow Beams for Atom Guiding

Chapter 6: Laguerre-Gaussian Beam Guiding of LVIS

There is a theory which states that if ever anyone discovers exactly what the universe is for and why it is here it will instantly disappear and be replaced by something even more bizarrely inexplicable. There is another theory which states that this has already happened...

The Hitchhikers Guide to the Galaxy

Chapter 1:

Introduction

1.1 Wave-Particle Duality

It is now well known that light has both wave- and particle-like properties. However, it was not until the beginning of the 20th century and the formulation of quantum theory that the nature of light as both a particle and a wave could be understood. Before this the exact nature of light was unclear as experiments designed to show the wave-like properties of light (Young's double-slit experiment) showed light to be an electromagnetic wave and experiments designed to prove the particle nature (the photoelectric effect) succeeded in demonstrating light exists as a particle. This chameleon behaviour of light could finally be explained using the quantisation of electromagnetic fields. The quantisation of light came about as a solution to

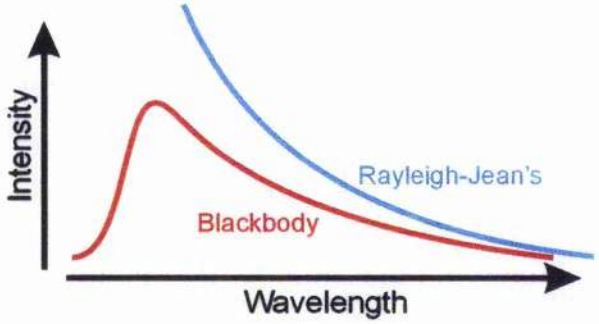

Figure 1.1: Blackbody radiation curve. The Raleigh-Jean's curve is shown as the blue line; the total energy is the area under the graph, at high frequencies the Rayleigh-Jean's approximation diverges rapidly from the observed radiation curve and the total energy becomes infinite.

the ultra-violet catastrophe encountered whilst explaining the energy curve of a blackbody, see figure 1.1. Before 1900 the closest fit for this curve was the Rayleigh-Jeans law: $E \propto \nu^2$, where E is the energy and ν is the frequency of the light. This produced an approximate fit at low frequencies but at high frequencies the Rayleigh-Jeans law diverges to an infinite energy – the UV catastrophe. Planck proposed that the absorption and emission of light occurred in discrete packets (quanta) with each packet having an energy, $E = h\nu$, where h is Planck's constant. From this postulate the probability of emission of a photon can be found by Einstein-Bose statistics, previously the probability of emission was assumed to be the same for all frequencies. Planck's theory of quantised energy leads to the probability of emission of a photon decreasing the further away the photon is from the average temperature of the blackbody, therefore, the total energy released no longer tends to infinity at high frequencies. However, Planck was unable to properly justify his idea of the quantisation of energy until Einstein explained the photoelectric effect. Einstein showed that this quantum of light, or photon,

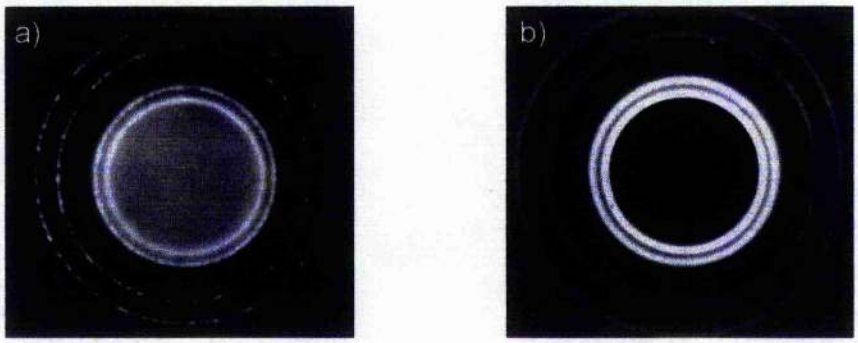

Figure 1.2: Diffraction pattern of a wave-like beam. A powder of aluminium is used as a target of an incident beam, the diffraction pattern of an x-ray beam (a light wave) is shown in a). The diffraction pattern of an electron beam (matter wave) is shown in b). Note the similarities of the patterns. Reproduced from Halliday, Resnick and Walker. "*Fundamental of Physics, extended, 5th edition,*" John Wiley and Sons Inc. (1997)

has an associated momentum of $h\nu/c$, where c is the speed of light; de Broglie then postulated that the momentum, p, was related to the wavelength, λ, by $\lambda = h/p$. This connection between momentum and wavelength demonstrated that all matter, and not just light, has this dual nature.

This, naturally, led to experimental activity to prove the wave-like nature of massive particles. Electrons and neutrons were the first particles to have their wave-like properties demonstrated (fig. 1.2), however, whole atoms could also display their wave-like nature depending on the experimental conditions. One of the most important applications of the wave-like nature of particles is the electron microscope. The highest resolution that can be distinguished is dependent on the wavelength of the viewing light (resolution ~$\lambda/2$); electrons can have a de Broglie wavelength which is 10^{-5} times that of visible light

permitting much more detailed examination of tiny structures that would not even be visible using optical microscopes.

If we look at the de Broglie equation above we see that as momentum is reduced the longer the wavelength of the particle becomes, so to maximise the wave-like nature (this is in contrast to the electron microscope when smaller wavelengths are desired) of particles we need to minimise the velocity, and hence the momentum, of the particle. Only recently, with the advances over the last 20 years in laser cooling has this become experimentally possible to realise using optical forces. Laser cooling exploits the particle nature of light and utilises the momentum transfer when photons are absorbed by an atom; essentially the massive particle (usually an alkali metal atom) is bombarded with a stream of photons in order to reduce the velocity of the particle. Considering this on a more real world scale it would be similar to trying to stop a free-wheeling car by throwing golf balls (this is the University of St Andrews after all) at it; one ball is not going to make any noticeable difference but if you throw enough of them then you can move the car (you'll probably also need a new car after the experiment).

Temperature

The use of the term cooling in this context is, however, somewhat of a misnomer; thermodynamic temperature is defined for a *closed system* in *equilibrium*, i.e. there is heat exchange between the entity and the surrounding environment. This is not the case in laser cooling. Atoms are

constantly absorbing and emitting photons, this is an exchange of energy not of heat so although the system can be in a steady state condition there is no thermal equilibrium. It is, nevertheless, convenient to use temperature as a label to describe an ensemble of atoms with a well defined velocity distribution whose average kinetic energy, $<E_k>$, in one dimension is given by:

$$< E_K >= \frac{1}{2} k_B T \qquad (1.1)$$

where k_B is Boltzmann's constant and T is the temperature. Therefore an atom with a temperature of 1K has a corresponding velocity of a few m/s, room temperature atoms move with velocities of a few 100m/s.

BEC

The further you can cool the particles the larger the de Broglie wavelength you can create. Eventually it is possible to obtain a particle whose associated wavelength is larger than the separation between two particles, at this point the atomic ensemble forms a Bose-Einstein condensate (BEC) and the whole system can then be considered as a coherent source. The BEC could be used in a similar fashion to laser beams with interference effects being used to act a delicate sensors, these can offer better sensitivity than their laser counterparts because the particles have a mass and will therefore interact with the environment to a greater extent. Not all atoms, however, can form BEC. Atoms can be split into two separate types: Bosons and Fermions. Only Bosons can produce a BEC, where all the atoms are in the same energy

state and therefore have the same associated wavelength. Fermions cannot occupy identical energy levels so are incapable of forming a coherent ensemble; instead they form a "Fermi sea" with exactly one atom in each low-level energy state.

This fact that the wave-like nature of particle is being used - whether as a single coherent source (BEC with large wavelengths) or in electron microscopes and lithographic contexts (where very short wavelengths are required for high resolution) - has led to the field being known as atom optics. The aim of this thesis is to use optical forces to generate cold atoms (reducing the temperature of the atoms lowers the guiding potentials required in order to manipulate them), generate cold atomic beams and to also use optical forces to create devices that mimic the effects of optical beam splitters for an atomic beam.

1.2 Synopsis of thesis

After this initial introduction chapter 2 will describe the optical forces that can be utilised to manipulate an atomic ensemble. The mechanisms of laser cooling will be presented along with the limitations to the minimum obtainable temperatures using near-resonant light, the use of light tuned further from resonance can be used to cool atoms to even lower temperatures. This is followed by a brief overview of the techniques for neutral atom traps where

the magneto-optical trap (MOT) has had a profound effect due to the ease of construction and stability of the design. A review of atom guiding experiments is given in chapter 3. The use of magnetic forces and hollow fibre guiding are discussed but the emphasis of this chapter is on the use of free space light beams and the use of the optical dipole force in order to place the experimental work performed during this thesis into some form of context.

Once this overview is complete chapter 4 goes on to describe the methods for building a vacuum system for a MOT, the lasers employed and the locking and stabilisation electronics used in the cooling and guiding beams. The last section of this chapter is used to describe the three traps built during this thesis, explains the reasoning behind the different designs and gives the properties of the MOTs then formed. Attempts to create a molasses cycle for reducing the temperature of the MOT even further are detailed at the end of this chapter. The key aims of this thesis have been to use low powered, non-TEM_{00} beams to manipulate the cold atoms; chapter 5 describes the experimental generation of hollow Laguerre-Gaussian beams, using holograms and spiral phase plates, and Bessel beams and outlines their properties as light tubes within which atoms may be guided. The use of a spatial light modulator as a dynamic, computer-controlled hologram has also been investigated; this allows a rapid change of the optical parameters with minimal realignment of experimental optics.

The last three chapters highlight three different experiments performed. Chapter 6 details the guiding and splitting of a low-velocity intense source (LVIS, this is a cold atomic beam extracted from a running MOT) of atoms

using Laguerre-Gaussian beams. A comparison of the use of Laguerre-Gaussian and Bessel beams for guiding a free falling cold atomic cloud is given in chapter 7. Chapter 8 uses a spatial light modulator (SLM) to generate the optical guides; the versatility of the SLM allows us to compare the effect of different orders of Laguerre-Gaussian beam for guiding a falling cloud of atoms. Finally the SLM was also used to create several beam shapes for the generation of optical beam splitters and interferometers.

Chapter 2:

Interactions between Light and Matter

2.1 Introduction

This chapter will discuss the radiation pressure and the dipole forces which a light field can exert on matter. The cooling cycle and the techniques for using the radiation pressure for cooling atoms down to temperatures that will display their wave-like nature will then be considered (the dipole force is utilised primarily in the guiding of atoms along light beams, a review of guiding experiments is given in chapter 3), finally we will describe some of the methods for the subsequent trapping of neutral atoms.

2.2 Optical Forces

When light passes through a medium its velocity is reduced and the beam can be subject to refraction. The scale of this effect is given by the refractive index, n. The refractive index of an atom about a transition is defined by the Kramers-Kronig relation. This index has both real and imaginary components which lead to two separate means of interaction between the medium and the light; the real component results in the dipole force and the radiation pressure is due to the imaginary factor.

2.2.1 Radiation Pressure

Radiation pressure can be attributed to the particle like nature of photons, and utilises the conservation of momentum. If an atom absorbs a photon then the photon ceases to exist but the momentum associated with it is transferred by imparting a momentum kick to the atom in the direction of the beam of light. The force produced by a laser resonant with an optical transition of an atom is given by [1]:

$$F = \frac{\Delta p}{\Delta t} = \frac{\hbar k}{\tau / f} \tag{2.1}$$

where $\hbar k$ is the photon momentum along the propagation of the beam ($\hbar = h/2\pi$, and the wavevector, $k = 2\pi/\lambda$), τ is the natural lifetime of the excited state, f is the fraction of time an atom spends in the excited state and λ is the

wavelength of the light. This is the force used to cool thermal atoms to the μK regime, it is a weak force since photons have very little momentum (each recoil can change the velocity of an atom by ~1cm/s), but this can become significant with a sufficiently high flux of photons. At large scales this is the force that pushes the tail of a comet away from the sun. The process by which photons are absorbed and re-emitted is known as the cooling cycle.

2.2.2 Optical Dipole Force

A second force of light on matter is the dipole (or gradient) force. Whereas the radiation pressure can be considered as absorption followed by the spontaneous emission of a photon, the dipole force occurs as the result of absorption and stimulated emission.

Classically the dipole force, F_d, can be defined by:

$$F_d = p.\nabla E \tag{2.2}$$

where p is the dipole moment and E is the electric field. When placed in an optical field an atom acquires an induced dipole moment:

$$p = \alpha E \tag{2.3}$$

with α as the polarisability of the atom. For an atom in the ground state α is dispersive, linked to frequency by the Kramers-Kronig relation; at frequencies below resonance it is positive, zero exactly on resonance and negative above resonance (figure 2.1a). The resultant force, the optical dipole force, pulls

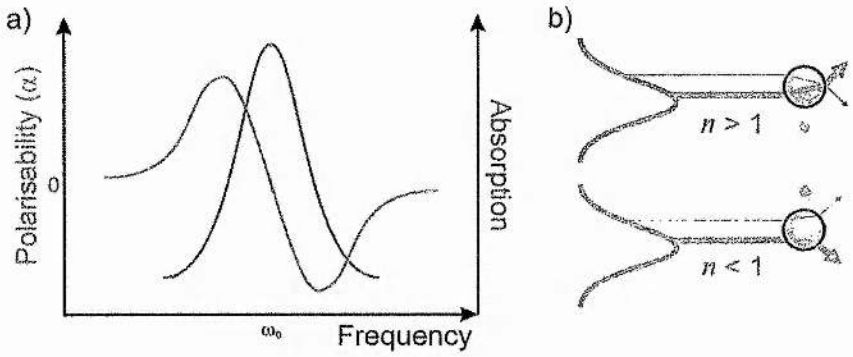

Figure 2.1: a) Classical description of the dipole force. For an atomic transition at the frequency ω_0, with the absorption profile shown in red, the atomic polarisability, α, is given by the blue curve, with a positive value when the laser frequency is tuned below resonance, zero on resonance and negative above resonance. This results in the atom being attracted or repelled from the light depending on the sign of α.

b) A physical analogy of the dipole force. For a microscopic sphere in a light field the direction of refraction depends on the relative refractive index, n, between the sphere and the surrounding medium. For n>1, the light is refracted away from the centre of the beam and the particle recoils toward the high intensity, a lower than unity n results in the momentum kick pushing the particle away from the high intensity. This can be related to the case of an atom in a light field since the refractive index of an atom, $n = 1+ \alpha$.

atoms into regions of high intensity for detunings below resonance (red-detuning) and pushes atoms away form these regions for a beam tuned higher than resonance (blue-detuning).

It can be useful for understanding this effect to consider an analogy with dielectric spheres first proposed by Ashkin in 1980 [2]. Consider a microscopic dielectric sphere placed within a laser beam, as shown in figure 2.1b. If the sphere is not exactly on axis the beam of light will be subject to

refraction and gain momentum in a transverse direction. By conservation of momentum the resultant force on the sphere is in the opposite direction pushing the sphere either towards or away from the intense part of the beam depending on the refractive index of the sphere.

This force does not give the atoms a "push" as does the radiation pressure and is used for confining already cooled atoms either in a tight focus to be used as a trap or within an extended optical beam and used as a guide. Using the dipole force to guide atoms is described more in chapter 3.

2.3 Cooling atoms

The primary goal when cooling atoms is to increase the *phase space density* (PSD), $n(\lambda_{dB})^3$, where n is the density of the gas and λ_{dB} is the de Broglie wavelength. The PSD is the probability of finding a particle at the position (r, t) with a momentum p. This increase in PSD is what separates cooling from velocity selection. Laser cooling can significantly increase the PSD of an atomic vapour, the effect is greatest when used as part of a trap, however it is not sufficient on its own to generate BEC conditions. Lower temperatures and higher densities than can be achieved using laser cooling are required to get a high enough PSD (>2.612) to produce a coherent ensemble. The temperature actually required is dependent on the density of the ensemble; atoms closer together require shorter de Broglie wavelengths (i.e. hotter atoms) to achieve an overlap with adjacent atomic wavefunctions.

2.3.1 The cooling cycle

As mentioned in the previous section the momentum transfer from a single absorbed photon to an atom is very small (a single recoil causes a velocity change of only ~1cm/s), for this force to be properly utilised to control atomic motion many such transfers must take place (in an intense field an atom can scatter some 10^7photons/s). Therefore the atom must be in an appropriate state to absorb a photon and then return to that same state in order to absorb further photons. This cycle can be understood simply by treating the atom as a two level system.

When a photon with energy, $E=\hbar\omega$, interacts with a ground state atom of mass, m, (assuming the energy of the photon matches the energy difference between the two levels of the atom) the photon is absorbed and the energy is used to raise the electronic state of the atom to an excited level. The momentum associated with the photon, $\hbar k$, is conserved resulting in a recoil to the atom ($\delta v=\hbar k/m$) in the direction of the photon. After a characteristic lifetime, τ, depending on the excited state, the atom will spontaneously decay back into the ground state by emitting a photon. Again the atom will be subject to momentum recoil as the photon is ejected, this time in the direction away from the photon motion. As this decay is spontaneous the photon is emitted in a random direction so over many such emissions the net force is zero. Now that the atom is in the ground state so the cycle can begin again (this cycle is shown in figure 2.2). However, at any one moment the re-emission of a photon does cause a force and it is this turbulence of many

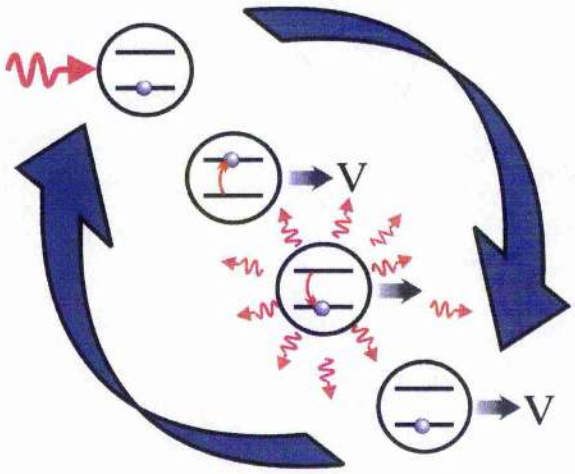

Figure 2.2: A two level atom interacting with a photon. An atom in its ground state (top) absorbs a photon from an oncoming laser beam, this raises an electron into the excited state imparting a momentum "kick" on the atom in the direction of the beam of light (upper middle). Spontaneous emission of a photon can occur in all directions (lower middle) resulting in zero net change in the atom's momentum and leaving the atom in the ground state to absorb another photon and begin the cycle again (bottom).

such spontaneous emissions that imposes a limit on the minimum velocity (temperature) that can be reached, the *photon recoil limit*, where the atom is constantly jostled in $\hbar k$ steps, this temperature is typically a few μK.

This description, however, is an idealized closed cycle. A photon of the correct frequency of the transition is absorbed and re-emitted with the atom returning to its initial ground state. Real life is slightly fuzzier, atoms are not two level systems which introduces the possibility of exciting the atom into the wrong energy level. Once an atom has decayed into a different ground state it is outside the cooling cycle and no further cooling will occur. This is resolved, practically, with the use of a second "hyperfine pumping" laser. The

hyperfine laser is tuned to a frequency that excites the atoms from the un-cooled ground state to an excited state where it then re-enters the cooling cycle. The hyperfine pumping laser will be referred to as the hyperfine laser in future chapters since this is the practice in our lab.

2.3.2 Zeeman Slowing

The simplest way to cool a source of hot atoms would be to counter-propagate a laser with a hot atomic beam and use the radiation pressure, as described above, to decelerate the beam of atoms. However, as the atoms slow down the change in velocity will result, due to the Doppler shift, in the observed frequency of light moving away from resonance with the atom and thereby reducing the cooling effect. For laser cooling to be useful over large velocity ranges some way to overcome the drift away from resonance must be found. One such technique, called Zeeman Slowing [3], places an atomic beam in a varying magnetic field. In a magnetic field the different energy levels within the atom can be shifted - the degeneracy of the energy levels is lifted; this is the *Zeeman effect*. So, if the decrease in frequency seen by the atoms can be compensated for by reducing the resonant frequency of the atomic transition then an extended cooling range of velocities can be obtained. This can be achieved by placing the atomic beam within a tapered magnetic field (figure 2.3).

The hottest atoms see the greater Doppler effect and therefore the highest laser frequencies, the large magnetic field at the start of the slower splits the

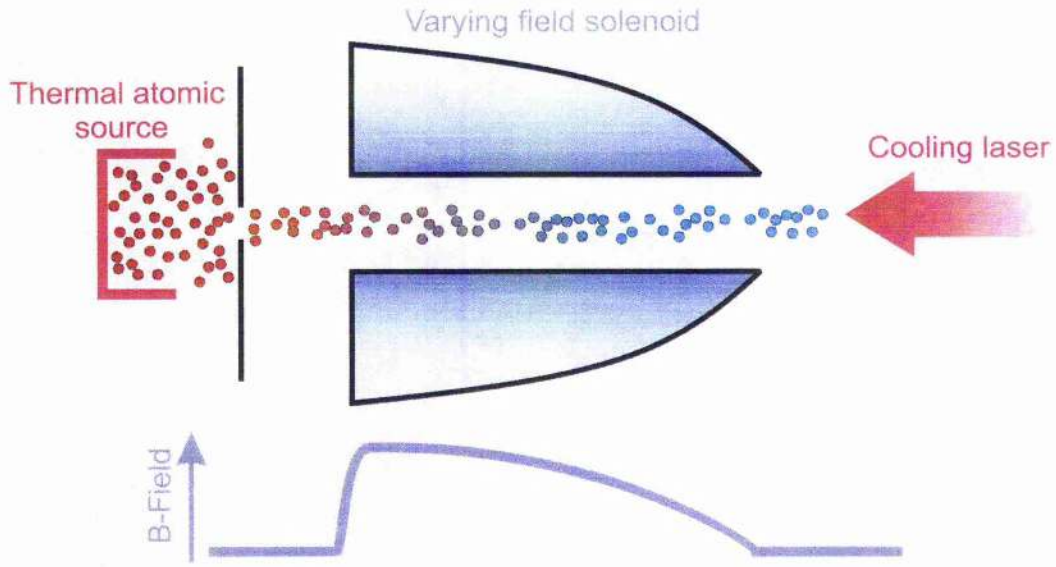

Figure 2.3: A Zeeman Slower. As the thermal atoms propagate along the tapering magnetic field the Zeeman splitting of the atomic levels is reduced; combined with the reduction in the Doppler shift this allows the cooling beam to continue to interact with the light. The lower line shows how the magnetic field varies along propagation length.

cooling levels so that the new energy levels are resonant with the Doppler shifted cooling light. As the atom slows it undergoes a reduced Doppler effect and sees a lower laser frequency than before, during this time, however, the atom has moved to a position of lower magnetic field with the resultant reduction in Zeeman splitting keeping the cooling laser on resonance with the atom and continuing the cooling process. An advantage of this technique is that initially slower moving atoms will continue along the magnetic field unperturbed until reaching the position in the field appropriate for that velocity to see the cooling beam as resonant light. At this point the atom will begin cooling and continue to do so at the same rate as atoms originally much hotter but which have undergone the cooling cycle over a longer distance. In

this way we get a very uniform velocity range output from the Zeeman slower with only the very hottest atoms, which are not Zeeman split enough to bring the laser light into resonance, passing through the system without slowing. Other techniques to keep the laser on resonance include using chirped [4] or broadband [5] sources. The chirped source slows a bunch of atoms during the pulse but hot atoms arriving after the start of the pulse pass through unaffected, broadband sources output a range of frequencies so there is always some fraction of the laser light with the correct energy to be on resonance with and cool the atoms. These techniques, however, require a lot more power (greater than 100 times the intensity) than the Zeeman slower because there is only a small fraction of the laser light used to interact with and cool the atoms.

2.3.3 Doppler Cooling

The Zeeman slower is, as described above, mostly a method for decelerating a beam of atoms but it does produce a compression of the velocity distribution to cool the atoms in one dimension. One method for three dimensional cooling of the atoms is to illuminate the atoms from all directions and to actively exploit the Doppler shift [6] that we were trying to avoid in the Zeeman slower. If we consider an atom in a laser beam tuned not to resonance with the atomic transitions but frequency shifted to the red (lower frequencies) then an atom travelling towards a beam will see the light Doppler shifted towards resonance, undergo increased absorption of the photons and thus have its

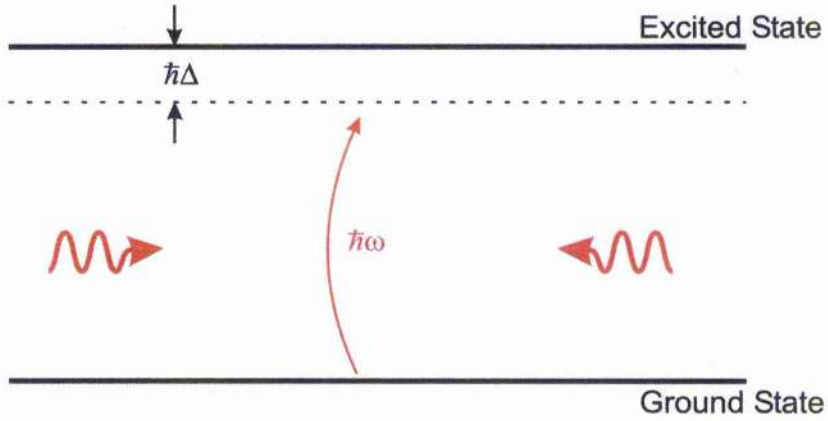

Figure 2.4: Doppler cooling in one dimension. The laser frequency is detuned by an angular frequency, Δ, below the atom resonance. An atom travelling towards one of the beams sees a frequency closer to resonance and is cooled. The two beams create a damping force around v = 0m/s, the zero velocity point.

velocity reduced. An atom travelling away from the laser will see light Doppler shifted even further from resonance and the laser will have a much reduced effect. If we expand this idea to involve three orthogonal pairs of counter propagating beams we create what is known as an optical molasses (see figure 2.4 for the process in one dimension). An atom moving in this field will always interact more with the beam that opposes its motion and will be subject to a balanced force only when the atom is not moving in relation to the beams. In this way the atom is slowed regardless of direction of motion. This method is only a technique for cooling atoms and **not a trap**, atoms in a molasses are free to move around (albeit very slowly) anywhere within the overlapping molasses beams. Once an atom leaves this region it is no longer subject to cooling forces and is free. Since this is a cooling method based on the radiation pressure there is still a constant jostling of the atoms which limits

the minimum temperature which can be achieved, however, we do not reach the photon recoil limit. Here the temperature limit is dependent on the amount of detuning and occurs when the viscous forces of the optical molasses counteract the heating of the atoms due to the continuous absorption of photons [7]:

$$T_D = \frac{\hbar\Gamma}{2k_B} \tag{2.4}$$

where T_D is the Doppler Temperature and Γ is the natural linewidth of the atomic transition. The Doppler temperature is generally a few hundred μK, corresponding to velocities of ~30cm/s. This method of cooling is the basis of the magneto-optical trap discussed in section 2.4.2.

2.3.4 Sisyphus Cooling

Using these optical methods for cooling should bring us to the Doppler Limit and no further, however many experimental groups were able to record temperatures below this limit just by using optical techniques [8]. This occurs because atoms are not the simple, two level systems described for basic understanding of the cooling cycle, and the polarisation of the light itself does not remain constant over the cooling volume but is subject to interference effects with the other beams. The increase in cooling efficiency can be attributed to two effects: optical pumping of the energy levels and an AC stark effect. If we consider an atom with levels as shown in figure 2.5 we have several different possible sublevels to excite the electron into, E_j and G_j

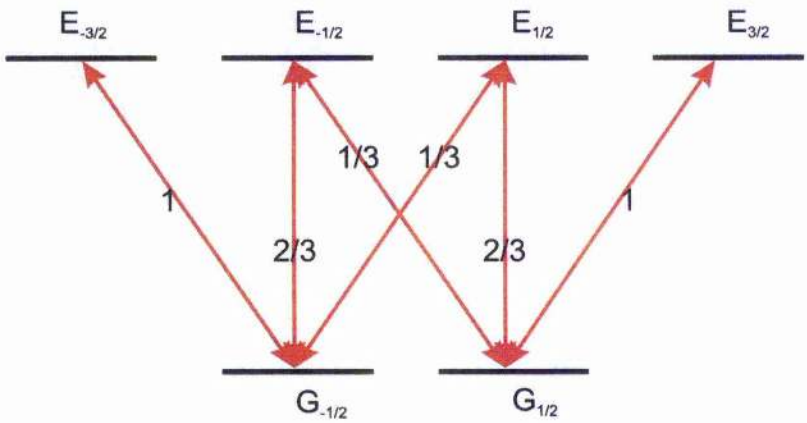

Figure 2.5: The energy levels for an atom in a polarisation gradient. The relative probabilities for each transition are indicated by the numbers on the joining lines. G_j and E_j represent the ground and excited states respectively

representing the excited and ground states respectively with an angular momentum, j. The relative probability of each transition is shown by the number between the levels. Optical pumping is dependent on polarisation of the light to define which new energy level the atoms will be excited to, right-hand circularly polarised light, σ^+, will always pump the atom into a $j \rightarrow j+1$ angular momentum state, i.e. $G_{-1/2}$ will be excited to $E_{1/2}$. Emission is still a random decay, controlled by the probabilities indicated, but over many cycles the atom will be pumped towards the highest j value. From here it is only possible to decay into the $G_{1/2}$ state so under constant illumination of suitably tuned σ^+ light the atom is optically pumped into the $G_{1/2}$ ground state. Left hand circularly polarised light, σ^-,pumps the atom into a $j \rightarrow j-1$ angular momentum state, in this case pumping the atom into the $G_{-1/2}$ state. Therefore the ground state an atom can be in is dependent on the polarisation of the incident light. The AC Stark effect shifts the energy levels of the atomic

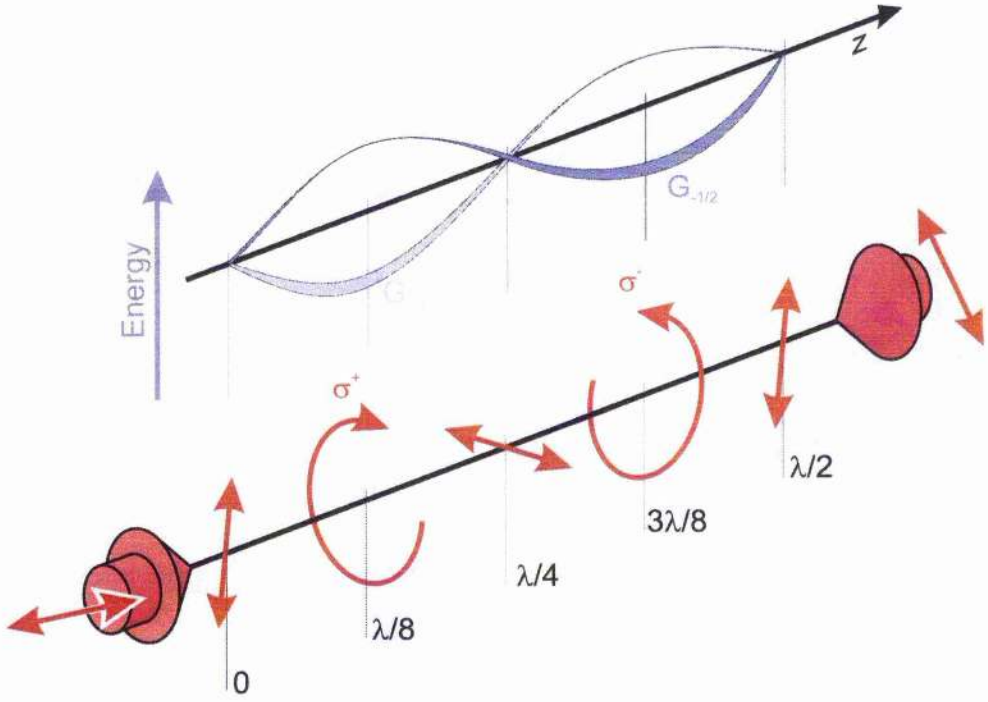

Figure 2.6: Polarisation gradients. The lower line describes the resulting varying polarisation of two co-propagating linearly polarised beams. The polarisation changes from linear and circular every eighth of a wavelength. The upper line shows the effect these gradients have on the ground state of an atom. Where the polarisation is σ^+ the $G_{1/2}$ level is shifted lower due to the AC Stark shift, where the light is σ^-, $G_{-1/2}$ is lowest level. The relative populations of each level are indicated by the thickness of the lines.

ground state in a similar way to the Zeeman effect. The ground states are shifted down for incident laser frequencies lower than resonance and increased for frequencies higher than resonance; the effect on the different j sub-levels depends on the polarisation of the light. In a σ^+ field there is a larger effect in the $G_{1/2}$ state, and in a σ^- field the $G_{-1/2}$ undergoes the larger shift. Now, if we consider two counter-propagating beams with linear but orthogonal polarisation we produce a field whose polarization changes from

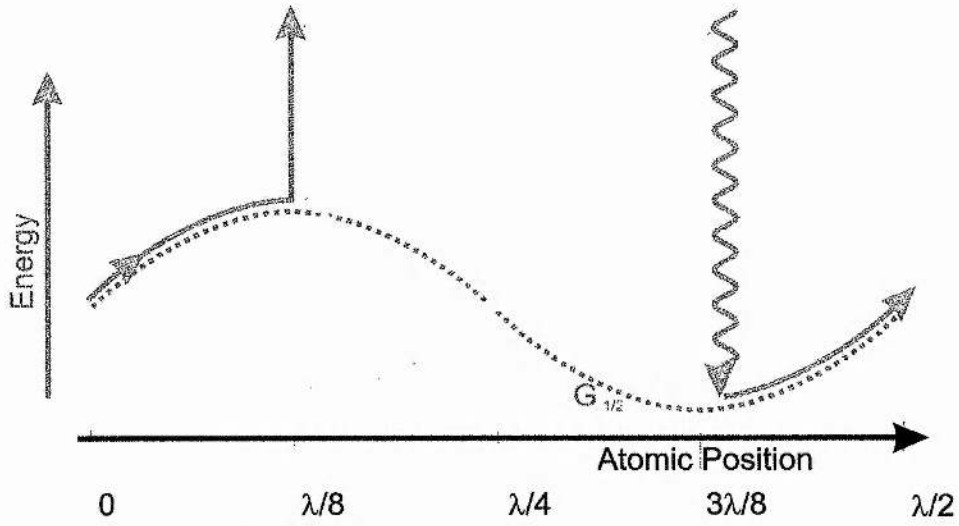

Figure 2.7: Sisyphus cooling in 1-dimension. An atom travelling from left to right in the $G_{-1/2}$ state experiences a potential hill, at the top of the hill it is optically pumped into the $G_{1/2}$ state and is now in a potential valley, and again travels up a potential hill. This cooling effect is a maximum when the time taken to travel to the top of the potential is the same as the time to be pumped into the other ground state, as shown here.

linear to circular periodically as shown in figure 2.6. Combining this polarisation gradient with the AC Stark shift and optical pumping we generate an oscillation between the different ground states, with a population in these levels strongly related to position along the optical field. Consider an atom moving along this polarisation gradient starting in the $G_{1/2}$ state (figure 2.7), if the atom remains in the $G_{1/2}$ state (as it should do due to optical pumping of the σ^+ beam) then as the atom moves to the right is travels up a potential "hill" and looses energy. Once it reaches the top of this "hill" it will have travelled through the polarisation gradient and reached a position where the light is circularly polarised in the other sense, σ^-, and, therefore, has a high

probability of being optically pumped into the $G_{-1/2}$ state where it will be in a potential "valley" again and the process can be repeated. In this way the moving atom always has to travel up a hill and so constantly loses energy and is cooled. This is known as *Sisyphus Cooling* after Sisyphus in Greek mythology who betrayed the secrets of the Gods and was condemned to push a block of stone to the top of a steep hill, every time the rock reached the top it rolled down and Sisyphus had to start all over again continuing his labour for all eternity. This cooling method is finally limited by the individual recoils of the atoms with each absorption event resulting in a recoil velocity of $\hbar k/m$ [8]:

$$T_r = \frac{\hbar^2 k^2}{m k_B} \qquad 2.5$$

where T_r is the photon recoil temperature and m is the mass of the atoms. T_r is typically a few μK which corresponds to velocities of ~1cm/s.

Although laser cooling has shown itself to be a powerful tool for cooling atoms its reliance on the absorption and emission of photons to transfer momentum limits the final temperature that can be achieved to that of a single photon recoil, T_r. In order to reduce the temperature of the atoms further and reach high enough phase space densities for BEC a different cooling method must be used.

2.3.5 Evaporative Cooling

If we can cool a vapour of atoms to a sufficiently low temperature and high density the atomic ensemble can form a Bose-Einstein condensate (BEC) [9].

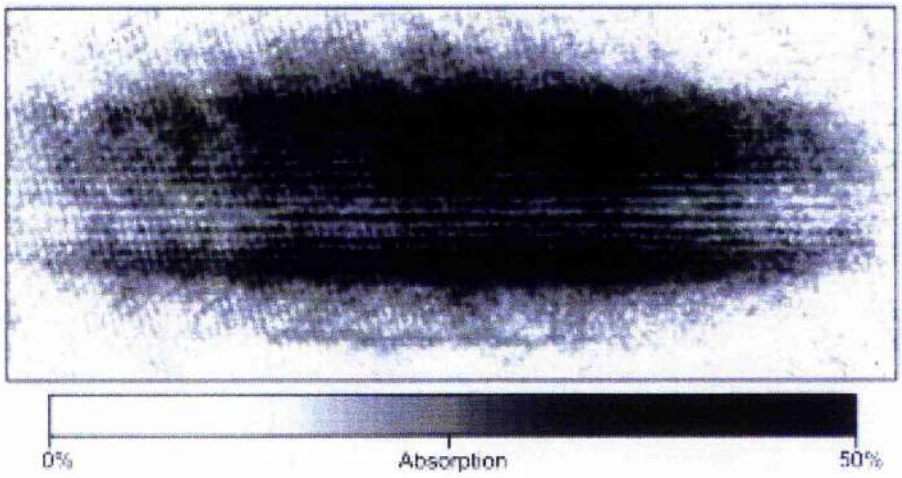

Figure 2.8: Interference between two BEC clouds. Image reproduced from W. Ketterle's Nobel lecture; "*When atoms behave as waves: Bose-Einstein condensation and the atom laser.*" Les Prix Nobel 2001, pp.118-154 (2002)

The atoms reach a temperature where the thermal de Broglie wavelength, $\lambda_{dB} = h/(3mk_BT)^{1/2}$, becomes larger than the mean spacing of the atoms (the phase space density is 2.612), i.e. the atomic wave functions must overlap each other and the resultant ensemble of atoms can be considered as a coherent source in a similar way to a laser beam and subject to similar effects, such as interference (see figure 2.8) [10].

The temperatures required for BEC are many times colder than the photon recoil limit. This precludes the use of near resonant light to create the required temperatures (on top of this emitted photons from one atom can be absorbed by neighbouring atoms causing a repulsive force, thus preventing near resonant optical cooling from achieving the required densities either), however, the simplicity of the optical techniques described earlier offer a good "springboard" to start from.

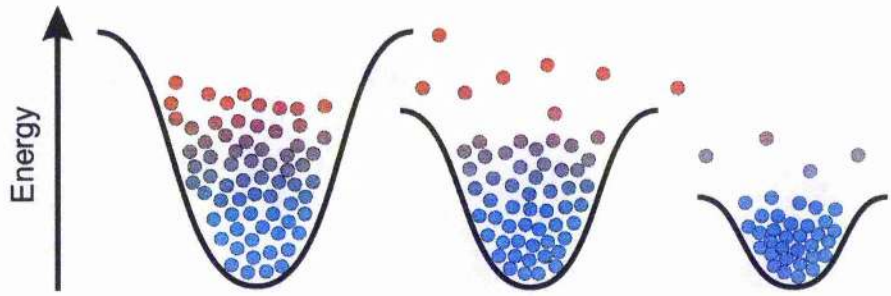

Figure 2.9: Evaporative cooling. The potential confining the atoms is lowered, the highest energy atoms can now escape, leaving the remaining atoms re-thermalise at a lower temperature. The cooler atoms can now sink further into the potential occupying less space and increasing the density of the ensemble.

Once you have your initial cold ensemble of atoms, at a few μK, the most promising technique is evaporative cooling [11]. The basic idea is the same as occurs in nature; the most energetic atoms are allowed to escape and the whole ensemble re-thermalises to a lower temperature - in the same way as a cup of coffee cools. The remaining atoms will occupy a smaller volume and increase the density of the sample (see figure 2.9). The potential "cup" for forming a BEC can be generated using optical [12] or magnetic forces [13], the hotter atoms being allowed to escape by lowering the depth of this potential.

2.4 Trapping Atoms

While the cooling methods described above provide a damping to the motion of the atoms there is no actual confinement of the atoms (with the exception of the potential "cup" for evaporation cooling). During interaction with the beam atoms are slowed but are still free to move in any direction; if an atom reaches the edges of the cooling beams then is can escape into the surrounding environment. Thus having cooled the atoms we still need a technique to spatially confine them.

2.4.1 Magnetic-field trap

Earnshaw's theorem prohibits stable trapping of a charged particle in a fixed electrostatic field, dipoles, however, can be trapped within local minima. An atom with a magnetic moment, μ, can be confined by an inhomogeneous magnetic field. Inside a magnetic field, B, an atom has a potential energy $-\mu.B$, and within a field gradient the atom experiences a force:

$$F = \mu.\nabla B \qquad (2.6)$$

To confine the atoms there is an exchange of kinetic energy for potential energy (stored as atomic energy), for this to occur the angular momentum of the atoms must be anti-parallel with the magnetic field where they are trapped within potential minima, atoms cannot be trapped in potential maxima. Convenient magnetic fields (up to ~2T) produce potentials <1K deep, so a

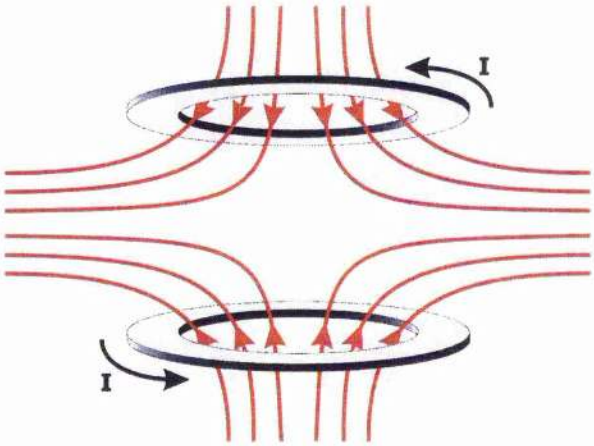

Figure 2.10: Schematic of a magnetic quadrupole trap. Because the currents in the coils are in opposite directions there is zero magnetic field in the centre in which to confine the atoms.

magnetic trap needs a source of cold atoms to begin with, also because the trap depth is so shallow high vacuum conditions (10^{-7} mbar) are required to reduce collisions that would otherwise knock atoms out of the trap. The first magnetic trap used anti-Helmholtz coaxial coils to create a simple magnetic quadrupole with a zero field in the centre [14] (figure 2.10) This was neither a harmonic or a central trap and angular momentum was not conserved in the field minima, atoms were ejected from the zero-field centre as the direction of the atomic moment could spin-flip into the un-trapped state.

A different kind of field is created in the Ioffe scheme [15]; four rods create a minimum in the centre with two coils placed at either end to close the potential, this is not, however, a zero-field position. This stops the atoms flipping into the un-trapped state and greatly increases the lifetime of the trap. This type of arrangement is used typically for the generation of BEC. The state of the art of magnetic traps is very high nowadays and modern traps

often do not make use of large coils and external wires to create the necessary fields but make use of miniaturisation methods to etch the wire structure onto chip surfaces trapping atoms very close to these surfaces in much higher magnetic gradients [16].

2.4.2 Magneto-optical Trap and Low-velocity Intense Source of Atoms

Although a 3D optical molasses is an effective method for cooling atoms, as mentioned earlier the radiation pressure alone cannot be used to spatially trap an ensemble of atoms. This is for a similar reason as Earnshaw's theorem for electrostatics and is therefore called the Optical Earnshaw theorem; we cannot have a radiation pressure inwards over the whole trapping volume so the force is fundamentally unstable [17]. Thus, for the radiation pressure to be the basis of a trap we need to "break the symmetry" of the system by making the force dependent on position. The most widely used trap is a hybrid trap utilising magnetic fields and the radiation pressure to make a magneto-optical trap [18]. The MOT uses circularly polarised light for the molasses beams in order to exploit the Zeeman shift of atoms as they move through a magnetic gradient. For a simple scheme of an atom excited from the $j_g=0 \rightarrow j_e=1$ (j is the total angular momentum quantum number) there are three Zeeman components, that can be excited by each of three polarisations, whose frequencies tune with field and therefore position as shown for one dimension in figure 2.11.

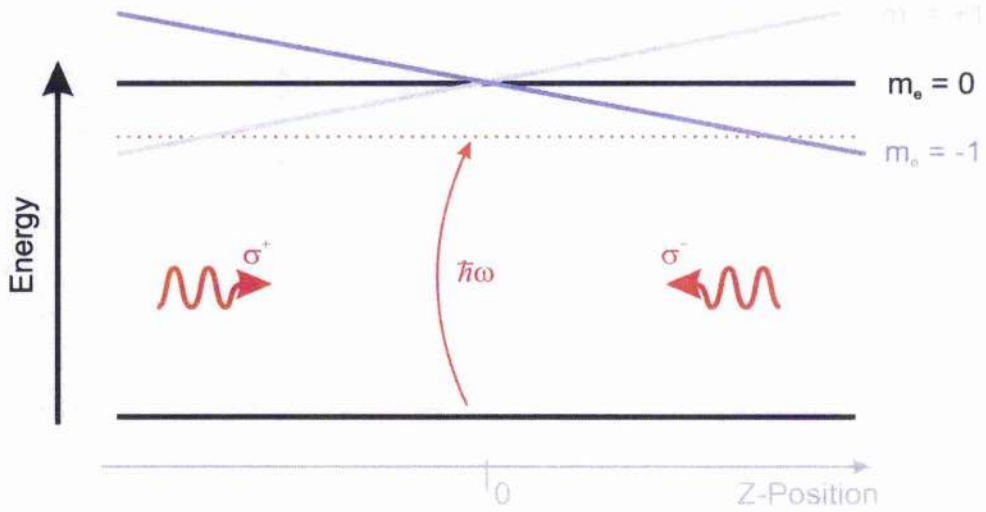

Figure 2.11: The magneto-optical trap in one dimension. The magnetic quadrupole field varies linearly with distance from centre so the m=±1 sub-levels see a linear Zeeman shift. An atom in the negative z-direction sees the m=+1 level brought closer to resonance and the σ^+ beam pushes it back to the centre. For an atom with a positive displacement the σ^- beam is brought into resonance and the atom is again pushed into the centre.

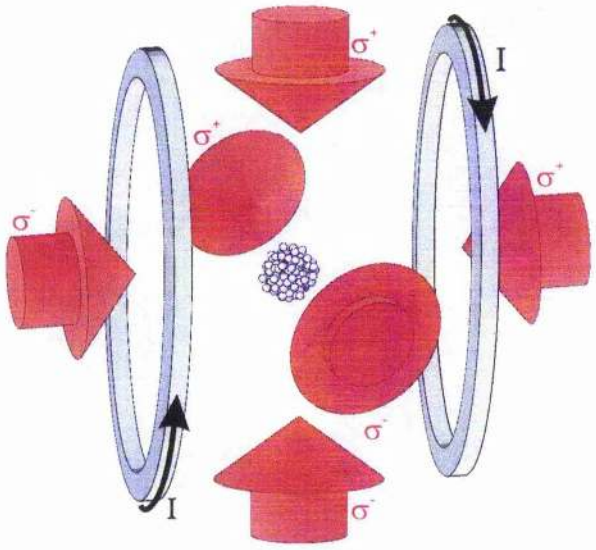

Figure 2.12: Schematic of a MOT. Six mutually orthogonal, circularly polarised beams create a 3-dimensional molasses while the anti-Helmholtz coils produce a positional dependent force

The Zeeman shift for the state m_e=+1 (the projection of the total angular momentum on the quantisation axis has been increased by +1) is up in a positive field and down in a negative field. Looking at figure 2.11 we see that at a position left of centre the m_e=+1 state is shifted closer to the frequency of the laser, the m_e =+1 state then absorbs more light in the σ^+ polarisation so the atom will be pushed back towards the centre of the trap. If the atom drifts to the right of centre the m_e=-1 state is shifted closer to the laser frequency, this state absorbs the opposite polarisation and is again pushed back into the centre of the trap. In 3-dimensions the magnetic gradient is created using anti-Helmholtz coils with the polarisation of the beams orientated to the magnetic field as shown in figure 2.12. In order to generate a large enough positional dependence and overcome the optical Earnshaw theorem a field of ~10G/cm is required. This combination of forces results in a very robust trap able to cool atoms from a room temperature cell with atoms captured directly from vapour in an initial cooling cycle in the molasses beams. This type of trap requires much lower magnetic gradients than the purely magnetic trap because the magnetic field is not used to cool or confine the atoms, it is simply required to create the positional dependence of absorption. A MOT is also quite insensitive to any imbalance in the beam powers or deviations from perfectly circular polarisations making it the workhorse for obtaining atoms with temperatures of 100μK and densities of 10^{12} atoms/cm^3. The number of beams to be manipulated within a trap has been reduced using mirror MOT's, where atoms are trapped close to a mirror surface with one of beams incident to the surface at 45° and retro-reflected back. In the cross over region near

the mirror this beam provides a cooling force in four of the six required directions [19]. Controlling a source of cold atoms close to a surface is important as a method of loading magnetic guides built into the surface of a substrate for the realisation of miniaturised "atom chips." The number of beams needed has been reduced further using conical and pyramidal mirrors to reflect a single beam onto a central point so as to create the required, orthogonal beams between the mirror surfaces [20].

The very stability of the MOT allows for minor modification to the setup and permits simple extraction of atoms and generation of a cold atomic beam (an ensemble of cold atoms with a low longitudinal velocity and narrow velocity distribution, and with minimal kinetic energy in the transverse direction). This is important for atom lithography or interference experiments or simply for moving atoms to a "clean" chamber for further experimentation. For a pulsed, simple extraction of atoms from the MOT you can simply turn off the trapping forces and let the atoms fall under gravity. However, a continuous extraction might also be required. One of the simplest and most effective methods of creating a continuous wave (CW) atomic beam is a *Low-velocity Intense Source* (LVIS) [21]. The system for this is nearly identical to a normal MOT with six beams and a quadrupole magnetic field, the only difference is one beam has a narrow dark region in the centre (see figure 2.13). This dark region can be generated by drilling a hole in the retro-optic or by placing a small obstruction in the retro-beam, (typically MOTs are generated using three mutually orthogonal beams, these are then retro-reflected to propagate back along the same path and generate the six cooling beams; it is in the retro-

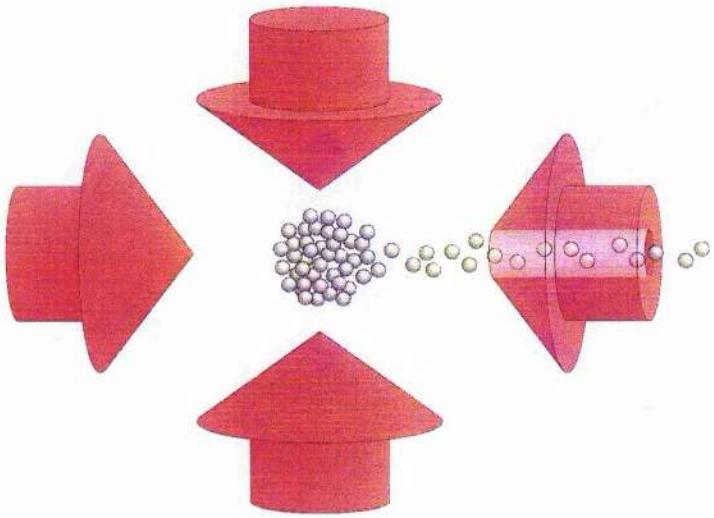

Figure 2.13: A schematic of an LVIS beam. One of the beams is generated with a hole in the centre; the radiation pressure imbalance along the hole creates the beam of atoms. The magnetic coils and third pair of trapping beams (perpendicular to the page) are not shown.

reflected beam that the obstruction in placed). This creates an intensity imbalance in the centre of the trap; the radiation pressure then accelerates the atoms out of the trap along the hollow beam. This technique has the advantage that it constantly apertures and recycles the beam as any atom with enough transverse velocity to move out of the hollow region will find itself back in the MOT beams and are returned to the centre of the trap just as in a normal MOT. For optimised flux it was found that the detuning of the cooling beams should be 5Γ below resonance, for a MOT the optimal detuning is only 3.2Γ [21]. This can be explained by increased scattering near to exiting the MOT region: if there is an imbalance in the transverse beams then the atom beam will get deflected and leave the hollow region early. Increasing the detuning of the MOT beams decreases this radiation pressure effect, resulting

in a smaller cloud but a greater LVIS flux. Using this method atomic beams with velocities of 14m/s ± 2.7m/s can be generated. The relatively large distribution of velocities is due to the atoms not all being accelerated out of the trapping region at the same position and so are being subjected to different radiation pressure forces.

The value of $\Delta v/v$ is the significant figure for an atomic beam as the variation of velocity gives a measure of how "monochromatic" the source is. For smaller values of $\Delta v/v$ the atom funnel [22] can be used. The funnel is essentially a stretched MOT. The magnetic field is generated using "hairpin" wires to produce an extended zero field for the atoms to move along, the relative detuning or intensity of the cooling beams along this axis is changed to apply a drift velocity and form a slow atomic beam. Atomic beams from this setup have produced a Δv of only ~20cm/s with a controllable velocity between 3 to 10m/s, however these atomic funnels lack the simplicity of LVIS.

There have also been several variations on the basic design of LVIS; one of these has been to use Laguerre-Gaussian beams as the source of the hollow beam [23]. Since the LG beam is a free space light beam it propagates without diffractively filling, unlike the obstruction generated hollow beams used in the description above. This results in a more robust atomic beam which is better confined and with a flux that is a constant percentage of the atoms trapped. Another method for creating a force imbalance within the MOT is to use an extra push beam [24]. A weak near resonant beam can be used to push the atoms in an arbitrary direction unlike the fixed LVIS, but the

Δv is a lot worse than the standard LVIS with velocities of 14m/s ± 9m/s. Single beam MOTs have also been used to produce an LVIS beam [25]. A hole can be placed at the apex of the conical trap to produce a force imbalance and the atoms can then propagate along that axis and out of the conical mirrors.

2.4.3 Optical Dipole Traps

In contrast to the previous traps the optical dipole trap uses only light fields to confine the atoms. While the radiation pressure cannot be used to trap atoms by itself, its interaction with the atoms must be considered as well as the dipole force we want to use. Optical potentials are usually very shallow with the absorption and re-emission of a photon often enough to kick the atoms out of the trap, therefore we want to minimise this scattering rate. For most experiments, where there is a large detuning of the laser with negligible saturation of atoms, the dipole potential in a beam of power P, waist w_0 and detuning from resonance, Δ, is given by [26]:

$$U_0 = -\frac{\hbar P}{4{w_0}^2 \Delta \tau^2 I_{sat}} \tag{2.7}$$

where I_{sat} is the saturation intensity, and τ is the natural lifetime of the upper state. The scattering rate is:

$$\gamma_s = \frac{I\Gamma^3}{8I_{sat}\Delta^2} \tag{2.8}$$

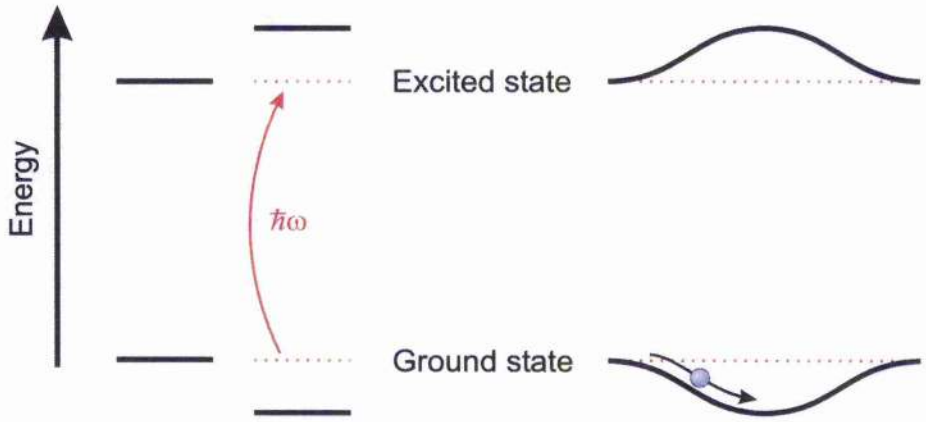

Figure 2.14: Light shift for a two level atom. Red-detuned light shifts the gound state down and the excited state up by the same amount, (left). In a inhomogeneous field like a Gaussian beam a ground state potential well is produced in which atoms can be trapped (right).

These equations show two important factors; different scaling factors with respect to the detuning of the laser. The dipole potential is proportional to I/Δ whereas the scattering rate is proportional to I/Δ^2, therefore, you usually use large detunings and high intensities to reduce the scattering rate. The dipole potential is also seen to be proportional to the sign of the detuning, red detuned light ($\Delta<0$) attracting the atom to the light field, blue detuned light repelling the atoms. If we look at the energy levels of the atoms we observe a light shift (AC Stark effect) perturbing the position across the profile of the laser beam (see figure 2.14). In a low saturation case the atoms spend most time in the ground state and see the varying light shift across the beam creating a potential well for trapping. The dipole potential and scattering rate can be defined in several ways; in later chapters different definitions will be given to be more convenient for the application described.

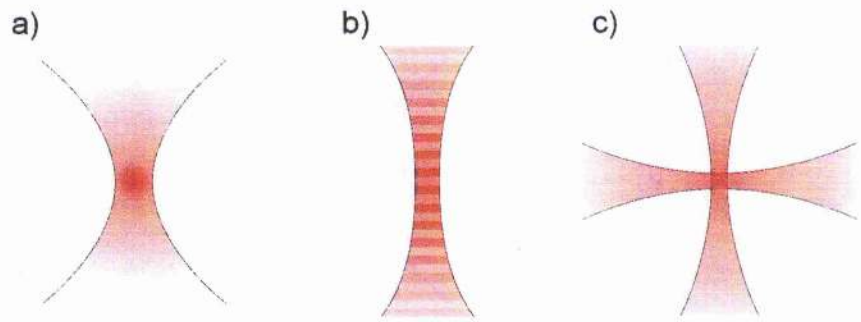

Figure 2.15: Beam configurations for red-detuned optical dipole traps. a) Focused beam trap. b) Standing wave trap, the potential depth is four times deeper than the focused beam trap. c) Crossed beam trap, this type of trap can be used to create deep, nearly symmetrical traps, in contrast to the case in b).

The simplest dipole trap is a focused Gaussian beam red-detuned as in figure 2.15a with the atoms attracted to the intense focus [27]. Most traps are limited to a few mK and other cooling methods, such as MOT's, are required to load the dipole traps [28]. Of course a single focus laser beam is not the only way to create a trap, combining beams can offer higher intensities and tighter confinement (figure 2.15b and 2.15c). Micro optical arrays [28], and spatial light modulators [29] have also been used to create many trap sites for trapping ensembles or single atoms.

The scattering problem occurs only when the laser is red-detuned since it is in this regime where atoms are attracted to the highest intensities. Blue-detuned trapping minimises the scattering forces by forcing atoms into low light intensities. The basic idea is to surround a spatial region with repulsive light. Trapping in the dark region reduces the rate of unwanted scattering events, allowing the use of weaker beams that generate lower light shifts of the

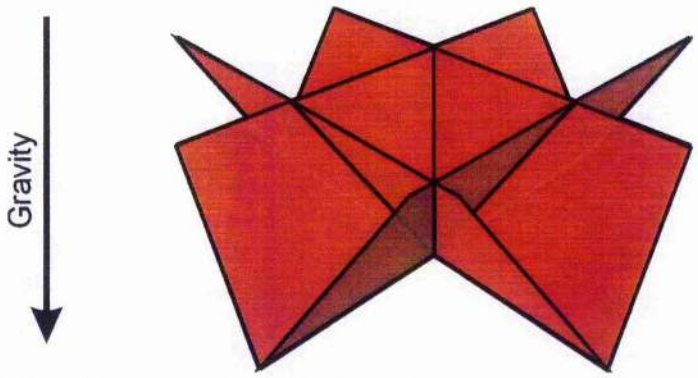

Figure 2.16: Schematic of a blue-detuned crossed light sheet trap. The four light sheets create a potential well, with gravity used to pull the atoms to the bottom of the trap. Reproduced from [31]

atomic levels and other light assisted losses. Experimentally these types of traps are not as simple and straight forward as the red-detuned case. We require repulsive walls of light, and three main ideas have been put forward for these ends: using light sheets, hollow beams and evanescent waves. In most cases gravity is used to confine the atoms in the vertical direction. In the simplest case crossed light sheets are used to create a "V" shaped trap that atoms can sit in, two beams can be used to create a trapping volume with 3-dimensional confinement achieved as the potential closes around the centre due to tight focusing of the trapping light [30], however a more sturdy trap with increased trapping volume can be made using four crossed light sheets in an inverted optical pyramid pattern [31] (see figure 2.16). Hollow beam traps contain the atoms in a tube of light, two plug beams [32] can be used to add 3-dimensional confinement, or if non-free space propagating beams have been used then focusing can be used to close the ends of the trap creating either conical potentials [33] or shaped bubbles of light by interfering Laguerre-Gaussian beams [34].

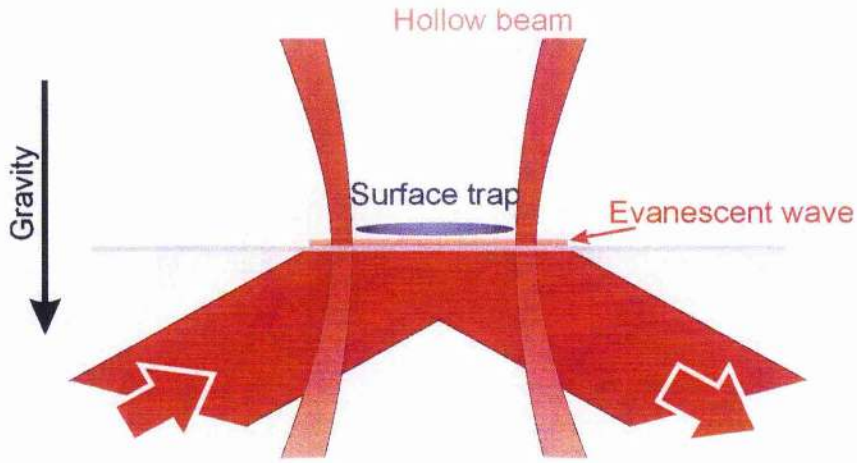

Figure 2.17: Blue detuned optical surface trap. The blue-detuned evanescent field traps the atoms above the surface against gravity and a detuned hollow beam provides horizontal confinement. Reproduced from [35].

A third method of exploiting the dipole force is in the use of evanescent waves. The evanescent wave realises a hard flat potential from a dielectric surface, this evanescent field drops off exponentially as we move further from the surface so it can be used to levitate atoms a few μm from the surface where the repulsion of the blue-detuned light balances with gravity. Further optical confinement can be achieved using a blue detuned hollow beam to create vertical walls around the surface of atoms [35] (see figure 2.17).

Bibliography

[1] A. Ashkin, "Atomic-beam deflection by resonance-radiation pressure," Phys. Rev. Lett. **25** 1321 (1970)

[2] A. Ashkin, "*Applications of laser radiation pressure*," Science **210** 1081 (1980)

[3] W. D. Phillips and H. Metcalf, "*Laser deceleration of an atomic beam*," Phys. Rev. Lett. **48** 596 (1982)

[4] W. Ertmer, R. Blatt, J. L. Hall, and M. Zhu, "Laser manipulation of atomic beam velocities: demonstration of stopped atoms and velocity reversal," Phys. Rev. Lett. **54** 996 (1985)

[5] M. Zhu, C. W. Oates and J. L. Hall, "Continuous high-flux monovelocity atomic beam based on a broadband laser-cooling technique," Phys. Rev. Lett. **67** 46 (1991)

[6] T. W. Hänsch and A. L. Schawlow, "*Cooling of gases by laser radiation,*" Opt. Comm. **13** 68 (1975)

[7] H. J. Metcalf and P. van der Straten, "*Laser Cooling and Trapping*," Springer-Verlag New York (1999)

[8] P. D. Lett, R. N. Watts, C. I. Westbrook and W. D. Phillips, "*Observation of atoms laser cooled below the Doppler limit*," Phys. Rev. Lett **61** 169 (1988)

[9] S. N. Bose, Z. Phys. **26** 178 (1924)

A. Einstein, Sitzungsber. Kgl. Preuss. Akad. Wiss. **1924** 261 (1924)

[10] M. R. Andrews, C. G. Townsend, H-J. Miesner, D. S. Durfee, D. M. Kurn and W. Ketterle, "*Observation of Interference between Two Bose Condensates*," Science **275** 637 (1997)

[11] K. B. Davis, M. O. Mewes and W. Ketterle, "*An Analytical Model for Evaporative Cooling of Atoms*," App. Phys. B. **60** 155 (1995)

[12] M. D. Barrett, J. A. Sauer and M. S. Chapman, "*All-Optical Formation of an Atomic Bose-Einstein Condensate*," Phys. Rev. Lett. **87** 010404-1 (2001)

[13] M. H. Anderson, J. R. Ensher, M. R. Matthews, C. E. Wieman and E. A Cornell, "*Observation of Bose-Einstein Condensation in a Dilute Atomic Vapour*," Science **269** 198 (1995)

[14] A. Migdall, J. Prodan, W. Phillips, T. Bergeman and H. Metcalf, "*First Observation of Magnetically Trapped Neutral Atoms*," Phys. Rev. Lett. **54** 2596 (1985)

[15] T. Bergeman, G. Erez and H. Metcalf, "*Magnetostatic Trapping fields for Neutral Atoms*," Phys. Rev. A. **35** 1535 (1987)

[16] R. Folman, P. Krüger, D. Cassattari, B. Hessmo, T Maier and J. Schmiedmayer, "*Controlling Cold Atoms using Nanofabricated Surfaces: Atom Chips*," Phys. Rev. Lett. **84** 4749 (2000)

[17] A. Ashkin and P. J. Gordon, "Stability of radiation-pressure particle traps: am optical Earnshaw theorem," Opt. Lett. **8** 511 (1983)

[18] E. L. Raab, M. Prentiss, A. Cable, S. Chu and D. E. Pritchard, "*Trapping of neutral sodium atoms with radiation pressure*," Phys. Rev. Lett. **59** 2631 (1987)

[19] M. A. Clifford, G. P. T Lancaster, R. H. Mitchell, F. Akerboom and K. Dholakia, "*Realisation of a mirror magneto-optical* trap," J. Mod. Opt. **48** 1123 (2001)

[20] K. I. Lee, J. A. Kim, H. R. Noh and W. Jhe, "*Single-beam atom trap in pyramidal and conical hollow mirror,*" Opt. Lett. **21** 1177 (1996)

[21] Z. T. Lu, K. L. Corwin, M. J. Renn, M. H. Anderson, E. A. Cornell and C. E. Wieman, "*Low-Velocity Intense Source of Atoms from a Magneto-optical Trap,*" Phys. Rev. Lett. **77** 3331 (1994)

[22] E. Riis, D.S. Weiss, K. A. Moler and S. Chu, "*Atom funnel for the production of a slow, high-density atomic beam,*" Phys. Rev. Lett. **64** 1658 (1990)

[23] G. P. T. Lancaster, "*Experimental Studies of Diode Lasers and Cold Atom Guiding,*" PhD Thesis, University of St Andrews (2001)

[24] W. Wohlleben, F. Chevy, K. Madison and J. Dalibard, "*An Atom Faucet,*" Eur. Phys. J. D. **15** 237 (2001)

[25] K. H. Kim, K. I. Lee, H. R. Noh, W. Jhe, H. Kwon and M. Ohtsu, "*Cold atomic beam produced by a conical mirror funnel,*" Phys. Rev. A. **64** 013402-1 (2001)

[26] C. S. Adams and E. Riis, "*Laser cooling and trapping of neutral atoms,*" Progress in Quantum Electronics **21** 1 (1997)

[27] S. Chu, J. Bjorkholm, A. Ashkin and A. Cable, "*Experimental observation of Optically Trapped Atoms,*" Phys. Rev. Lett. **57** 314 (1993)

J. D. Miller, R. A. Cline and D. J. Heinzen, "*Far-Off-Resonance Optical Trapping of Atoms*," Phys. Rev. A. **47** R4567 (1993)

[28] R. Dumke, M. Volke, T. Müther, F. B. J. Buchkremar, G. Birkl and W. Ertmer, "*Micro-optical Realisation of Arrays or Selectively Addressable Dipole Traps: A Scalable Configuration for Quantum Computation with Atomic Qbits*," Phys. Rev. Lett **89** 097903-1 (2002)

[29] S. Bergamini, B. Darquié, M. Jones, L. Jacubowiez, A. Browaeys and P. Grangier, "*Holographic generation of micro-trap arrays for single atoms*," J. Opt. Soc. Am. B. **21** 1889 (2004)

[30] N. Davidson, H. J. Lee, C. S. Adams, M. Kasevich and S. Chu, "*Long optical coherence times in an optical dipole trap*," Phys. Rev. Lett. **74** 1311 (1995)

[31] H. J. Lee, C. S. Adams, M. Kasevich and S. Chu, "*Raman Cooling of Atoms in an Optical Dipole Trap*," Phys. Rev. Lett. **76** 2638 (1996)

[32] T. Kuga, Y. Torii, N. Shiokawa, T. Hirano, Y. Himizu and H. Sasada, "*Novel optical trap of atoms with a doughnut beam*," Phys. Rev. Lett. **78** 4713 (1997)

[33] R. M. Herman, T. A. Wiggins, "*Hollow beams of simple polarisation for trapping and storing atoms*," J. Opt. Soc. Am. A. **19** 116 (2002)

[34] R. Ozeri, L. Kaykovich, N. Friedman and N. Davidson, "*Large-volume single beam dark optical trap for atoms using binary phase elements*," J. Opt. Soc. Am. B. **17** 1113 (2000)

[35] Yu. B. Ovchinnikov, I. Manek and R. Grimm, "*Surface Trap for Cs atoms based on Evanescent-Wave Cooling*," Phys. Rev. Lett. **79** 2225 (1997)

Chapter 3:

Review of Guiding Experiments

3.1 Introduction

Once a source of cold atoms has been obtained (such as a MOT or LVIS) we must then consider how they can be utilised for experimental purposes.

The use of atomic beams has received a lot of interest in recent years. The relative ease in which atoms can now be trapped and cooled has led to the emergence of the field of atom optics. For total experimental control over an atom beam it is necessary to create atomic analogues to optical mirrors, lenses and beam splitters. Once this is achieved we can still use the atoms in several ways; by cooling the atoms to reveal their wave-like nature the atomic ensemble can be used for interferometry in similar ways to light beams or we can make use of the short wavelengths for accurate positioning of the atoms.

In certain applications the wave nature of particles offers advantages over the use of optical fields owing to the fact that an atom has a mass, whereas a photon has only momentum, and has a much greater ability to interact with its local environment. Thus an interfering atomic beam would offer an increase in sensitivity of several orders of magnitude for measuring non-inertial frames (such as accelerating and rotating frames) over laser based technologies and open the possibility of creating gravity sensors sensitive enough to measure the slight fluctuation in the earth's gravitational field and result in maps based on these fluctuations (a system that is independent of other, external factors such as the use of satellites in GPS). The use of BEC provides a single wavelength in atomic beams making their use in interferometers advantageous, but just as white light can be used in optical interferometry it is also possible to use a multimode matter wave to produce interference fringes [1, 2]. The high resolutions possible with atomic wavelengths (the resolution of an imaging system is limited to ~$\lambda/2$) leads to very accurate deposition for applications such as lithography and in such circumstances a controllable guide is still necessary to channel the atoms to the desired location. In reducing the energy of the atoms by cooling we make them easier to manipulate and reduce the powers needed to guide them (the atoms are travelling more slowly and can be confined within much shallower potentials than thermal atoms). In applications such as atom lithography it is actually beneficial to avoid cooling the atoms too far, as this would increase the wavelength of the atom beam and reduce the resolution when writing the

pattern. Of course, it is often desirable to simply transport atoms to a "clean" science chamber for further study without other experimental contaminants.

There are two main forces that have be used to generate guides for atomic beams: the first uses magnetic field gradients to influence the atoms, the second technique is to optically guide the atoms using the dipole force as described in section 2.2.2. The use of optical forces can be further split into two categories: Hollow optical fibre guiding where the light confining the atoms is itself contained within an optical fibre, and free space light beam guiding where the light travels naturally through space.

This chapter is written to give a flavour of the concepts and results in this field, in order to give a background to the experimental area of this thesis, and is not meant to be an exhaustive study on all areas of this rapidly advancing field. Since this project aims to demonstrate the guiding of atoms with free space light forces this section will concentrate on areas leading to this goal.

3.2 Magnetic Guiding

The earliest experimental results for the guiding of neutral atoms were demonstrated using magnetic fields generated around a current carrying wire. This was proposed and shortly after demonstrated by Schmiedmayer in 1995 [3, 4]. When a current flows through a wire there is a resultant magnetic field, B, and an associated guiding potential around the wire (figure 3.1).

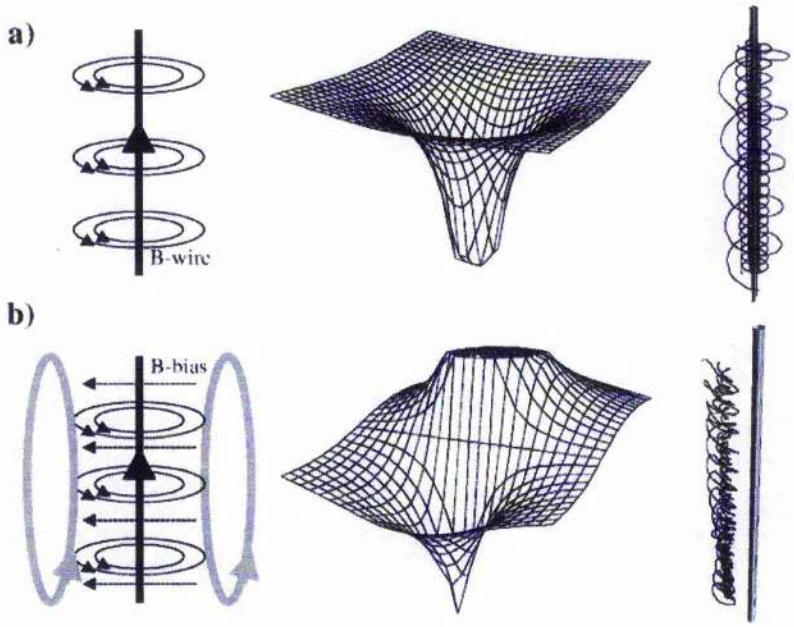

Figure 3.1: Two configurations for magnetic guiding of neutral atoms along current carrying wires. The left images show the wire and magnetic field potentials, the centre images show the guiding potentials and the right images show typical trajectories of the guided atoms. a) describes this process when only a wire is used to create the guide and b) shows the effect of a bias field to create a side guide. Reproduced from [5]

Thermal atoms were guided within this field. An atom with a magnetic moment, μ, in a field will experience a potential, U_{mag}:

$$U_{mag} = -\vec{\mu}.\vec{B} \qquad (3.1)$$

Atoms in a high field seeking state (where $U_{mag} < 0$) are attracted towards the wire, however, instead of simply falling onto the wire the interaction between the field of the wire and the angular moment of the atoms result in the atoms moving in Kepler-like orbits around the wire [5]. In Schmiedmayer's experiment (the basic schematic is shown in figure 3.2a) a thermal beam of

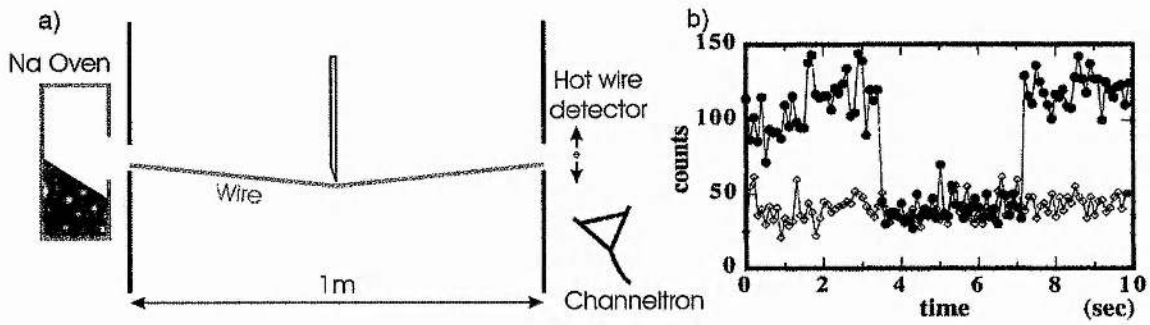

Figure 3.2: a) Diagram of wire guiding experiment. Sodium atoms are emitted from an oven (the beam is collimated using two apertures) and guided along the field minimum produced by a current of 2A in a 1m wire. A bend of up to 1mrad is incorporated in the guide to bypass an obstruction, and the guided atoms are detected at the end of the guide by a hot wire and channeltron. The results of guiding around a 0.5mrad bend are shown in b); measurements were taken every 100ms for current on (•) and off (◇). The current was turned off between 3.5s and 7.2s where both counts rates agree. Reproduced from [3]

sodium atoms is guided with an overlapping wire and finally detected using a hot wire and channeltron (the hot wire surface ionises the atoms and the ejected electron is detected by the channeltron). The wire is bent in the centre to bypass an obstruction used to block the straight through, unguided atoms. The results obtained (figure 3.2b, no current is applied between t=3.5s to 7.2s) demonstrates clear guiding and a fall to background levels when the guiding current is removed.

A further refinement of the Kepler guide is the side guide. Here atoms in low-field states are attracted to the side of the wire; this is usually achieved by using an external bias field [5] as in figure 3.1b, but it has also been achieved using extra wires along side the main guide [6]. The use of extra wires offers

more control over the atoms; the use of two wires with counter-propagating currents creates a main guide potential which permits guiding along both directions of the potential when used with a vertical bias field [7], i.e. the direction of the atoms can be reversed. For a single wire guide the atoms are only free to move in one unconfined direction along the potential perpendicular to the bias field, because the guide direction is dependant on the orientation of the wire in the bias field it can be difficult to maintain the potential around curves in the guide track.

Atom guiding can also be implemented close to a substrate surface upon which trapping/guiding tracks have been patterned using photolithography techniques. Work towards the miniaturisation of the magnetic structures in this way has been motivated by the idea of integrated optics and aided by the use of well-established lithographic methods to create the guides. This production method allows micron-sized wires to be used, which provide steeper potential gradients for confining the atoms, and the ability to manufacture a vast range of guide geometries. Use of substrate-grown, surface guides was demonstrated by Müller and co-workers in 1999 [8]. A cold atomic beam from an LVIS (low-velocity intense source) was overlapped with two parallel wires and guided 10 cm around an obstruction (see figure 3.3 for schematic) into a separate detection chamber where the flux is measured with a hotwire and channeltron. Direct loading of these microscopic guides from a MOT is hindered by the proximity of the substrate blocking the use of the standard six-beam configuration MOT. The above experiment used LVIS and loaded the guide from a MOT positioned several cm away from the

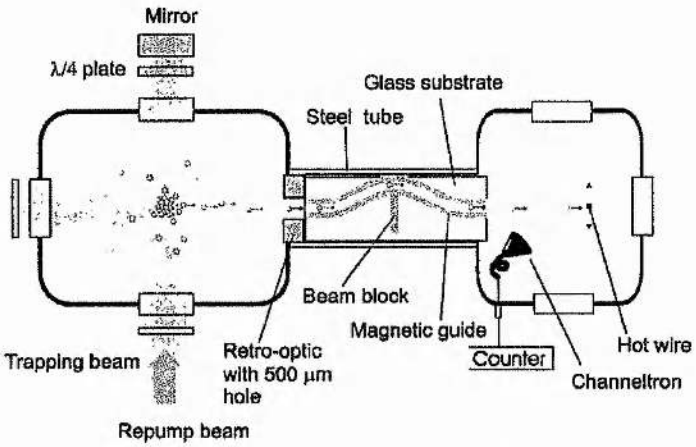

Figure 3.3: Magnetic guiding above a substrate. An LVIS in the left chamber provides a beam of cold atoms that is coupled into the magnetic guide. The guide is in a 2" diameter tube used to separate the source and detection chambers. Three 15cm radius curves in the guide escort the atoms around an obstruction, to stop unguided atoms travelling straight though the tube, where they are detected in the second chamber with a hot wire and channeltron. Reproduced from [8].

substrate. A second solution, which further aids miniaturisation, is the use of the mirror MOT [9]; the surface of the substrate is made reflective to allow two of the beams to be reflected from the surface and create a MOT using only four beams, in this way a cloud of atoms can be formed only 1mm away from the surface of the substrate and the magnetic guides.

The success of the side-guide and substrate grown guide tracks has allowed the creation of compact multi-component experiments for atoms optics. More recently experiments have produced a reduction in size of chip based, surface guides to scales of only a few μm (the fundamental limits of magnetic guiding along atom chips are discussed in [10]) and generated more complicated

guiding shapes such as coils [7] or multiple trap sites [11] which can be used as conveyor belts for precise movement of cold atoms.

Beam Splitter

Beam splitters are key elements in optics and an atomic beam splitter is vital to any interferometer. Previously atomic beam splitters had been limited to small splitting angles, interacting with periodic potentials, gratings and semi-transparent mirrors. Advances in magnetic guide manufacture have resulted in the generation of large angle splitters of compact size.

Cassettari *et al* in 2000 [12] designed and manufactured a Y configuration beam splitter (see figure 3.4). A cold atom cloud from a MOT is transferred to a magnetic trap close to the surface of an atom chip; a wire in the shape of a "Y" is used to guide the atoms. By varying the current in each arm of the wire they could control the probability of an atom emerging out the left of right arm, however due to the experimental setup at the splitting position there is an extra potential minimum backwards, between the magnetic potential split and the geometrical split of the wires, where losses occur as atoms following this extra port are directed towards the surface of the chip. The use of two-wire guiding would remove this extra port and also remove any bias in the guide direction as described earlier. In 2001 Müller and co-workers [13] demonstrated a beam splitter based on this idea. Atoms were split into each arm by alternating the guiding scheme from a centre guide (entering the

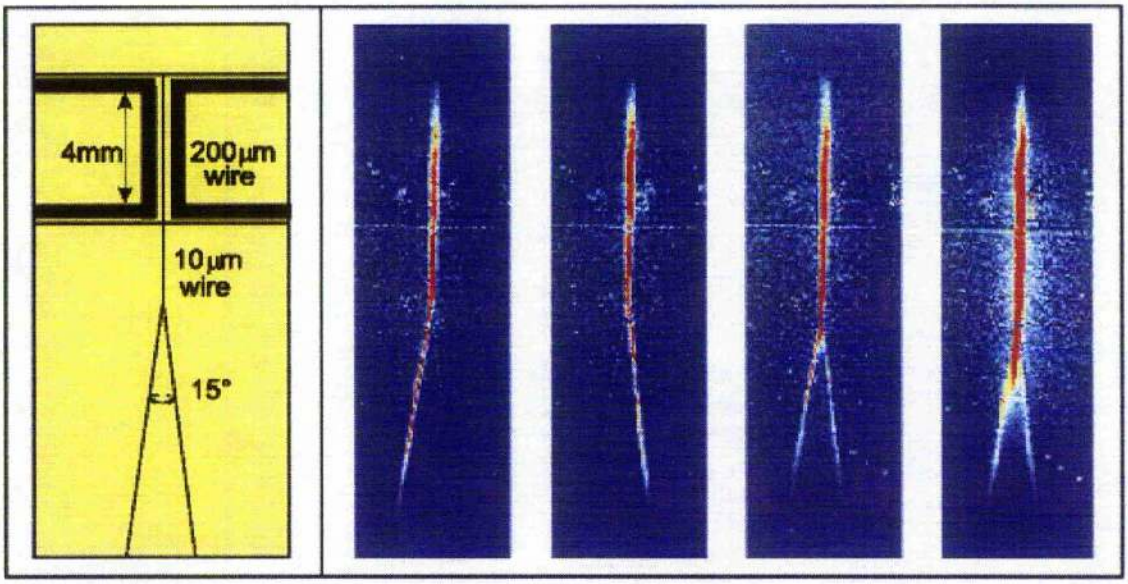

Figure 3.4: A magnetic beam splitter. The chip schematic is shown in (a), over 10^6 atoms are transferred into the 10μm wire guide, the fluorescence of the atoms in the guide at 16ms are shown in (b), the two left images show the results of only driving the current through one of the arms (acting as a beam deflector), the right two images show the effect of different bias fields (12G and 8G respectively) with equal splitting of the current into both arms. Note that the splitting does not take place above geometrical split of the wire. Reproduced from [12].

splitter) to a side guide configuration (during the splitting process) and then back to centre guides once the two paths were separated.

Building atom guides using current carrying wires and magnetic fields has been very successful, has been used to demonstrate many atom optic devices and has been shown to produce multi-element devices with prefabricated atom chips. However, using such fixed devices has certain

restrictions and complications in experimental realisation. First, with a prefabricated design inside a vacuum system, the MOT (or other source of cold atoms) must be positioned with great care with respect to the guide to maximise the coupling into the magnetic potentials, and once this is set up further modification can be very difficult. Second, the currents necessary for the guiding potentials are quite high and with the micro- and nano-chip guides the size of the wires are often unable to continuously pass the required currents and must be used in a pulsed operation. Third, since these guides are based on magnetic forces, just like with the magnetic traps described in the previous chapter, only atoms with certain m_F sub-levels (magnetic dipole moments) will be attracted to the low-field potentials, and unless a specific population pumping is applied the remaining cold atoms are lost. This results in only a small percentage (usually <25%) of the initial atom flux incident on the guide which can then be observed at the detection region. A final problem with the use of magnetic field wires is an observed fragmentation of a BEC placed within 200μm of the guide wires. Whilst the guide wires are manufactured to be very narrow, the electrons, as they flow though the wires, do not travel perfectly parallel to the direction of the wire (as illustrated in figure 3.5), this could be due to sub-micron imperfections in the manufacture of the wires. Any motion traverse to the wires produces corrugated variations to the magnetic field (in the order of a few hundred nK) which in turn causes the break up of a BEC held in this potential and fragments the atomic ensemble into separate parcels within the potential.

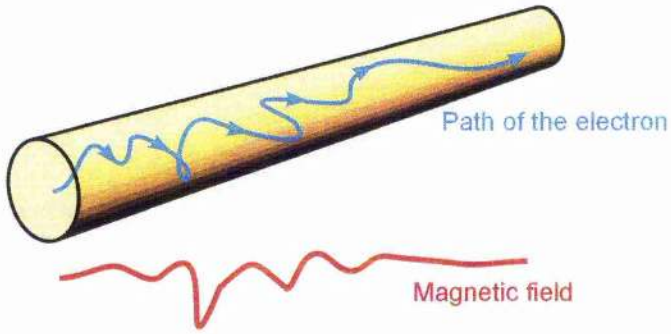

Figure 3.5: Current flowing along a wire. The deviations from a parallel path cause slight fluctuations in the magnetic field, in the order of 10^{-3} of the trapping potential, and results in the break-up of BEC.

Optical forces can be used to overcome some of these problems; the dipole force can be used to guide atoms irrespective of the spin state of the atom and use of light forces to guide the atoms should remove the problems arising from the minute variations in magnetic field wires. The use of light beams would ease modification to the experimental set up as potentials can be created outside of the MOT and then imaged inside the trap, unlike the permanent design of the magnetic guides. This type of access to the MOT will also remove the atoms from surface and any interactions that proximity may involve. The complicated pattern design possible with magnetic guiding is, however, difficult to replicate owing to the linear propagation of light. Coupling the guide light into a hollow fibre is one method for guiding around curves and offers a robust geometry (however this does fix the position and shape of the guide) another method is the use of holographic elements to sculpt the shape of the beam (this is the technique chosen for use in this thesis), both phase and amplitude information can be encoded onto a hologram allowing a vast range of beam shapes for guiding.

3.3 Optical Guiding

The optical dipole force was described in the previous chapter as a method for trapping atoms, this force can also be used to guide atoms regardless of spin states. From the Kramers-Kronig relation (the relationship between absorption and the refractive index is given in figure 2.1) the frequency of the light, compared with the absorption of the atomic transition, can result in the potential seen by the atom to be either attractive or repulsive from areas of high light intensity. This force can be exploited in either free-space laser beams or with light trapped in hollow waveguides and optical fibres.

3.3.1 Hollow Optical Fibre Guiding

By coupling light into a hollow-core fibre the light and, therefore, the dipole potential is confined to the hollow region of the fibre. However, atoms within the fibre will also be attracted to the surface by Van der Waals interactions, if we treat the waveguide as a slab this interaction is given by [14]:

$$U_{Vdw} = \frac{-1}{4\pi\varepsilon_0}\left(\frac{\varepsilon-1}{\varepsilon+1}\right)\frac{\langle g|d^2|g\rangle}{8k_B x^3} \qquad (3.2)$$

where ε is the dielectric constant, ε_0 is the absolute permittivity of free-space, $\langle g|d^2|g\rangle$ is the matrix element of the dipole operator and x is the distance to the wall. Therefore, to be able to guide atoms along the fibre the guiding

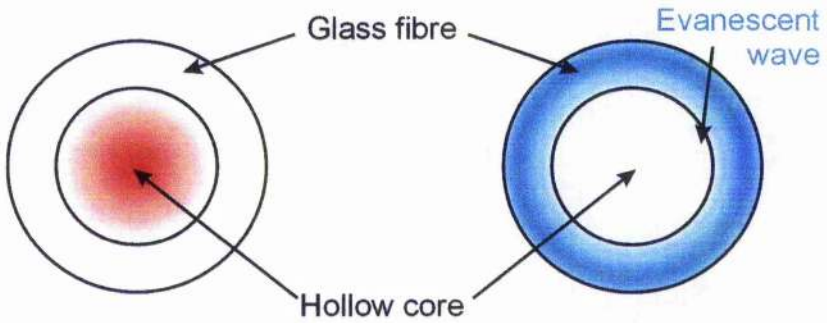

Figure 3.6: Guiding schemes for light within a hollow fibre. Red-detuned guiding is shown left; the atoms are attracted to the light at the centre of the fibre, and blue-detuned guiding; where the evanescent field keeps the atoms away from the wall of the fibre.

potential must overcome this attraction to the walls of the fibre. For a two-level atom the potential from the dipole force is given by [15]:

$$U(r) = \frac{h\Delta}{2} \ln\left(1 + \frac{I(r)/I_{sat}}{1 + 4\Delta^2/\Gamma^2}\right) \qquad (3.3)$$

where Δ ($=\omega_l - \omega_0$) is the detuning of the laser frequency, ω_l, from the atomic transition, ω_0. I_{sat} is the atomic saturation intensity and Γ is the natural linewidth of the transition.

Since the dipole force can be either attractive or repulsive we have two schemes for optical guiding along a fibre (figure 3.6). For red-detuned guiding the atoms are attracted to high intensity regions so light propagating along the centre of the fibre will "pull" the atoms away from the walls. This scheme was first proposed in 1993 by Ol'Shanii and co-workers [16]. The equivalent scheme for a blue-detuned guide was proposed the next year by Marksteiner *et al* [17]; here blue-detuned light is coupled into the glass fibre around the

hollow core, evanescent leaking through the fibre walls providing the potential to counteract the attractive Van der Waals forces.

The use of fibres offers several advantages over other methods of guiding atoms. Since the atoms are contained within a fibre they can be transported between two vacuum systems, also as the fibres are glass then optical probes of the atoms can be made through the fibre wall whilst it is outside of the vacuum system. This allows optics to be placed closer to the atoms and avoids performing beam alignment within the vacuum chambers. Fibres can be bent and light will still propagate along the centre guiding the atoms, bending fibres can even be used as a velocity selective element as the faster atoms are the ones that will escape the guiding forces when travelling around bends and hit the fibre walls, increasing the curvature of the fibre would select decreasing velocities.

The first capillary guiding experiments were performed by Renn and co-workers in 1995 [18]. A short capillary fibre length of 3.1cm was used to separate two chambers as shown in figure 3.7. The modes of the laser supported at the grazing angle used decayed exponentially through the fibre and limited the guide distance to only a few cm for the experiment. The decay constant is proportional to a^3/λ^2, where a is the radius of the hollow and λ is the wavelength of the light. Rubidium entered the fibre from a hot background vapour in the first cell and was detected upon exiting the fibre in the second cell by a hot wire and channeltron. The effect of guide detuning was investigated, the laser was tuned from 1 to 30GHz red of the atomic transition and a maximum flux was measured at 3GHz. Although these results showed

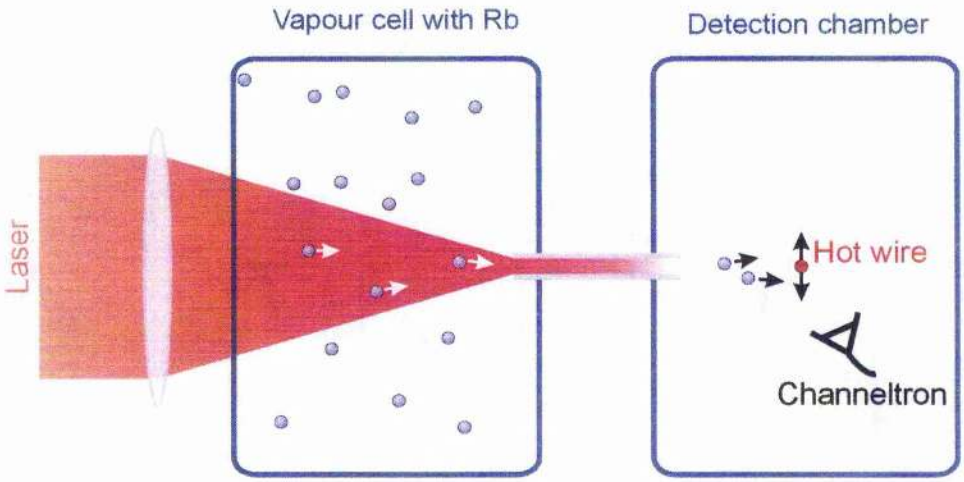

Figure 3.7: Red-detuned guiding in a hollow-core fibre. Light from a 45mW Ti-Sapphire laser is coupled into the 144μm diameter hollow core of the fibre; a 3.1cm length of fibre separates the two vacuum chambers. Rubidium atoms with low transverse velocities are extracted from background vapour in the first cell and guided along the fibre into the detection cell. Reproduced from [18].

similar profiles for the different laser intensities further work [19] reported that at higher intensities a "hole" is burnt into the flux spectrum, figure 3.8. This is due to a combination of the AC Stark effect distorting the energy levels of the atom and spontaneous scattering (which occurs predominantly at low detunings); the Stark effect causes a variation in the energy levels across the guide beam, as shown in figure 3.9. An atom in the ground state will simply oscillate within a potential bowl in the same way as an atom in an optical dipole trap, occasionally absorption will take an atom into the excited state, from here spontaneous emission returns the atom to the ground state, however, due to the curvature of the energy levels the atom can "roll" down the surface before emission thus gaining kinetic energy.

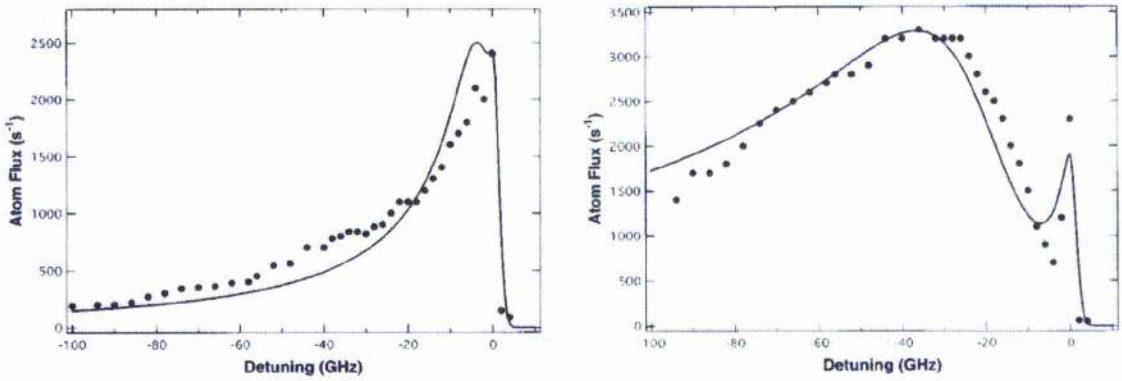

Figure 3.8: Guiding flux versus guide detuning from resonance for different intensities. The graph on the left shows the results for an intensity of 7 MW/cm^2, and 50 MW/cm^2 for the right hand graph. As the intensity is increased a substantial flux is seen at significantly higher detunings. The spike observed near to resonance is due to the rapid turn off of the scattering force relative to the dipole force. The solid lines are theoretical fits. Reproduced from [19].

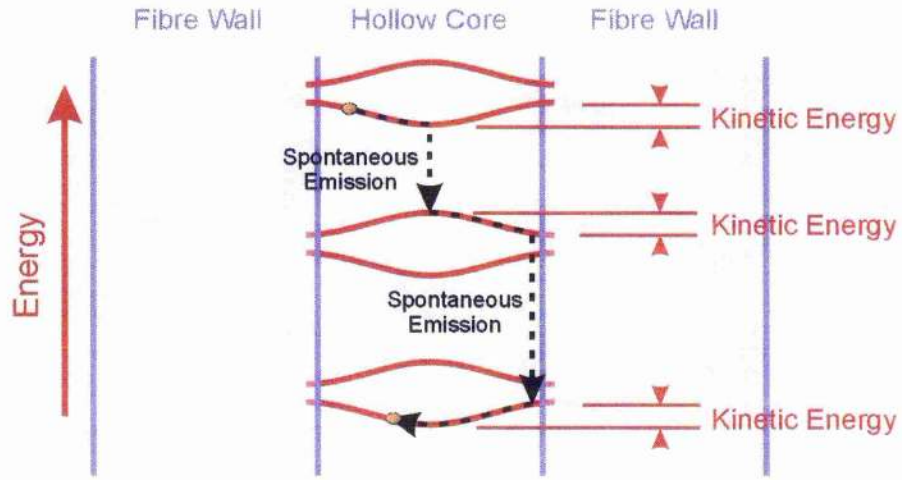

Figure 3.9: Heating processes in a fibre guide. The spatial variation of the energy levels allows the atoms to roll down an energy level gaining kinetic energy before a spontaneous emission event. Reproduced from [19].

Guiding atoms using red-detuned light in this way does pose several problems, the severe limiting of propagation distance due to exponential decay into the fibre and the excess heating of the atoms within an intense laser beam. The use of blue-detuned guiding offers a solution to these problems.

Blue-detuned guides exploit evanescent fields, noted by Ito *et al* in 1995 [15] whilst investigating coupling light into hollow core optical fibre. In contrast to the capillary fibre used by Renn for the early red-detuned guides, these investigations used actual optical fibre complete with cladding. By modelling the supported propagating modes in the fibre it was determined that there was, like any waveguide, an exponentially decreasing field that leaked into the cladding and core regions – evanescent waves. These fields only propagated a few hundred μm out into the core, however, as the Van der Waals force is very short ranged (it is inversely proportional to the seventh power of the separation between atoms) it was experimentally possible to obtain evanescent fields large enough to overcome the attraction to the walls of the fibre. The use of evanescent fields to guide atoms was experimentally reported a year later by Renn *et al* [14]. In an experimental setup similar to the red-detuned guides, blue-detuned evanescent fields were used to guide thermal rubidium along a 6cm length of fibre (beyond the distance possible with the early capillary guides). Difficulty in coupling the blue-detuned light into the fibre resulted in a lot of scattered light into the core at the end of the fibre, which would repel atoms from entering the guide in the first place. To counteract this an extra, red-detuned escort laser was focused into the hollow

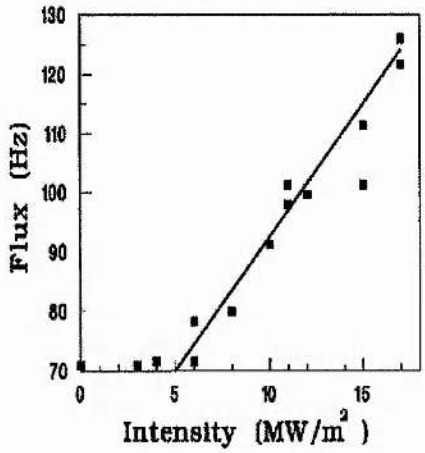

Figure 3.10: Intensity dependence of evanescent wave guiding. The threshold for overcoming the Van der Waals attraction is clearly seen at ~5 MW/m^2, after this threshold the atomic flux increased linearly with intensity. Reproduced from [14].

core of the fibre. Since both the scattering and escort potentials are in the core of the fibre they quickly decay and once the atom is through the entrance region of the fibre (a few cm) the evanescent potential dominates and guides the atoms along the remainder of the fibre length. Optimising of the detuning of each beam resulted in an increase of atomic flux of a factor of 4; however, the effect for guiding efficiencies is markedly different to those of red-detuned guiding schemes. Red-detuned guiding relies in confining atoms to the centre of the fibre so that it has only very weak interactions with the walls. Blue-detuned guides are required to actually overcome the Van der Waals attractions, this results in a clear threshold for guiding where the evanescent field potential overcomes the Van de Waals forces, figure3.10.

Both the above experiments have used thermal atoms, in order to display the wave-like nature of the atomic beams it is necessary for the atoms to be cooled. Müller and co-workers (2000) [20] made the first step by guiding laser cooled atoms from a MOT. Again the experimental setup is similar to before with two vacuum systems connected by a length of optical fibre. Atoms are trapped in a MOT and loaded into the fibre using an LVIS beam with the guiding forces generated using blue-detuned light and the detection equipment contained in the second vacuum chamber. The internal state of the atoms is detected in the second chamber, 90% of the LVIS atoms are in the lower hyperfine state (the un-cooled state), a probe beam tuned to the cooling cycle is introduced perpendicular to the atomic beam at the end of the fibre. Atoms in the cooling state absorb photons and are deflected and, therefore, not detected. At low guide beam detunings there are enough spontaneous emission-absorption events to pump the atoms back into the cooled state where spontaneous heating reduces the overall flux guided. Increasing the detuning increases the number of atoms remaining in the lower hyperfine level and lengthens the guiding time.

The advent of photonic crystal fibre (PCF) offers promising possibilities for fibre guiding. Hollow-core PCF allows light to be guided without any leaking by using a band gap structure, this enables red-detuned guiding over much longer lengths to be realised with a constant guiding potential along the centre of a very narrow core. Using this band gap structure it would also be possible to excite higher order laser modes within the hollow region and permit the

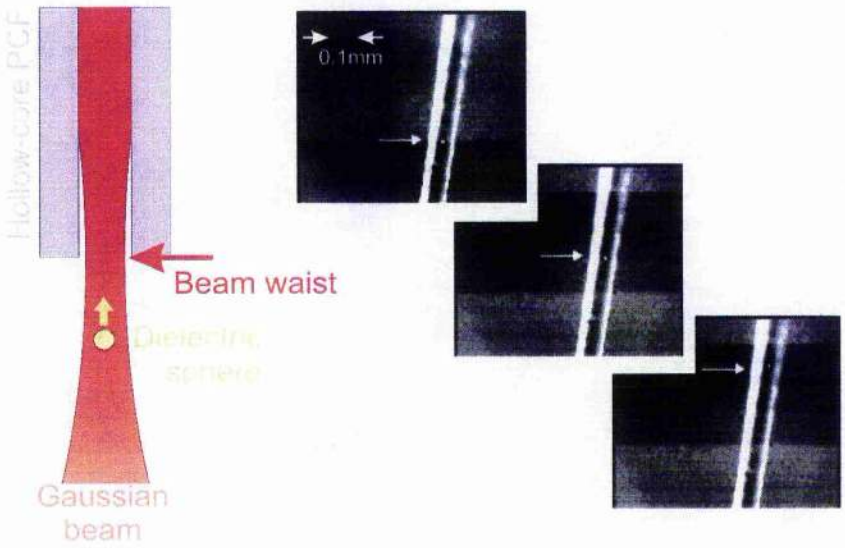

Figure 3.11: Guiding of particles in photonic crystal fibre. The schematic of the particle levitation is shown left; 5μm polystyrene particles are levitated into the 20μm diameter core of the PCF. The images on the right show the particle, indicated by the arrow, as it propagates along the fibre. The separation of the adjacent frames is 67ms. Reproduced from [21].

propagation of doughnut shaped beams along the core allowing stronger blue-detuned guiding as the optical potentials are maintained further from the fibre walls and are more intense as they use all the power of the laser, not just the small evanescent leaking. A proof of principle experiment has been performed along these lines by Benabid and co-workers in 2002 [21]. Small, 5μm diameter, particles were levitated into a hollow-core PCF (see figure 3.11) and then guided along the fibre using an argon ion laser as a guide beam. Although no results have been obtained at time of writing there is ongoing work at St Andrews to guide cooled rubidium atoms along these fibres.

The use of hollow fibres for guiding atoms provides a robust experimental setup; the fibres allow precision alignment of the atomic beam and permit bending of the atomic beam which would allow the generation of interferometers. The use of hollow fibres exhibits a number of drawbacks; the rapid intensity decay along the fibre length may be removed by the use of PCF, however, whilst PCF fibres do allow guiding along significantly longer distances than capillary guides it is still an emerging technology and has not yet realised its potential as a near lossless guide. Beam splitting and combining also cannot be achieved within the fibres, this would have to be performed outside the fibres and the atoms then coupled back into the fibres adding another layer of complexity to an experimental arrangement. Finally the use of fibres has the same drawback of magnetic guides, once the experiment has been built it is fixed, the source of atoms has to be positioned with great care to optimise coupling (this can be complicated further by the need to couple light into a fibre held within a vacuum system) and further modification within the vacuum system is nearly impossible.

3.3.2 Free Space Optical Guides

When using optical fibres to guide atoms the fibre itself does not contribute to the guiding forces, it is simply a means to confine the laser light. By choosing suitable beams and geometries of laser light we can remove the need for fibres in the trap. This offers advantages due to the simplicity of focusing a laser into a vacuum to generate the potential in contrast to the manufacture

and physical alignment of fibres and magnetic guides and therefore implies an ease of modification that is not possible with the "fixed" guides using magnetic field wires and hollow optic fibre. The lack of a fibre also removes the guide from surfaces and associated Van der Waals attraction, however the action of bending atomic beams using a light guide becomes a lot more problematic.

Red-detuned Guiding

Bjorkholm *et al* [22] experimentally demonstrated one of the earliest uses of a free space light guide in 1978. A laser tuned close to one of the transitions of sodium was shown to be able to focus, defocus and steer a thermal beam of sodium atoms. The atom beam was overlapped with a guide through a hole in a mirror. The atomic flux was detected downstream of this by use of a hot wire detector scanned across the beam as shown in figure 3.12. By tuning the guide above and below resonance the effects of the dipole force are clearly seen (figure 3.13). Detuning the laser to the red attracted the atoms to the intense region of the guide and resulted in a sharp increase in the atomic beam intensity in the centre of the guide, blue–detuning, by contrast repels the atoms and a clear drop in intensity was observed. In this type of scheme, where only small detunings are used, there is a significant heating of the atomic beam from absorption of the near resonant light. One method to overcome this is to use a far from resonance red-detuned guide as the dipole potential is proportional to $1/\Delta$ (Δ is the detuning) and the scattering (which causes heating) is proportional to $1/\Delta^2$ (see section 2.4.3 on optical dipole

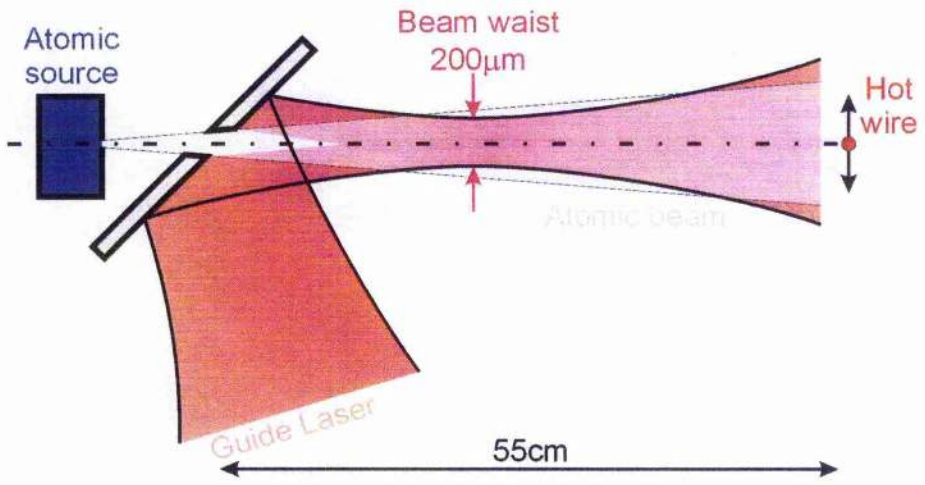

Figure 3.12: Focusing an atomic beam using red-detuned light. A 50mW focused laser beam is co-propagated with a thermal beam of sodium atoms. Note the difference in scale between the horizontal and vertical axes. Reproduced from [22]

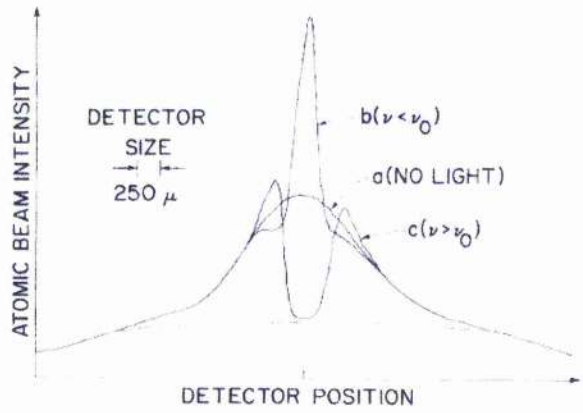

Figure 3.13: Atomic flux at the detector for the experiment in figure 3.12 at detunings above and below resonance. Atoms are clearly attracted towards the red-detuned beam and repelled from the blue detuned beam. The dashed line shows the approximate background intensity. Reproduced from [22].

traps for further explanation). This has been demonstrated by Szymaniec *et al* [23] and by Pruvost and co-workers [24]. Both groups used greater than 10W of power from a Nd:YAG laser with a wavelength of 1064nm (more than 1.5×10^7 Γ from the atomic transition) for the guide beam to make the heating from scattering negligible. Szymaniec used an atomic fountain as the source of atoms. The atoms are projected vertically upwards though an aperture, an increase in flux of 60 times was observed above the aperture when a 12W guide beam was present. The shape of the cloud was observed to closely follow that of the guide beam. The Pruvost experiment dropped rubidium atoms from a MOT into a 15W vertical guide, the guide realised was also shown to offer simple manipulation of the temperature of the atoms and cloud size. When the guide is focused the atomic cloud is compressed as it falls along the guide. This results in a flux increase of three, but the transverse velocity and temperature of the ensemble increase by more than a factor of ten. Similarly if the guide beam is divergent a cooling of the atoms is observed, but this is in parallel to a reduction in atomic density.

More recently Wolschrijn *et al* [25] have demonstrated a red-detuned guide for rubidium using only 85mW after assessing that a detuning of ~70GHz resulted in an acceptable optical scattering rate. Under these conditions 40% of the original cloud can be guided; at still lower detunings the fraction seen to be guided is larger but at this stage the radiation pressure starts to play a significant role, accelerating the atoms to the detection region so more can be detected before they have had time to escape the guide beam.

Blue-detuned Guiding

Increasing the detuning of the guide is one solution to reducing the interactions found within a red-detuned guide beam; however, this then requires the use of high powers to maintain an adequate dipole potential. The use of a blue-detuned beam has certain advantages over the use of red-detuned guides. Atoms are repelled from regions of high light intensity; this reduces the interaction between the atoms and the guide since the atoms are confined in dark hole within a ring of light. This allows lower detunings to be used (as there will be fewer heating events) and therefore guide powers required to generate the dipole potentials can be reduced. Hollow beams can be generated in a variety of different ways. One of the earliest proposed was by Balykin in 1987 [26] in which the use of a focused Laguerre-Gaussian (LG) beam (Laguerre-Gaussian beams are described in Chapter 5) as a means of focusing an atomic beam was considered. Increasing the order (the number of phase changes around the beam) of these LG beams reduces the thickness of the ring of light creating a more intense light field for guiding the atoms leading to guides with higher potentials and tighter focusing properties [27].

A guide based on a hologram generated LG beam was demonstrated by Schiffer *et al* [28] to guide a beam of cold neon atoms, the atoms were laser decelerated to speeds of 28 ± 4m/s. The beam of atoms was then directed through a hole in a mirror, in a similar way to that of Bjorkholm's [21] red-detuned guide, and the doughnut shaped LG beam was reflected to co-

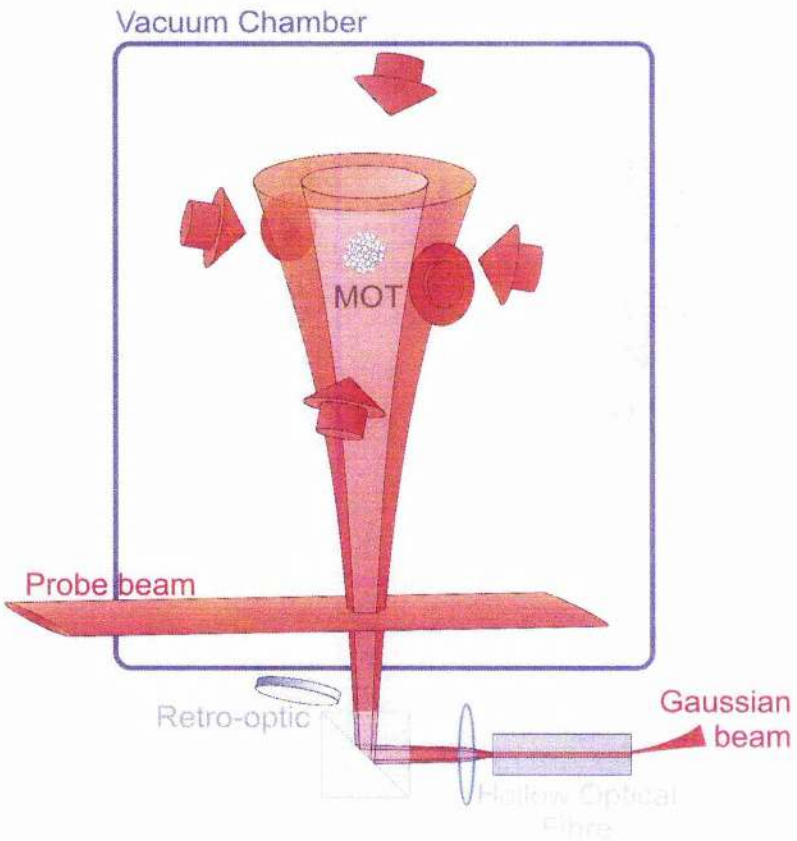

Figure 3.14: Guiding a dropped MOT in a blue-detuned hollow beam. A hollow, LP_{01}, beam is generated from the collimated output of a mm-sized hollow optical fibre. A hyperfine laser, not shown is propagated along the guide through the beam splitting cube. The probe beam induces fluorescence in the atoms which allows the guided flux to be measured. Reproduced from [29]

propagate with the Ne* beam. Due to focusing of the guide beam the transverse velocity of the atoms had to be reduced and a 2-dimensional optical molasses was used around this focus to contain the atoms within the guide. Guiding of cold atoms was achieved shortly after this by Yin and co-workers [29], a cloud of rubidium atoms from a MOT was dropped into a vertical hollow, guide beam (figure 3.14). The hollow beam was generated using the output of a hollow optical fibre and was projected upwards to

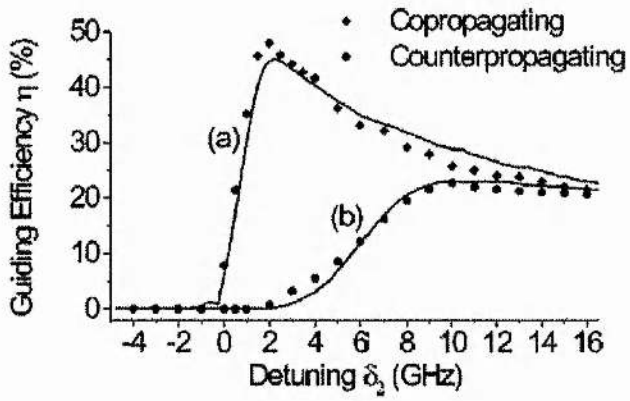

Figure 3.15: The guiding efficiency as a function of the detuning δ_2 in the co-propagating (a) as well as the counter-propagating (b) scheme. The solid curves represent the numerical simulation results. Reproduced from [30]

counter-propagate with the falling atoms. A further study using this type of experimental setup compared the guide efficiencies for co- and counter-propagating guide beams [30] (see figure 3.15) and achieved guiding efficiencies of 50%, noting that 80% should be possible with improved hollow beam modes. These schemes all act to focus the dropped atoms, extended guiding and collimation has also been proposed. Yin and Zhu, in 1998, [31] designed a horizontal, collimated guide based on a doughnut mode generated by a hollow optical fibre. Because of the horizontal geometry the atoms required an initial push to start them along the guide; this is achieved using a force imbalance in the cooling beams as in an LVIS.

Beam Splitters

A linear waveguide for atoms is all well and good, but for full exploitation of atomic beams we need a way to separate and combine beams, in this way we can generate interferometers. The first all optical beam splitter was realised by Houde and co-workers [32] using two crossed far from resonance dipole guides to guide rubidium. A vertical beam was used to guide a dropped cloud of atoms from a MOT, with a second beam crossing the first at a slight angle a few mm below the trap. As the atoms fall down the vertical guide they oscillate within the potential from side to side, the crossover region of the two beams must be long enough to allow this oscillation to occur once and permit the atoms to "jump" potentials. The oblique guide is left off initially so that no atoms from the MOT can be caught, it is then turned on when the atoms reach the cross over region of the guides, the sudden potential change from turning the oblique guide on results in a slight momentum kick to the atoms and assists in transferring the atoms across the guides. Transfer of up to 40% was achieved and the separation of the two atom beams was complete after only 10mm.

A more complicated crossed beam pattern was demonstrated by Dumke *et al* [33], with an array of crossed dipole guides producing many possible splitting sites. An array of 2-dimensional guides was generated by illuminating cylindrical micro-lenses positioned outside the vacuum and then focusing resulting beams inside the trap. The guides in this case are perpendicular to the propagation of the laser beam, unlike the previous examples where the

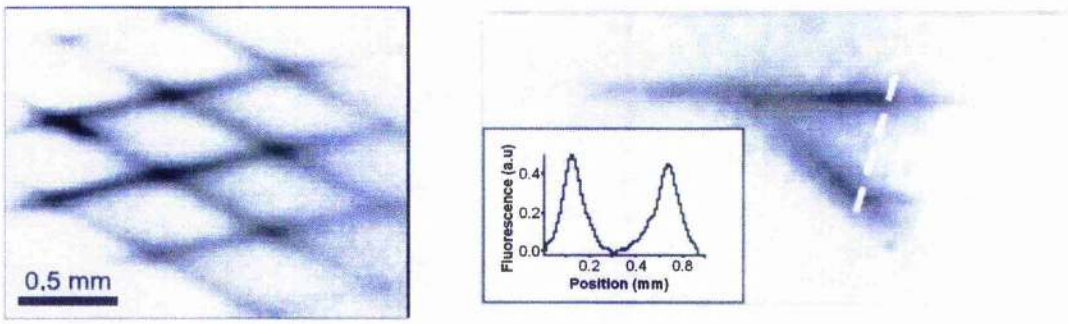

Figure 3.16: Multiple path interferometer structure. The left image shows the fluorescence of Rb atoms in the crossed beam pattern. The profile of the splitting of the atoms is shown on the right, the line profile is the atom distribution taken across the dotted line. Reproduced from [33].

atoms were guided along the beam; the atoms are trapped in the propagation-direction by using very tightly focused light. Two arrays of guides were then crossed to create multiple interferometer patterns with arbitrary splitting angle (figure 3.16). By controlling the intensities of the cross pattern both Mach-Zehnder and Michelson type interferometers were created; Mach-Zehnder interferometers are made by simply propagating the atoms across the pattern. Generating the Michelson type involves centring a Gaussian intensity profile at one of the intersections; atoms can fall into the intersection and split as they escape out the other side but the higher dipole potential in the centre attracts the atoms back, as they reach the intersection again they are split again with part of the cloud now moving along the output port. High loading efficiencies were achieved in this set up as the initial dipole trap was formed by illuminating only a small part of the micro-lens arrangement, thus loading into the guide has no significant loss of atoms or increase in temperature. The total area of each of these interferometer paths is below $1mm^2$.

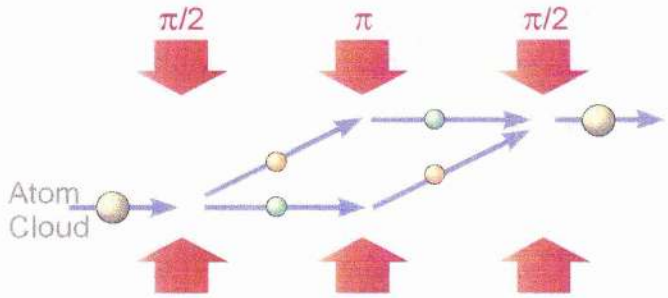

Figure 3.17: Atom interferometry using stimulated Raman transitions. As the atomic cloud propagates a $\pi/2$ pulse pumps the atom into a superposition of two ground states, one ground state undergoes a recoil separating the cloud. The π pulse changes the ground states, with the separate packets recoiling in opposite directions, the final $\pi/2$ pulse combines the atoms. Based on [34].

Interferometers have also been demonstrated without the longitudinal guiding of the beam. Raman pulses [34] from two counter-propagating laser beams have been used to split an atomic packet by exciting some of the atoms into a different ground state, thus imparting a recoil velocity on these atoms. By using a $\pi/2$-π-$\pi/2$ sequence of pulses the atomic ensemble can be split and recombined to form an interferometer as shown in figure 3.17. Because of the lack of confinement of the atomic ensemble as it propagates the cloud will continue to expand thus limiting the area this type of interferometer can achieve. More recently Shin *et al* [35] have demonstrated interferometry with BEC. Here the atoms are held in an optical dipole trap which is deformed and separated, using an AOM, by up to 13μm before being recombined where fringes could be observed.

A blue-detuned beam splitter was reported in 2000 by Yan and co-workers [36]. A hollow guide beam was generated using a pair of axicons, this was

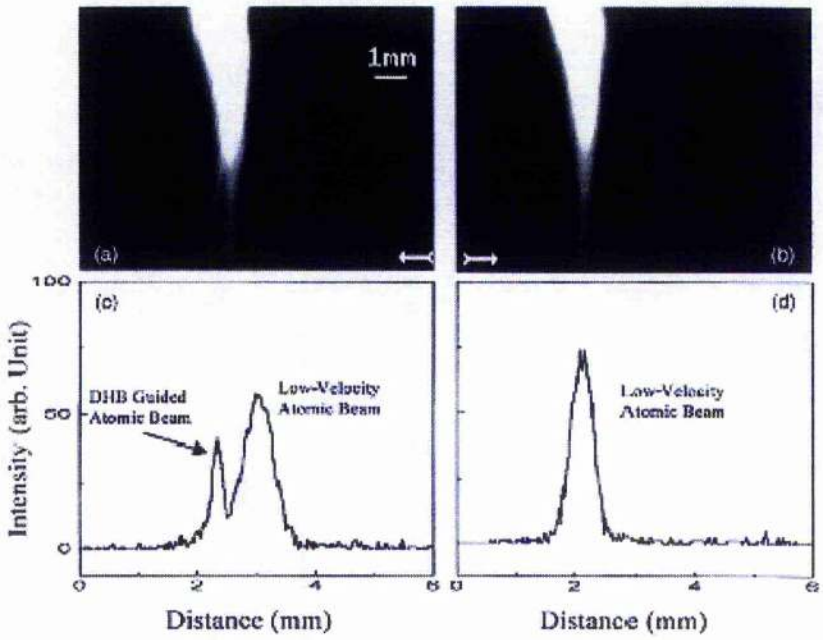

Figure 3.18: Splitting LVIS with a blue-detuned hollow beam. (a) and (b) show CCD images of LVIS with the guide beam present and absent respectively. Profiles taken across the images at the point indicated are given in (c) and (d). Reproduced from [36]

then overlapped with an LVIS, generated in a standard MOT, propagating in the downwards direction. The coupling into the guide was found to be best with the dark centre of the beam approximately equal to the diameter of LVIS (~1mm). Figure 3.18 shows the splitting of LVIS using a counter-propagating guide angled at 8°. The maximum transfer of atoms into the guide was ~50% of the total atomic flux.

At St Andrews we have performed a similar experiment in splitting an LVIS beam. A Laguerre-Gaussian beam was used for the guide and was co-propagated with a horizontal LVIS, however, our experiments show marked differences to the resultant guiding of cold atoms. A full description of our

experiment along with the results seen and a physical model to explain these findings are given in chapter 6.

Near-surface Guides

While one of the advantages of light beams for generating potentials is the ability to remove the atoms from any surface interactions, it can sometimes be desirable to manipulate the atoms near a surface, perhaps for integration into an array of experiments. Working close to a surface can also allow light beams to be focused more tightly leading to increased intensity and higher dipole potentials. Birkl *et al* [37] have proposed the possibility of micro-fabricating lenses as wave guides (the first examples demonstrated being the interferometer pattern described earlier [33], however, this pattern was imaged inside a vacuum, not positioned so the atoms are guided over the structure), in this way complicated wave guides can be built up in a similar way to the magnetic chip guides. An example of a micro-lens beam splitter is shown in figure 3.19.

Barnett *et al* [38] in 2000 proposed the use of evanescent fields above a linear wave guide to guide cold atoms, in a similar way to magnetic chip guides. The differing decay rates of TE and TM modes allows the combination of red- and blue-detuned light in this scheme (figure 3.20, left). The blue-detuned field is used to counteract Van der Waals forces and keep the atoms above the surface and a red-detuned field, in the slower decaying TM mode, is used to guide the atoms along the waveguide. A red-detuned wave guide with

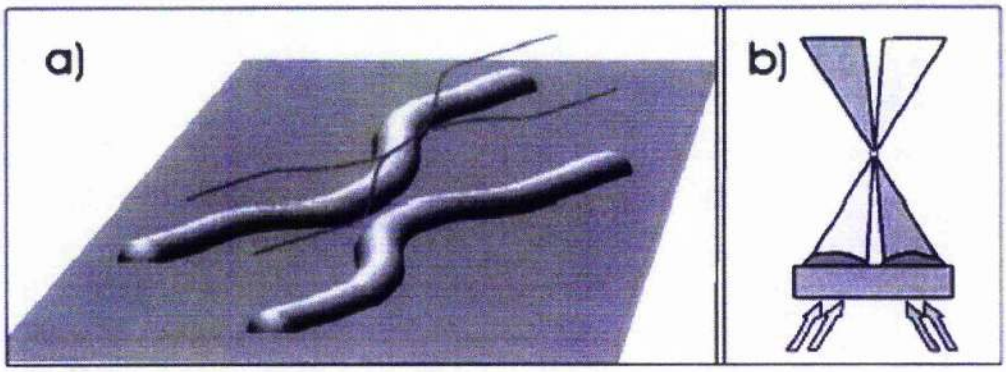

Figure 3.19: Micro-lens waveguides for creating an atomic beam splitter (a). The arrays are illuminated at an angle in order to make the foci overlap (b). Reproduced from [37]

integral detection was demonstrated in 2003 by Schneble and co-workers [39] (figure 3.20, right). The atom source is a magneto-optical surface trap (MOST), a combination of a MOT and an evanescent wave mirror (EWM) which is continuously loaded from a cold atomic beam. A series of planar waveguides are generated above the surface by reflecting a laser beam of the top surface of the EWM, and producing interference fringes. The laser is red-detuned so the atoms are confined to the high intensity regions of the standing wave. Atoms are coupled into the guide using a further evanescent wave (OPW) to pump the atoms in the MOST into an untrapped state and the atoms are then preferentially transferred to the surface waveguides. The atoms can then be detected using an integral detector on the surface or by simply turning off the waveguides and letting the atoms fall onto the surface and recording the distribution of injected electrons. By blocking portions of the waveguide it is even possible to control the flow of the atoms along the surface.

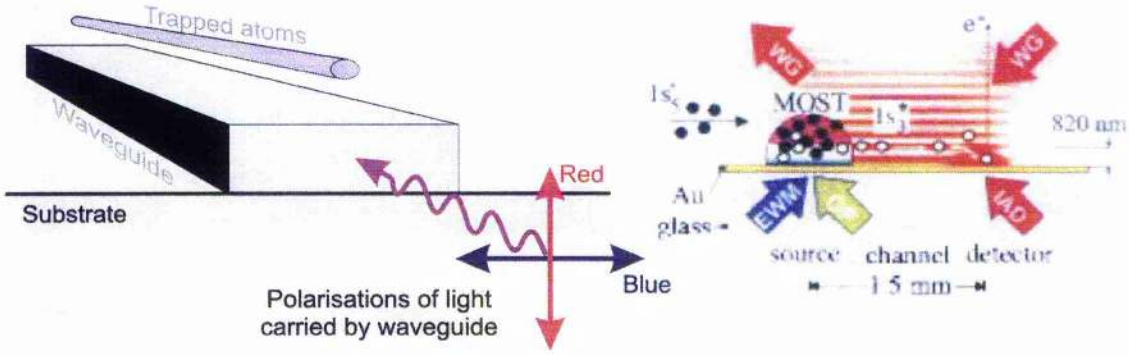

Figure 3.20: Near surface wave guides. The differing decay rates of TE and TM evanescent fields means a blue-detuned field can be used to counteract Van der Waals forces, the red-detuned light extends further from the surface and attracts the atoms towards the surface trapping them where the attractive and repulsive forces balance, left. Reproduced from [38]. The right hand image shows the use of a standing wave to guide the atoms. Atoms in a magneto-optical surface trap are transferred into the guide by pumping the atoms into an untrapped MOST state and allowing the atoms to "fall" into the dipole guide. Atoms were detected downstream by releasing the atoms and detecting the locally injected electrons on the surface. Reproduced from [39].

3.4 Motivations for Thesis

These last sections highlight the basic methodology for the different optical guiding regimes. Red-detuned guides can be generated using the output direct from a laser, this type of guide has been demonstrated to enhance the flux of atoms from a free-falling MOT [24] and an LVIS beam [40], however, with the exception of the Wolschrijn experiment [25] (which only succeeds in guiding over a few mm before the heating effects overwhelm the dipole

potential) these guides all require a large detuning and high beam intensities to guide without significant losses of flux due to heating effects. Our preferred method for atom guiding is to use lower powered beams, which leads to the use of hollow beams to confine the atoms.

The experiments performed previously have generated hollow beams using several techniques; the use of Laguerre-Gaussian modes as a guide beam has been exploited for guiding atoms from a MOT [28] and as a guide for BEC [41]. The LG beams are free space beams; the profile of the guide expands due to diffraction but otherwise retains its profile allowing extended guiding regimes. However, the dipole potential of low azimuthal index LG beams is relatively shallow and allows significant penetration into the walls as reported by Xu [30]. The time spent within the walls increases the probability of heating of the ensemble and a loss of guiding efficiency. In order to reduce this effect one needs to increase the intensity in the guide walls and reduce the thickness of the ring. One method to achieve this was demonstrated by Song *et al* [42]; their guide beam uses an array of axicons (conical lenses) to generate a tube of light with very narrow, intense walls. Even with this narrow-ringed guide the position and velocity of the falling cloud was still significantly affected by the guide in a similar manner to the results reported by Xu [30], even though the atoms only interacted with the beam for short periods. However, this method of creating a doughnut mode does not result in a free space mode that will propagate indefinitely nor will the dark centre be preserved if it is focused through an ordinary lens.

In this thesis we have explored the use of high order LG beams to guide both atoms from a free-falling cloud from a standard MOT and a continuous atomic beam from LVIS. Splitting of an atomic beam from LVIS has also been investigated where we find the nature of the hollow guide imposes significant coupling problems. The use of higher azimuthal index guides, previously neglected in the literature, produces narrower ring sizes that retain their shape as they propagates though free space unlike the fibre [29] and axicon [42] generated guide beams. This should reduce the interaction with the guide beam from previous LG experiments and result in an increase in the guiding efficiency. The use of Bessel beams has also been investigated as a potential guide beam. These "non-diffracting" beams create a light tube of constant size along their entire propagation length unlike the other guide beam described in this chapter which do suffer from divergence along the propagation distance of the guide. The Bessel beam is not a true free space mode and the non-diffracting nature is only valid in the near field, however, it is still possible to create a beam with an effective propagation distance of a few meters, with the appropriate dimensions for guiding a beam of atoms, over which the dipole potential will remain constant.

Holographic techniques have been used primarily for the production of our guide beams. The use of spatial light modulators (SLM), in particular, to generate the holograms aids rapid modification to the guide parameters. These holographic methods have also been used to create beam splitter, and interferometer patterns similar to those proposed in [37] but without the need for manufacturing micro-lenses.

Bibliography

[1] D. E. Miller, J. R. Anglin, J. R. Abo-Shaeer, K, Xu, J. K. Chin and W. Ketterle, "*High-Contrast Interference in a Thermal Cloud of Atoms*," cond-mat/0412672 (Pre-print)

[2] E. Anderson, T. Calarco, R. Folman, M. Andersson, B. Hessmo and J. Schmiedmayer, "*Multimode Interferometer for Guided Matter Waves*," Phys. Rev. Lett. **88** 100401 (2002)

[3] J. Schmiedmayer, "*Guiding and trapping a neutral atom on a wire*," Phys. Rev. Lett. **52** R13 (1995)

[4] J. Schmiedmayer, "*A wire trap for neutral atoms*," Appl. Phys. B. **60** 169 (1995)

[5] J. Denschlag, D. Cassettari and J. Schmiedmayer, "*Guiding Neutral Atoms with a Wire*," Phys. Rev. Lett. **82** 2014 (1999)

[6] N. H. Dekker, C. S. Laa, V. Lorent, J. H Thywissen, S. P. Smith, M. Drndić, R. M. Westervelt and M. Prentiss, "*Guiding Neutral Atoms on a Chip*," Phys. Rev. Lett. **84** 1124 (2000)

[7] X. Luo, P. Krüger, K. Brugger, S. Wildermuth, H. Gimpel, M. W. Klein, S. Groth, R. Folman, I. Bar-Joseph and J. Schmiedmayer, "*An atom fibre for guiding cold neutral atoms*," e-print Quant-Ph/0311174 (2003)

[8] D. Müller, D. Z. Anderson, R. J. Grow, P. D. D. Schwindt and E. Cornell, "*Guiding Neutral Atoms Around Curves with Lithographically Patterned Current Carrying Wires*," Phys. Rev. Lett. **83** 5194 (1999)

[9] J. Reichel, W. Hänsel and T. W. Hänsch, "*Atomic Micromanipulation with Magnetic Surface Traps*," Phys. Rev. Lett. **83** 3398

[10] C. Henkel, P. Krüger, R. Folman, and J. Schmiedmayer, "*Fundamental limits for coherent manipulation in atoms chips*," App. Phys. B. **76** 173 (2003)

[11] W. Hänsel, J. Reichel, P. Hommelhoff and T. W. Hänsch, "*Magnetic Conveyor Belt for Transporting and Merging Trapped Atom Clouds*," Phys. Rev. Lett. **86** 608 (2001)

[12] D. Cassettari, B. Hessmo, R. Folmn, T. Maier and J. Schmiedmayer, "*Beam Splitter for Guided Atoms*," Phys. Rev. Lett. **85** 5483 (2000)

[13] D. Müller, E. A. Cornell, M. Prevedelli, P. D. D. Schwindt, Y. Wang and D. Z. Anderson, "*Magnetic switch for integrated atom optics*," Phys. Rev. A. **63** 041602(R) (2001)

[14] M. J. Renn, E. A. Doneley, E. A. Conell, C. E. Wieman and D. Z. Anderson, "*Evanescent-wave guiding of atoms in hollow core optical fibre*," Phys. Rev. A. **53** R648 (1996)

[15] H. Ito, K. Sakaki, T. Nakata, W. Jhe and M. Ohtsu, "*Optical potential for atom guidance in a cylindrical-core hollow fibre*," Opt. Commun. **115** 57 (1995)

[16] M. A. Ol'Shanii, Y. B. Ovchinnikov and V. S. Letokhov, "*Laser guiding of atoms in a hollow optical fibre*," Opt. Commun. **98** 77 (1993)

[17] S. Marksteiner, C. M. Savage, P. Zoller and S. L Rolston, "*Coherent atomic waveguides from hollow optical fibres: quantised atomic motion*," Phys. Rev. A. **50** 2680 (1994)

[18] M. J. Renn, D. Montgomery, O. Vdovin, D. Z. Anderson, C. E. Wieman and E. A. Cornell, "*Laser-Guided Atoms in Hollow-Core Optical Fibres*," Phys. Rev. Lett. **75** 3253 (1995)

[19] M. J. Renn, A. A. Zozuluya, E. A. Doneley, E. A. Cornell and D. Z. Anderson, "*Optical-dipole-force fibre guiding and heating of atoms*," Phys. Rev. A. **55** 3684 (1997)

[20] D. Müller, E. A. Cornell, D. Z. Anderson and E. R. I. Abraham, "*Guiding laser cooled atoms in hollow core fibres*," Phys. Rev. A. **61** 033411 (2000)

[21] F. Benabid, J. C. Knight and P. St. J. Russel, "*Particle levitation and guidance in hollow-core photonic crystal fibre*," Opt. Express **10** 1195 (2002)

[22] J. E. Bjorkholm, R. R. Freeman, A. Ashkin and D. B. Pearson, "*Observation of Focusing of Neutral Atoms by the Dipole Forces of Resonance Radiation Pressure*," Phys. Rev. Lett. **41** 1361 (1978)

[23] K. Szymaniec, H. J. Davis and C. S. Adams, "*An atomic fountain guided by a far-off resonance laser beam*," Europhys. Lett. **45** 450 (1999)

[24] L. Pruvost, D. Marescaux, O. Houde and H. T. Duong, "*Guiding and cooling of cold atoms in a dipole guide*," Opt. Commun. **166** 199 (1999)

[25] B. T. Wolschrijn, R. A. Cornelussen, R. J. C. Spreeuw and H. B. van Linden van den Heuvell, "*Guiding of cold atoms by a red detuned laser beam of moderate power*," New J. Phys. **4** 69.1 (2002)

[26] V. I. Balykin and V. S. Letokhov, "*The possibility of deep focusing of an atomic beam into the Å region*," Opt. Commun. **64** 151 (1987)

[27] J. Arlt, T. Hitomi and K. Dholakia, "*Atom guiding along Laguerre-Gaussian and Bessel light beams*," Appl. Phys. B **71** 549 (2000)

[28] M. Schiffer, M. Rauner, S. Kuppens, M. Zinner, K, Sengstock and W. Ertmer, "*Guiding, focusing and cooling of atoms in a strong optical potential*," Appl. Phys. B. **67** 705 (1998)

[29] J. Yin, Y. Zhu, W. Jhe and Z. Wong, "*Atom guiding and cooling in a dark hollow laser beam*," Phys. Rev. A. **58** 509 (1998)

[30] X. Xu, K. Kim, W. Jhe and N. Kwon, "*Efficient optical guiding of trapped atoms by a hollow laser beam*," Phys. Rev. A. **63** 063401 (2001)

[31] J. Yin and Y. Zhu, "*Doughnut-beam-induced Sisyphus cooling in atomic guiding and collimation*," J. Opt. Soc. Am. B. **15** 2235 (1998)

[32] O. Houde, D. Kadio and L. Pruvost, "*Cold Atom Beam Splitter Realised with Two Crossing Dipole Guides*," Phys. Rev. Lett. **85** 5543 (2000)

[33] R. Dumke, T. Müther, M. Volk, W. Ertmer and G. Birkl, "*Interferometer-Type Structures for Guided Atoms*," Phys. Rev. Lett **89** 220402 (2002)

[34] M. Kasevich and S. Chu, "*Atomic Interferometry Using Stimulated Raman Transitions*," Phys. Rev. Lett. **67** 181 (1991)

[35] Y. Shin, A. E. Leanhardt, M. Saba, T. Pasquini, W. Ketterle and D. E. Pritchard, "*Atom interferometry with Bose-Einstein condensates in a double well potential*," Phys. Rev. Lett. **89**, 040401 (2002).

[36] M. Yan, J. Yin and Y. Zhu, "*Dark-hollow-beam guiding and splitting of a low-velocity atomic beam*," J. Opt. Soc.Am. B. **17** 1817 (2000)

[37] G. Birkl, F. B. J. Buchkremer, R. Dumke and W. Ertmer, "*Atom optics with microfabricated optical elements*," Opt. Commun. **191** 67 (2001)

[38] A. M. Barnett, S. P. Smith, M. Olshanii, K. S. Johnson, A. W. Adams and M. Prentiss, "*Substrate-based atom waveguide using guided two colour evanescent light fields*," Phys. Rev. A. **61** 023608 (2000)

[39] D. Schneble, M. Hasuo, T. Anker, T. P. Fau ad J. Mlynek, "*Integrated atom-optical circuit with continuous wave operation*," J. Opt. Soc. Am. B. **20** 648 (2003)

[40] J.G. Livesey, D.P. Rhodes, D. McGloin and K. Dholakia, "*Transient response of a cold atomic beam in the presence of a far-off resonance light guide*," J. Mod. Opt. **50** 1751 (2003)

[41] K. Bongs, S. Burger, S. Dettmer, D. Hellweg, J. Arlt, W. Ertmer and K. Sengstock, "*Waveguide for Bose-Einstein condensates*," Phys. Rev. A **63** 031602(R) (2001)

[42] Y, Song, D. Milan and W. T. Hill III, "*Long, narrow all-light atom guide*," Opt. Lett. **24** 1805 (1999)

Chapter 4:

Magneto-optical Trap Realisation: Vacuum and Laser Systems

4.1 Introduction

During the course of this PhD a number of ultra high vacuum (UHV)* systems have been designed and built, each offering different arrangements for the guiding of cold atoms either from a cold atomic beam or a dropped cloud. The basic construction techniques are the same for each system so a generic guide to building a trap will now be described followed by the laser systems employed to produce an ensemble of cold rubidium atoms (in the basic MOT

* UHV is defined as a system whose pressure is less than 10^{-7} mbar.

we trap the ^{85}Rb isotope). The specific designs of each trap will then be considered along with the motivations for their construction.

4.2 General Construction

This section will detail the actual construction of the vacuum system, including the considerations for optical access and a source of atoms. Preparations necessary for creating and maintaining an ultra-high vacuum are detailed next. Finally the operation of a MOT is discussed; the magnetic fields required and the orientation, frequency and polarisation of the cooling beams.

4.2.1 Assembling a Vacuum System

The basic considerations for a simple MOT are an ability to pump the system down to UHV, a source of atoms and adequate optical access for the cooling beams while leaving enough room outside the vacuum to position the anti-Helmholtz coils for creating the magnetic field and completing the trap.

The skeleton of the traps built were based around standard, stainless steel UHV components (available from Helma and Vacuum Products), such as cross-pieces and tee-pieces, with all the other components connected to these via the flange ends of these parts. The flanges have a knife edge ring around the centre of the tubes. All metal-to-metal connections were bolted together with copper gaskets between the knife edges to make a good

vacuum seal, the exception to this was where a viewport was needed in which case an annealed copper gasket was used as it reduces the stress on the windows. When constructing the trap care was taken when handling all the vacuum components and latex gloves were used at all times to avoid contaminating the surfaces with dirt or oil from contact with hands; also when joining the flanges together opposite pairs of bolts were tightened in sequence to reduce the stresses on the metal and ensure a high quality seal.

The trap itself is positioned so that light can be incident on the trapping volume from six mutually orthogonal directions, and also ensure that there is space to place the magnetic coils around the MOT region. Completing the six directional beams usually required the trap to be positioned on top of a six-way cross piece, attaching a viewport in the opposite side of the six-way cross piece allowed the MOT region to be illuminated from underneath (this is not always necessary; placing a retro-optic in the trap region itself negates the need for a sixth beam from below, however, since this optic will be within the vacuum it can no longer be repositioned which might complicate the alignment of the other beams). From this six-way cross piece the other elements can be attached (a simple arrangement is shown in figure 4.1).

A background vapour of atoms must be present in the vacuum system in order to load the trap. We used getter ovens (SAES Getters, UK) as a source of rubidium atoms. The getter is several milligrams of Rb contained in a small metal envelope with a wire across the top as a seal (figure 4.2), when a current (3.5A-7A) is passed through the getter it heats up, the wire closing the envelope expands, opening the getter and allowing Rb vapour to escape into

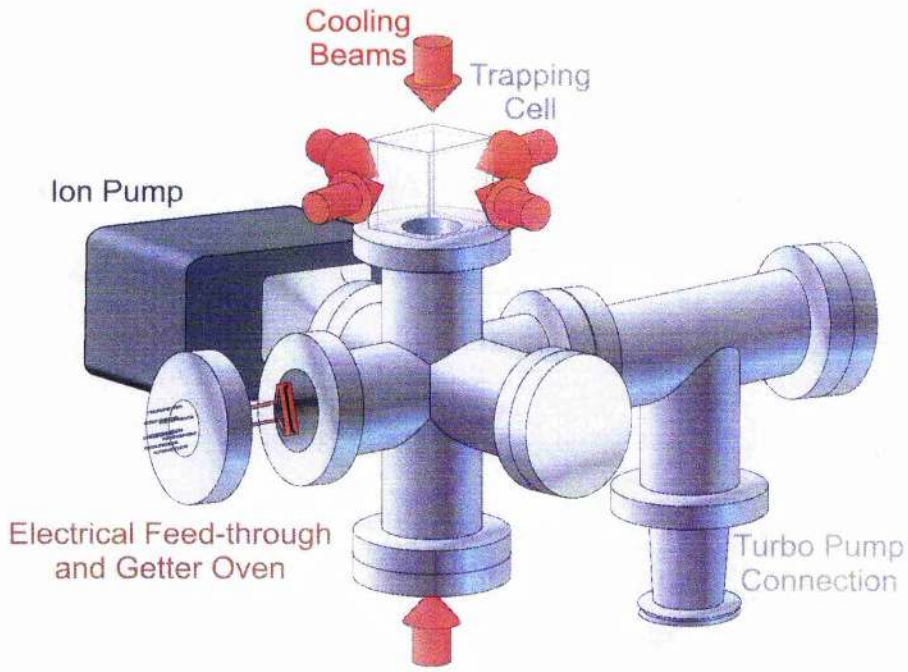

Figure 4.1: A simple MOT vacuum set up. Atoms are trapped within the glass cell, this is attached to a flat flange at the top of the six-way cross piece using a UHV epoxy resin, a viewport beneath the trap allows illumination from all six directions (magnetic coils are not shown). Two of the remaining flanges of the cross piece connect to turbo and ion pumps to maintain a vacuum and the Rb getters can be connected via a electrical feed-through as shown.

the trap. The getters are spot welded to the pins of an electric feed-through which can then be attached to one of the vacuum pieces. Using getters in this way allows us a simple method of controlling the vapour pressure within a vacuum from a highly localised position (i.e. the atom source can be positioned directly in the trapping region if required).

Finally a vacuum must be maintained in the trap, although trapping can be achieved with a pressure of only 10^{-7} mbar this pressure is still high enough to cause significant collisions within the MOT due to interactions with thermal

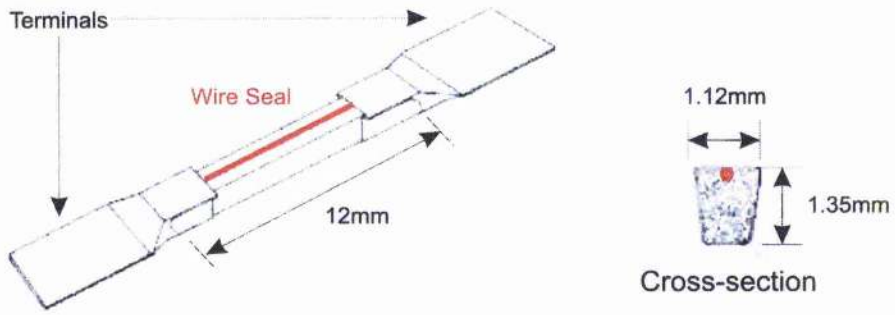

Figure 4.2: A diagram of the getter ovens.

background vapour and thus results in a reduced trap lifetime. To increase the trap lifetime a pressure of ~10^{-9} mbar was maintained with an ion pump (a $401s^{-1}$ Varian, Vaclon Plus 40 Triode). A tee-piece that can be attached to a turbo pump (Varian, Turbo-Dry 70) was also used, this is to enable us to take the trap from air pressure to 10^{-6} mbar rapidly whereupon it is switched off and the ion pump can be turned on and used to bring the trap to the experimental pressures required (the ion pump is a diffusion pump; particles have to diffuse into the ion pump itself for them to be ionised and attracted to the inside walls of the pump, the turbo pump is a turbo backed diaphragm pump which physically draws the particles out). However, simply turning on the vacuum pumps is not enough to reach the UHV requirement; at room temperature contaminants on the interior surfaces of the trap will not all be removed, during an experiment these contaminants will evaporate from the surface raising the background pressure of the trap and increasing unwanted collisions within the trapping volume. To remove these contaminants the trap has to be baked when it is brought down to UHV.

4.2.2 Bake Out

One of the major contaminants in the vacuum is water vapour, in order to remove this and other contaminants on the interior surfaces the trap is baked at temperatures higher that 100°C (so that all the water is converted to steam which can be drawn out with the pumps) whilst the initial evacuation with the turbo pump is performed; this evaporates the contaminants from the surfaces and ensures all the water vapour can be evacuated from the trap. Several thermocouples are positioned on different areas of the trap to monitor the temperature during the bake out and watch for high temperature gradients across the trap. The entire vacuum system, including the ion pump (so that the interior surface of the ion pump, where the particles will be trapped, can be evacuated as well), is wrapped as evenly as possible with electrical heat tape and any optical elements are covered completely in aluminium foil. The whole apparatus is then wrapped in foil for insulation and then placed in a metal oven. The turbo pump is connected and started and the electrical heating tapes are turned on. The temperature of the trap is raised to ~150°C where it is left for about two days, with the turbo pump remaining on. After this the current through the heat tape was reduced and the temperature was brought down to ~70°C whereupon the turbo pump was turned off and the ion pump was started. The bake out continued at this temperature for another day before the heat tapes were finally turned off. On cooling, the vapour pressure in the trap can be inferred from the ion pump current and pressures of approximately 10^{-9} mbar are observed, which is the desired value for the

trapping experiments. The rubidium is protected from the baking process inside a protective metal case within the getter envelope itself, in order to start releasing the Rb this case needs to be opened. The case has a score along one side which has to be split; this is achieved by running a high current though the getter and heating the case until it cracks open. Before this can be done the getter needs to be degassed and opened so any contaminants inside the envelope of the getter can be removed before the Rb is released. This is done by running the ovens at low currents (not enough to break the Rb seal but enough to cause the closing wire to expand and open the getter) and slowly increasing the current; the contaminants are slowly evaporated off the ovens into the surrounding vacuum where they are then removed by the ion pump. This out-gassing of the ovens needs to be monitored quite closely because if the ovens are out-gassed too quickly the increased vapour pressure could result in the ion pump reaching a current high enough to trip the safety switch to the pump. Because of this the current to the ovens was increased in steps, out-gassing the getters for a short while before reducing (or turning off) the current in order to give the ion pump time to recover. As the ovens are out-gassed the currents can be slowly increased, once the getters reach a current of ~5A the ovens can be considered safely out-gassed and increasing the current beyond this up to 9A would break the seal on the Rb case. Once the seal is broken the current must immediately be reduced to 1A-2A or turned off entirely as these currents are well above the normal operating values of the getters and would result in all the Rb being evaporated out within a few minutes. The release of the Rb can be monitored by directing a beam from one of the trapping lasers, tuned to the Rb transition, into the

area around the getters, once the getter has been opened a line of fluorescence, from the absorption and spontaneous emission induced by the laser beam, can be observed by use of a near infra-red viewer. It is also important to note that due to chemical reactions and physisorption of Rb the walls of the trap will usually remove more Rb than the ion pump does, the rate of this removal depends on how well coated the walls have become, and results in a "creep" of Rb along the surfaces as the vapour slowly saturates the walls and diffuses further inside the vacuum. The absorbed Rb will slowly evaporate off the surfaces when the source of atoms is removed and vapour can linger for several days, in this way it can take several days of experiments before the vapour is distributed evenly throughout the vacuum and an equilibrium can be reached.

With a suitable pressure and a controllable source of Rb we now need to align the molasses beams and magnetic coils to actually cool and trap the atoms.

4.2.3 Operation of a MOT

The magnetic field required for a MOT is generated using a pair of symmetric coils, approximately separated by the diameter of the rings, with oppositely directed currents, an anti-Helmholtz arrangement. This creates a field with a zero point in the centre (at the trap position) and a simple linear gradient in the x-, y-, and z-axes, a gradient of 10-15G/cm is all that is needed to trap the atoms (For coils of ~4cm diameter made up from 60 wraps of wire a suitable field can be created by using only 2A).

Diode lasers are used for the trapping beams because they are inexpensive, compact, and can easily be made narrow linewidth, tuneable sources using extended cavity geometries. The choice of rubidium as a trapping substance is made because there is a transition from the ground state to an excited state in the near infra-red region, ~780nm, which is in a wavelength range covered by these simple diodes. We have used a few variations of laser systems for the trapping beams described in this thesis, (the laser systems will be described in next section) but all of them are based around an extended cavity diode laser (ECDL).

The output from one of the diodes is used as the cooling beam and was expanded up to ~20mm diameter (as large a beam as permitted when using 1" diameter optics at 45°). It is then split into three beams of approximately equal power (the total power needed for trapping Rb is only about 10mW, so it can be provided with the use of only a single diode laser). The beams were then directed into the trapping region. Before entering the trap each of the beams was passed though a quarter-wave plate to produce circularly polarised light of the correct orientation with respect to the magnetic coils (figure 4.3 shows the handedness of the laser beams required), once each of the three beams are through the trapping region they pass through another quarter-wave plate and are retro-reflected backwards by a dielectric mirror. The beam does not need be reflected exactly 180° straight backwards, just as long as the overlap inside the trapping volume is good, because the MOT is such a stable trap. However, because of the susceptibility of diode lasers to feedback any beam that is reflected straight back to the diode laser will

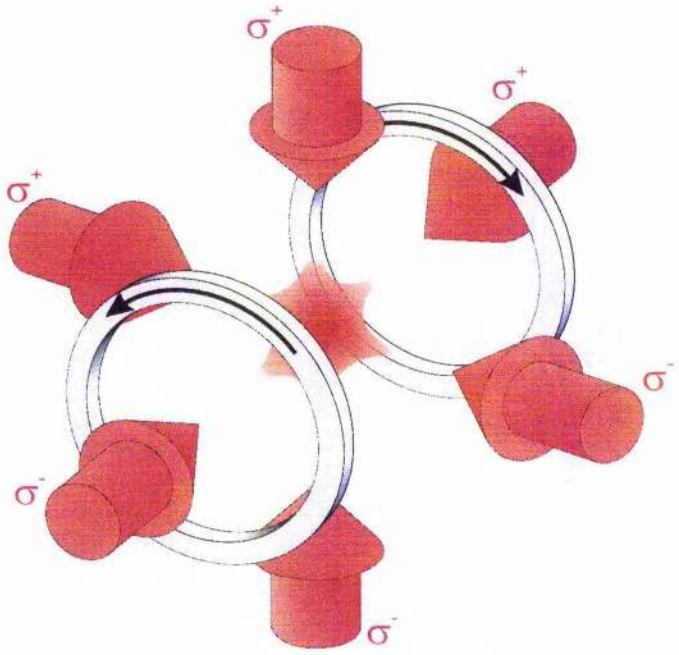

Figure 4.3: The polarisation of the trapping light in a MOT for the six mutually orthogonal cooling beams. The current in the coils is in the direction shown by the arrows (anti-Helmholtz configuration); this produces a zero field in the centre of the trap.

dramatically affect the laser frequency so an optical isolator is required at the source to stop this. While silvered mirrors can be used for all of the beam steering optics the retro-reflecting mirrors are chosen to be dielectric because the high reflectance (~99.9%) means that the trap beams end up more symmetric (this is useful for a molasses cycle, described in section 4.4.3). This generates the six mutually orthogonal beams polarised with the correct handedness. It can simplify the orientation procedure of the circular polarised light by positioning the input quarter-wave plates with their axes at 45° and keeping the polarisation of the cooling beams either horizontal or vertical, in this way the handedness of the circularly polarised beam can be reversed by simply rotating the whole optic mount through 180° about the post axis and

illuminating the wave plate from the other side rather than rotating the wave plate within the mount itself. As the incident beam on the retro-optics is circularly polarised the orientation of the second quarter-wave plates is not important. The hyperfine beam is taken from a second ECDL but here the orientation and direction of the beam is not important for trapping (though this can be of consideration when guiding the atoms outside of this region, which will be discussed later) and can just be gently focused to overlap with the trapping region, for example: by using a lens of focal length ~300mm at a distance of 200cm.

With the beams correctly aligned the laser needs to be tuned to the correct frequency. The cooling laser was tuned and locked approximately 2Γ (where Γ is the natural line-width of the transition) below the frequency (red-detuned) of the $5S_{1/2}$ (F= 3)$\rightarrow$ $5P_{3/2}$ (F'= 4) transition for ^{85}Rb while the hyperfine laser was locked to the $5S_{1/2}$ (F= 2)$\rightarrow$ $5P_{3/2}$ (F'= 3) transition (Rubidium has two natural isotopes, the transitions for trapping the ^{87}Rb isotope are $5S_{1/2}$ (F= 2)$\rightarrow$ $5P_{3/2}$ (F'= 3) for the cooling laser and $5S_{1/2}$ (F= 1)$\rightarrow$$5P_{3/2}$ (F'= 2) for the hyperfine). A scan across the Rb lines is given in figure 4.4, the energy level diagrams for the cooling transitions are given later in figures 4.5 for Rb^{85} and 4.6 for Rb^{87}. In practice, because the hyperfine laser is only pumping atoms that have fallen out of the cooling cycle (approximately only one in every thousand transitions results in the atoms falling out of the cooling transition), it does not need to be as finely stabilised as the cooling laser; in fact it is possible to maintain a MOT for several minutes without the hyperfine laser being locked at all.

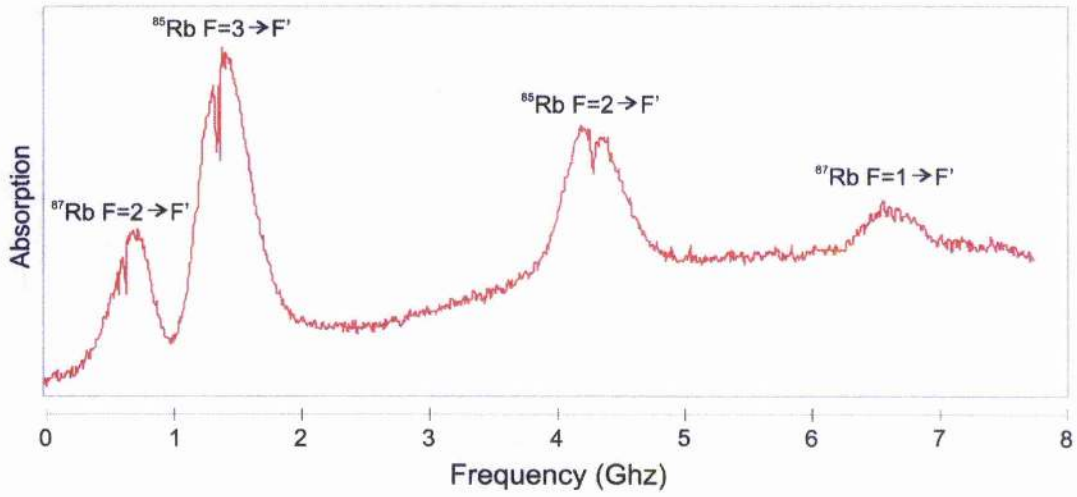

Figure 4.4: An absorption scan across the rubidium transitions. The two left hand side peaks are the cooling transitions, the hyperfine transitions are on the right.

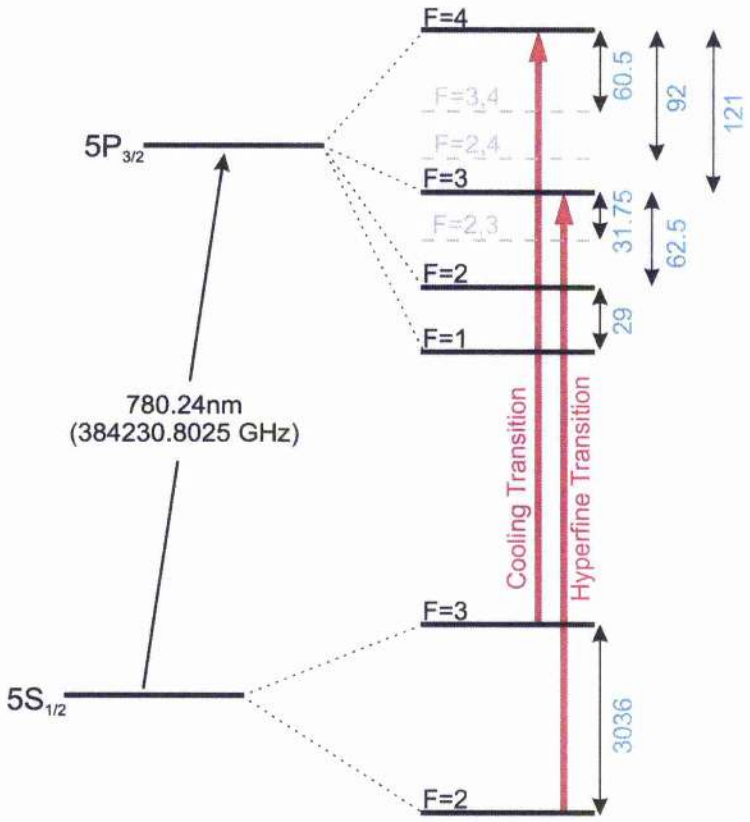

Figure 4.5: Energy level diagram of the ^{85}Rb D2 lines. The values in blue are all MHz.

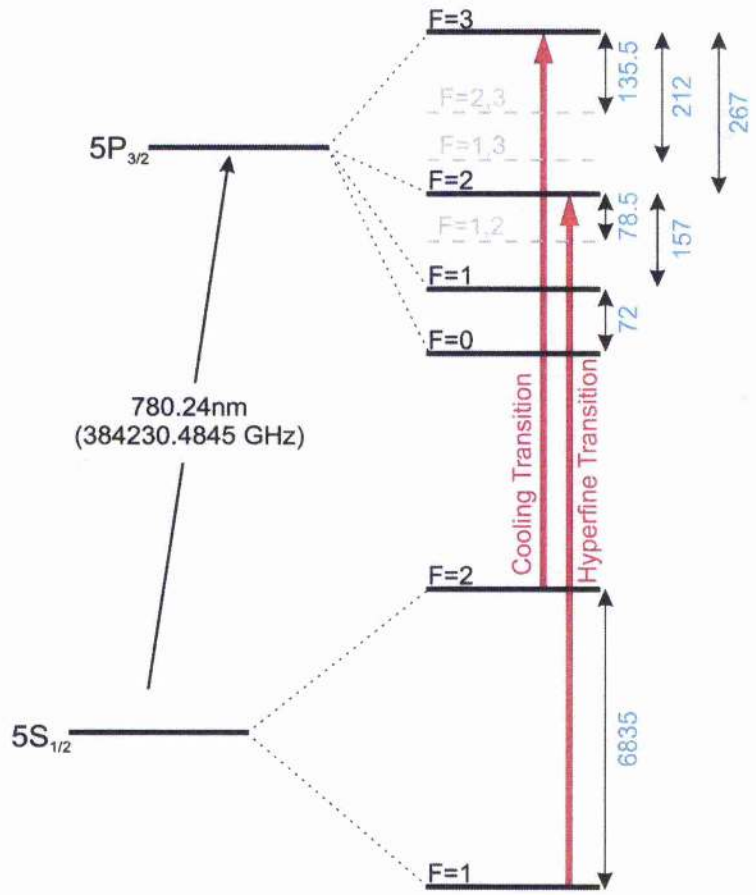

Figure 4.6: Energy level diagram of the ^{87}Rb D2 lines. The values in blue are all MHz.

With the magnetic field in place and the lasers locked to the correct frequencies the trapped atoms can be observed using a CCD camera sensitive in the near infra-red which is orientated towards the trapping region. The fluorescence of the atoms can then be observed on a TV monitor.

4.3 Laser Systems

In this section we shall first detail the construction and characteristics of the different lasers used for creating the MOT and for generating the guide beams. Second; precise control over the frequency of the lasers is required for generating a MOT, narrow linewidths and stabilisation are required. A description of the generation of a reference signal through saturated absorption spectroscopy and the use of a dual current/PZT locking system to stabilise the lasers is given.

4.3.1 Lasers Employed

Trapping Beams

As mentioned earlier the transitions of rubidium are of the correct wavelength for us to be able to exploit simple diode lasers. The D1 and D2 transitions of Rb are 795nm and 780nm respectively, we use the D2 lines of ^{85}Rb to trap with. The ease by which these diodes can be tuned, by way of current or temperature control makes them ideal candidates for locking to the specific wavelengths of the atomic transitions. Selectively feeding back some of the laser power by way of an extended cavity design reduces the linewidth of these devices by some two orders of magnitude, to a few hundred kHz, and allows us to stably lock the laser to a specific transition using a basic feedback circuit to control the cavity length.

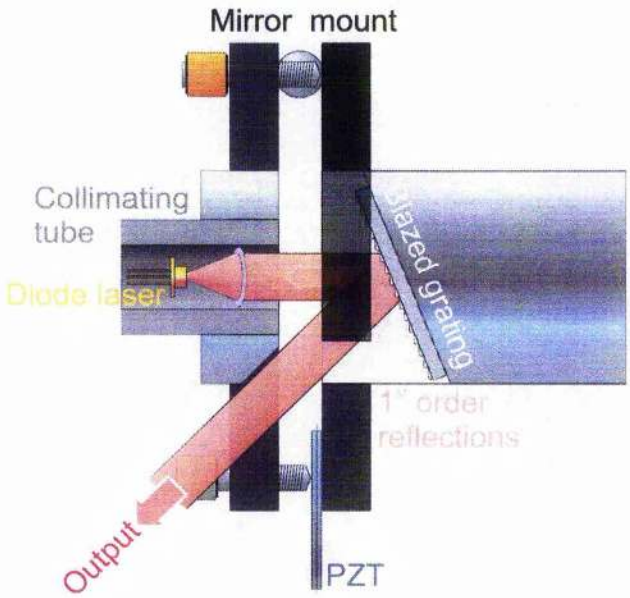

Figure 4.7: Schematic of our extended cavity diode laser. The output of a circularised diode is collimated and reflected off a grating, the first diffracted order is fed back into the diode. The cavity length is controlled by adjusting the mirror actuators with a PZT disk placed in the horizontal arm to permit fine tuning and scanning of the laser wavelength.

The first laser system used was a home made ECDL in the Littrow geometry [1] based around a diode laser built onto a commercial clear quadrant mirror mount (Newport, P100-AC) which also holds the grating [2]. Figure 4.7 shows a schematic of our laser. One consideration when using diode lasers is the elliptical output, which could cause distortions in the shape of a trapped cloud of atoms. This would need to be corrected for typically by using anamorphic prisms, a pair of cylindrical lenses or coupling into a fibre optic which complicates the experimental setup and can result in a severe loss of power. To eliminate the need for these extra, corrective optics we used Circulase diode lasers (Blue Sky Research), these are Hitachi HL7851G diode lasers

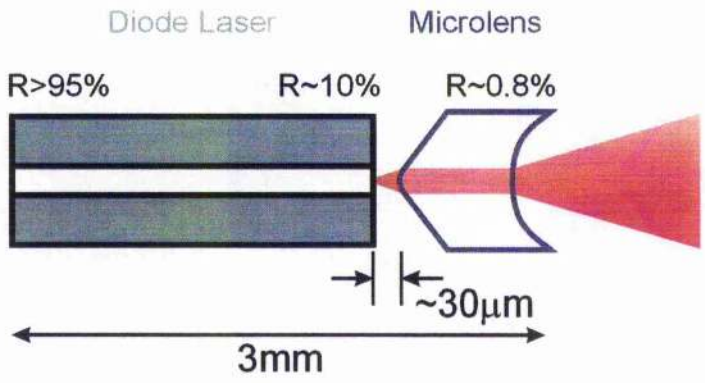

Figure 4.8: A diagram of the laser diode and microlens array. The microlens is only 250μm thick.

(maximum output power 50mW at 785nm) which have had a small microlens placed a few μm from the output facet, this generates a diverging, circular output (aspect ratio ~1:1.1) direct from the diode output facet that is then collimated in a commercial collimating tube. A diagram of the diode and microlens array is shown in figure 4.8. The collimating tube was placed in a custom built holder for attaching to the mirror mount, a second custom machined holder was built for the grating, 1200lines/mm, blazed wavelength at 300nm, (Optometrics, UK) which was positioned on the other side of the mirror mount so the mirror adjust screws can act to control the cavity alignment. The angle of the grating can be found from (figure 4.9):

$$m\lambda = d(\sin\theta \pm \sin\theta') \qquad (4.1)$$

where m is the diffracted order, θ is the angle of incidence, θ' is the angle of reflection and d is the line spacing of the grating. The grating feeds back about 20% of the incident light into the laser with ~30mW output power in the zeroth order beam which can be sent to the trap. The laser should be rotated

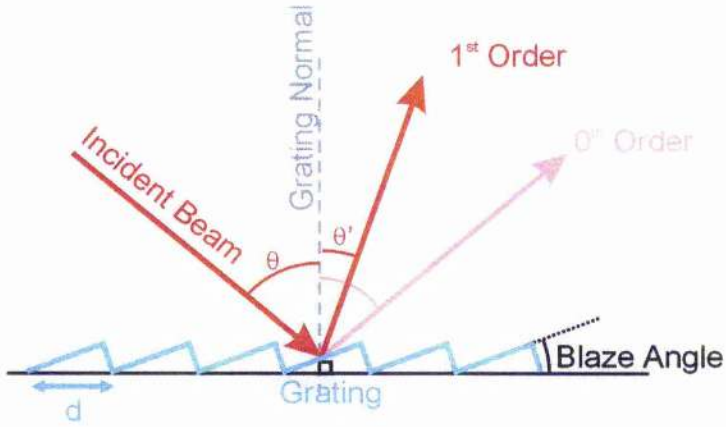

Figure 4.9: If there is an angle across the grating edges then the light will be preferentially diffracted into one specific order, the wavelength which diffracts the highest intensity into the first order is known as the blaze wavelength. A blaze wavelength away from the laser wavelength is used to ensure most light is reflected into the zeroth order as only a little light is required for feedback to the diode.

in its mount so that the polarisation of the laser matches the grating orientation, this optimisation is achieved by simply measuring the reflected beam power off the grating. The extended cavity is aligned by observing the zeroth order output from the grating; using a drive current of ~80mA, when the grating is positioned correctly a second very faint spot should be observed next to the main beam. The faint spot is the first diffracted order reflecting off the diode facet and back onto the grating again. Once this faint spot is found the mirror adjust screws are used to overlap the spot with the main output (as it is moved closer the faint beam will disappear in the glare of the main beam so a best guess should be made by eye), with the spots overlapped the drive current is reduced to just below threshold, in our case ~37mA. Once again looking at the zeroth order output from the grating the mirror mount is then

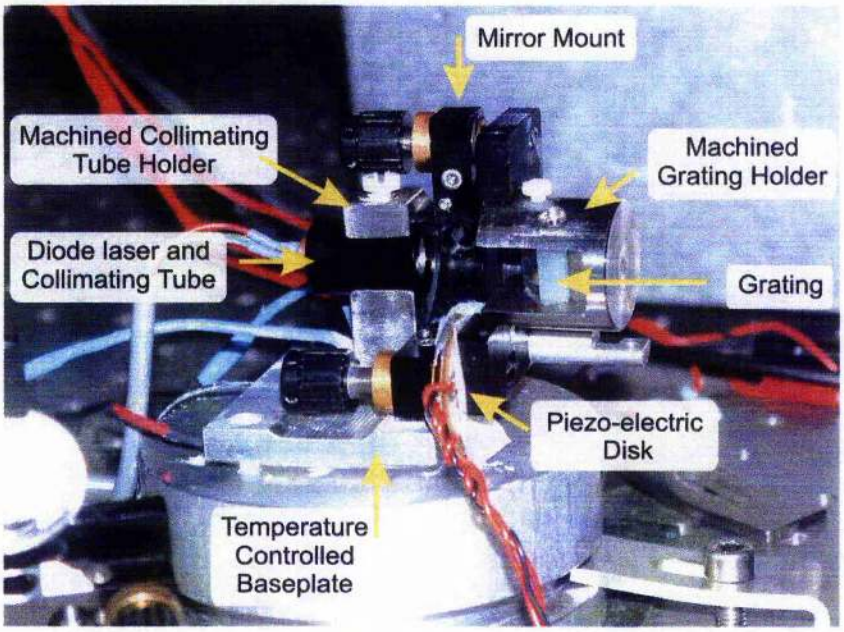

Figure 4.10: A digital photograph of the extended cavity diode laser used in these trapping experiments. For scale the machined grating holder is 1" in diameter.

mechanically scanned back and forward looking for a characteristic bright intensity "flash" when the diode starts to lase because of feedback lowering the threshold current. Experimentally the horizontal mirror adjust is rotated to scan over the overlapping region (we found rotating the mirror screws half a turn each way kept the laser on extended cavity), if no flash is seen then the vertical adjust is moved very slightly and the horizontal is scanned again (the vertical adjust is the most sensitive because the grating is mounted with the grating lines vertical). The whole thing is then mounted on a 90mm diameter, 40mm high block of aluminium via a peltier element, driven by a commercial TEC controller (Wavelength Electronics, Inc.), to stabilise the temperature (a photograph of one of the lasers used throughout this project is shown in figure 4.10). The diodes are initially cooled to ~14° to pull the laser

wavelength down to approximately 780nm, the frequency can then be controlled by altering the external cavity length; this can be done coarsely by rotating the horizontal adjustment screw of the mirror mount while fine tuning is achieved by applying a voltage to a piezoelectric transducer (PZT) placed beneath this screw, a continuous, mode-hop free tuning range of ~5GHz is achieved using the PZT to scan the frequencies. Whilst a simple feedback circuit controlling just the PZT can be used to lock the laser extra stability is found when using control of the diode current (this is used to counter high frequency fluctuations) as well as the PZT voltage, this will be described in the next section.

The useful output from one of these diodes is ~30mW, this is enough power to create a MOT with but the number of trapped atoms is proportional to the area of the beam (with the intensity of the beam greater than I_{sat}) so a method of increasing the usable power was then considered. Sanyo make a higher power diode (75mW at 780nm, DL-7140-201, this can also be bought circularised through Blue Sky Research) than the Hitachi model we have used previously but the spectral quality is slightly lower. It has a larger linewidth making it less practical for locking to the atomic transitions. A solution to this is to injection lock the higher power Sanyo laser to the output from the Hitachi ECDL; seeding a free running (slave) laser with a few μW of light from a second (master) laser will cause the slave laser to run on an identical mode to the master. If the slave laser is running at a frequency close to the master laser the presence of the injected beam reduces the threshold for the specific cavity mode of the master and results in that mode being preferentially

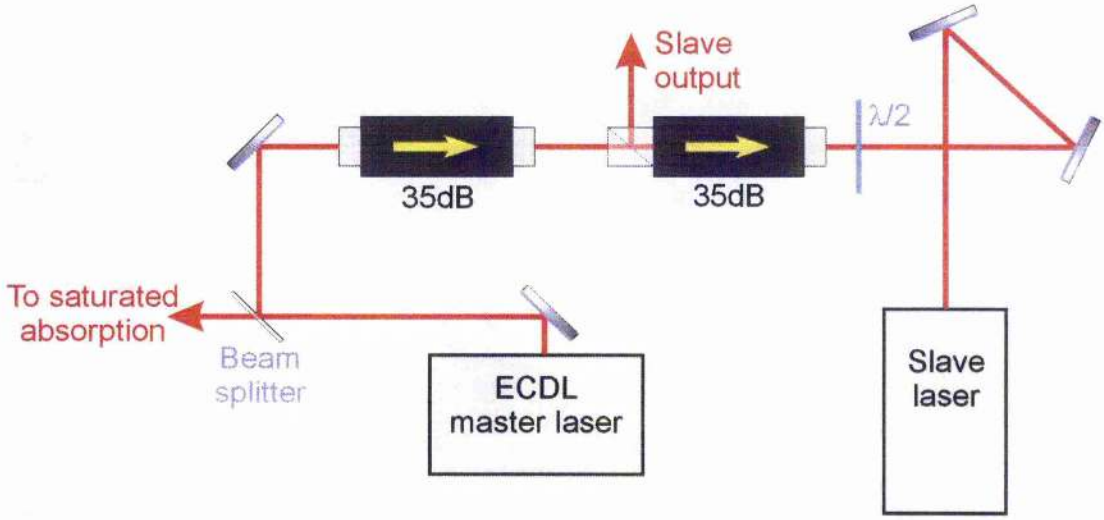

Figure 4.11: Diagram of injection locking of a diode laser. Isolators are required to stop any light from the slave returning to the master laser and causing unwanted feedback. The half-wave plate is included to match the polarisation of the two lasers (similarly the slave laser could be rotated in its mount).

selected by the slave laser. In this way we can get a beam with the higher power of the Sanyo diode and the spectral quality of the Hitachi. The seeding was set up as shown in figure 4.11 with a beam splitting optical isolator used to separate the two beams. The beams are aligned by overlapping the two beams at the isolator and at the diode output facet; with both points overlapped the beams are co-propagating. As with the ECDL when the diode laser is injection locked the threshold is reduced slightly, if the slave is operated just below the normal threshold limit a "turning on" of the laser can be observed in the slave once the beams are properly aligned.

The cooling beams for the trap were achieved using this slave setup but the hyperfine source, because it requires less power was left just as a single ECDL, constructed as described above.

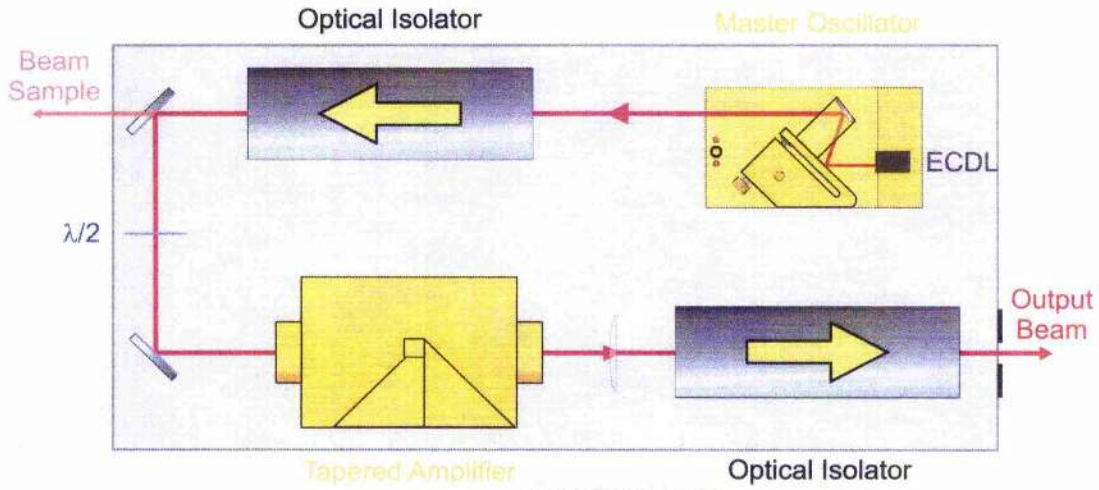

Figure 4.12: A schematic of the TA100. The master oscillator (MO) is an extended cavity diode laser in the Littrow geometry. The output from the MO is collimated but not circularised, lenses on the front and back facets of the tapered amplifier collimate the amplified beam and the cylindrical lens acts to circularise the output.

Detection of the atoms was also performed using these lasers. Some of the cooling light was separated from the trapping beam and passed through two acousto-optic modulators (AOMs) to bring the light exactly onto resonance with the transition. Because the laser power from these diodes is limited a second laser system was used to create the cooling beams, this freed up one of the ECDL's to be used solely as a probe source and provided enough power to run a dual pass AOM system for adding a molasses cycle to the MOT (this molasses cycle will be describe later in section 4.3.3). The second cooling laser system used was a commercially available tapered amplifier diode laser system (TUI Optics TA-100), this is an ECDL that is then passed through a tapered amplifier to give a maximum output of 500mW (a schematic is shown in figure 4.12) [3]. The extended cavity is again in the Littrow geometry, and the beam from the diode can be sampled through a <90%

mirror for the purposes of locking the laser. The beam from the ECDL is then passed through a tapered amplifier to give a high power output. The diode used in the extended cavity is not circularised, however, the optics system around the tapered amplifier includes cylindrical optics to beam-shape the beam upon exiting the amplifier. Because the tapered amplifier is a gain medium it also generates amplified spontaneous emission (ASE) "wings" around the, now circularised, output which need to be apertured independently, outside of the laser system.

Guide Beam

The guide light was provided by a Titanium-doped Sapphire (Ti:Sapphire or $Ti:Al_2O_3$) laser (Spectra-Physics, Model 3900S) pumped by a diode pumped Neodimium Yttrium Vanadate ($Nd:YVO_4$) laser (Spectra-Physics, Millennia Vs). The guide beam is not required to have as narrow a linewidth as the cooling beams, this is because the atomic transition has a linewidth of 6.1MHz and the guide beam is typically detuned by a few GHz. The Millennia laser provides 5W of 532nm light to optically pump the Ti:Sapphire crystal resulting in a final output of ~1W with a tuning range of 650-1000nm (dependent on the intra-cavity optics used), this gives use the versatility to experiment with both red- and blue-detuned guiding regimes. The number of laser modes in the Ti:Sapphire is reduced by several intra-cavity optics, a birefingent filter and two etalons. The cavity arrangement is shown in figure 4.13 [4]. The first of these is the birefringent filter; this made up form three retardation plates at

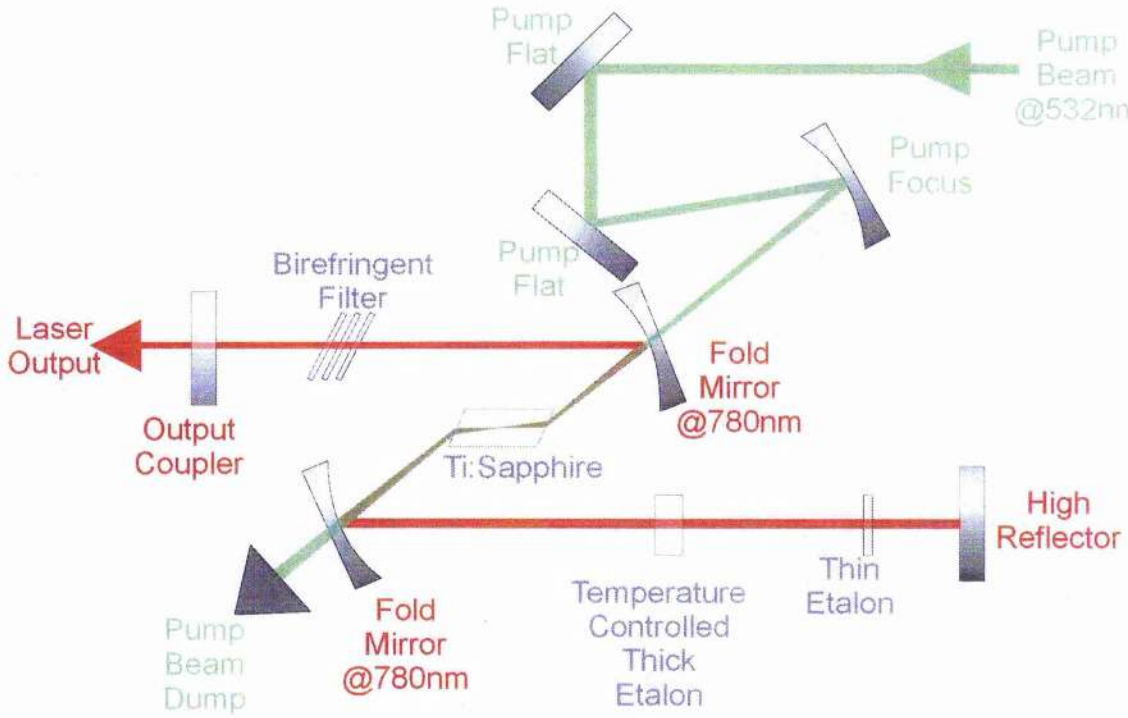

Figure 4.13: Schematic of the Ti:Sapphire cavity. The birefringent filter and thick and thin etalons act to select two cavity modes.

Brewster's angle, on passing through these plates the linearly polarised light becomes slightly elliptical, only one frequency will be unchanged through one pass of the filter and see negligible loss when oscillating in the cavity. The birefringent filter is the coarsest tuning element with a bandwidth of 100GHz (~0.2nm). The next coarsest element is a thin etalon, ~0.5mm thick; this etalon has a free spectral range (FSR) of 200GHz and reduces the bandwidth of the laser to 15GHz. The etalon can be tilted to tune this bandwidth over the whole 100GHz permitted by the birefringent filter. The finest tuning is achieved by way of a thick etalon; this is 5mm thick etalon mounted in a temperature controlled housing. The FSR of the etalon is 20GHz and has a bandwidth of 500MHz, this reduces the number of allowed cavity modes to

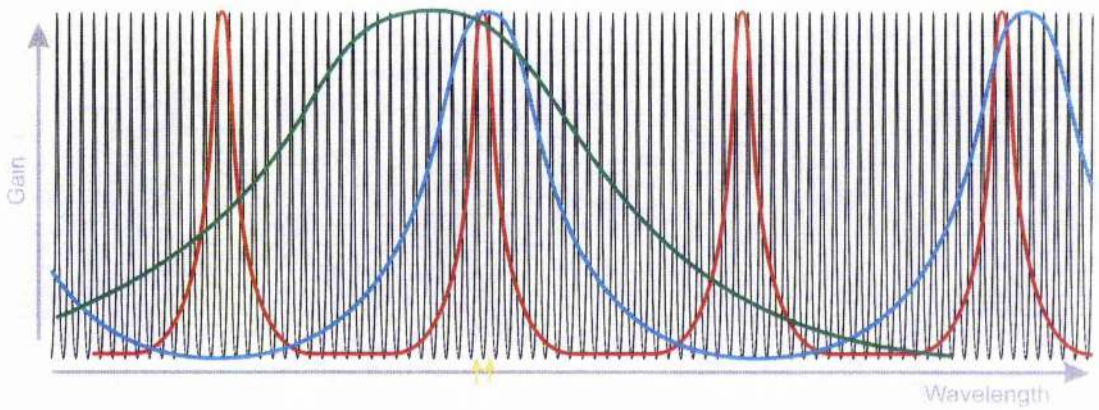

Figure 4.14: Mode selection of the intra-cavity elements. The black lines are the cavity modes, the green line shows the allowed modes for the birefringent filter, the allowed modes for the thick and thin etalons are given by the red and blue lines respectively. With all three elements in place only two of the cavity modes, indicated by the arrows, are allowed. This figure is not to scale.

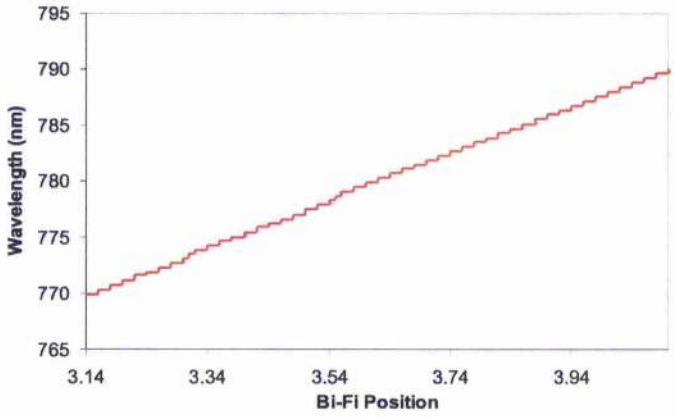

Figure 4.15: Tuning properties of the birefringent filter (Bi-Fi), with the other cavity elements in place. The steps occur as the laser jumps to run on a new pair of cavity modes. Bi-Fi position relates to the reading on the control actuator.

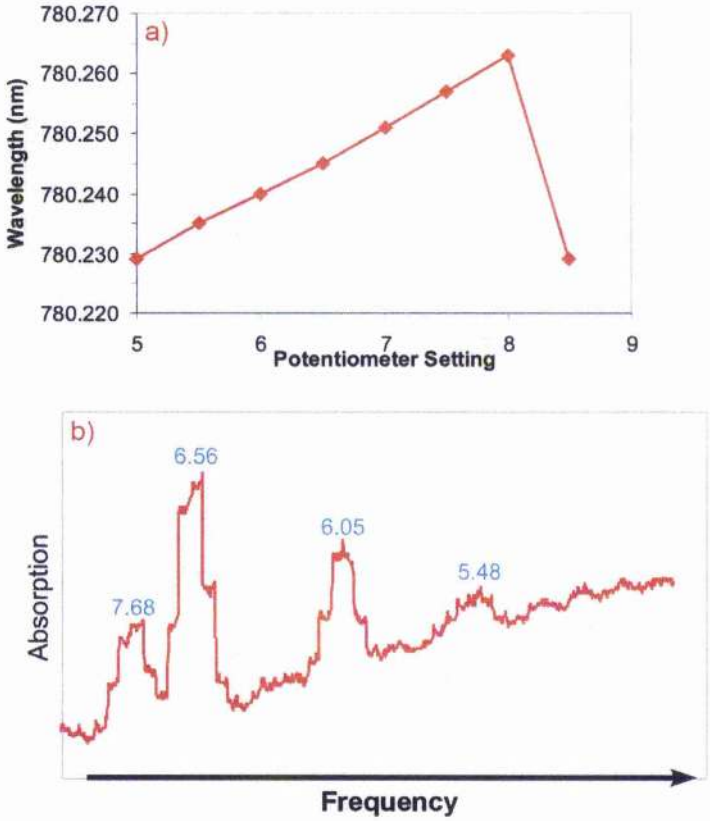

Figure 4.16: Tuning properties of the thick etalon. (a) shows how the wavelength of the laser varies as the thick etalon is heated up, the drop at the end is the mode hop back to the start of the thin etalon bandwidth. A scan across the absorption line of rubidium is shown in (b), the numbers in blue give the potentiometer values at the peak of each transition. The stepped nature of the scan is due to the laser hopping across the cavity modes.

two modes, separated by 200MHz. Tuning of this etalon can also be controlled by tilting (this can only be done when the laser casing is open) butthe main method for controlling the tuning of this element is achieved by regulating the temperature (by way of a potentiometer), and hence the thickness, of the etalon. The effect of each cavity element on the lasing mode is shown in figure 4.14. Graphs of the tuning characteristics of the birefringent filter and the thick etalon are given in figures 4.15 and 4.16, respectively.

4.3.2 Frequency Locking Methods

The ECDL's described above have the required beam characteristics for trapping the atoms: they are narrow linewidth, single mode tunable sources, but the frequency of the light also needs to be stabilized to a very precise value to within a few hundred kHz (less than the natural linewidth of the transition). This is accomplished by using a negative feedback circuit to lock the atoms to the atomic transition.

Servo-locking System

A basic servo locking system is shown in figure 4.17; it requires a measure of the signal and a reference signal with which to compare it. This comparison is used to create an error signal which is then fed through some compensation electronics which provides a negative feedback signal that is sent to the laser.

The feedback is negative to cancel the effect of the noise and return the laser to the reference level. The error signal is inversely proportional to the gain of the feedback circuit, increasing the gain will pull the signal closer to the reference level (the dc response) but this is at the expense of the bandwidth of the system (increasing the "tightness" of the lock reduces the range of frequencies which can be compensated). This leads to a trade off between the transient response time and dc sensitivity of a servo locking system.

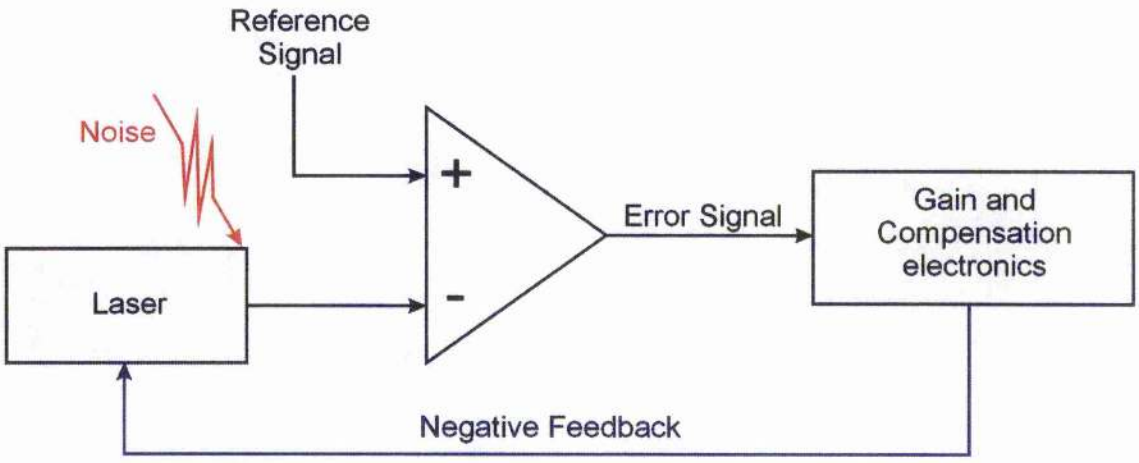

Figure 4.17: A basic servo loop for stabilisation of a laser.

There is also a form of time lag in these systems; if the feedback signal sent to the corrective element is at a frequency below the resonance of that element then the correction will follow the phases of the feedback signal and correct for the noise. If, however, the feedback frequency is above the natural resonance of the corrective element then the correction is delayed by π radians and the feedback becomes positive, acting as an oscillator to the noise and moving the laser even further from the reference. Thus a simple negative feedback circuit, with constant gain across all frequencies, cannot correct for all frequencies of noise in a system.

In order to extend the bandwidth of the locking whilst still keeping the dc sensitivity we implemented a dual-servo system. The ECDL's constructed have a feedback control to the PZT controlling the grating position which was used to correct for broadband deviations with a slow response time, high frequency noise was corrected for with feedback to the diode current. The current of the diode laser can be modulated at up to 100MHz, two orders of

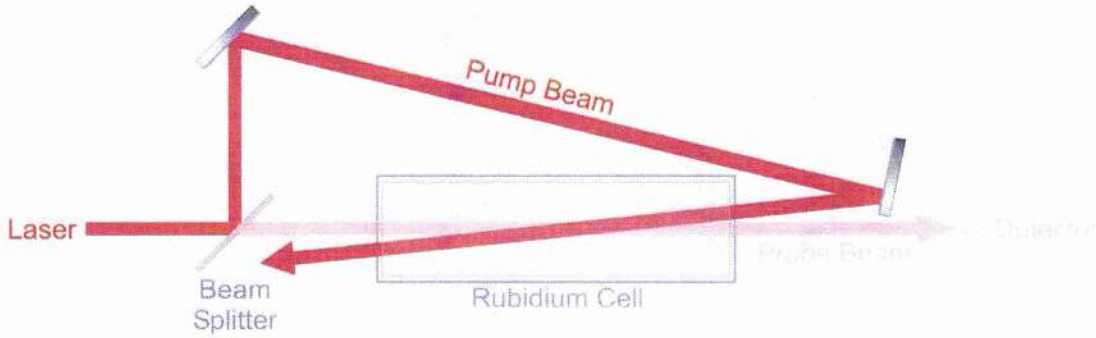

Figure 4.18: Schematic of the saturated absorption arrangement. A high power pump beam is alligned to overlap a weak probe beam, saturating the atoms and resulting in absorption "holes" in the probe beam signal.

magnitude faster than the PZT which is why current feedback is used for the transient deviations, with the PZT used for low frequency, dc shifts.

Doppler-free Saturated Absorption

The reference signal for lock was obtained from a saturated absorption signal generated using a portion of the laser output passing through a Rb cell. This technique is a method to observe the hyperfine features of the atomic transitions using a thermal cell of Rb which would otherwise be washed out due to Doppler broadening of the laser signal from the motion of the atoms. Two counter propagating beams of exactly the same frequency are overlapped inside a vapour cell, as shown in figure 4.18. Only atoms with zero velocity along the directions of the beams will see identical frequencies from both directions and be able to interact with both beams. Atoms moving in a direction along the path of beams will observe opposite Doppler shifts in the two beams and will therefore only absorb light from one beam. If one of

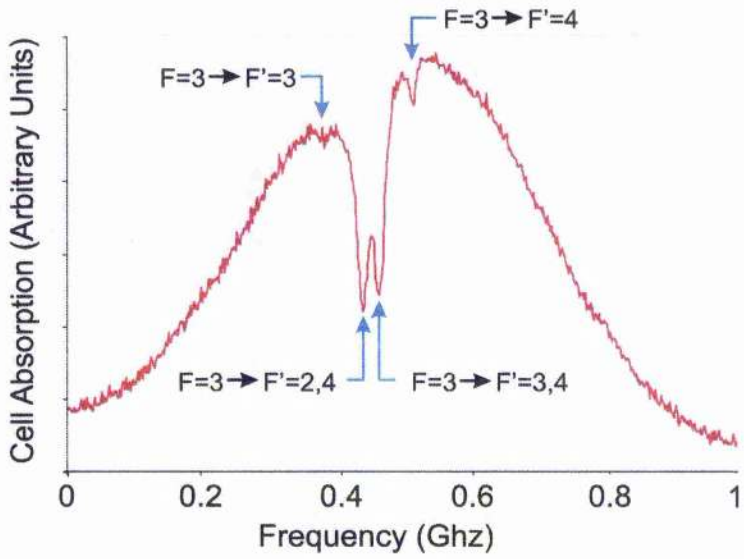

Figure 4.19: The saturated absorption signal for the ^{85}Rb F=3 →F' transitions with the hyperfine transitions labelled (the F'=2 line is not visible). The crossover transitions are clearly the largest features detected.

the two beams is more intense than the other (the intense beam is known as the pump beam, the weaker beam is the probe) when an atom with a velocity that permits interaction with both beams does absorb a photon then it will most likely be from the pump beam (the pump beam saturates the atom), leaving the probe beam to pass though unabsorbed leaving dips in the overall Doppler broadened signal. These dips correspond to the atomic transitions within the atom. A typical saturated absorption spectrum is shown in figure 4.19. As well as dips due to the atomic transitions we also observe larger features in between the transitions. These cross-over transitions occur when the laser is tuned exactly between two transitions, at this point an atom moving along the beams can observe a Doppler shift that will bring it into resonance with one transition for a beam travelling in one direction and a different transition for the beam travelling the other way. These cross-over

features are more prominent than the actual atomic resonances because more atoms can interact with the beams in this way. For absorption of the exact atomic transitions the atoms must have zero velocity with respect to the beams so there is zero Doppler effect, however, the cross-over transition can be excited by atoms moving in both directions, the Doppler shift will bring the light into resonance with one transition regardless of the direction of the beam, so more atoms can be involved in absorbing the beams.

Dual Current/PZT Lock

This saturated absorption signal can now be fed into a locking circuit to stabilise the laser. The locking system used here is a top-of-peak locking method, a simplified diagram of the locking electronics is shown in figure 4.20 (this is the locking method for the home-made ECDL's only, the TA-100 has its own built in locking circuit which will be described next). The PZT is modulated by feeding a triangular waveform into the "Ramp in" socket, this allows us to scan across the atomic transition of interest. A sinusoidal dither was applied to the diode current (up to 100kHz) to ramp the frequency of the laser across the peak hyperfine feature that we are trying to lock to. The saturated absorption signal from a photodiode is sent to an amplifier tuned to the dither frequency and then to a phase sensitive detector. A dispersive signal is generated, and can be viewed via the "Signal Monitor" output. Integrating the dispersive signal over a short time base results in a high frequency error signal which is sent to the "current output", integrating over a

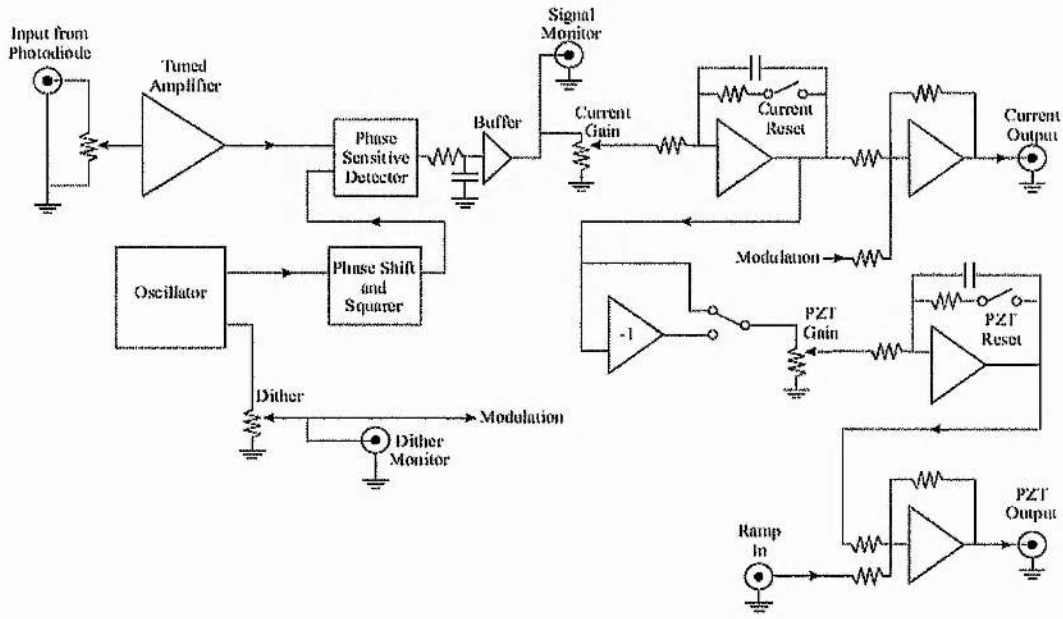

Figure 4.20: Simplified diagram of the dual current/PZT locking electronics.

longer time base gives the dc error term which is sent to the "PZT output". This gives us a method to stably lock the lasers for several hours to one of the atomic transitions. An example of the locking signal generated from the cooling transition is given in figure 4.21, the error signal is a DC value and we lock to the point at zero voltage. A more thorough explanation of the locking electronics can be found elsewhere [5].

Since this method is a peak-locking method we still need to offset the frequency of the laser to the red side (~12MHz) of the cooling transition for creating a MOT. This can be done by passing the beam through an acousto-optic modulator (AOM). The AOM was placed in the saturated absorption setup, not directly in the cooling beam because tuning the AOM has an associated spatial shift which can cause problems with the alignment of the beams at the trap. Placing the AOM in the saturated absorption setup (shown

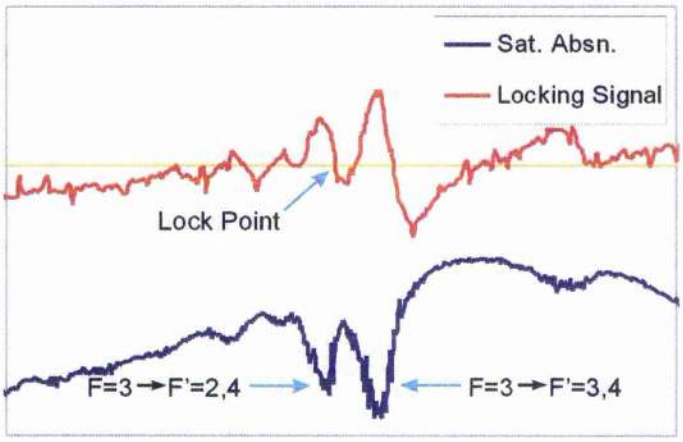

Figure 4.21: Example of the locking signal obtained with the dual current/PZT lock box. The lock point is the crossover point of the dispersive signal (red) with 0V (the orange line), the corresponding saturated absorption signal is shown in blue.

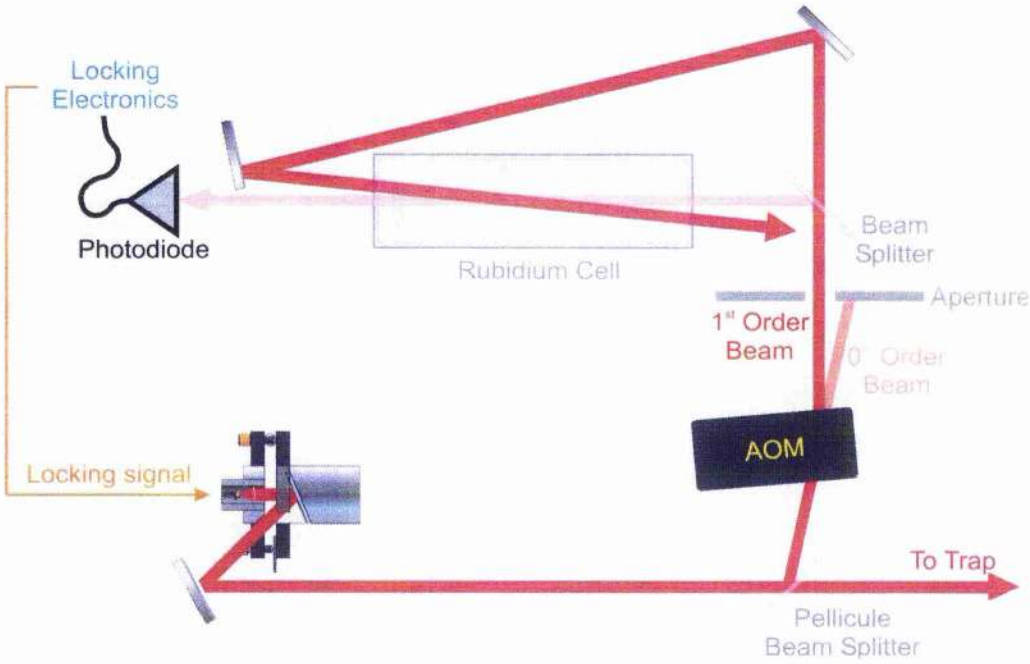

Figure 4.22: Schematic diagram of the experimental acousto-optic modulator setup for the cooling beams. The ECDL is operated at the cooling frequency; the AOM shifts the frequency of the sampled beam to one of the crossover resonances which offer a better signal to lock to.

in figure 4.22) removes the problem of beams shifting whilst tuning the laser, this also negates any loss of trapping power due to diffraction into different orders of the AOM. The AOMs used (Isle Optics, LM080 and Gooch and Housego plc., M080) had a nominal frequency shift of 80MHz with 23MHz tuning either side controlled by the voltage input to the AOM driver. This means it is not possible to lock the laser directly to the cooling transition and use the AOM to provide the small frequency shift required. The cross-over resonances provide much larger signals for locking to and would therefore provide a more stable locking point, ideally it would be best if we could lock to one of these transitions and tune the laser from this lock to the cooling frequency. The D2 transitions are used for cooling ^{85}Rb, shown in figure 4.5, from this diagram it can be seen that the F'= (2,4) crossover transition is of the correct frequency range to be useful with our AOM's. Thus, by locking the laser to the $5S_{1/2}(F= 3) \rightarrow 5P_{3/2}(F'= (2,4))$ line with a 80MHz shift from the AOM we can obtain a frequency at the correct 12MHz detuning for trapping. By changing the control voltage of the AOM we can easily tune the laser around this transition to optimise the trap size.

The TA-100 has a modular control box with its own, optional, locking controls built into the driver; this was a PID (proportional-integral-differential) stabilisation circuit that was automatically fed back to the master laser's PZT and current values, via the scan control (SC110) and current control (DCC110) modules respectively. Whereas the dual current/PZT lock described earlier was locked to an ac error signal (integration gave an error signal around a zero level) the PID lock is referenced to a dc value. This

means the saturated absorption signal had to be carefully isolated from other light sources (an interference filter with transmission at 780nm was used to cut out all other light sources from being detected on the photodiode) to avoid a dc variation which would pull the signal away from the reference level and therefore change the lock point.

The laser is locked by setting a reference level so that it crosses the saturated absorption signal at the desired point, the scan range of the PZT is reduced to zero and the PID regulator module is turned on. The regulator scans the PZT across a set range and stabilises to the point the locking signal crossed the reference level, if the reference level is not found the scan continues to a threshold value and starts again. The PID parameters were set initially by zooming in the PZT scan of the laser to the desired set point and turning the P, I and D values to zero. The PID board is turned on and the Integrator contribution (I) is increased until some feedback is observed in the outputted error signal (it may be necessary to unlock the laser and reset the laser scan to centre on the reference level again as the laser can drift across the desired atomic feature whilst increasing the I value since it is not properly stabilised yet), the proportional (P) and differential (D) levels are then increased until feedback is also seen on the error signal. Once these levels are found the P, I and D controls are turned down about one turn so the laser is less susceptible to jumping across the scan to other points where the reference level crosses. It was found that the factory settings in the PID control board are not adequate for locking to an atomic transition; the scan range and scan limit values (controlled by potentiometers inside the board) are set too high so

when the PID regulator is turned on it scans too fast (and too far, scanning well above the dc level of the saturated absorption signal)) across the signal and misses the lock point reference. This was solved by turning both the scan range and scan limit levels to their minimum values, now the searching scan was made over a much smaller range, the reference level could be found and the laser stably locked.

4.4 Specific Trap Design

The designs of the three traps built for this thesis will now be presented. The uses of each design, the characteristics of the MOTs formed and the reasons for changing the traps will be given. The traps built during this thesis were: a glass trap which allowed all round optical access, a ten-way cross trap based on a standard UHV piece and the drum trap, this also uses a UHV piece as the trap but allows much greater optical access than the ten-way cross.

The MOT produces a cloud of atoms at a temperature of approximately 100μK. During the guiding experiments using the Bessel beam (discussed in chapter 7) we found the dipole potential of the guide was severely limited due to the nature of the beam. In order to improve the effectiveness of the guide a method of further reducing the temperature of the cloud was considered. An extra molasses cycle was established to cool the atoms further; while we were unable to detect consistent cloud temperatures, due to beam variations, the methods used and results obtained are described in the last section.

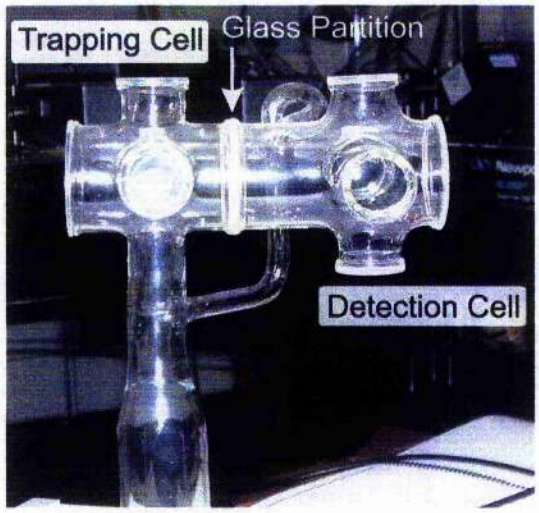

Figure 4.23: A digital photograph of the glass trap.

4.4.1 Glass Trap Design

The first trap used was a two chamber glass trap, based on two six-way cross cells, blown in house by the school's glass blower, Fritz Akerboom. The trap was two glass crosses with 30mm windows on the top and sides with 50mm windows along the horizontal axis, a photograph of the cell is shown in figure 4.23. The glass crosses were joined together at one of the 50mm windows with access between the cells by a 1.5mm hole permitting the guiding of atoms from one cell into a second, "clean," cell for detection. The base of the first cross cell was blown and affixed to a blank flange piece with a hole in the centre to allow access for the sixth trapping beam. The glass was glued to the flange using a two part epoxy (EpoTek H77) which does not outgas in vacuum. The second cell had a narrow tube connection to the blown glass at this flange joint to improve the evacuation of the second cell and maintain it as

a clean cell, both access holes into the second detection cell were considered small enough that the probability of Rb vapour diffusing into the clean cell without the aid of a guide was negligible. This flange piece was then attached to a six-way cross piece upon which the ion pump, turbo-pump connection and getter ovens could be attached.

Operation

Initial experiments with this trap were the guiding of thermal Rb with a Bessel beam, however, the temperature of the atoms was too great to be guided in the beam intensities used so a cold atom source was required. The quadrupole magnetic field for the MOT was created by wrapping ~60 turns of 0.6mm diameter insulated wire directly around the arms of two opposite windows, an extra, shim, coil of ~20 turns was wrapped around the arm of the top window to provide a vertical control on the position of the cloud. The trapping beams were provided by the slave laser for the cooling beams and a simple ECDL for the hyperfine. The cooling beams were sent in perpendicular to the flat window surfaces of the first cell, with the hyperfine being sent along the long axis of the trap angled over the top of the cooling beam mirrors. It was discovered that the hole separating the two cells caused a lot of distortion in the beams passing through it (for the guide beam this was less important as the beam was only required to guide the atoms to the hole not beyond it). Micro-cracks and imperfections created when cutting the hole caused phase and amplitude variations in the beams passing through it; the

end result of this was a large interference effect on the shape of the cloud with the hole itself creating an intensity imbalance in the laser beam and generating a greatly distorted LVIS when the trap was positioned on axis with the hole. Attempts to create a normal LVIS using a black spot in the beam to cover the hole in the glass partition were unsuccessful as the hollow in the laser beam was then too large to create a stable trap in that section of the beam at all.

As a result of these problems it was decided to change the trap design to one built around a stainless steel UHV trapping chamber with a ten-way cross.

4.4.2 10-Way Cross Trap Design

This trap used a ten-way cross UHV piece for the trapping region, six of the flanges around the piece were 70mm diameter; these were used for cooling beam access, four of these flanges had windows attached for cooling beam access, the other two were connected to a 70mm UHV cube with five windows attached, and a standard six-way cross piece for attaching to the other vacuum components. These two components shared a common axis which was used for the final trapping beams. The four remaining flanges on the ten-way cross were 35mm in diameter; these had windows attached and were used as viewports for imaging the cloud with CCD cameras. Imaging the cloud through these viewports offers a less distorted image than in the

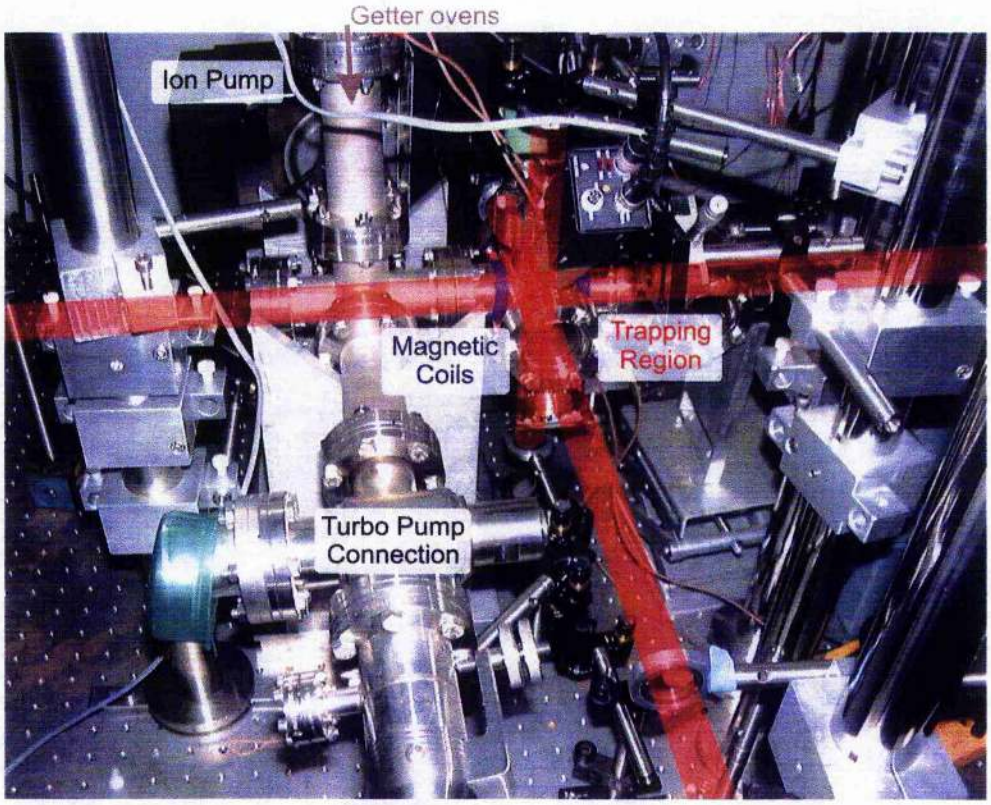

Figure 4.24: A digital photograph of the ten-way trap. The paths of the cooling beams are shown to indicate the trap centre. The cube for extended guiding is just visible to the right of the trapping region, the six-way cross is connected to the getter ovens and the ion and turbo pumps.

blown glass trap as the viewing is accomplished through flat surfaces. A photograph of the trap is shown in figure 4.24, a picture showing just the trapping cell is given in figure 4.25. The five remaining flanges of the UHV cube had viewports attached permitting observation 115mm from the trap centre. The flange separating this from the ten-way cross had a 26mm hole drilled through it to allow beam access along this, long, axis. The six-way cross had a viewport opposite the ten-way cross to continue the optical access along that axis, the other ports had the 40l/s ion pump, an electrical

Figure 4.25: Position of the trapping coils around the ten-way trap. The trapping coil is mirrored on the other side of the UHV piece, the shim coils are only individual coils to provide a 1-dimensional motion (the front and back flanges are open since the piece was removed from the rest of the trap apparatus for the photograph).

feed through for connected to two getter ovens and turbo pump connected to them, with the final flange terminating in a blank.

Operation

The quadrupole magnetic field was created by wrapping two sets of 70 turn coils of 0.6mm diameter insulated wire directly to the arms of the ten-way UHV piece, as shown in figure 4.25. Shim coils to give three-dimensional control of trap centre were added in the same way, by wrapping the wire directly around the UHV piece, because these are only needed to fine tune the position of the cloud only 23 turns of wire were used on two orthogonal

arms. Currents of ~1.4A provided an adequate magnetic gradient for trapping (a trap could be formed using currents below 1A but in these conditions the cloud is not of a practical size). The shim coils were only used to fine tune the position of the trap centre with respect to the optics and therefore only required ~0.5A.

The cooling beams were provided by the slave laser arrangement and a single ECDL was used for the hyperfine beam. The hyperfine was gently expanded over the trap centre and could be introduced to the trap along any axis with no observable difference in trapping, although the orientation would have to be considered if guiding was going to extend outside of the trapping region.

Observation of the cloud was made by CCD cameras looking in through the smaller viewports in the ten-way cross. A short focal length lens (f=38mm or 40mm) was placed as close to the viewport window as possible to image the cloud onto the CCD. Accurate focussing was obtained by placing the CCD camera on an x-translation stage. Although the imaging obtained from the CCD cameras is adequate for observing the fluorescence of the atoms in the centre of the trap, and fluorescing due to the cooling beams, the flange arms used for imaging were too restrictive and prohibited analysis of the cloud outside of a narrow viewing angle seen by the camera (see figure 4.26), the cube piece offers enough optical access for probe beams and detailed study of an atomic flux, however at this time in the experiment we were not in a position to guide atoms far enough to be observed in this region. To improve

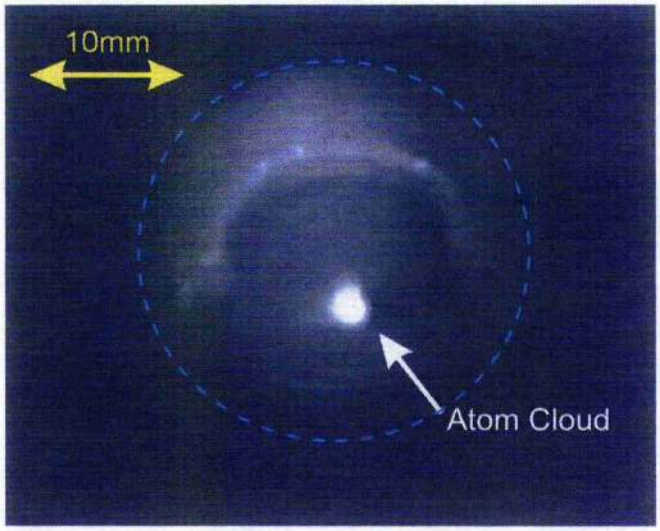

Figure 4.26: Field of view through the ten-way cross viewports. The blue circle shows the view of the inside of the trap, we can only observe up to 10mm from the atom cloud.

optical access for more detailed probing of the atomic flux beyond the trap centre a further trap was designed and built.

4.4.3 Drum Trap Design

The core of the drum trap is a custom built UHV piece; this is a short stainless steel cylinder with two large flanges on the flat face and eight smaller flanges around the circumference, a photograph of this trap is shown in figure 4.27. The large flanges hold 150mm diameter windows allowing a large amount of optical access, permitting access for one of the pairs of trapping beams, various probe beams (absorption and fluorescence imaging could be

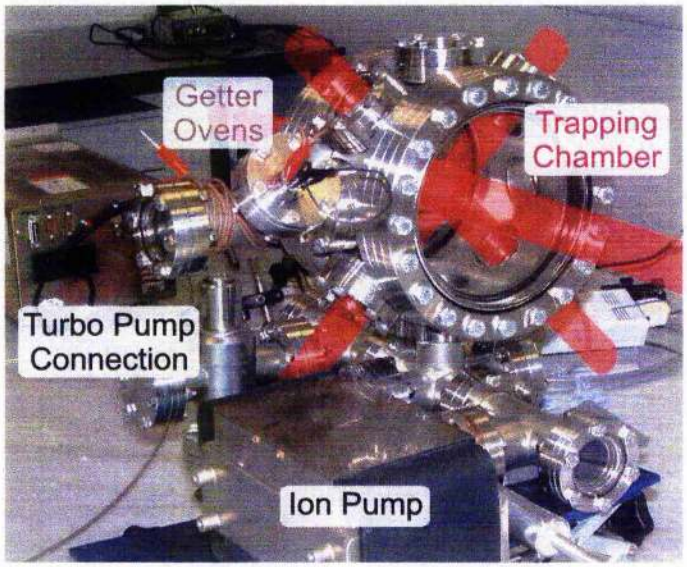

Figure 4.27: A digital photograph of the drum trap. The large front and back viewports afford a large field of view around the cloud. The paths of the cooling beams are shown to illustrate the position of the trap centre. Diagonal beams are used for trapping to allow access for a vertical guide beam. The magnetic coils are mounted on a separate, water cooled, ring and are positioned just inside the bolts of the large windows (see figure 4.28). Here the getter ovens have been positioned next to the trap, initially they were attached to a tee-piece next to the turbo pump connection.

performed up to 50mm below the trap centre) and guide beams and still providing a viewing angle for the CCD camera. Instead of using a single lens to image onto the CCD, as in the ten-way cross, the camera was used with a zoom lens, which allowed much greater control over the focus, size and aperture values of the final image. Seven of the flanges on the circumference had 35mm windows attached with the final flange, at the bottom of the trap (unlike the previous trap, which was used to create horizontal LVIS and guide beams this newest trap is in a vertical geometry letting us drop the ensemble into our guide beams), connecting to a six-way cross piece with connections

to the other vacuum pieces. This six-way cross can be used as a further probe region 150mm below the trap so the vacuum pumps and getters were connected to this via tee-pieces to allow optical access below the trap from four directions. Because this cross piece was the route for Rb vapour to diffuse into the main trapping region the vapour density in this region proved too high to allow probing of atoms dropped or guided into this position, the thermal vapour caused too much scattering of the guided atoms for any to be detected. A further development of this trap was to move the position of the getter ovens onto one of the smaller flanges, on the horizontal, around the drum; this would reduce the diffusion distance to reach the trapping volume and hopefully reduce the amount of hot vapour below the trap and allow detection of guided atoms in the six-way cross. At this time although the atom source has been moved no experiments have been performed to examine guiding at this larger distance.

Operation

The size of the trapping cell has serious implications for the magnetic field, whereas in the earlier traps the coils had diameters of a few cm and were able to be placed within a few cm of the trap centre, we therefore needed only moderate currents of 2 to 3A to generate the required magnetic gradient. The drum trap is much thicker and in order to maintain the optical access though the large viewports the coils were required to be 140mm in diameter, placed 190mm apart around the trap. In order to create the necessary magnetic field

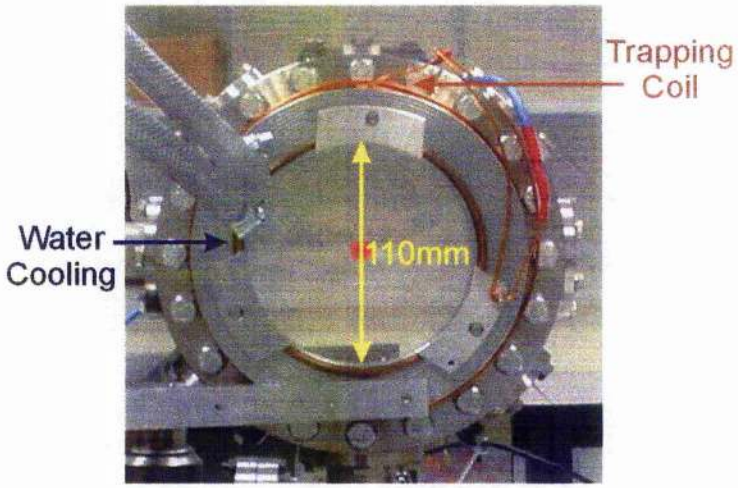

Figure 4.28: Position of the magnetic field coils around the drum trap. We have a field of view of 11cm diameter into the trap, the position of the MOT is indicated by the red spot.

gradient 83 turns of wire were used at currents of ~15A (Kingshill Electronics current supply). Because of the large currents involved the wires become much hotter, the 0.6mm diameter wire is not suitable for these conditions so a thicker core than before was used, 1.5mm diameter insulated wire. Temperature is still an issue because, although the wire can pass the applied currents they still become very hot during operation and necessitated extra cooling of the coil mounting. The coils were wrapped around an aluminium ring, the ring had grooves cut into the aluminium to increase the surface area and aid in cooling, the whole mount then had a copper pipe attached around the outside of it, the pipe was attached to the high pressure (120psi) water outlet and used to water-cool the coil mount. In this way we were able to keep the temperature of the coils below ~35°. A photograph of the position of the coils around the trap is given in figure 4.28.

Trapping beams are generated using the slave arrangement for the cooling beam and single ECDL for the hyperfine as before. The beam alignment is slightly different to allow for the vertical guide arrangement; a retro-reflected beam is sent horizontally through the large viewport and polarised correctly for the magnetic field coils, the other two pairs of beams are sent into the trap at 45°, this leaves the vertical viewport clear for access for a guide beam. Probe beams can be sent into the trap horizontally around the cooling optics in the large viewport or along the small viewports on the horizontal axis, though the latter position limits the probe region to within 10mm of the cloud centre.

In the MOT the cooling cycle produces a spontaneous re-emission of photons by the atoms in the cloud. By measuring the fluorescence of the cloud over a known solid angle, and by dividing this by the emission rate of a single atom the total number of atoms in the trap can be calculated. A 2", f=90mm focal length lens was used to collect the light emitted by the cloud, it was positioned ~180mm from the trap centre, by the small horizontal viewport as shown if figure 4.29, and the focused light was collected on photodiode. A black cardboard tube was placed around the lens and photodiode to stop stray light entering the photodiode. The level of fluorescence was measured by comparing the photodiode voltages of the trapped atoms with a background signal. The background signal was taken with the cooling beams on but with the magnetic coils turned off; this was done because the background vapour in the trap will also fluoresce in the cooling beams and this background level also needs to be eliminated from the voltage level of the photodiode (the

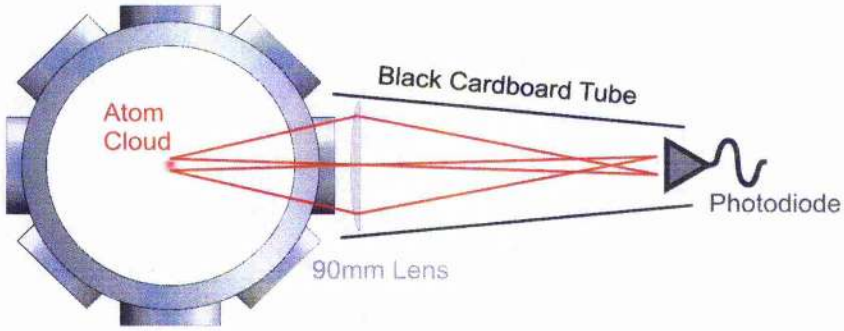

Figure 4.29: Diagram of the setup for measuring the fluorescence of the cloud, and therefore the number of atoms in the trap.

background fluorescence does change slightly with the magnetic fields off, because of the Zeeman effect, but the total change is negligible compared to the fluorescence of the cloud). Calibration of the photodiode was achieved by illuminating the photodiode with a fraction of the cooling light of known power and relating this to the photodiode signal, thus a difference in power between the cloud being present and the background level can be found. This power is the value over a fraction of the total solid angle, thus a simple calculation will provide the total power emitted over all space and the total number of photons emitted per second. The scattering rate (number of photons scattered per second) of single atoms is given by [6]:

$$R = \frac{(I/I_{sat})\Gamma/2}{1+(I/I_{sat})+4(\Delta/\Gamma)^2} \qquad (4.2)$$

where I is the total intensity of the illuminating beams (the cooling beams) I_{sat} is the saturation intensity of rubidium (1.63 mW/cm^2), Γ is the natural linewidth of the transition (2π x 6.1 MHz) and Δ is the detuning of the illuminating light from resonance. Cloud sizes for this trap were found to be about 2x10^7 atoms.

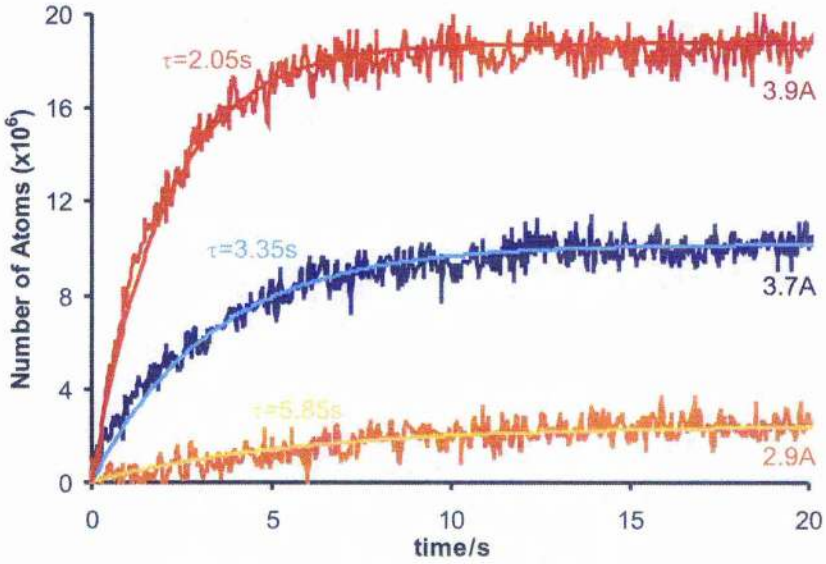

Figure 4.30: Cloud size as a function of time. The results are for the getter currents indicated; the recorded photodiode values are given by the darker lines, the lighter lines representing a theoretical fit to the data using equation (4.3). The trap filling time, τ, decreases as the background vapour level increases.

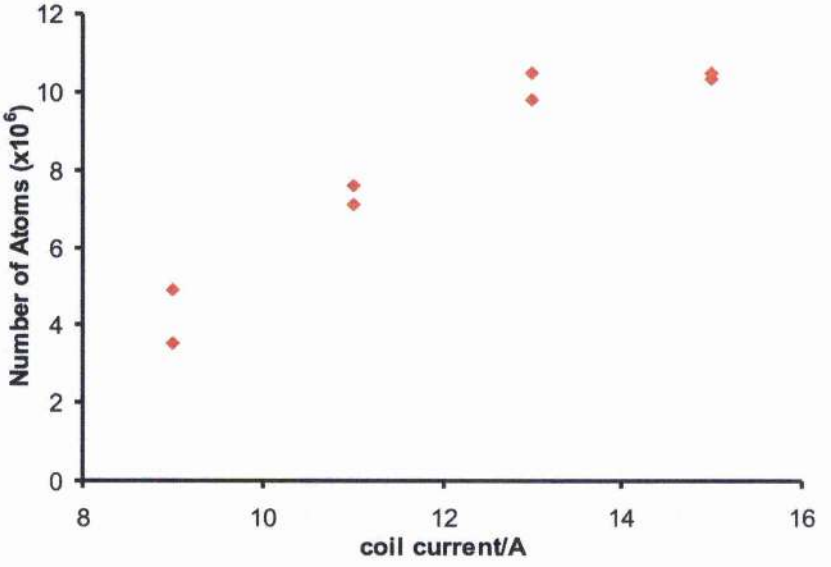

Figure 4.31: Final cloud size as a function of the magnetic coil current. The points are plotted with respect to the current through one of the coils, the second coil was set to keep the position of the trap constant throughout; since the trap was not in the exact centre of the magnetic coils, the second coil deviated from the given value by ~20%.

By recording the build up of the fluorescence signal on a digital oscilloscope (Tektronix TDS360) we can also measure the trap filling time. When the trap is turned on the number of atoms build up in an exponential form, similar to that of a capacitor charging, and can be described by:

$$N(t) = N_0(1 - e^{-t/\tau}) \qquad (4.3)$$

where τ is the time constant for the trap filling time (it is also the average time a single atom will remain in the trap). The filling time of the trap was explored by increasing the getter oven currents, releasing the Rb at different rates and thus changing the background vapour pressure in the trap. Graphs showing the number of atoms and the filling times for given getter currents are shown in figure 4.30. The effect of the magnetic coil current on the size of the cloud is given in figure 4.31. The higher magnetic gradients increase the positional dependence of the atoms giving a tighter confinement but this also reduced the size of the MOT.

Molasses Experiment

In order to increase the effectiveness of the optical guides used an experiment to reduce the temperature of the atoms by way of an extra cooling cycle was attempted. A molasses cycle is applied over only a few tens of ms before the cloud is finally released. The cooling beams are shifted in frequency further to the red of the transition and reduced in power for a few ms, then the magnetic field is extinguished until finally, after another few ms,

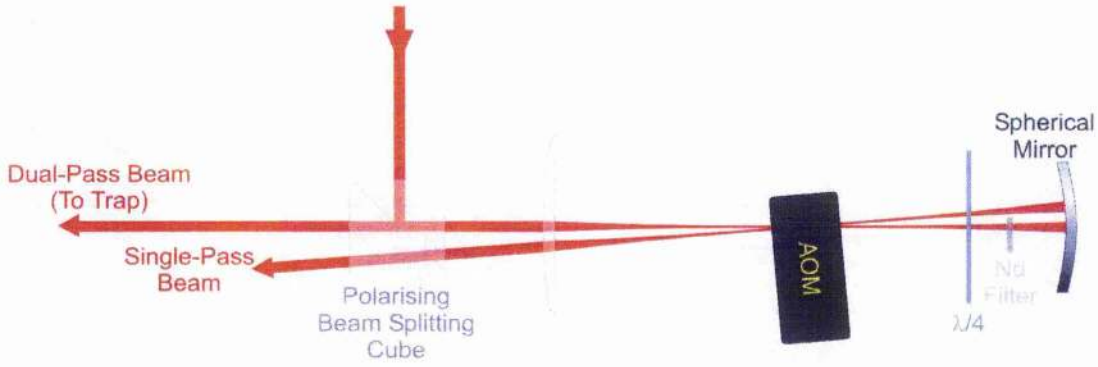

Figure 4.32: Experimental setup of a dual-pass AOM. The dual-pass beam is diffracted away from the straight through beam on the first pass of the AOM and is diffracted back onto the original beam path at the second pass. The λ/4 plate allows separation of the input and output beams at a polarising beam splitting cube. The straight through beam, unshifted in frequency, is reduced in intensity by a nd filter to ensure it has a negligible effect whilst trapping the atoms with the dual-pass beam and still offers reduced power when the AOM is turned off for the extra cooling cycle.

all the beams are turned off and the cloud is allowed to fall. The exact delays for each of these sections were varied between 0 and 40ms.

The frequency of the light is again controlled by an AOM, this time we want to change between two values of the detuning without changing the alignment of the laser beams. This can be achieved by using a dual-pass system as shown in figure 4.32; light passing through the AOM is diffracted different amounts depending on the change in frequency required, effectively steering the beam from a pivot at the AOM, by sending the light onto a spherical mirror placed at twice the focal distance from the AOM we can reflect the beam straight back along the same path. Once again the light is frequency shifted and deflected by the AOM, the end result is a beam propagating straight back

along the path of the incident beam to the AOM but which is frequency shifted by twice the single pass frequency. The incident and shifted beams can then be separated by using a polarising beam splitter and a quarter-wave plate placed in front of the spherical mirror.

For the purpose of locking the laser a suitable feature is required between 114 and 206 MHz away from the cooling line (twice the frequency range of our AOM's), this means we lock the laser in the far from resonance position and use the AOM to bring the beam to the cooling frequency, for the extra cooling cycle all we do is turn the AOM off. In this case the straight through beam of the AOM has a neutral density filter placed in the beam so the final power of the undiffracted beam – the beam at the molasses frequency – has a lower power than the diffracted, cooling beam. The frequency considerations of the AOM do not correspond to any of the ^{85}Rb transitions (see figure 4.5), however, the other isotope of rubidium, ^{87}Rb, has crossover resonances at 212 and 133.5MHz (for the F= 2→F'= (1,3) and F=2→F'= (2,3) crossover transitions respectively). An energy level diagram for ^{87}Rb is given in figure 4.6, and a typical saturated absorption signal is shown in figure 4.33. The MOT requires the cooling beams to be tuned 2Γ from resonance (~12MHz) so the larger frequency shift of the F→F'= (1,2) was chosen to lock to as it gives the greatest frequency shift and could still be brought onto the cooling frequency with the AOM. This means locking the probe and hyperfine lasers to different frequencies as well, the hyperfine is locked to the features of the F= 1→F'= 2 hyperfine transition in the same manner as before but the probe laser needs to be locked to the F= 2→F'= (1,3) transition as this is the only

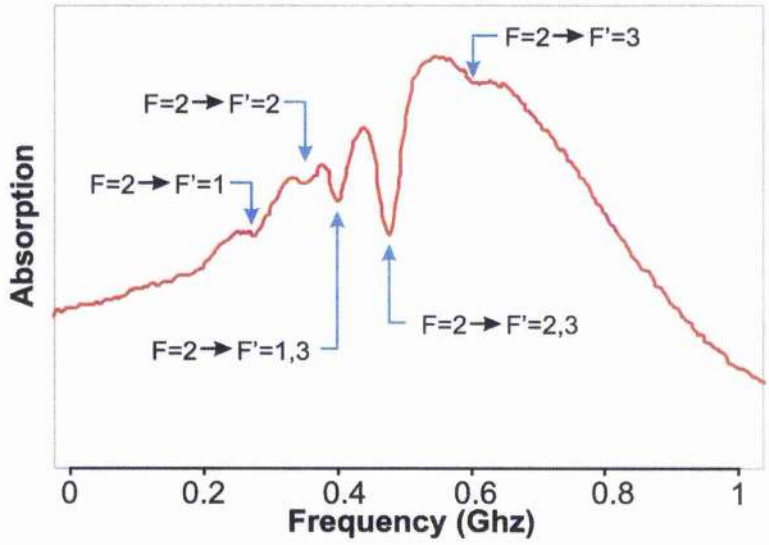

Figure 4.33: The saturated absorption signal for the ^{87}Rb F=2→F' transitions.

feature that can be frequency shifted with the AOMs to hand. This also requires a double pass though the AOM, but because the frequency is not switched, i.e: the zeroth order beam is not used, the use of a spherical mirror is unnecessary.

The double pass through the AOMs has a very low overall efficiency; we recorded an efficiency of only 10% in the required output. Because of this the tapered amplifier laser was used for the cooling beams to ensure enough power arrives at the trap.

Alignment of the cooling beam is critical in this experiment as any deviation in the beam direction when switching the frequency of the cooling beams will distort or move the position of trap centre. To aid the alignment of the dual pass spherical mirror an Ultima mount (Newport, U100-A) with precision actuator screws on all three pivot points was used, this allowed not only

control over the angle of the mirror but, by moving all actuators in synch, control over the z-position of the mirror in the beam, improving our ability to position the focus of the mirror at the correct position on the AOM.

If a molasses cycle is successful the signal of a dropped cloud though a probe beam will be narrower as the atoms are cooler and, therefore, the cloud does not expand as fast. Unfortunately, we were unable to consistently generate these cooled signals. To calibrate our molasses cycle a weak absorption probe was aligned 5mm below the MOT. The exact timing of the frequency shift and magnetic field shut off was varied up to 40ms before the cooling beams were extinguished and the atom cloud is allowed to fall. While we were unable to reproduce the results over several days figure 4.34 gives examples of the increase in the absorbed signal measured 5mm below the MOT as we increase the time of the optical molasses, the magnetic field is turned off when the cooling beams are finally extinguished. The largest signal was recorded with a 8ms molasses cycle, the number of atoms detected is increased by a factor of 4. The narrowing of the signal corresponds to a temperature reduction from ~160μK to 36μK, using a time of flight analytical model as a fit [7].

We believe the lack of consistency is because of alignment issues with the dual pass AOM and the subsequent crossover of the different frequency beams in the trap centre, a slight interference effect in the output of the tapered amplifier beam may also have contributed to this. If the interference pattern is altered upon passing the AOM then the intensity profile in the trap centre will change and distort the MOT during the molasses cycle.

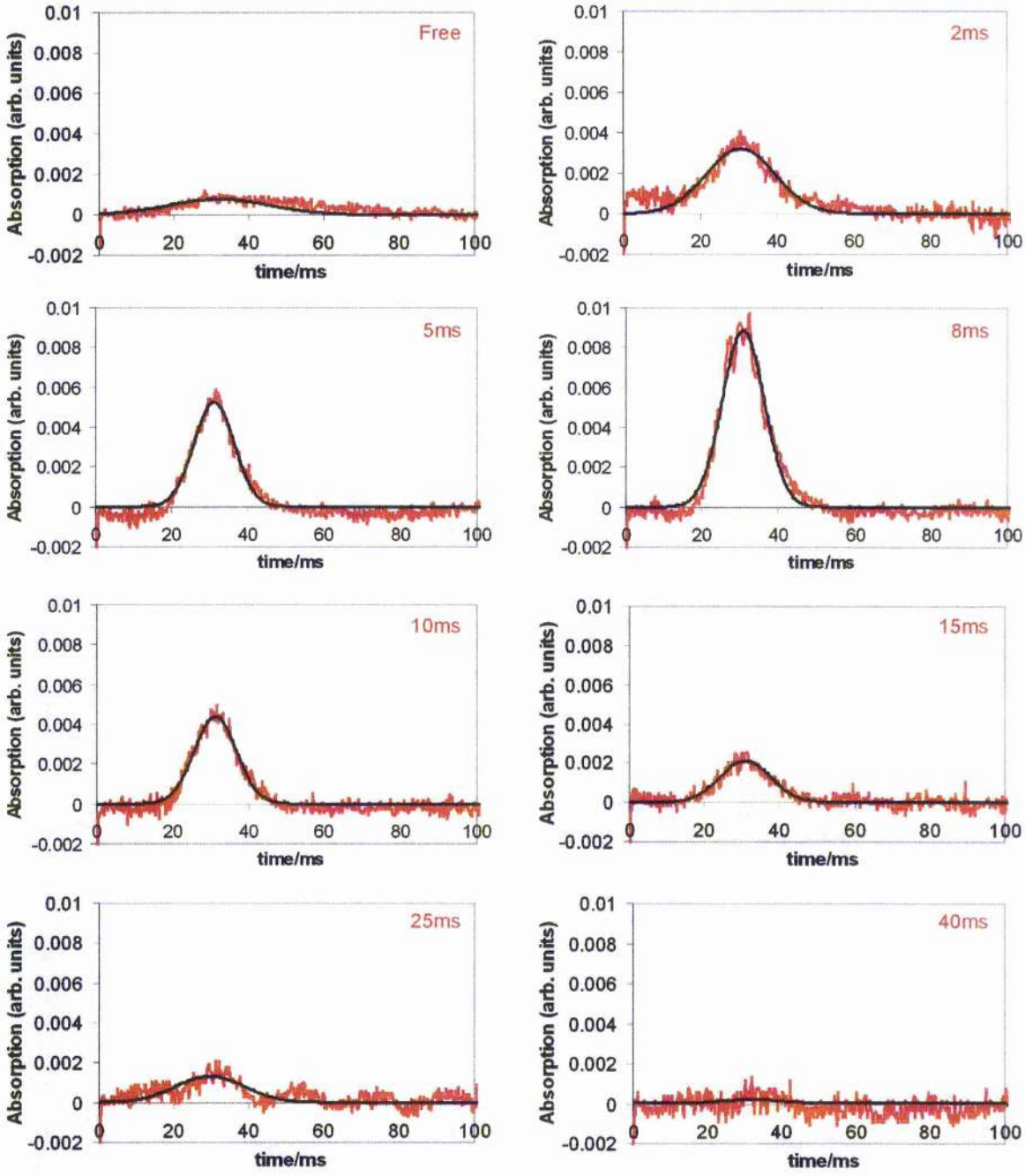

Figure 4.34: Increasing the length of the molasses cycle. The optimum length of the molasses cycle is ~8ms before the beams are extinguished. The width of the signal at this point is less than half that of the free falling cloud. The black line is a best fit Gaussian.

4.5 Summary

We have designed, built and characterised three different MOTs in order to exploit a variety of different geometries. The first was the glass trap which was ultimately discarded because the aperture separating the two cells prevented the formation of a stable LVIS. The second trap was the ten-way cross trap, in this an LVIS could be generated and this MOT was used for the guiding of a cold atomic beam in chapter 6. The drum trap was the final MOT built and allowed optical access to probe beams guided over 5cm. This trap was used for the dropped MOT experiments in chapters 7 and 8 and is the trap currently in use at St Andrews.

Several laser systems have been used to provide the beams for trapping and guiding the atoms. The main laser used in the trapping of the atoms has been the home-made ECDLs (though a commercial system, the TA-100, was used when more power was required in the molasses experiments), these were then stabilised to the atomic transition using a combined current/PZT locking circuit also built in-house. A Ti:Sapphire laser was used as a guide beam; the power and tuning characteristics have been carefully categorised as the use of blue-detuned guides allows the laser to be tuned very close to resonance, a difference of 2GHz could be the difference between a red- or blue-detuned guiding regime.

Finally a molasses cycle for cooling ^{87}Rb to ~36μK was incorporated into the drum trap. Whilst we achieved some success and were able to observe an

increase and narrowing of the detected flux signals using this system we were unable to consistently create the molasses temperatures and due to time constraints it was decided to abandon their use for the experiments described in this thesis.

Bibliography

[1] M. W. Fleming and A. Mooradian, "*Spectral characteristics of external-cavity controlled semiconductor lasers*," IEEE Journal of Quantum Electronics **QE-17** 44 (1981).

[2] M. A. Clifford, J. Arlt, J. Courtial and K. Dholakia, "*High-order Laguerre-Gaussian laser modes for studies of cold atoms*," Opt. Commun. **156** 300 (1998)

G. P. T. Lancaster, W. Sibbett and K. Dholakia, "*An extended-cavity diode laser with a circular output beam*," Rev. Sci. Instrum. **71** 3646 (2000)

[3] "*TA100 Tapered Amplifier Diode System User's manual*" TUI Optics (now Toptica)

[4] "*Model 3900S, CW Ti:Sapphire Laser User's Manual*," Spectra-Physics.

[5] G. P. T Lancaster, "*Experimental Studies of Diode Lasers and Cold Atom Guiding*," PhD Thesis, University of St Andrews (2001)

[6] H. J. Metcalf and P. van der Straten, "*Laser Cooling and Trapping*," Springer-Verlag Inc., pages 219-229 (1999).

[7] T. M. Brzozowski, M. Mączyńska, M. Zawada, J. Zachorowski and W. Gawlik, "*Time-of-flight measurement of the temperature of cold atoms for short trap-probe distances*," J. Opt. B: Quantum Semiclass. Opt. **4** 62 (2002)

Chapter 5:

Hollow Beams for Atom Guiding

5.1 Introduction

The spatial structure of a laser beam can be described using transverse and longitudinal modes. In this work we are interested in the transverse mode of the laser beam since we desire the beam cross-section to be an annulus of light for blue-detuned guiding of atoms along a dark core. Most lasers typically operate in the fundamental transverse mode (TEM_{00}) producing a Gaussian profile as the output. In this chapter we will look at the properties of two types of beam that produce either a circular symmetric ring of light around a dark centre; a Laguerre-Gaussian (p=0) beam, or an array of rings; Laguerre-Gaussian ($p\neq0$) and Bessel beams, and examine some of the

methods for generating these beams from the conversion of the Gaussian mode output of a laser.

Transverse laser modes are generally described by the product of two independent Hermite polynomials with a Gaussian, and are known as Hermite-Gaussian (HG) beams. This is one solution to the free-space paraxial wave equation which has a rectangular symmetry. HG modes are characterised by two integer subscripts *m* and *n*, which give the order of the polynomial in the x- and y-directions and correspond to the number of nodes in the electromagnetic field in those directions. Examples of these HG modes are shown in figure 5.1(a) and 5.1 (b). HG modes are also known as TEM_{mn} modes with the indices again corresponding to the number of nodes in the x- and y- directions. The fundamental, Gaussian, output of a laser is the TEM_{00} mode. The transverse mode structure remains constant along the propagation direction of the beam.

5.2 Laguerre-Gaussian Beams

The HG modes are described using Cartesian co-ordinates and result in transverse modes with rectangular symmetry. An alternative, but equally valid set of solutions to the paraxial wave equation is to use cylindrical coordinates, which produce solutions with radial symmetry. This basis set of solutions are called Laguerre-Gaussian (LG) modes, and are similarly described by a single Laguerre polynomial with the superscript l and the subscript p. The index l

gives the number of 2π phase cycles around the circumference of the mode while p+1 gives the number of rings in the mode profile. The electromagnetic field amplitude of the mode LG_p^l is given by:

$$u_p^l = \sqrt{\frac{2p!}{\pi(p+|l|)!}}\frac{1}{w}\left(r\frac{\sqrt{2}}{w}\right)^{|l|} \times L_p^{|l|}\left(\frac{2r^2}{w^2}\right)e^{\frac{-r^2}{w^2}}e^{\frac{-ikr^2}{2R}}e^{-i(2p+|l|+1)\arctan\left(\frac{z}{z_R}\right)}e^{-il\phi} \qquad (5.1)$$

where L_p^l is the generalised Laguerre polynomial, the other terms follow the standard definitions for Gaussian beam parameters:

spot size $$w(z) = w_0\sqrt{1+\left(\frac{z}{z_R}\right)^2} \qquad (5.2)$$

wavefront curvature $$R(z) = z\left(1+\left(\frac{z_R}{z}\right)^2\right) \qquad (5.3)$$

Rayleigh range $$z_R = \frac{\pi {w_0}^2}{\lambda} \qquad (5.4)$$

where z is the distance from the beam waist, r is the radial distance from the beam axis and λ is the wavelength. The spot size, $w(z)$, is the radius at which the Gaussian term falls to $1/e$ of its on-axis value, w_0 is this value at the beam waist and the Rayleigh range, z_R, is the propagation distance from the waist at which the area of the beam has doubled. The Gouy phase, $\Psi=(2p+|l|+1)\arctan(z/z_R)$, is the phase shift a Gaussian beam undergoes compared to a plane wave as it passes though a focus. The intensity profiles of some example LG beams are shown in figure 5.1(c) and 5.1(d).

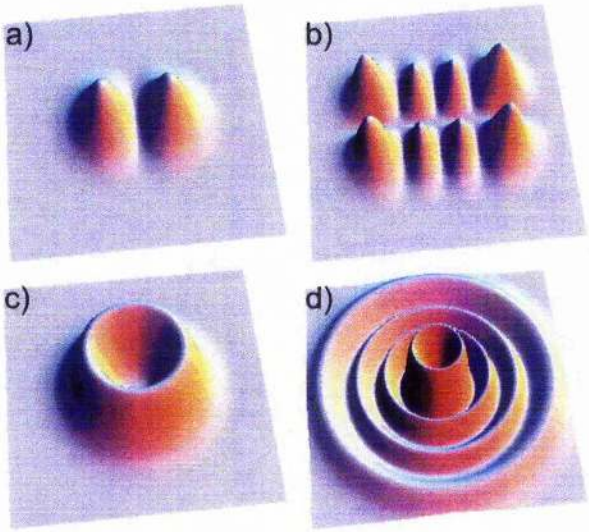

Figure 5.1: The intensity distribution of a Hermite-Gaussian mode m=1, n=0 (a) and m=3, n=1 (b), and of Laguerre-Gaussian modes l=2, p=0 (c) and l=2, p=3 (d).

The phase structure around the circumference of the beam is described by the $e^{-il\phi}$ term in equation (5.1) which results in a phase singularity (where all phases are present) at the beam axis and thus leads to a zero field in the centre of the beam. For an azimuthal index l=0 then there is zero phase change around the circumference of the beam and the innermost ring fills in to produce an on axis spot. Increasing the value of l >0 produces a phase change around the ring (phase structure =$2\pi\, l$) leading to a hollow beam profile. Higher azimuthal index beams have a greater number of phase changes at the singularity and larger hollow regions in the centre of the beams. LG beams have a characteristic helical wavefront due to this phase change in contrast to the plane wavefronts of an HG mode, (figure 5.2). For the guide beams that concern us in this thesis we are only interested in a

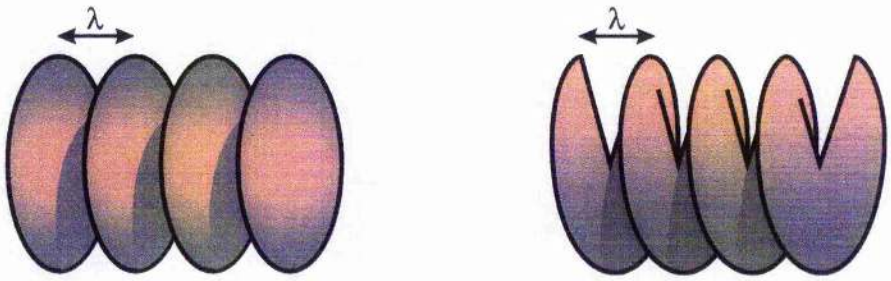

Figure 5.2: Phase structure of a TEM_{00} and LG mode. A normal TEM_{00} beam (left) is a series of plane wavefronts, the LG beam (right) has helical wavefronts. The beams are propagating horizontally.

single tube of light, i.e: p=0. For LG beams with p=0 and l >0 the beam forms a single ring with its maximum intensity at:

$$r_l = w(z)\sqrt{\frac{l}{2}} \tag{5.5}$$

The higher azimuthal index beams also have a narrower annulus of light; this results in a steeper gradient between areas of high and low intensities in the beams and has the effect of creating a higher dipole potential for guiding. Taken on its own this should lead to higher index beams offering more desirable properties for guiding atoms or particles, however, increasing the azimuthal index causes the peak intensity of the LG beam to fall rapidly and for the beam to diverge faster than a lower index beam of equivalent ring diameter. Thus high index beams are better at compressing and focusing over shorter distances because the higher potential at the beam waist (focus) will better contain atoms, which have gained transverse momentum as a result of oscillating between the walls of the LG beam [1]. Figure 5.3 shows the dipole potential as a function of propagation distance for l=1 and l=4 LG beams. The

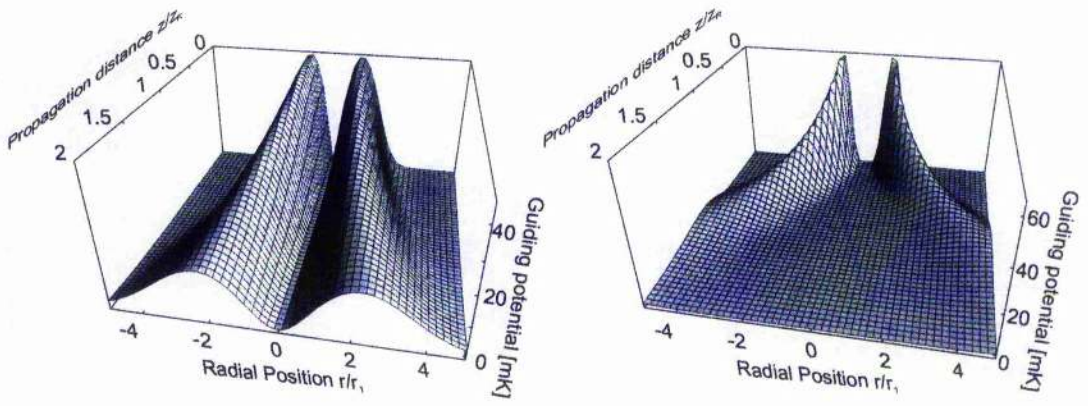

Figure 5.3: Dipole potential of l=1 (a) and l=4 (b) Laguerre-Gaussian beams. The dipole potential increases with higher index beam but also become more divergent. Note the difference is vertical scales between the two plots.

azimuthal phase also gives rise to a well defined angular momentum of $l\hbar$ per photon in addition to any momentum the light may posses due to its polarisation state. This can be of interest for momentum transfer onto atoms [2], however, in this thesis we are attracted to the LG beam purely in regard to the intensity profiles that can be created by increasing the azimuthal index, not for any intrinsic properties of the phase structure.

The LG beam, as a free-space solution to the paraxial wave equation, only diffractively expands as it propagates (in the same way as a HG beam does), thus the profile of a guide beam will remain constant and the hole in the beam remains through a focus. This can be of use when guiding atoms over extended distances; several of the hollow beams used for atom guiding are generated using fibres and axicons (see chapter 3 for examples), these beams maintain their shape only over limited propagation distances, in contrast to the LG beams.

5.3 Generating Laguerre-Gaussian Beams

Whilst Laguerre-Gaussian beams are a suitable solution to the free-space wave equation they are not usually generated as transverse modes within a laser cavity. Asymmetries within the cavity such as Brewster windows give rise to rectangular symmetry which results in Hermite polynomials providing the best solution for the laser beam. Modification to the laser cavity, such as the insertion of crossed wires, can force the laser to generate high order HG modes, however, the cavity losses for the LG mode are much higher ensuring that the HG modes lase. High order HG modes can be converted to an LG mode by a cylindrical lens mode converter. Two cylindrical lenses at the correct position around the focus of the beam introduces a π phase difference (the Gouy phase term) between two orthogonal HG modes resulting in an LG beam [3]. Central to using this technique is the ability to generate high order HG modes within the cavity, which is impractical for many laser designs, especially diode lasers and the Ti-Sapphire laser used for these experiments. Instead we must convert the fundamental output, TEM_{00}, of the laser using external optical elements. There are two main techniques for generating LG modes from a TEM_{00} beam: the use of computer-generated holograms [4] and spiral phase plates [5]. In this thesis we have made use of both of these methods to generate the LG beams required, the different methods used will now be described.

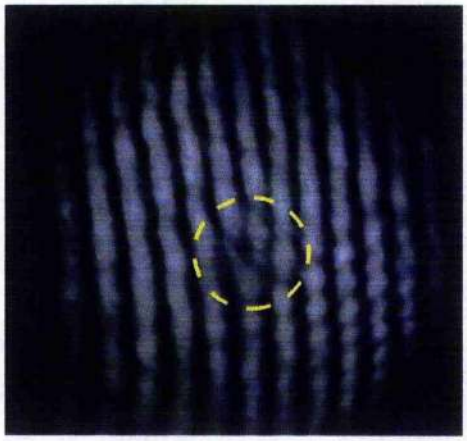

Figure 5.4: The interference pattern of an l=1 LG beam with a TEM_{00} beam. The dislocation in the grating pattern is indicated by the yellow circle.

5.3.1 Generation with Holograms

Essentially a hologram is the recording of an interference pattern between the beam of interest with a simple reference, illuminating the recorded interference pattern with the reference beam reconstructs the beam of interest in the diffracted light. In the case of a LG beam with a TEM_{00} reference beam the pattern takes the form of a simple grating with a number of dislocations equal to the index of the LG beam, l, producing a forked pattern in the centre of the grating. An example of the interference pattern between an LG and TEM_{00} beam is shown in figure 5.4. Illuminating a hologram of this type with a TEM_{00} beam results in a screw phase dislocation being applied to the incident beam, this results in the characteristic, $e^{il\phi}$ phase structure required and gives an annular intensity pattern in the far field.

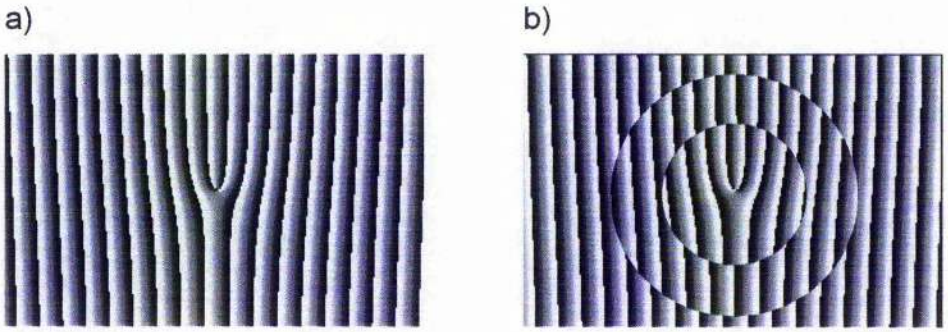

Figure 5.5: The holographic patterns used to produce Laguerre-Gaussian beams. The modes of the beams are (a) *l*=2, *p*=0 and (b) *l*=2, *p*=2. The phase shift applied to the incident light is 0 to 2π going from black to white.

For a binary forked grating the boundaries between the transparent and opaque areas of the hologram are given, in polar co-ordinates, by the formula [6]:

$$l\frac{\phi}{\pi} = n + \frac{2r}{\Lambda}\cos\phi \qquad (5.6)$$

where Λ is the grating period and n=0, ±1, ±2... Efficiency of the holograms can be increased by converting them into phase holograms; by adding a blaze to the pattern the power into a chosen diffracted order can be maximised. Examples of these holograms are shown in figure 5.5.

To generate LG modes with p>0 a circular discontinuity can be introduced around the forked dislocation of the hologram, about which the phase is changed by π (see figure 5.5b); higher p modes are generated simply by adding additional circular discontinuities of larger radius [7].

The first LG holograms used were manufactured in house [6] and were generated using the above equations to define the grating. The pattern was

printed onto standard holographic film (Edmund Scientific Ltd.) which was then developed and placed in a mount creating a slide to be used as a transmission hologram which could be placed into the TEM_{00} output from our guide laser. The desired LG beam is found in the first diffracted order through the hologram. Efficiency of these holograms is ~40% of the incident power diffracted into the first order. The azimuthal index of the diffracted beams increases as a multiple of the diffracted order $l_n = nl$ (where n is the diffracted order and l is the nominal order of the hologram), thus the second order diffraction produces LG beams of azimuthal index of $2l$, third order of $3l$ and so on. Higher efficiencies than those achieved using these holograms are possible by using specialist holographic glass plates, but not by using the simple techniques utilised in the creation of these holograms.

In order to obtain higher efficiencies a different method of hologram production than could be made in house was required. The Universität Erlangen (Germany) provided the etched glass holograms that would produce the high efficiencies desired. These holograms essentially use the same design parameters as before to produce a dislocated grating, the etching process is slightly different to the blazing of the previous holograms but produces similar results. This opened up the possibility to create high efficiencies, of up to 90%, into the required diffracted order. The holograms are etched into the glass substrate in 8 discrete levels to create a phase transmission hologram. The first holograms purchased from Erlangen offered ~50% efficiency, better than our photographic film based holograms, but, unfortunately, before they could refine the manufacturing process and get

closer to the theoretical efficiencies technical difficulties with their etching machine meant they were unable to provide any further holograms after the prototypes.

The static holograms described above are not the only way to sculpt the mode of a HG beam into a LG beam, recent advances in spatial light modulators have resulted in the ability to generate dynamic computer controlled holograms which can then be modified in real time.

Spatial Light Modulators

A spatial light modulator (SLM) can be considered as an array of discrete pixels (similar to a LCD screen), where each pixel acts as a variable wave plate. There are two basic types of devices, which can act as phase or amplitude modulators; these are nematic and ferroelectric liquid crystals (FLCs). Nematic SLMs are slow speed devices, FLCs are considerably faster but are limited to producing only binary holograms (there are only two, discrete, modulation levels, e.g. a phase change of only 0 and π). The individual pixels can also be addressed in one of two ways; electrically or optically. Electrically addressing involves locally isolating the pixels, in the same way as an LCD screen, which leads to an inherent pixelisation of the image and diffraction of the light from the grating-like nature of the pixel array leading to unwanted noise in the final beam, optically addressing the SLM removes this pixelisation but adds further complications to the device as extra imaging optics are required to actually address the SLM module. In this

thesis we have used programmable phase modulators only, which will be described here.

The SLM can encode an input light beam with a phase structure such that it produces the desired output beam. Hence the output from the SLM can be given by [8]:

$$A(r) = A_0(r)e^{i\psi(r)} \tag{5.7}$$

where $A_0(r)$ is the complex amplitude of the incident beam, and $e^{i\psi(r)}$ is the phase term that we modulate using the SLM. In the case of the Laguerre-Gaussian beam the phase of the beam is known as $e^{il\phi}$, where l is the azimuthal index and ϕ is the azimuthal angle. By encoding this phase pattern onto the SLM we can create LG beams of any index. The pattern displayed on the SLM is controlled from a computer; the hologram can be displayed by the computer as a grey-scale image, with white and back corresponding to 0 and 2π phase shifts respectively (the exact phase calibration of the device is set by controlling the voltage applied across the SLM pixels). The hologram designs are the same as for the static holograms; see figure 5.6 for an example of one of these holograms and the image it creates. The computer control of the image sent to the SLM screen permits a rapid change of design to the hologram allowing an iterative "clean-up" method to be performed for optimising the hologram designs and permitting the use of many holograms in the same experimental set up without any further alignment issues. Computer control also opens the possibility for creating dynamic holograms that change shape in real time over the course of an experiment, controlling the motion of

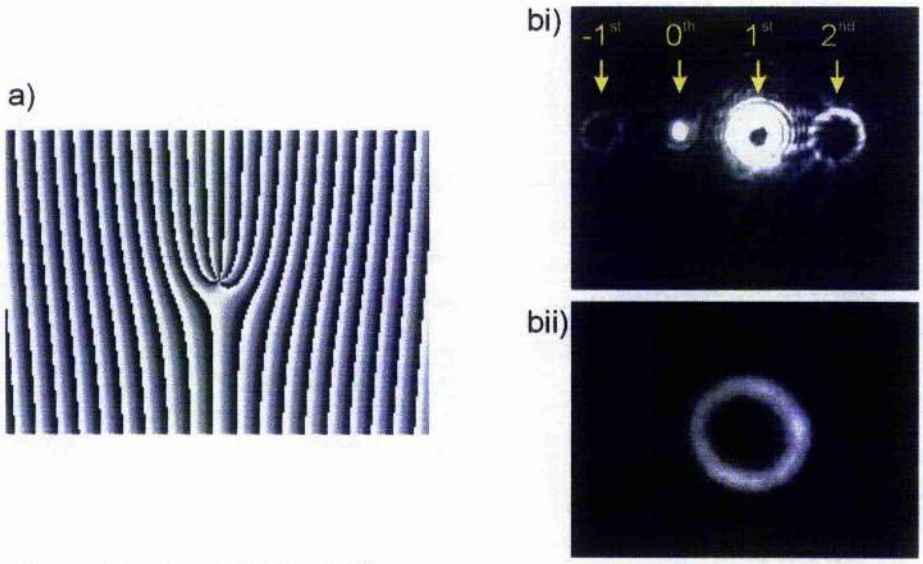

Figure 5.6: A detail of the LG^{5}_{0} hologram projected onto the SLM is shown in (a). The reflected beam produced (bi) is a diffraction pattern, the 1st order beam is the desired mode and had most power diffracted into it due to the blaze on the hologram, the higher diffracted orders give a higher order LG beam. The interference seen around the 2nd order beam is due to overlapping of adjacent modes, this can be removed by decreasing the grating separation at the expense of the efficiency of the hologram. A filtered image of the 1st diffracted order is given in (bii).

the atoms to an even greater extent with ensembles of atoms being manipulated around circuits, as in the magnetic conveyor belt [9], or separated and recombined for interference experiments, in a similar manner to the splitting of a dipole trap demonstrated by Shin *et al* [10]. However, current technology limits the refresh rates of nematic, phase SLM devices to a few tens of Hertz, this is too slow for atomic experiments where atoms can escape the potentials created in between the frames (dynamically changing holographic patterns have be applied successfully in the field of optical tweezers [11, 12] using these devices). Refresh rates of several kHz are

required before the optical potentials can be modified without excessive loss of atomic flux during these field refresh times. FLC SLMs (producing binary holograms) can be refreshed at kHz rates and work towards the manipulating BEC within arrays of microtraps has been performed using these devices [13]. The binary nature of the FLC devices results in a significant degree of inefficiency and loss of power. However, manipulation of BEC requires much lower potentials compared to the work described here using cold atoms from a MOT.

In this thesis we have used a Hamamatsu X8267 SLM for shaping our Ti:Sapphire guide beam. This is an optically addressed nematic liquid crystal SLM with an active area of 2x2 cm, made up from an array of 768x768 pixels, a diagram of the SLM is shown in figure 5.7. A laser diode writes the image onto the LCD screen, this display is transferred to the SLM by a set of coupling lenses to remove the pixelisation of the image. The SLM reads data as if it was a second monitor to the controlling computer, therefore a simple greyscale image is displayed on the SLM, with black and white pixels corresponding to 0 and 2π phase changes respectively. The SLM can be operated in both phase and amplitude modulation regimes. Operation of the SLM for phase modulation requires the incident light to be polarised in the direction of the axis of the liquid crystals in the SLM (if the liquid crystals are aligned at 45° to the beam polarisation the SLM operates as an intensity modulator). The SLM acts as a reflective hologram, the incident light should be a linearly polarised plane wave that illuminates the whole of the active area at normal incidence; the reflected beam will then have the properly encoded

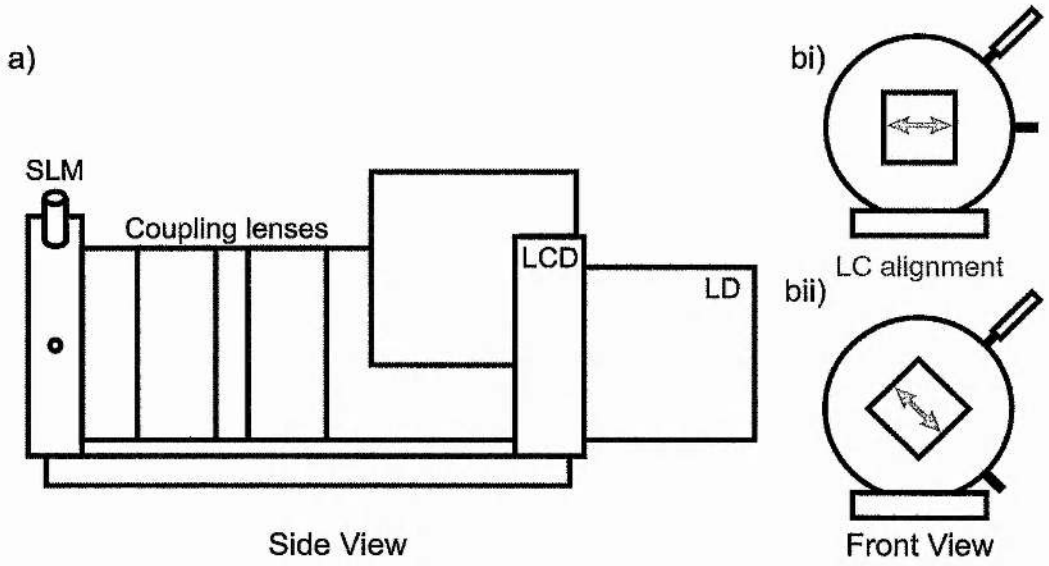

Figure 5.7: A schematic of the Hamamatsu X8267 SLM. LD is the laser diode for writing the image to the LCD screen. This is focused onto the SLM itself by means of a pair of imaging lenses. The LCD screen is 1024x768 pixels whereas the SLM is only 768x768, therefore, there is clipping at the edge of the computer screen image sent to the SLM. When illuminated by horizontally polarized light if the SLM is aligned with light (bi) the SLM acts as a phase modulator and as an amplitude modulator if the liquid crystals are orientated at 45° to the input beam.

phase information in it. Experimentally illuminating the SLM at normal incidence can lead to difficulties as to how to separate the incident and reflected beams without loosing a significant percentage of the total power by simply placing a beam splitter placed in front of the SLM (because the incident beam must be linearly polarised we cannot use a quarter wave plate and a polarising beam splitter to completely separate the reflected beam). The most practical solution we have found is to direct the beam onto the SLM at a slight angle, approximately 5°, the reflected beam is now spatially separated from the incident beam and can be easily directed towards the experiment. The

slight angle when going onto the SLM will offset the calibration of the SLM, at this slight angle the maximum phase delay through the liquid crystal will no longer correspond exactly to a phase change of 2π, at small angles, though, this was not observed to effect the quality of the resultant beams. The holograms are encoded based on a input beam with a flat wavefront and constant intensity (the holograms can be encoded for a specific beam shape, but this would also require the phase and intensity structure of the illuminating beam to be measured) so, ideally, we would like to use plane waves to illuminate the SLM, however, this also leads to experimental concerns. To project a plane wave onto the hologram from a TEM_{00} laser source would require the expanding of the beam so that only the central, approximately flat, portion of the Gaussian profile hits the active area of the SLM. Expanding the beam in such a way will result in the loss of a significant fraction of the power in the beam. For this reason the incident beam is expanded to fill as much of the SLM as possible without clipping the edges. We found that the Gaussian profile of the incident beam did not affect the quality of the converted beam significantly. For the generation of the LG beams only the central dislocation of the hologram is necessary for imparting the required phase information so the loss of information at the edges of the hologram are unimportant. For more complicated holograms that use the whole device to encode the phase information such a loss of information at the edges may result in a reduction of beam quality or efficiency. However, in the experiments performed in this thesis using such holograms (the beam splitter shapes described in chapter 8) the desired beam shape was still clear and the overall efficiency of the device

remained at ~50%. Please note that it would also be possible to compensate for the shape of the incident beam by altering the information encoded on the SLM itself, however, this would also require us to measure the properties of the laser beam leading to added complexity to not only the hologram parameters but in experimental equipment required to measure the beam properties.

For the generation of LG holograms a LabView program, written by David McGloin, was used to generate a greyscale hologram image which was then projected onto the SLM. Since the atom guides are only required to be a single tube the radial index, p, is kept at zero, just as with the static holograms, and this parameter cannot be altered in our program. The azimthal phase, l, can be controlled by increasing an integer value allowing arbitrary orders of index to be created. Simply controlling the azimuthal phase of the light can be used to generate an LG beam (this is the idea behind using a spiral phase plate), however, because the SLM is a reflective hologram there is a fraction of the incident beam that undergoes a normal reflection from the surface. The normal reflection does not pass through the phase modulation of the SLM and results in the dark singularity at the core of the LG beam still containing some light. In order to ensure the LG beam has zero intensity in the centre a blazed grating is used, this is overlaid onto the spiral pattern and puts the desired LG beam in the first diffracted order (figure 5.8). Since the normal rays do not pass through the SLM they do not see the grating pattern and thus remain in the zeroth order, leaving the first order "clean" for use in the experiment. The number of lines in the grating, the

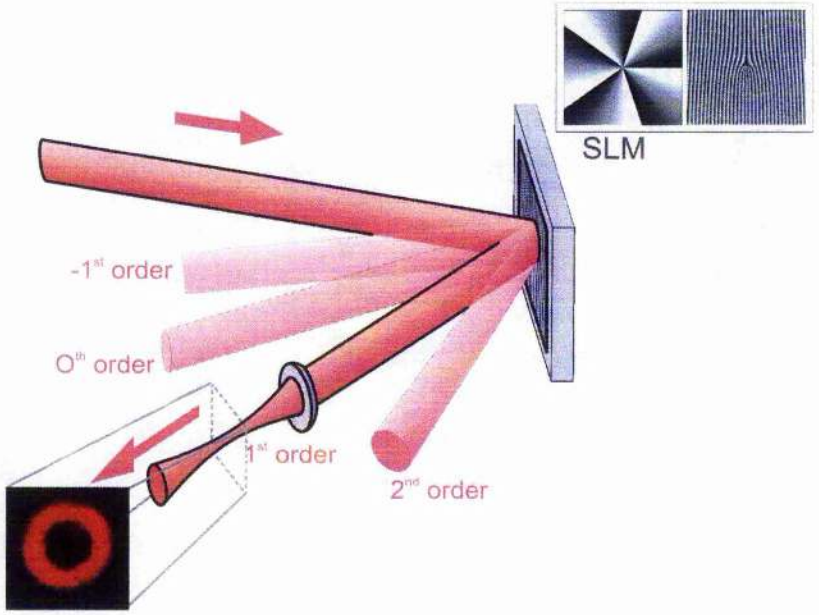

Figure 5.8: Generation of Laguerre-Gaussian beams using a spatial light modulator. The SLM is encoded with a hologram (inset right, showing the spiral phase structure without and with the blazed grating). A collimated beam is incident on the SLM and the output LG beam is then imaged into the trap at the desired size. The first diffracted order is used to ensure that no undiffracted (zero-order) light is present in the centre of the LG beam.

grating separation, is controlled by the program, this allows us to increase the diffraction angle of the beams and ensure that the experimental beam (first diffracted order) does not overlap with any adjacent diffracted orders that might result in interference fringes and excess light within the dark centre of the beam. Examples of some of the different LG beams be created are shown in figure 5.9. The overall efficiency of the SLM depended on the SLM parameters, the size of the hologram array remains constant so the only parameters we can adjust using this program are the azimuthal index, l, and the number of lines in the grating, N. Increasing the grating parameters resulted in the largest effect in the efficiency of the LG generation into the first

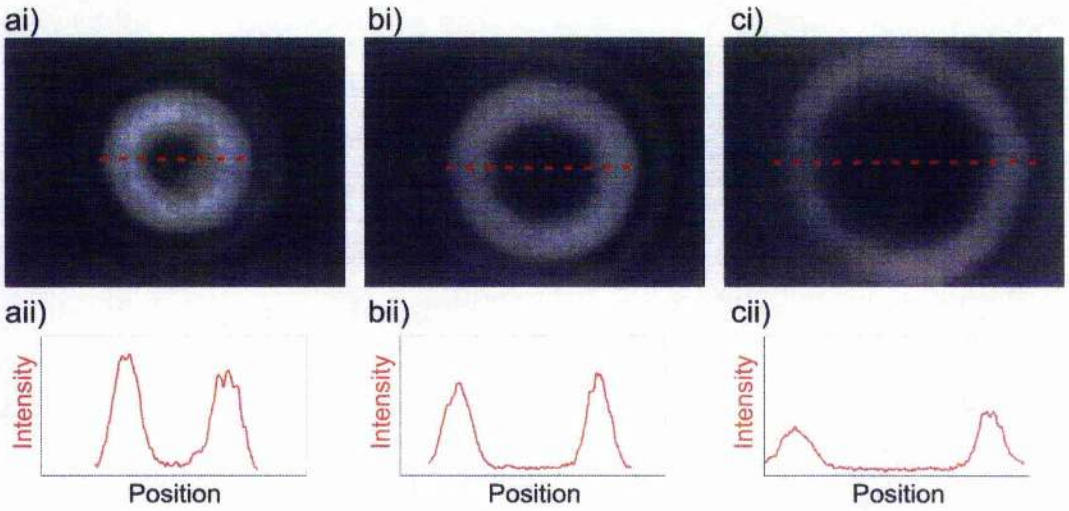

Figure 5.9: Examples of the LG beams generated by the SLM. The cross-section of l = 2, 5 and 10 beams are shown in (ai), (bi) and (ci) respectively; an intensity distribution taken across the beam is shown below in (aii), (bii) and (cii).

order; increasing the grating lines from N=20 to N=200 resulted in an efficiency drop from 72% to 27% for a fixed azimuthal index of l=2, this is because the decrease in separation of the lines results in fewer pixels between each line and therefore the blaze on the grating becomes less smooth and reducing the power diffracted into the first order. For a fixed value of N (N=70, was used as this permitted the use of l=10 Laguerre-Gaussian beams without any interference effects from overlapping of higher order diffracted beams) the efficiency of the SLM was found to only vary from 55% to 50% for l=0 and l=10 respectively. A table of hologram efficiencies is given in figure 5.10. Overall, for moderate values l and N, we find the SLM compares favourably with our static holograms, and the possible 256 grey levels of the pixels allows a much smoother variation across the features of the hologram than the etched glass designs.

Number of lines (l=2)	1st order efficiency
20	72.5%
30	66.5%
40	62.1%
50	59.6%
60	57.3%
80	53.0%
100	48.1%
150	38.5%
200	27.4%

LG order (N=70)	1st order efficiency
0	55.6%
1	55.2%
2	55.2%
3	54.7%
4	54.3%
5	53.8%
10	50.2%

Figure 5.10: Efficiencies of the SLM holograms. For a fixed azimuthal index (left) the number of lines in the grating is increased, by N=200 the efficiency has dropped significantly, however, at the resolution of the SLM there is only 3 pixels in each line which does not permit a smooth blaze to be applied. For a fixed grating size (right) the efficiency remains more constant.

Arbitrary Beam Shapes

Other beams with known phase structures, such as Bessel beams (these will be discussed in section 5.4) and bottle beams [14] (this is a beam with zero intensity at its focus surrounded by regions of high intensity) can be created in a similar manner to that described above by encoding the phase information onto a fixed hologram or SLM. However, it is not necessary to have a known phase structure in the beam in order to create a hologram capable of generating it. Arbitrary beam shapes can be created using iterative algorithms such as the Gerchberg and Saxton algorithm. A flow chart of the algorithm used in this thesis is given in figure 5.11 [15]. Using these methods any beam shapes can be created from simple arrays of spots to complicated

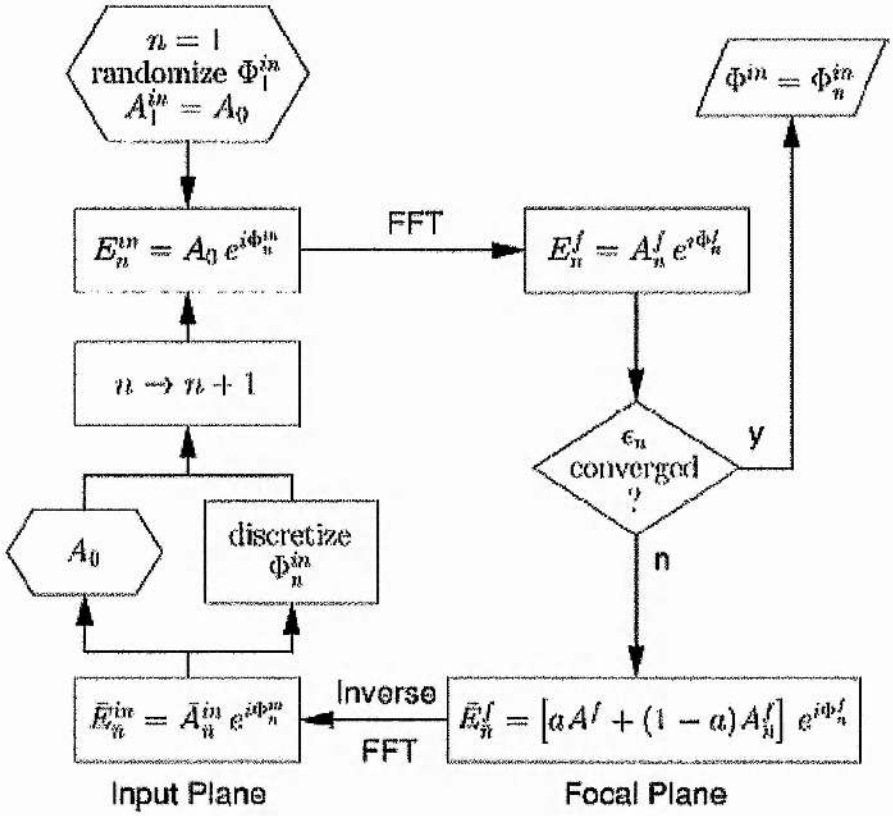

Figure 5.11: Flow chart of the adaptive-additive algorithm. The phase modulation, $\Phi^{in}_n(\mathbf{r})$, can be quantized into discrete steps with every iteration, as shown, or after the algorithm has converged. Reproduced from [15].

pictures, see figure 5.12 for examples of iteratively generated holograms and their images. Using this method we have created the non-standard beams used for creating atomic beam splitters and interferometers, these beams will be described in chapter 8.

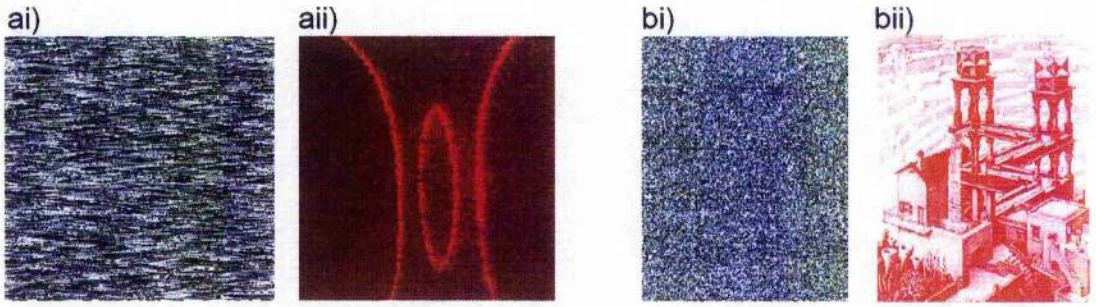

Figure 5.12: Iteratively generated holograms (i) and their resultant beams (ii). The resultant beam images are taken at the focus of the beam in the plane transverse to the beam propagation. These patterns do not propagate in free space like the LG beam, which maintains its shape as it propagates; away from the beam waist these patterns rapidly become out of focus.

5.3.2 Generation with Spiral Phase Plates

Instead of manipulating the shape of the beam by passing it through a hologram pattern and interfering the HG beam with a grating another method of creating the form of an LG beam is to simply adjust the phase of the beam around the circumference using a fixed spiral phase plate. A spiral phase change can be displayed simply on an SLM, in fact it is the first step in generating our holograms, however, because of the reflective nature of the SLM a grating is still necessary to move the final beam shape away from any normal reflections off the surface. The use of a transmission phase plate opens up the possibility to increase efficiency to almost 100% because we are not diffracting the beam into a range of order but simply passing it through a glass slide. By creating a phase plate with a spiral variation in height (a spiral ramp) we can change the phase of an incident beam as it passes through the

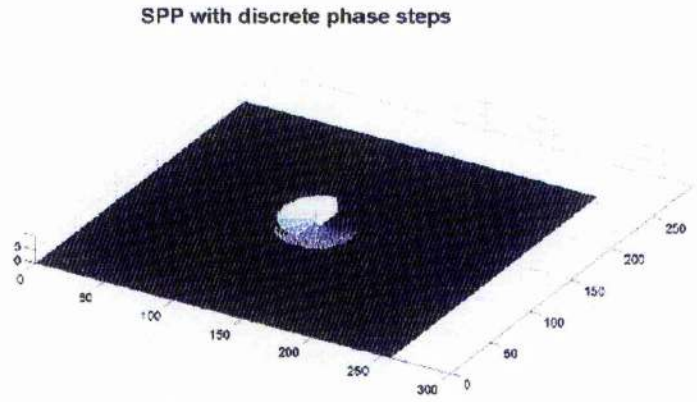

Figure 5.13: A diagram of an l=1 spiral phase plate. The spiral is built up from 12 steps each of $\pi/6$ radians. The total height of the spiral is λ_n, the length of a single wavelength inside the substrate of refractive index n. Image from Nanyang Technological University.

different parts of the phase plate. If the highest part of the spiral is an integer number of wavelengths thick then as we look at the phase of the beam across this position to the lowest point on the ramp we will see a smooth change in phase; for an l=1 beam the thickness of the SPP is increased by one wavelength around the spiral, for higher order beams the thickness of the SPP can be increased by integer values of the wavelength resulting in a greater etching depth, or the spiral can be "reset" each time the phase is changes by 2π giving a saw-tooth shape to the circumference of the SPP. A diagram of an l=1 SPP is shown in figure 5.13.

We were provided with several examples of l=1 SPP's from Nanyang Technological University (N.T.U), Singapore [16]. These SPP's were made to a diameter of 500μm in order to facilitate the potential integration of these devices into any existing micro-optical beam shaping apparatus (larger diameter devices of this type have also been manufactured by other groups

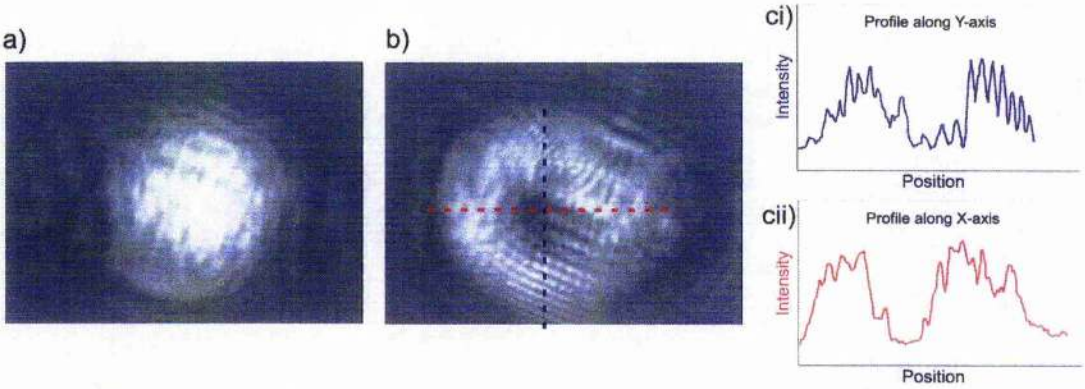

Figure 5.14: Intensity profile of a spiral phase plate generated LG^{1}_{0} beam (b). The horizontal and vertical intensity distributions are shown in (c). The incident beam is given in (a).

[17]). SPP's were produced for each of 405nm and 780nm and were then tested at St Andrews. These phase plates were etched using electron-beam lithography, the spiral pattern was built up from 12 discrete phase steps in $\pi/6$ radian increments in the prototype slide, which was subsequently increased to 24 steps in $\pi/12$ radian increments for the next set of SPPs; the size of the SPPs were also increased to include 1mm diameter wave plates, as well as the 500μm, at our request as it was hoped that the larger SPPs could be placed directly at the output of the laser diodes and provide the LG beams without the need for focusing optics; although the SPPs have yet to be used in such a way the larger diameter plates proved much easier to align when a focused beam was used to illuminate them.

Circularised diodes were used to illuminate the SPPs at both wavelengths; the TEM_{00} output from one of our home-made ECDLs (described in chapter 4) was used for the 780nm SPPs and a circularised blue diode at 405nm (VPSL-0450-N5B, Blue Sky Research). The incident light was focused down onto

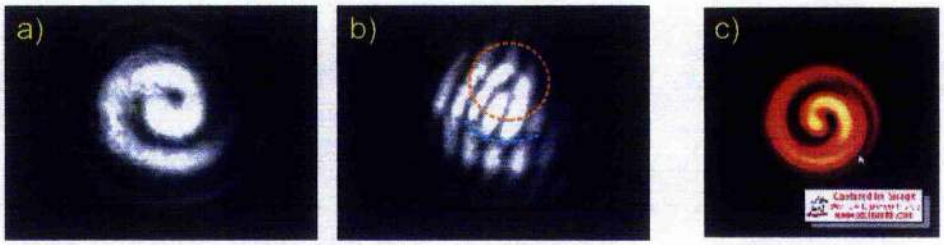

Figure 5.15: Overfilling the spiral phase plate. The results of illuminating a 500μm diameter SPP with a beam of diameter ~1mm (a), the interference of this beam with a TEM_{00} beam is shown in (b), the phase dislocations are highlighted by the dashed lines; the red circle indicates the characteristic phase dislocation of an LG beam, the blue shows the phase dislocation caused from the spiral artefact. The result of computer modelling by Moh Ken-Jin, N.T.U., is given in (c).

the spiral phase plates, using a lens of focal length 100mm, to ensure the input did not clip the edges of the SPP. If the beam waist is greater than the SPP radius there is a spiral pattern obtained in the resultant output beam, this was confirmed by modelling by Jonathan Moh Ken-Jin at N.T.U. The SPPs provided were all designed for generating an LG beam of order l=1. The measured efficiency of the mode conversion was found to be between 85-95% for the various plates supplied. Examples of the LG beams produced are shown in figure 5.14. The annular intensity of the LG beams generated varies by ~20%, approximately equal amounts in both horizontal and vertical axes. The results of mismatching the size of the beam and the corresponding computer models are shown in figure 5.15. Extended examination of the output beam confirmed that the beam propagated in free space as expected, without break-up of the beam shape. Subsequently the LG beam was examined in an interference experiment, the LG beam is generated in one

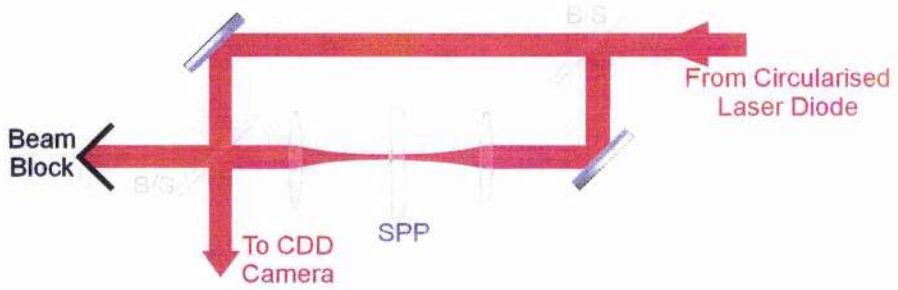

Figure 5.16: Mach-Zehnder interferometer for examining the LG beams. The output from a laser diode is split by a 50:50 beam splitter (B/S), one beam path is then focused through the spiral phase plate using 100mm focal length lenses, before being recombined using another beam splitter. The interference pattern is viewed with a CCD camera.

arm of a Mach-Zehnder type interferometer with the other arm remaining as the TEM_{00} output of the ECDL taken before the SPP, the set up is shown in figure 5.16. The resultant interference patterns showed the characteristic dislocated grating pattern as expected (there is also an extra π phase change observed around the diameter-mismatched spiral as indicated by the blue line in figure 5.15(b)). It is worth noting that the first SPPs provided for 780nm, unfortunately, suffered a manufacturing flaw such that the total height of the phase plate did not result in a phase change of 2π radians around the whole spiral, this resulted in very poor LG beam compromising of two intense regions of a beam on opposite sides of the ring (shown in figure 5.17) and with near zero intensity in between, as such the results shown earlier are for the 24 step SPPs. Whilst the efficiency of the SPPs is much superior to the hologram generated beams, up to twice the incident power is converted into the desire LG mode, these initial spiral phase plates did not offer as good a

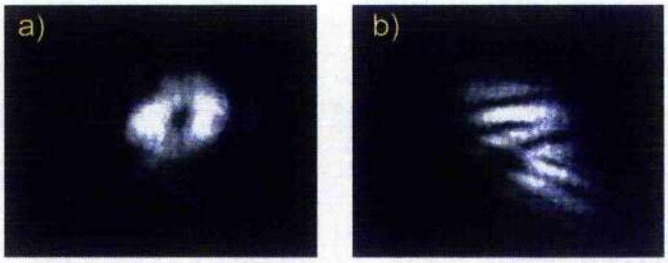

Figure 5.17: Beam profile of an LG beam when the height of the spiral phase plate is not equal to 2π (a) and the resultant interference pattern with a TEM_{00} beam (b).

quality of LG beam as the hologram generated beams which provided a much more uniform beam profile.

5.4 Bessel Beams

Any monochromatic beam travelling in free space is subject to diffractive spreading as it propagates. The characteristic distance over which a collimated beam can travel without significant spreading is given by the Rayleigh range. For this reason it is assumed that all beam-like fields (i.e: one that has an intensity along the axis of propagation but which tends to zero away from this axis) must eventually undergo diffractive spreading as it propagates. Whilst this is certainly true for Hermite-Gaussian and Laguerre-Gaussian beams, there are other solutions to the free space wave equation that remain propagation invariant for all time. One possible solution to the wave equation is the Bessel function which gives solutions with complete axial symmetry. The amplitude of these beams are given by [1]

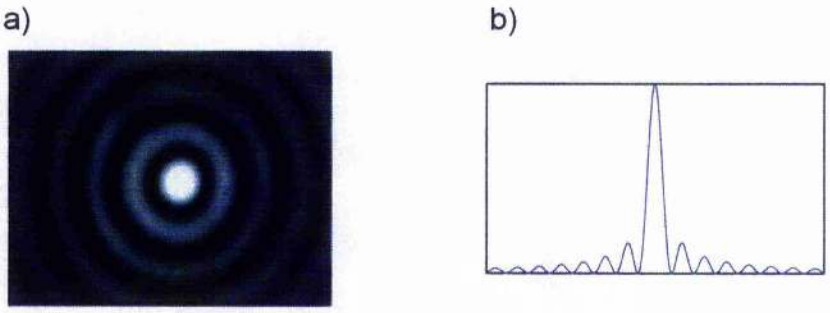

Figure 5.18: The cross-section of a zeroth order Bessel beam (a), the intensity profile of the Bessel beam (b) displays a very intense central feature.

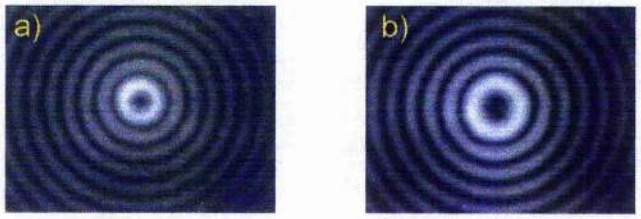

Figure 5.19: Cross-section of high order Bessel beams. A J_1 beam is shown in (a) and J_2 in (b). As the order of the beam is increased the central dark region becomes larger.

$$E(r,\phi,z) = AJ_l(k_r r)e^{ik_z z}e^{il\phi} \tag{5.8}$$

where J_l is the l^{th} order Bessel function, A is a constant and k_r and k_z are the radial and longitudinal components of the wavevector, k. The Bessel function can remain non-diffracting because it is not a true free space beam, it is instead the resulting interference pattern of conical wavefronts giving rise to a series of concentric rings in cross-section (see figure 5.18). The zeroth order Bessel function results a beam with a bright peak at the centre of the beam. Higher order Bessel beams have a phase singularity in the centre of the beam (the $e^{il\phi}$ term) in a similar manner to the LG beams described earlier and have a central dark region, the size of which increases with the order of the Bessel

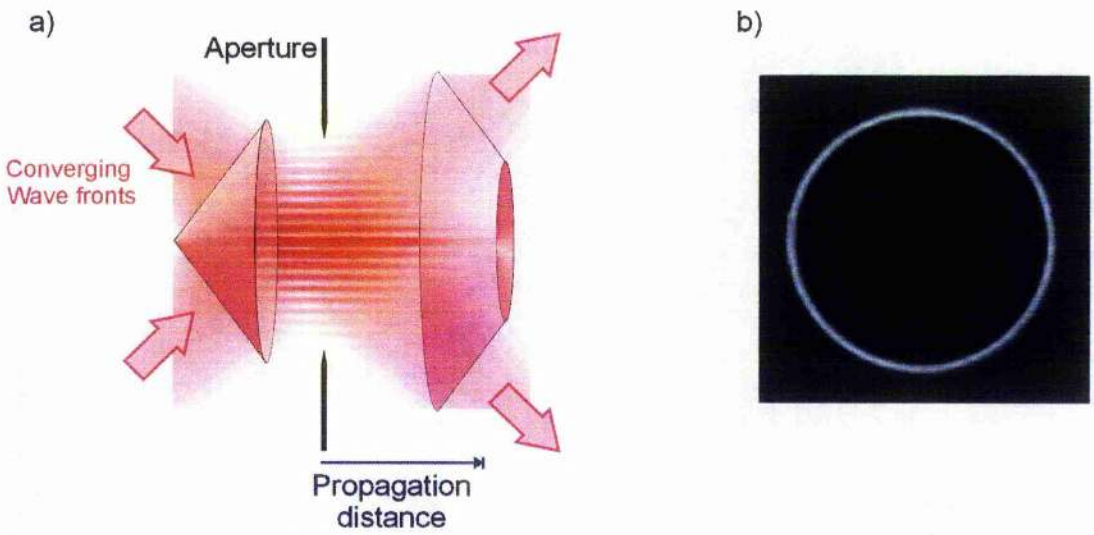

Figure 5.20: Experimental Bessel beam approximation. The longitudinal cross-section of a Bessel beam (a), the propagation direction of the conical wavefronts is indicated by the arrows. The Bessel beam is a near field effect, in the far field of these wavefronts we get a narrow annular light beam (b). Figure (b) is reproduced from [17].

beam, as shown in figure 5.19. Each ring of the Bessel beam has roughly equal amounts of energy. It would require an infinite amount of energy to produce a beam of this type that extends over an infinite plane and which would, therefore, propagate indefinitely without diffracting. The use of an aperture to limit the extent of the beam eliminates the energy concern, but introduces edge diffraction effects and introduces a limit to the range over which the beam can propagate. Thus any experimentally produced Bessel beam is only a valid approximation over a short distance, see figure 5.20. Considering the conical wavefronts of the beam whilst the beams are overlapping the Bessel beam is formed from the interference effects, if these wavefronts are finite in size then eventually these wavefronts will pass each

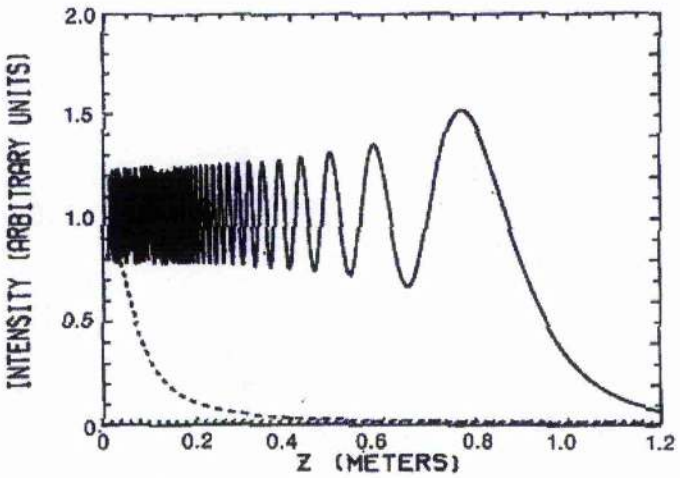

Figure 5.21: Fluctuation in the intensity of the central maximum of the J_0 Bessel beam. As the cross-section of the Bessel beam is increased the magnitude of these oscillations decrease. The dashed line is the propagation of a Gaussian beam with a beam waist equal to the central feature of the Bessel beam. Reproduced from [19]

other to finally produce a ring shaped beam in the far field, figure 5.20(b) (the far field pattern in fact has a very narrow ring pattern offering high dipole forces and has been used by several groups as a hollow beam for guiding [20], however, since this is not a free space beam the profile of the ring is not constant over the propagation distance unlike the overlapping Bessel-like portion of the beam). The aperture of the wavefronts also introduces an intensity fluctuation in the central peak of the Bessel beam, the magnitude of this fluctuation decreases with increasing aperture size [20] (figure 5.21). Despite these factors limiting the maximum distance the beam can propagate, during this distance the central core of the Bessel beam remains non-diffracting for lengths far in excess of those possible with an equivalently sized Gaussian beam. Figure 5.22 shows the beam profile of a Bessel beam as it

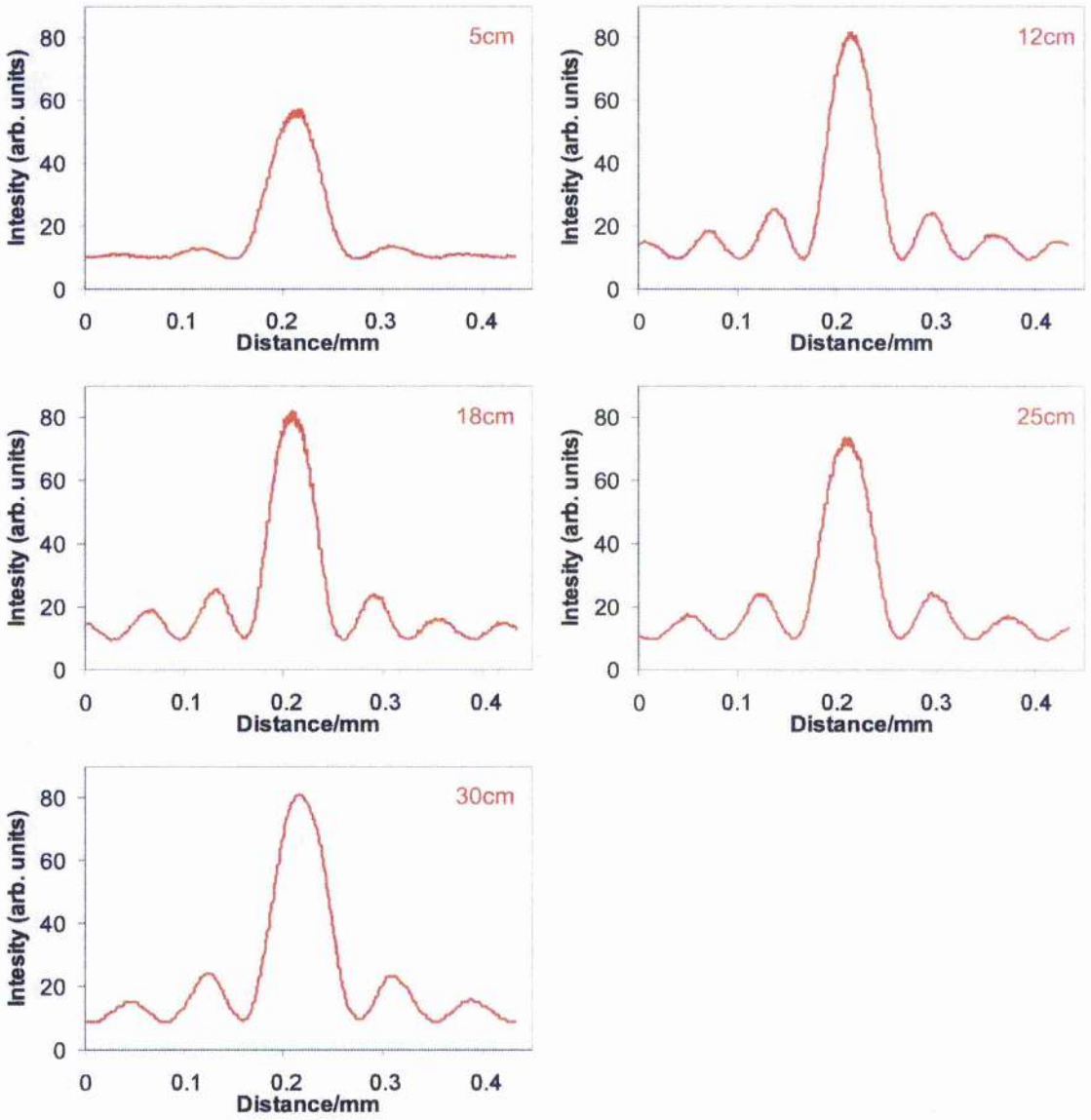

Figure 5.22: Beam profile of the Bessel beam as it propagates. The distances marked give the position of the profile from the axicon used to generate the beam.

propagates through 30cm. The central spot size remains constant at 26.5μm ± 1μm for 16cm, over the whole propagation distance the beam had only expanded by 4μm at the edges of the Bessel approximation. A comparison of the spot size of the experimental Bessel beam shown in figure 5.22 with a

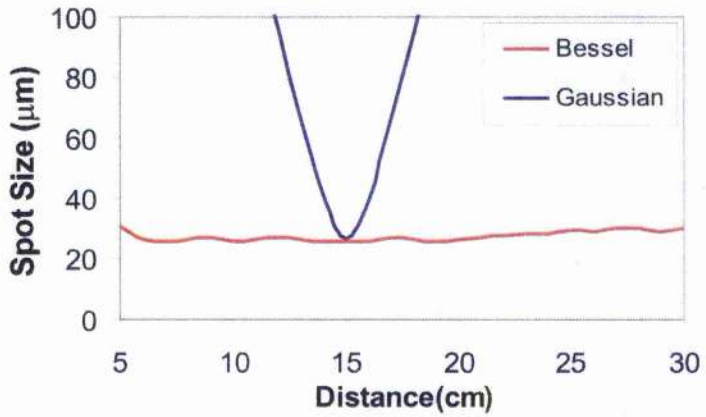

Figure 5.23: Comparison of the spot size of a Bessel and Gaussian beam. The spot size of the beam shown in figure 5.22 is plotted in red, a model of a Gaussian beam focused to a waist of 27μm, at the 15cm position, is given in blue.

computer modelled Gaussian beam, with a 27μm beam waist is given in figure 5.23. This clearly illustrates the advantages of using the Bessel beam for extended guiding and small beam waists.

The intensity structure of the Bessel beam leads to much steeper intensity gradients between areas of low and high intensity than an equivalent sized HG or LG beam and the non-diffracting nature of the beam means this potential is approximately constant along its propagation distance. Ignoring the outer rings this would seem to be of great advantage for optical guiding of atoms and particles as the dipole potential that these beams can impart is significantly higher. The overall structure of the beam, however, reduces the advantages afforded by this increased dipole potential. The total power in the beam is distributed evenly between all the concentric rings of the Bessel

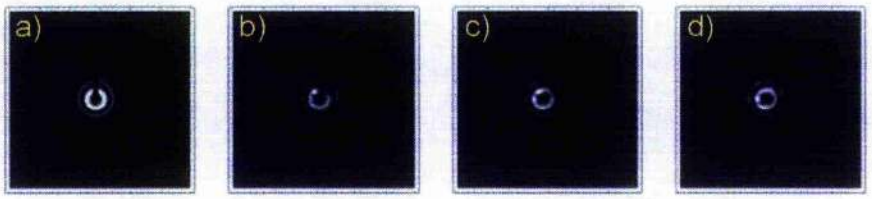

Figure 5.24: A simulated reconstruction of an obstructed Bessel beam. The rectangular obstruction has a width of 50μm. The Bessel beam has an azimuthal index l =3 and a peak radius of 150μm. (a) shows the profile of beam at z=0 (at the plane of the obstruction), (b) when z=3.6cm, (c) when z=7.2cm and (d) when z=10.8cm. The inner ring of the Bessel beam is closed by (b), less than the Rayleigh range of an equivalently sized LG beam. Simulation by David McGloin.

beam thus the actual intensity of the central ring ends up becoming much lower than can be achieved in a LG beam.

Another result of the conical propagation of the Bessel beam wavefronts is a reconstructive ability of the beam. If an obstruction is placed in the beam the shadow that the obstruction casts is quickly removed by the conical rays from around the obstruction recreating the beam further down its propagation length [21]. An obstruction placed in a Gaussian beam would only be diffractively filled, this would usually take a longer distance to achieve and result in a distortion to the final beam, whereas the centre of the Bessel beam will be reconstructed to be identical to the beam before the obstruction. The shadows that the objects cast still exist but since they propagate in the direction of the conical wavefronts they are seen in an increasing diameter ring as it propagates further along the beam. A computer model of the reconstruction of a Bessel beam is shown in figure 5.24.

5.5 Generating Bessel Beams

Experimental approximations to a Bessel function can be made by the use of an axicon [22] (a conical shaped lens), illuminating an annular slit placed at the focal plane of a lens [20] or by the use of holograms [23]. However, in the case of holograms and annular slits there is generally a high degree of inefficiency. Higher order beams can be generated by illuminating the beam converter with light with a non-zero azimuthal index, such as an LG beam.

5.5.1 Generation with an Annular Slit

The set up for generating a Bessel beam with an annular slit is shown in figure 5.25. A 4mm diameter annulus, mounted on a x-y axis translation stage, was illuminated with a collimated beam from a HeNe laser, the laser beam was expanded to illuminate the whole annulus using a simple telescope arrangement of two lenses with focal lengths f=20mm and 320mm. An f=75mm lens was placed at its focal length past the annulus to generate the Bessel beam, which was viewed using a 10x microscope objective and imaged onto a CCD camera. The annulus acts as a ring of point sources such that the light is collimated after the lens, when all points around the annulus are considered a conical wavefront is produced. The propagation length of this beam, Z_{max}, can be approximated using the thin lens formula and using the similar triangles formed by extrapolating rays from the lens back

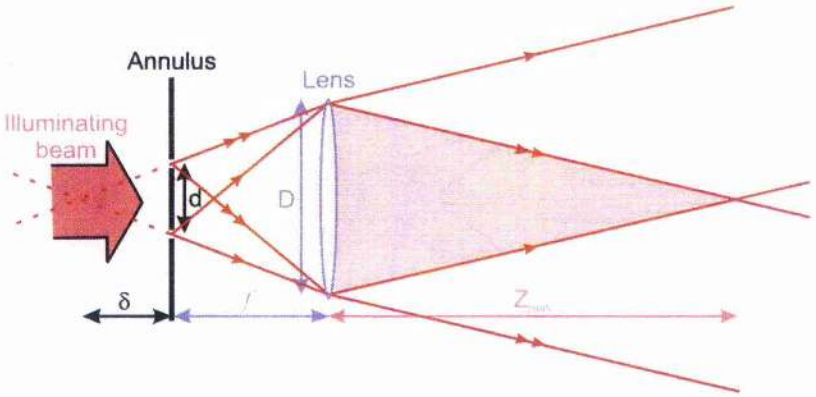

Figure 5.25: Ray diagram of annulus generation of a Bessel beam. The Bessel beam is formed in the shaded triangle after the lens.

through the annulus to an image point [24], the propagation distance of the Bessel beam is therefore given by:

$$Z_{\max} = \frac{(f+\delta)f}{(f+\delta)-f} = \frac{fD}{d} \tag{5.9}$$

where f is the focal distance of the lens, D is the diameter of the beam at the lens, d is the diameter of the annulus and δ is the point source found when extrapolating the rays backwards. For the set up described above this equation gives us a Z_{max} of ~110mm which agreed with the experimental results.

High order Bessel beams were created by illuminating the annulus with an LG beam. As with the LG beams increasing the order of the beam leads to larger rings sizes and hollow regions. An l=1 LG beam was generated using the slide holograms built in house. The hologram was placed in the beam after the beam expander and an aperture was placed in front of the annulus to remove the unwanted diffracted orders from the hologram. This higher order

Bessel beam produces a dark region in the centre of the beam, alignment of the annulus is found to be very critical here. The phase vortex in the centre of the Bessel beam is very susceptible to aberrations; if the input beam is not correctly positioned, ie: normal and centred to the annulus, the phase vortex breaks up on focusing through the lens. This effect also occurs in the zeroth order besel beam but since there is no break up of a phase singularity the effect for small misalignments is less obvious, instead resulting in intensity "hot spots" around the rings of the beam, with large misalignments the circular pattern of the Bessel beam is seen to break up in all orders of Bessel beam, but with only minor errors the phase singularity is the first to break up. Examples of some of the aberrations are given in figure 5.27

The use of LG beams to illuminate the annulus improves the overall efficiency of the conversion, even if we assume only 40% conversion efficiency into the LG beam, because the hollow beam can illuminate the annulus more effectively, however because we need the annulus to produce a point source for the light rays the thickness of the annulus must remain necessarily small and therefore the overall efficiency of this type of Bessel beam generation is kept very low.

5.5.2 Generation with an Axicon

In contrast to the annulus, in generation of Bessel beams with the axicon the whole of the input beam can be used to create the Bessel beam. This leads to very high conversion efficiencies as we are effectively just passing the

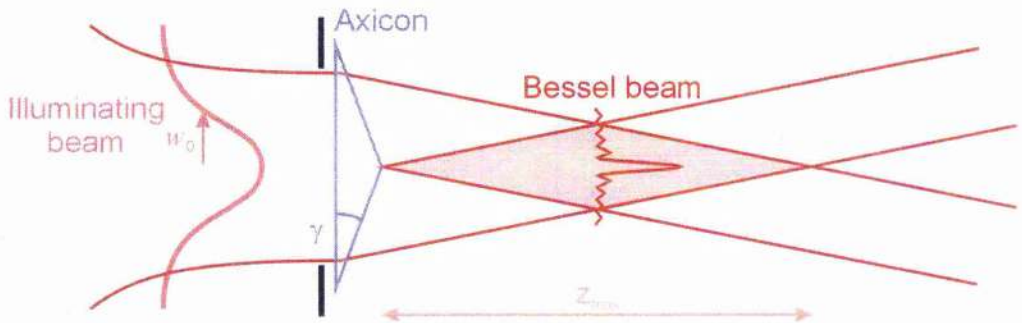

Figure 5.26: Ray diagram of axicon generation of a Bessel beam. The Bessel beam is formed in the shaded area after the axicon. The refractive index of the axicon is n.

beam through a lens. To generate a Bessel beam using an axicon the axicon is illuminated by a plane wave normal its flat face. Refraction through the axicon causes the output to be a conical wavefront, which acts to generate the required interference pattern to create the Bessel beam, a ray diagram of the set up is shown in figure 5.26. Altering the internal angle, γ, of the axicon varies the size and propagation length of the Bessel beam; larger axicon angles result in a greater crossover angle of the conical wavefronts so the beam propagates for a shorter distance but with narrower circular fringes. The propagation distance of a Bessel beam produced this way is given by [1]:

$$Z_{\max} = \frac{w_0 k}{k_r} \tag{5.10}$$

where w_0 is the input beam waist, $k_r \approx k(n\text{-}1)\gamma$ is the radial wavevector and n is the refractive index of the axicon.

Axicons with internal angles γ=1° and 5° were illuminated using the same HeNe beam as the annulus experiment. The axicon was mounted on an x-y

axis translation stage and the resulting beams were viewed using 10x and 20x objectives respectively. The 5° axicon produced the smallest pattern but a flaw at the apex of the axicon meant it was impossible to produce a clean zeroth order Bessel beam without aberrations breaking up the circular pattern. The 1° axicon produced a zeroth order Bessel beam with a central spot of full width half maximum of 45μm, the propagation distance depended also on the size of the illuminating beam.

Higher order Bessel beams were generated using hologram made LG beams as before. Holograms producing LG beams with azimuthal indices of l=1, 2 and 3 were used to generate higher order Bessel beams. The l=2 beam was of particular interest because of the break up of the phase singularity. It was observed that for small misalignments of the Bessel beam the vortex separated into l individual vortices; it was hoped that by careful control of the Axicon the phase vortex break up of an l=2 beam could act as a small angle beam splitter. An atom beam guided along the centre of the Bessel beam would split as the vortices separated.

5.5.3 Aberrations in Bessel Beams

Experiments into misalignment of the converting optics were carried out using both systems described above. Bessel beam are susceptible to aberrations, such as astigmatism, and this leads to separation of the phase vortices. It was found that if the axicon or annulus were not positioned normal to the incoming beam the Bessel pattern starts to decompose into a more linearly

Figure 5.27: Increasing the aberrations of a Bessel beam. An l =2 Bessel beam (a), the axicon is tilted about the vertical horizontal axis. A shallow angle (b) causes the phase vortex to break up. Increasing the angle of the axicon causes the Bessel beam to decompose into a linearly symmetric chess board like pattern, (c) shows the pattern of a decomposed J_0 Bessel beam.

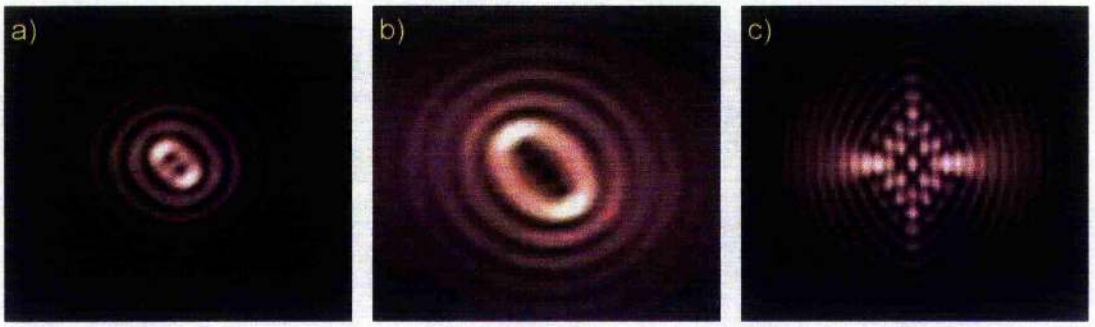

Figure 5.28: Computer simulation of aberrations in a Bessel beam. The phase vortex break up of a J_2 beam(a) and for a J_4 Bessel beam (b) shows separation into a number of vortices equal to the order of the beam. Increasing the spherical aberration results in the chess board pattern, (c).

symmetric pattern starting from the centre. In the higher order beams the centre ring decomposed first, for l =1 the ring split into 2 discrete spots, for the l =2 beam the vortex first split into two spots within the same ring, see figure 5.27, and the l =3 vortex became three dark spots in a line. Once the innermost ring has decomposed into an array of spots the next ring outwards starts to show aberrations and so on. In all cases the Bessel beam eventually

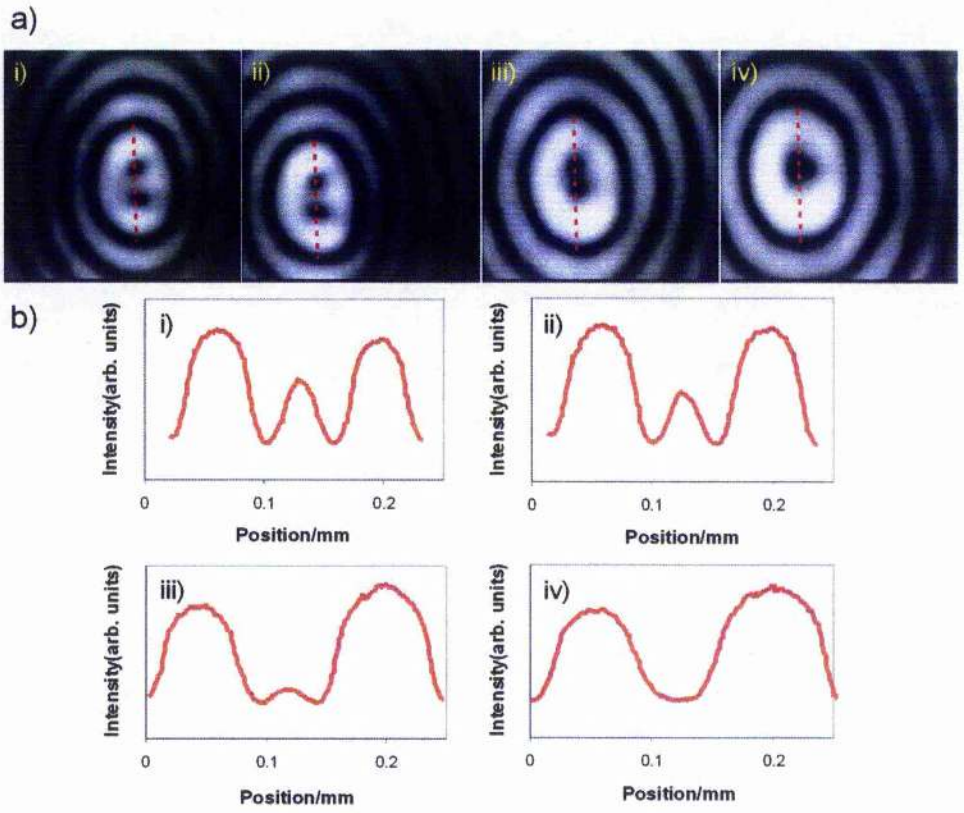

Figure 5.29: Phase vortex break up as a beam splitter. The profile of a J_2 Bessel beam (a) at positions 240mm (i), 320mm (ii), 450 mm (iii) and 540mm (iv) from a 1° axicon illuminated with a beam of waist ~5mm. An intensity profile taken across the central ring indicated by the dashed line is given in (b). The intensity beam between the split vortices is greater than 50% of the inner ring intensity at (i) and tends to zero at (iv).

decomposes into a regular chess-board like pattern, this has been confirmed by computer modelling, see figure 5.28, and is the same aberrated pattern as observed by Tanaka and Yamamoto for a J_0 Bessel beam [25]. The splitting generated using an l =2 LG beam on the axicon was examined more closely since the break up of the central ring decomposed into two holes before the eventual break up of the ring pattern. It was seen that for a given misalignment of the axicon (or annulus) the amount of splitting observed

between the two holes in the central ring varied along the propagation length. Starting with the double vortex in the central ring when the beam is close to the axicon, as the beam propagates the separated phase vortices slowly begin to coalesce into the normal single hollow region in the centre along its propagation length, once the vortices have coalesced they continue to cross over each other and separate again. This vortex separation may be used as the basis of a shallow angle atom beam splitter, in the experiment performed with the 1° axicon (figure 5.29) the splitting angle of the vortices is ~0.13mrad.

5.6 Summary

In this chapter we have generated both high-order Laguerre-Gaussian and Bessel beams from the standard TEM_{00} output of a laser for use as hollow all optical atom guides. LG beams have been generated using a variety of different methods, static holograms made either from photographic film or etched glass have been demonstrated. The use of the SLM as a dynamic, computer-controlled hologram has added great versatility to LG beam generation allowing us to alter the beam parameters in real time without the need for any experimental realignment. The SLM used has been characterised for the generation of $LG^{l}_{p=0}$ beams and has been shown to be at least as efficient as the static holograms in our possession (the etched glass holograms have a theoretical higher efficiency, however, we were unable to obtain any with efficiencies greater than ~50% for these experiments). As well as holographic generation, the use of spiral phase plates was

investigated. SPPs afford a very high efficiency, efficiencies up to 95% have been observed, but the beam quality resulting from the prototype SPPs tested in this thesis was lower than that of the hologram generated beams.

High-order Bessel beams have been generated using an annulus and lens and with an axicon. Alignment of the conversion optics is observed to be quite critical as the Bessel beams are very sensitive to aberrations and decompose into a linearly symmetric chess board pattern. The phase vortex of the high order Bessel beams breaks up initially for small misalignments; this effect has been used to construct a shallow angle beam splitter using the vortex break up of a J_2 Bessel beam.

Bibliography

[1] J. Arlt, T. Hitomi and K. Dholakia, "*Atom Guiding along Laguerre-Gaussian and Bessel light beams*," Appl. Phys. B. **71** 549 (2000)

[2] W. L. Power, L. Allen, M. Babiker and V. E. Lembessis, "*Atomic motion in light beams possessing orbital angular momentum*," Phys. Rev. A. **52** 497 (1995)

[3] M. Padgett, J. Arlt and N. Simpson, "*An experiment to observe the intensity and phase structure of Laguerre-Gaussian laser modes,*" Am. J. Phys **64** 77 (1996)

[4] N. R. Heckenberg, R. McDuff, C. P. Smith, H. Rubenstein-Dunlop and M. J. Wegener, "*Laser beams with phase singularities*," Opt. Quantum Electron. **24** s951 (1992)

[5] G. A. Turnbull, D. A. Robertson, G. M. Smith, L. Allen and M. J. Padgett, "*The generation of free-space Laguerre-Gaussian modes at millimetre-wave frequencies by use of a spiral phaseplate*," Optics Commun. **127** 183 (1996)

[6] M. A. Clifford, J. Arlt, J. Courtial and K. Dholakia, "*High-order Laguerre-Gaussian laser modes for studies of clod atoms*," Optics Commun. **156** 300 (1998)

[7] J. Arlt, K. Dholakia, L. Allen and M. J. Padgett, "*The production of multiringer Laguerre-Gaussian mode by computer generated holograms*," J. Mod. Optics **45** 1231 (1998)

[8] D. McGloin, G. C. Spalding, H. Melville, W. Sibbett and K. Dholakia, "*Applications of Spatial Light Modulators in Atom Optics*," Opt. Express **11** 158 (2003)

[9] W. Hänsel, J. Reichel, P. Hommelhoff and T. W. Hänsch, "*Magnetic Conveyor Belt for Transporting and Merging Trapped Atom Clouds*," Phys. Rev. Lett. **86** 608 (2001)

[10] Y. Shin, A. E. Leanhardt, M. Saba, T. Pasquini, W. Ketterle and D. E. Pritchard, "*Atom interferometry with Bose-Einstein condensates in a double well potential*," Phys. Rev. Lett. **89**, 040401 (2002).

[11] H. Melville, G. Milne, G. C. Spalding, W. Sibbett, K. Dholakia and D. McGloin, "*Optical trapping of three-dimesional structures using dynamic holograms*," Opt. Express **11** 3562 (2003)

[12] V. Bingelyte, J. Leach, J. Courtial and M. J. Padgett, "*Optically controlled three-dimensional rotation of microscopic objects*," App. Phys. Lett. **82** 829 (2003)

[13] V. Boyer, C. M. Chandrashekar, C. J. Foot and Z. J. Laczik, "*Dynamic optical trap generation using FLC SLMs for the manipulation of cold atoms*," J. Mod.Opt. **51** 2235 (2004)

[14] J. Arlt and M. J. Padgett, "*Generation of a beam with a dark focus surrounded by regions of higher intensity: the optical bottle beam*," Opt. Lett. **25** 191 (2000)

[15] E. R. Dufresne, G. C. Spalding, M. T. Dearing, S. A. Sheets and D. G. Grier, "*Computer- Generated Holographical Optical Tweezer Arrays*", Review of Scientific Instruments **72** 1818 (2001)

[16] W. C. Cheong, W. M. Lee, X.-C. Yuan, L.-S. Zhang, K. Dholakia and H. Wang, "*Direct electron-beam writing of continuous spiral phase plates in negative resist with high power efficiency for optical manipulation*," Appl. Phys. Lett. **85** 5784 (2004)

[17] S. S. R. Oemrawsingh, J. A. W. Van Houweligen, E. R. Eliel, J. P. Woerdman, E. J. K. Verstegen J.G. Kloosterboer and G. W. t Hooft, "*Production and characterization of spiral phaseplates for optical wavelengths*," Appl. Opt. **43** 688 (2003)

[18] J. Arlt, R. Kuhn and K. Dholakia, "*Spatial transformation of Laguerre-Gaussian laser modes*," J. Mod. Opt **48** 783 (2001)

[19] Y, Song, D. Milan and W. T. Hill III, "*Long, narrow all-light atom guide*," Opt. Lett. **24** 1805 (1999)

[20] J. Durnin, "*Exact solutions for nondiffracting beams. I. The scalar theory*," J, Opt, Soc. Am. A. **4** 651 (1987)

[21] J. Arlt and K. Dholakia, "*Generation of high-order Bessel beams by use of an axicon*," Opt. Commun. **177** 297 (2000)

[22] G. Indebetouw, "*Nondiffracting optical fields: some remarks on their analysis and synthesis*," J. Opt. Soc. Am. A. **6** 150 (1989)

[23] A. Vasara, J. Turunen and A. T. Friberg, "*Realisation of general nondiffracting beams with computer-generated holograms*," J. Opt. Soc. Am. A. **6** 1748 (1989)

[24] M. R. Lapointe, "*Review of non-diffracting Bessel beam experiments*," Opt. & Laser Tech **24** 315 (1992)

[25] T. Tanaka and S. Yamamoto, "*Comparison of aberration between axicon and lens*," Opt. Comm. **184** 113 (2000)

Chapter 6:

Laguerre-Gaussian Beam Guiding of LVIS

D. P. Rhodes, G. P. T. Lancaster, J. Livesey, D. McGloin, J. Arlt and K. Dholakia, "*Guiding a cold atomic beam along a co-propagating and oblique hollow light guide*," Opt. Commun. **214** 247 (2002)

6.1 Introduction

The use of blue-detuned hollow optical guides offers advantages for atomic guiding over red-detuned guides [1] because the repulsive dipole force results in the atoms being confined within a low intensity region at the centre of the beam. This reduces the time spent by the atoms within the light field and subsequently reduces spontaneous emission and heating effects. In this chapter the guiding of a cold atomic beam using an LG beam is described.

The LG beam is a free space beam so maintains its intensity structure as it propagates, unlike the fibre mode, LP_{01}, hollow beams [2], which makes it suitable for extended guiding.

First we will look at the effect of a co-propagating Laguerre-Gaussian beam for guiding atoms in an LVIS beam (low-velocity intense source, described in section 2.4.2). One of the important areas in atom optics is the generation of an atomic beam splitter which would permit the production of atom beam interferometers [3] so next we examine an oblique guide for splitting the atomic beam. We find that while an LG beam will enhance the flux of LVIS when co-propagating along the LVIS serious problems are encountered when trying to load atoms into an oblique hollow guide beam.

6.2 Generation of LVIS

The trapping apparatus used for these experiments is the 10-way cross stainless steel trap as described in section 4.4.2. The trap is evacuated to 10^{-10} mbar, and the MOT is formed using the standard configuration. The cooling light is provided by a stabilised extended cavity diode laser which is used as a master laser to injection lock an second circularised diode laser, this provided 70mW of light at the ^{85}Rb $S_{1/2}$ (F= 3) $\rightarrow$ $P_{3/2}$ (F'= 4) transition. A second ECDL supplied 20mW for the hyperfine repumping light. An optical table mounted on floated legs was used in order to minimise vibrations and further stabilise the frequencies of the diode lasers. Due to weight

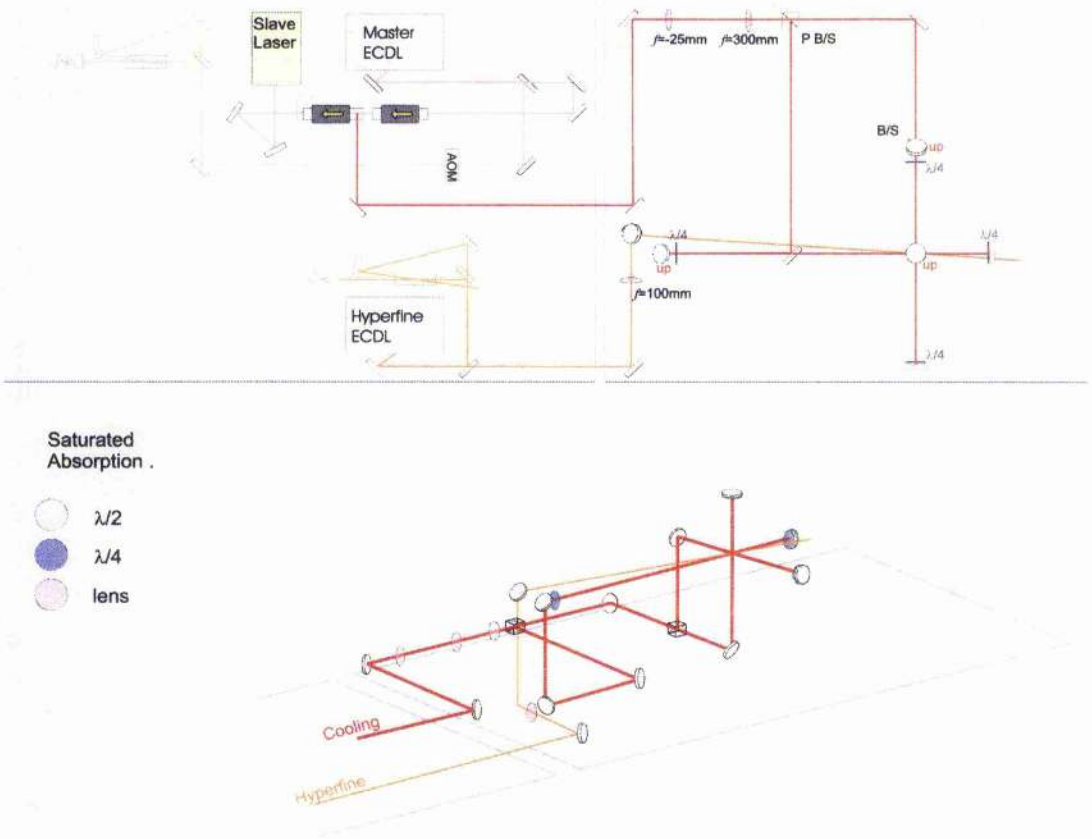

Figure 6.1: Experimental set up of LVIS. The surrounding boxes indicate the optical tables, the ECDL's are on the floating table, the trap itself is kept on a solid base. P B/S and B/S are polarising and 50:50 beam splitting cubes respectively.

considerations the trap itself was placed on a separate optical table. The cooling beams were expanded to approximately 1.5cm diameter beams before being directed into the trap, the hyperfine beam was focused gently so that it would expand over the volume of the MOT and was aligned to propagate in the direction of the LVIS beam. An experimental diagram of the trap set up is given in figure 6.1. The intensity imbalance for the LVIS beam was generated by placing an opaque spot in one of the horizontal retro-reflected beams [4]; the spots were produced on a microscope slide using two

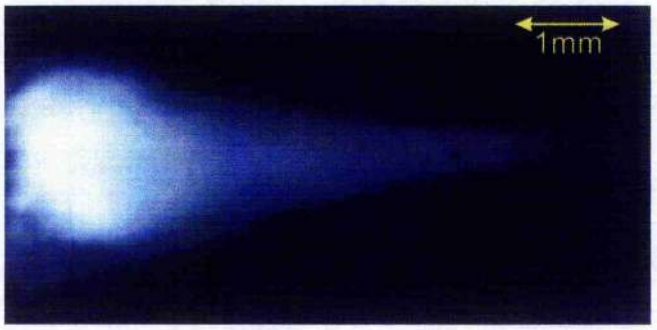

Figure 6.2: False colour image of LVIS.

methods; a fine OHP pen was used to make spots of ~1mm diameter; smaller obstructions of ~0.5mm diameter were made by scratching the surface of the slide with a hand drill. The resulting atomic beams were slightly smaller in diameter than the spots that created them due to diffractive filling of the beam. The atomic flux of the LVIS beams was $\sim 10^7 s^{-1}$. The fluorescence of the atomic cloud was viewed using two CDD cameras orientated at 90° to each other, while the cloud was imaged onto the cameras using 38mm and 40mm focal length lenses. Focusing of the cloud was performed by placing the CCD camera on an x-translation stage with the lenses attached directly onto the trap viewports; this arrangement produced an image with a field of view approximately 10mm around the centre of the MOT. A picture of the cloud fluorescence is given in figure 6.2.

6.3 Co-propagating LG Guide

Co-propagating Laguerre-Gaussian beams with azimuthal indices of l=1, 2 and 3 were used to guide the LVIS, a schematic diagram of this experiment

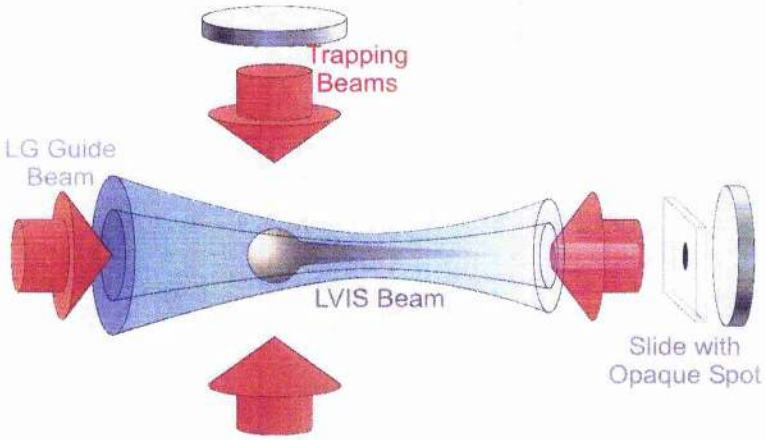

Figure 6.3: Experimental setup of blue-detuned Laguerre-Gaussian guiding of LVIS. The LVIS is generated using an opaque spot placed in one of the cooling arms, the guide beam is aligned to be co-linear with the LVIS.

showing the position of the guide is given in figure 6.3. The guides were generated by illuminating static holograms with output from the Ti:Sapphire laser. The beam was simply aligned to overlap with the dislocation in the hologram, rather than being expanded to overlap with the whole hologram. The maximum power of the resulting LG beams at the trap centre was measured to be 250mW, 220mW and 250mW for l =1, 2 and 3 respectively, the different beam powers are due to variations in the efficiency of the holograms. The set up used for generating the LG guide beams is given in figure 6.4. Focusing into the trapping region was achieved in two ways, the divergent output of the laser was simply focused into the trap by a lens of focal length f=1000mm placed ~2m from the trap centre, or by the use of two lenses separated by f_1+f_2, controlling the separation of these collimating lenses allows us to focus the beam inside the trap.

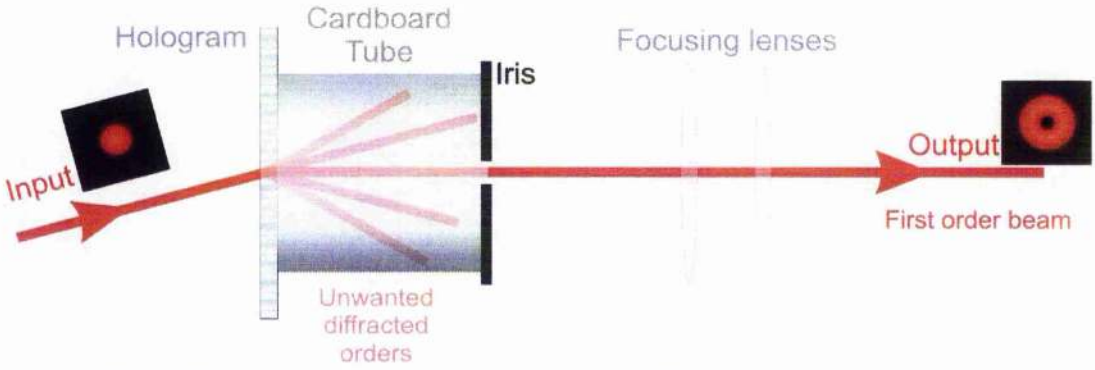

Figure 6.4: Experimental setup for Laguerre-Gaussian guide beam. The focusing lenses varied for the different order LG beams.

In contrast to guiding atoms in TEM_{00} laser modes where the laser is detuned far from the atomic resonance, for hollow beam guiding the light is blue detuned only slightly from the atomic transition. This creates difficulties when overlapping the guide beam; the LVIS is generated by an intensity imbalance along one of the cooling axes so the guide beam must also propagate along that axis. The close proximity of the two frequencies of the cooling and guide light (our typical guide detunings are only a few GHz) means a dielectric mirror cannot be used to reflect one beam and transmit the other in order to facilitate the overlapping of the two beams, as shown in figure 6.5a. The cooling beams are also circularly polarised before entering the trap. If we used polarising optics to combine the two beams the guide would have to pass through the quarter-wave plate as well (figure 6.5b), however, the exact effect of using a circularly polarised guide beam is uncertain. It was decided that, in order to properly compare our experiments to published results, we would have to keep the guide beam linearly polarised thus prohibiting the combination of the two beams in such a manner before a wave plate. Our solution is to steer the guide beam underneath the optics for the cooling beam

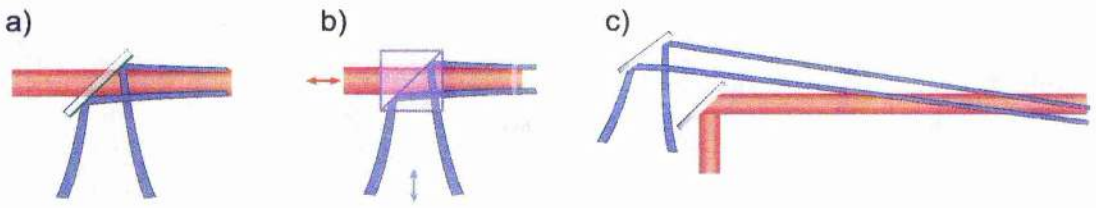

Figure 6.5: Co-linear alignment of Laguerre-Gaussian and cooling beam. A dielectric mirror (a) is unsuitable due to the nearness of the two frequencies, polarisation dependent optics (b) would result in a circular polarisation to the guide inside the trap. The LG beam is sent in around the cooling beam (c), which results in a slight angle to the guide.

(figure 6.5c), this imparts a slight angle on the guide beam, however, if the beams are far enough from the trap this angle should become negligible. In order to overlap the beams as co-linearly as possible, the final cooling mirror was place 1.4m away from the trap centre, a clear quadrant mirror mount was used for the final cooling mirror to allow the guide beam to be placed within 2cm of the centre of the cooling beam, this results in the guide beam having an angle of <15mrad to the direction of LVIS. At the distances now used the standard mirror mounts did not provide enough control over the beam direction for the necessary alignment within the trap. Instead the mirrors were mounted on ultima mounts (Newport, U100-A) and the standard actuators were replaced with micro controle actuators (Newport, SM-13) to provide greater control over beam direction.

The optical dipole potential for given intensity $I(\mathbf{r}_\perp)$ is given by:

$$U(\mathbf{r}_\perp) = \frac{\hbar\Gamma^2}{8\Delta}\left(\frac{I(\mathbf{r}_\perp)}{I_{sat}}\right) \qquad (6.1)$$

where $\Delta = \omega_L - \omega_A$ is the laser detuning from the optical transition frequency ω_A, Γ is the natural linewidth of the optical transition and I_{sat} is the resonant saturation intensity.

Firstly we examined the effect of l=2 and l=3 LG guides [5] on an LVIS generated using the ink spot. The size of the LVIS was ~800μm diameter, the guide beams were focused inside the trap to an equal size; the l=2 guide was focused using two 150mm focal length lenses so that the hollow region of the beam was ~900μm in diameter at trap centre, the l=3 beam was focused using f=500mm and f=300mm lenses to give at the trap centre a dark region ~800μm diameter. The dipole potentials of the l=2 and l=3 guides were 9mK and 13mK respectively from a beam detuned 2GHz from the atomic transition. The Rayleigh range of both beams was much larger than the trapping volume so the guide can be considered a non-diffracting tube for the guiding distances involved.

In order to observe efficient guiding the LG beam waist should be comparable to the size of the cold atomic beam from LVIS. Experiments using l=2 guide beams with a hollow region of only 450μm diameter did not produce any noticeable increase in the LVIS beam. This is because the guide beam actually restricted the size of the initial MOT cloud by producing a repulsive dipole force around the centre of the trap and limited the size of the LVIS flux.

The guide beams were detuned up to 9GHz away from resonance. As a crude measure of the frequency a rubidium cell could be placed in the beam, when the laser was on resonance a line of fluorescence in the cell due to

absorption and emission of the guide beam was clearly observable. This could not be observed when the laser was detuned by 1GHz so this could be used to check the calibration of our guide laser. The birefringent filter on the Ti:Sapphire laser could drift from day-to-day so the above method was used to ensure that it was positioned correctly at the start of the experiments.

Alignment of the guide beam was performed by tuning the beam onto resonance; the beam was passed through an ND (neutral density) filter to reduce the power to ~100mW. The path of the beam can be aligned by observing a dark line though the cloud where the spontaneous emission effects due to the guide beam heats the atoms out of the trap. The power of the guide was reduced in order to avoid completely ablating the cloud. Once the alignment was satisfactory the ND wheel was removed and the guide laser was detuned away from resonance. Images of the trap were recorded using the CCD cameras with individual stills being digitally captured to a PC using a National Instruments' DAQ card and Vision Builder software.

Typical CCD images for an $l=2$ guide beam are shown in figure 6.6; (a) shows the unguided LVIS, the results of a 220mW, 5GHz detuned guide beam is shown in (b) and the position and size of the guide beam over the LVIS is indicated by (c). This guide beam provides a dipole potential of 4mK at the focus, this corresponds to a maximum transverse velocity that may be guided at 100cm/s, the typical transverse velocity of an LVIS atom is 30cm/s [4] which implies all the atoms are guided long the LG beam. Analysis of the guide was achieved by taking intensity profiles along the lines indicated, line 1 is a longitudinal profile along the LVIS, line 2 is a transverse profile taken

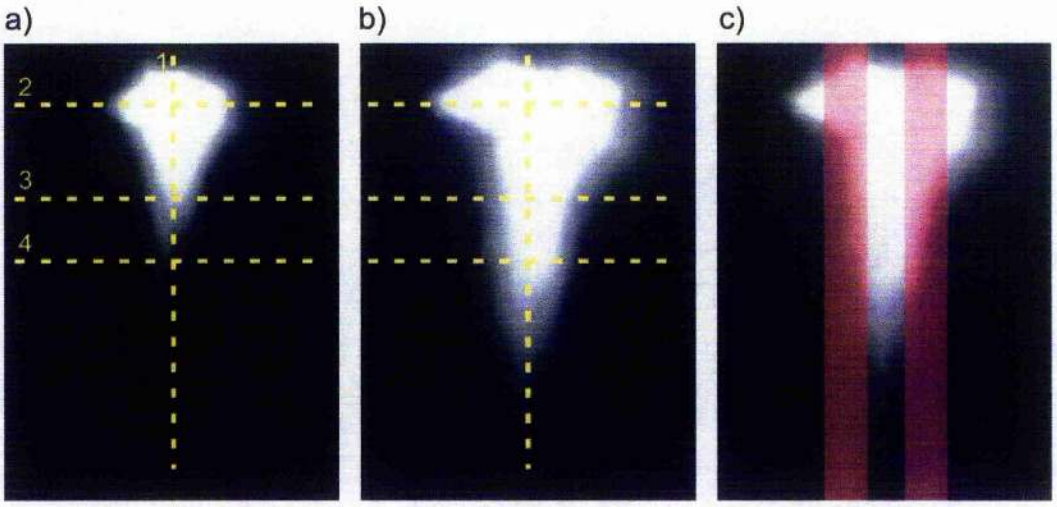

Figure 6.6: Guiding LVIS with an LG^2_0 beam. The LVIS is shown in (a), the result of the applied guide is given in (b) and the position of the guide is indicated by (c). Intensity profiles taken along the lines indicated are found in figure 6.7.

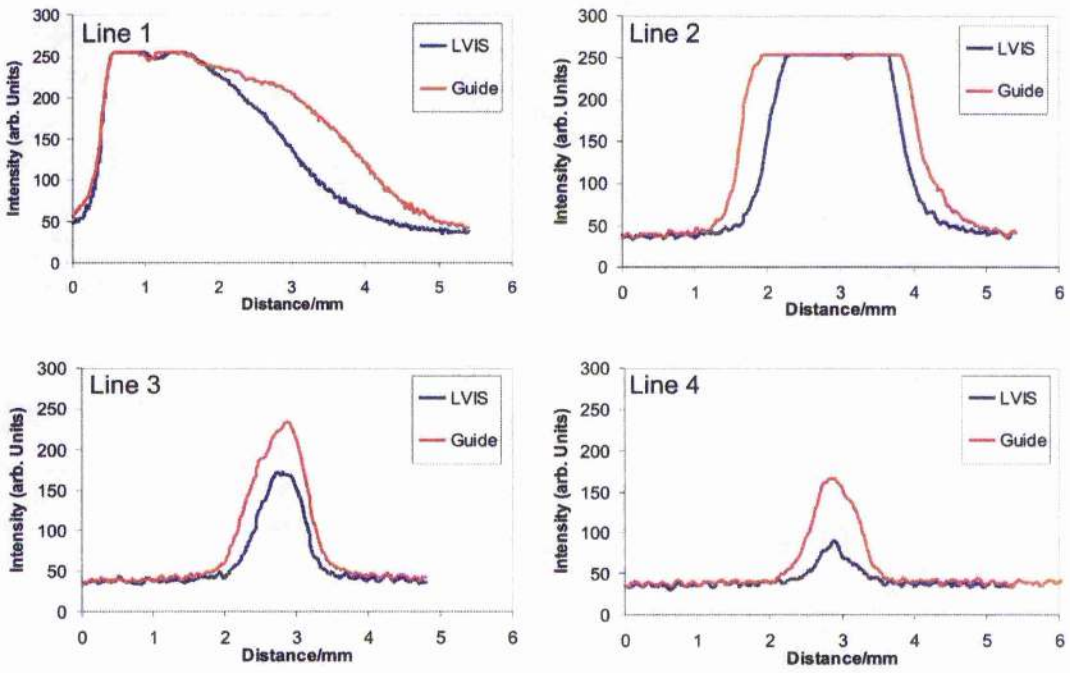

Figure 6.7: Intensity profiles taken along LVIS with and without an LG^2_0 guide beam present. The profiles are taken along the lines indicated in figure 6.6.

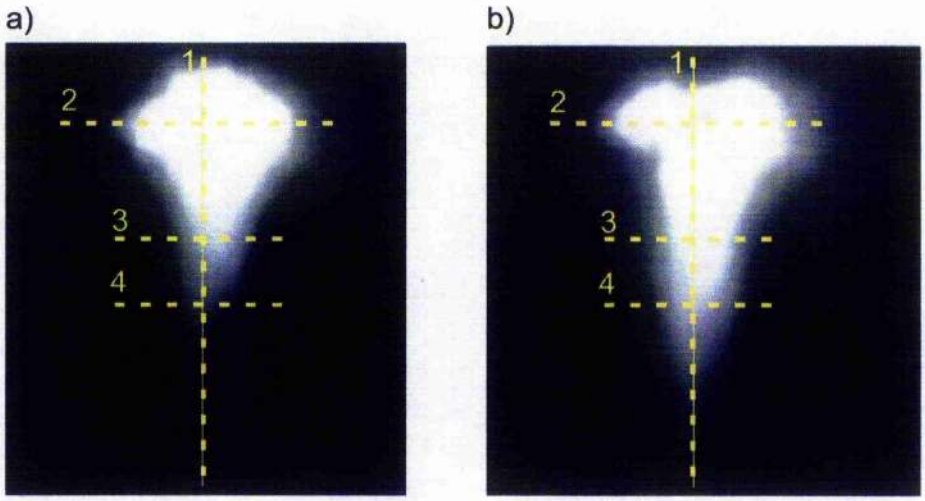

Figure 6.8: Guiding LVIS with an LG^{3}_{0} beam. The LVIS is shown in (a), the result of the applied guide is given in (b). Intensity profiles taken along the lines indicated are found in figure 6.9.

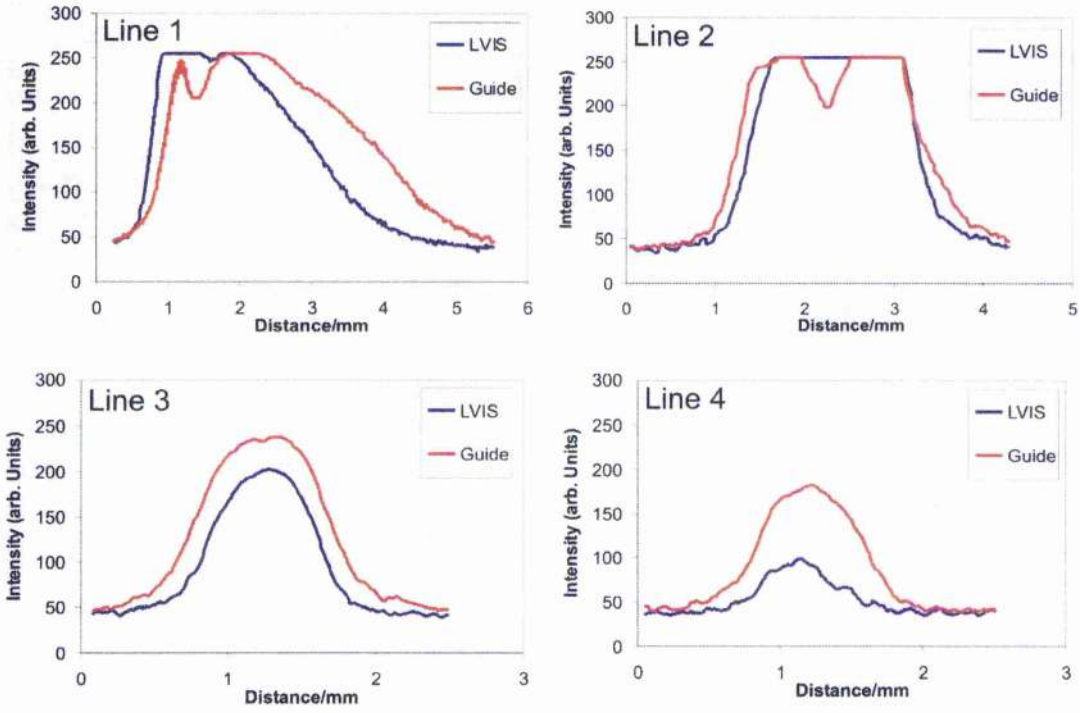

Figure 6.9: Intensity profiles taken along LVIS with and without an LG^{3}_{0} guide beam present. The profiles are taken along the lines indicated in figure 6.8.

across the cloud centre, and lines 3 and 4 are taken across the LVIS beam. The data from these graphs are shown in figure 6.7. Equivalent figures for a 250mW, l=3 guide detuned 5GHz from the atomic transition are given in figure 6.8 and 6.9 for the corresponding profiles. Here the dipole potential of the guide is 5mK.

These results for both LG beams clearly show the lengthening of LVIS and a widening of the centre of the MOT. Since the guide has zero intensity in the centre beam along the length of LVIS spontaneous emission due to the guide can be eliminated and the increase in fluorescence can be assumed to be due to the guiding beams. The widening of the centre of the MOT cloud is due to repulsion of the guide displacing the atoms from their normal equilibrium position. Both guide beams produce a significant increase in the length of LVIS; the l=2 guide produced an increase of 120% in the observed fluorescence of the atomic beam ~4mm from the centre of the cloud, and the l=3 beam produced an increase of up to 150% in the atomic fluorescence at the same distance.

The use of l=1 and l=3 guide beams was investigated more thoroughly to determine the role of guide detuning and power in the change of the efficiency of the guiding. For these experiments the LVIS was generated using the etched glass spot. The LG guide beam was imaged inside the trap to produce a hollow region ~500μm in diameter at the beam focus in order to match the size of the LVIS. Here the l=1 guide beam has a maximum power of 250mW and the l=3 had a maximum of 210mW. The power of the guide beams could be reduced to ~100mW by reducing the pump power to the

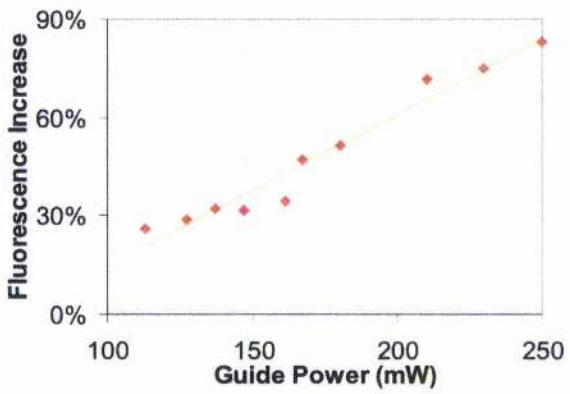

Figure 6.10: Graph showing the effect of increasing guide power for a 3GHz detuned LG^1_0 beam. This is a linear relationship as the dipole potential is proportional to the intensity of the beam. The solid line is a best fit plot.

Ti:Sapphire laser. The power was reduced in this way to eliminate any worries regarding slight misalignment of the beams that might occur if a filter was placed in the beam. The effect of the power of the guide beam was explored using constant detunings of 3, 5, and 7GHz. The power of the guide was then held constant at the maximum value and the guide was blue-detuned from 0 to 9GHz. The guide beam was kept at the high powers to maximise the observable tuning range.

The cloud images were recorded onto VHS video and then converted into digital format, using a Pinnacle studio DC10plus video card, in order to capture the desired images. The fluorescence of the LVIS was measured approximately 4mm from the MOT centre. The results on guiding efficiency of decreasing power with an l =1 guide beam at 3GHz is given in figure 6.10. We see increase in fluorescence falls off steadily with decreasing guide power due to the reduction of the dipole force imposed. From equation 6.1 the

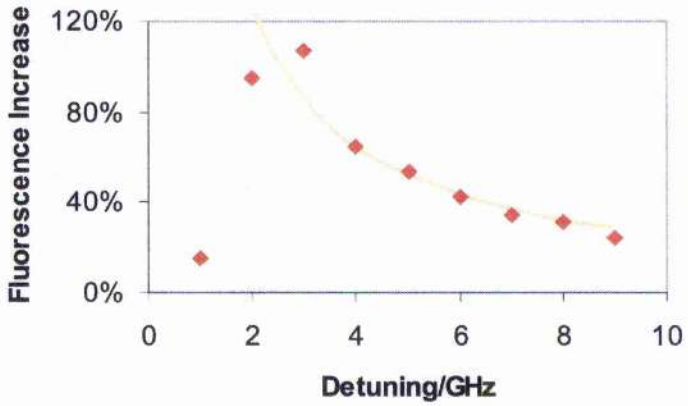

Figure 6.11: Graph showing the effect of increasing the detuning of the guide for a 250mW LG^1_0 beam. The solid line shows a $1/\Delta$ plot (where Δ is the detuning), the data deviates from the curve because of heating effects at low detuning.

dipole potential of a beam is linearly proportional to the intensity, and, therefore power, in the guide beam.

The effect of detuning the l =1 guide is shown in figure 6.11. We see that the measured increase in fluorescence does not vary as $1/\Delta$ as expected from equation 6.1, the fluorescence increases until a maximum is observed near 3GHz which then decays rapidly as the detuning is increased further. The loss of guiding efficiency at low detuning is due to the near-resonant light causing unwanted scattering, heating up the atoms which then destroys the MOT and LVIS. As the detuning is increased this scattering rate falls so there are more atoms available to guide and the efficiency of the guide is increased up to an optimum value beyond which the scattering force has a negligible effect and the efficiency falls due to the $1/\Delta$ reduction of the dipole force. Our observation of this optimum detuning near 3GHz is in agreement with work

performed by Xu *et al.* [2] for a guide beam co-propagating with the atomic cloud. We note that the experiment in [2] is performed on a free falling cloud with cooling and hyperfine beams turned off, as such some differences between our results and those of Xu's could be expected. The agreement observed in the two results implies that role of constant cooling and the presence of the hyperfine beams is not very significant.

Although these results are taken at a position ~4mm from the centre of the MOT these values for the percentage increase seen are roughly constant along the whole of the LVIS beam (graphs of the increase along the LVIS for an l=1 guide are given in figure 6.12), this implies the whole LVIS beam is enhanced by the guide beam and that we are not simply confining the atoms already in the LVIS beam beyond the range in which they would normally recycle back into the MOT.

The data recorded for these experiments are based only on the fluorescence as measured from a CCD camera. Although the fluorescence is directly linked to the atomic flux it is not a direct measure of the flux as it is also dependent on the intensity of the cooling light. We are also limited by the sensitivity of the CCD over the fluorescence level that can be measured. The LVIS beam has been measured beyond the distance observed with the camera using a low power probe tuned to the atomic transition, absorption of this beam has been measured at least 1.5cm from the centre of the MOT. We were not able to probe the beam any further than this due to limited optical access in the system.

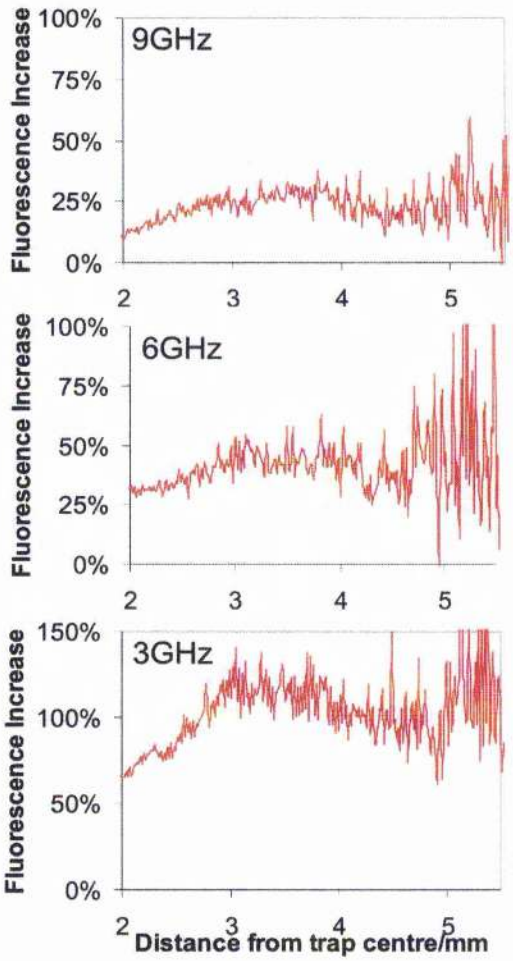

Figure 6.12: Graph showing the increase in fluorescence along the length of LVIS for 9GHz, 6GHz and 3GHz detuinings. The graph is more noisy towards the end of LVIS because of the smaller signals detected.

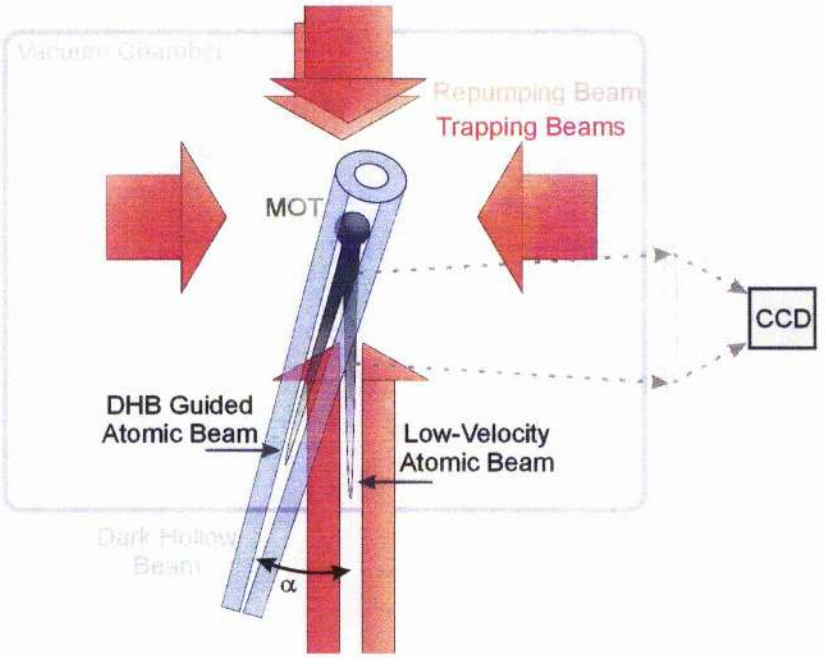

Figure 6.13: Schematic diagram of dark hollow beam (DHB) guiding of LVIS performed by Yan *et al*. Reproduced from [8].

6.4 Oblique Guide

Since the use of blue-detuned hollow beam guiding has been shown to improve the flux of an LVIS beam, and the advantages of using such a beam, zero intensity in the volume of atomic flux leading to closer detunings and lower power requirements, are still valid the next step would be to use a hollow beam for oblique guiding and splitting of an atomic beam.

Red-detuned guides [6] and Raman pulses [7] have been used to split an atomic ensemble. In 2000 Yan *et al* [8] reported on the splitting of a LVIS beam with a hollow optical guide, however, we believed some important details regarding the coupling of atoms into the dark hollow beam were left unanswered. The Yan experiment used a thin annulus of light, produced

using two axicons [9], as the blue-detuned guide. A Ti:Sapphire laser provided 200mW of tunable light for guiding the atoms. The LVIS beam was generated in the direction of gravity as shown in figure 6.13, with the guide beam propagating at 8° to LVIS. Yan reported a fraction (up to 50% of the total flux) of the LVIS beam was split from the vertical beam along the direction of the hollow beam, it was concluded that this fraction of LVIS was coupled into the hollow guide.

A similar experiment performed at St Andrews with a blue-detuned LG guide showed significant differences to the results of Yan *et al*, and highlighted some of the problems associated with coupling into hollow beams at oblique angles. The results of this experiment and a potential solution to the coupling problem will be described in the next section.

6.4.1 Laguerre-Gaussian Guide

The experiment performed at St Andrews showed some differences to that of Yan *et al*; we generated LVIS horizontally and used a co-propagating LG^3_0 as the guide beam (the DHB of Yan's experiment was counter-propagating with the direction of LVIS). The experimental geometry is given in figure 6.14. LVIS was generated using an ink spot to create an intensity imbalance in the cooling beams, the orientation of LVIS in the MOT was rotated by 90° to that in the previous experiment in order to align with the short axis of the trap, this permitted oblique guide angles of up to 20° (optical access was such that the maximum angle permitted along the long axis was <7°), the guide was aligned

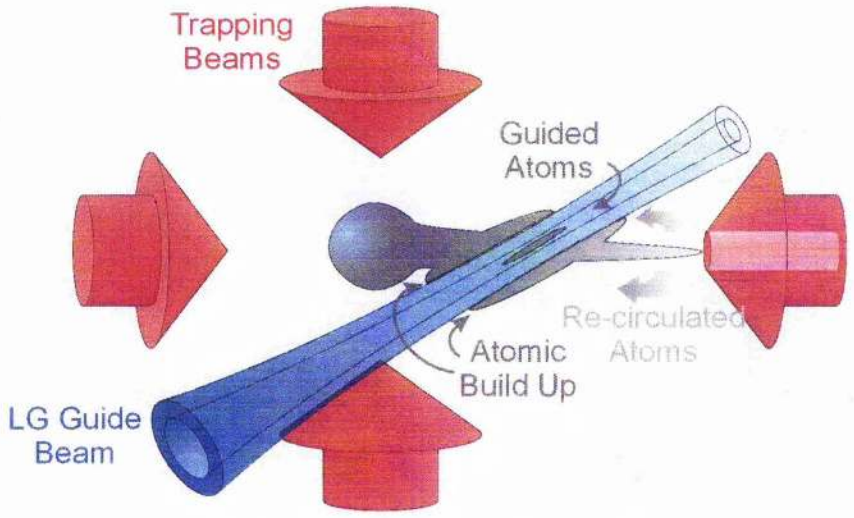

Figure 6.14: Schematic diagram of oblique LG guiding of LVIS. There is a build up of atoms around the LG beam due to LVIS and recirculating atoms with insufficient velocity to overcome the potential barrier imposed by the guide.

to ~8° to LVIS to compare with the results of Yan. The Laguerre-Gaussian guide beam was generated using a hologram designed for 1064nm, this produced only 25% efficiency when using 780nm light and resulted in a maximum power of 180mW. The beam was focused into the trap using a final lens with focal lengths 300mm to 600mm to produce a guide beam with a waist that varied from 100 to 300μm. Two CCD cameras placed orthogonally to each other were used for beam alignment and data capture.

From alignment of the on-axis guide beams we expect to see two dark lines across the cloud from heating of the atoms due to the walls of the guide beam. When the beam waist was ~100μm only a single ablated, dark line was visible across the cloud. In no position could we observe a flux of atoms along the centre of this beam. With the guide expanded to a beam waist of

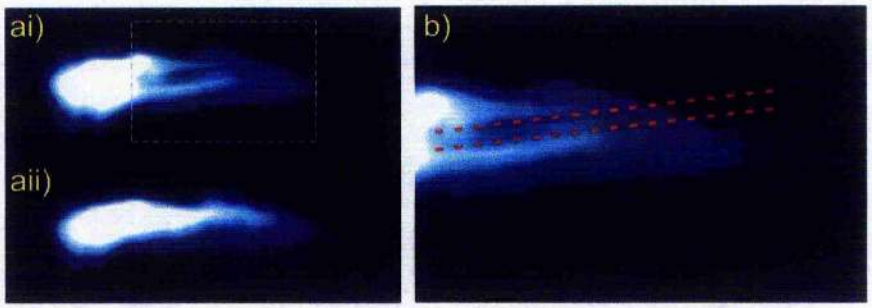

Figure 6.15: Images of LVIS with (ai) and without (aii) an LG^3_0 beam guide beam of waist 300μm. The guide beam is detuned 5GHz from resonance and has a power of 180mW. A close up of the guide (b) shows very few atoms in the hollow region, and an increase around the sides of the LG beam. The red line shows the path of the beam.

300μm two clear dark lines are observed with build up of atoms around both sides of the guide and visible in the dark centre of the beam. Figure 6.15 shows the typical behaviour observed.

These results show a large build up of atoms on the near side of the guide, very few atoms in the centre of the beam and finally another large build up of atoms on the far side of the guide. In fact the atoms within the guide are not observed to extend beyond the range of the initial LVIS beam. At the angle of the guide (8°) we calculate the maximum transverse velocity that can be caught by the guide is 1.3m/s. This can be explained as follows: atoms exiting the MOT along the LVIS first encounter the repulsive wall of the LG beam. The slower velocity atoms will be unable to overcome this potential and are deflected along the guide beam. Thus the atoms must first overcome the first potential wall to enter the guide centre. However, if the longitudinal velocity of the atoms is enough to overcome the dipole potential of the first

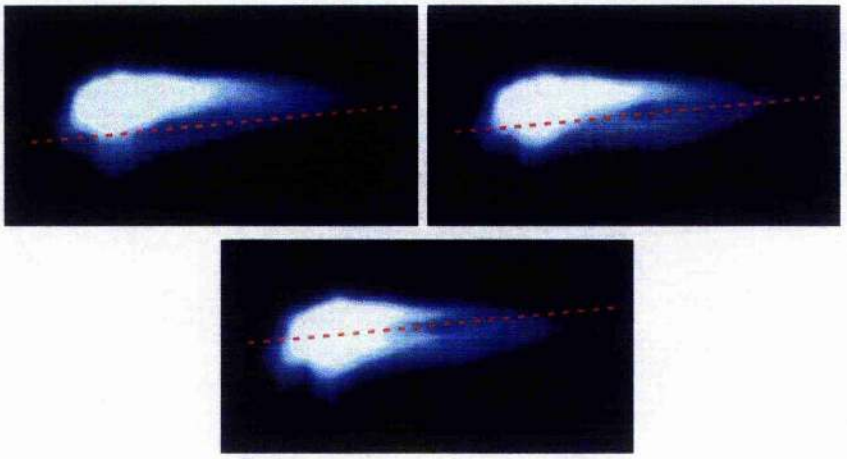

Figure 6.16: Images of LVIS with a blue-detuned TEM_{00} beam. The red line shows the path of the beam, the same build up of atoms as figure 6.15 is observed around the outside of the beam. The centre of the beam creates a dark line due to the heating of the atoms.

wall then they are likely to overcome the second as well and not be coupled into the oblique guide. The large build up of atoms on the downstream side of the LG beam can be accounted for as being fed by the recycled atoms from the LVIS. Once the LVIS atoms have escaped from the intensity imbalance in the cooling beams they once again undergo cooling in all three dimensions and they will be cooled and returned to the centre of the trap. It is these slow moving atoms that are encountering the LG beam that accounts for the large build up of atoms on the far side of the guide. In comparison the guiding reported by Yan (an image of the LVIS splitting is given in figure 3.18) showed no effect of the guide beam on LIVS itself and reported no difficulties with coupling atoms into a hollow guide beam.

This effect was verified by introducing a blue detuned TEM_{00} beam across the cloud. The hologram producing the LG beam was translated slightly so that

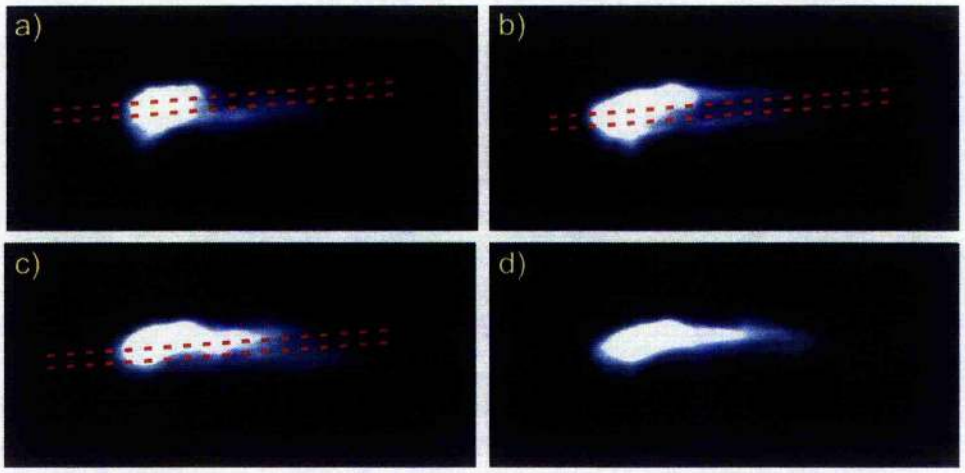

Figure 6.17: Moving the LG Guide beam across LVIS. The guide beam is positioned to completely overlap with the MOT (a), in the centre of LVIS (b) and close to the end of LVIS (c). (d) shows LVIS without a guide present. The red lines indicate the path of the guide beam.

the dislocation of the grating no longer overlapped with the laser beam, now the hologram acts just like a linear diffraction grating, in this way a TEM_{00} beam of the same power as the LG beam could easily be positioned over the cloud without the need for realigning any of the optics. The blue-detuned TEM_{00} beam clearly showed the same build up of atoms around the guide beam and a clear dark region in the LVIS due to heating of the atoms, see figure 6.16.

The effect of the position of the guide with respect to LVIS was also investigated. Figure 6.17 shows the results from crossing the guide beam at different positions along LVIS, here the LG beam is detuned 5GHz, with a beam waist ~200μm and a power of 180mW. With the cross over point near the end of LVIS (figure 6.17c) there is no significant coupling of the LVIS beam into the guide nor is there a large build up of atoms around the edges

of the guide at this point. Atoms at the end of LVIS have had a greater distance over which to accelerate. Thus the atoms have greater velocities and are less likely to be deflected by the guide beam so there is a reduction in the build up on the near side of the guide beam. There is still some build up of atoms along the far side of the guide, however, it is concentrated closer the MOT end of the guide beam since this is where the atoms are travelling at their slowest. As the guide beam is moved closer to the centre of the MOT more atoms are observed in the centre of the guide and there is a greater build up of atoms along the guide. If the guide is positioned too close to the centre of the MOT (figure 6.17a) the atomic cloud is distorted by the potential of the guide beam and no build up of atoms is observed around the guide or inside it. LVIS is still observed beyond the guide because atoms that form it can flow around the guide.

The effect the detuning of the guide beam has on the LVIS is shown in figure 6.18. The LG beam had a waist of ~300μm and the power was 180mW. At low detuning the scattering rate of the guide is large enough to heat up a large fraction of the atoms in the MOT and LVIS so there is only a very small signal observed, as the detuning is increased the scattering rate falls and the guide beam becomes clearer, the most intense region of the guide is the only place the heating effects are sufficient to allow atoms to escape the MOT. The clearest guiding was observed at 5GHz (6.18d), increasing the guide detuning beyond this resulted in a lessening of the effect of the guide beam.

From these results it can be seen that it is not a trivial undertaking to load atoms into an oblique hollow guide with any great efficiency. The guide beam

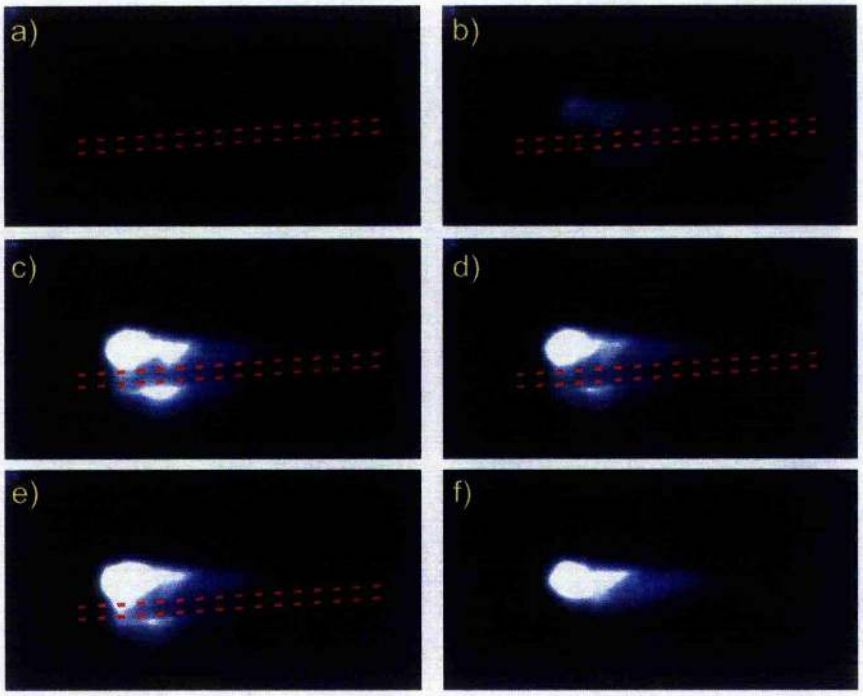

Figure 6.18: The effect of detuning of the guiding of LVIS. The guide beam in figures (a) – (e) have detunings of 2GHz to 6GHz respectively. The LVIS beam with no guide present is given in (f). The red lines indicate the path of the beam.

acts more like a velocity selective element, atoms with too much energy pass straight through the guide, those with too little never overcome the first potential barrier and are deflected along the guide beam. This effect may be overcome by the use of a counter-propagating guide beam with respect to the LVIS direction, a counter-propagating beam may assist in the coupling by slowing the atoms by radiation pressure forces, thus upon traversing the first potential wall of the guide beam the atom will be slightly decelerated which may reduce the velocity of the atoms enough to be contained by the second wall. This could explain the higher coupling efficiencies seen by Yan *et al*, however, the lack any visible ablation of the atoms due to the guide beam, as

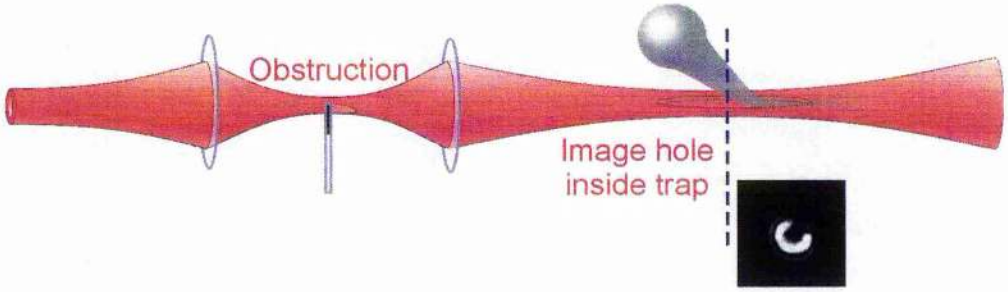

Figure 6.19: Geometry for imaging an obstruction into the trap region to allow LVIS to enter the guide.

predicted by our physical model, could imply the guide beam was just clipping LVIS and the observed coupling is, in fact, deflected atoms. Due to physical restrictions of our experimental arrangement we were unable investigate the effects of a counter-propagating guide beam.

6.4.2 Obstructed Laguerre-Gaussian Guide

The very guide beam and dipole forces we aim to utilise for guiding the atoms limits the coupling into the hollow region of the guide beam. In order to increase coupling efficiency into the LG guide we need to remove the first potential wall the atoms see, once the atoms are through the first wall they can be captured by the back wall of the LG beam and guided away from the LVIS atoms.

A hole in the LG beam was formed by imaging an obstruction into the guide. An obstruction was placed at the focal plane between two lenses and then focused inside the trap where LVIS intersected the guide beam, the geometry for imaging the obstruction is given in figure 6.19. Lenses of focal length

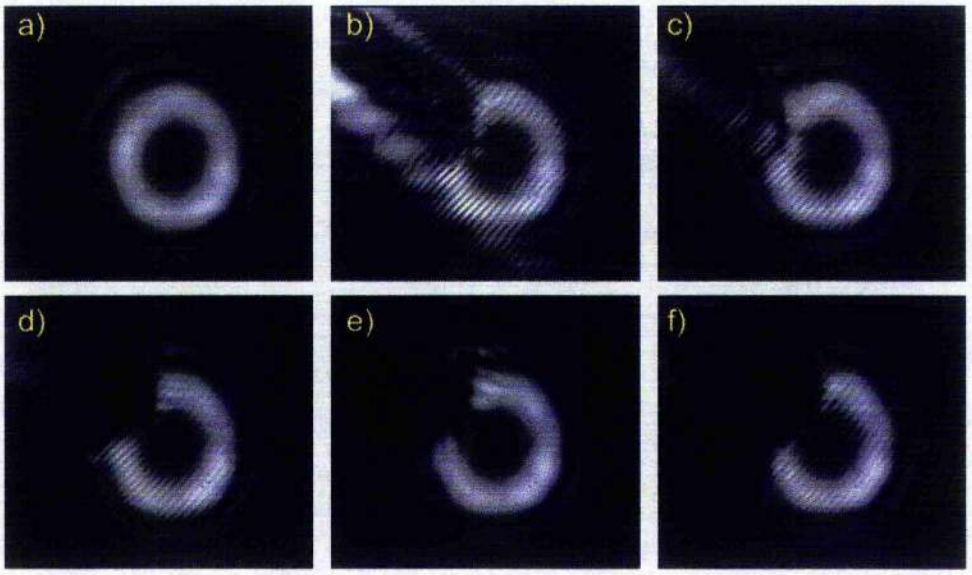

Figure 6.20: The results of using different obstructions to create a hole in the LG beam. (a) shows the original LG beam, obstructive elements used are: the corner of a microscope cover slip, clear (b) and opaque (c), a 60° corner of opaque cover slip (d) and 200μm (e) and 100μm diameter optical fibre (f).

500mm and 300mm were used to produce a beam with a waist of 300μm to better compare with the earlier guiding results. The image formed between these two lenses was less than 1mm in diameter and several methods for obstructing the beam with the minimum of interference effects to the rest of the LG beam were tested. The effect of various obstructions on the beam is shown in figure 6.20. The image with the sharpest shadow region was made using a microscope slide which had been cut to give an apex of 60°, this was then blackened and placed into the LG beam using a x-translation stage. A second method for generating a hole in the wall of the LG beam is to translate the hologram that generates the beam away from the optical axis; the phase vortex in the LG beam is positioned where the dislocation of the diffraction grating is on the incident beam. By positioning the dislocation to the edge of

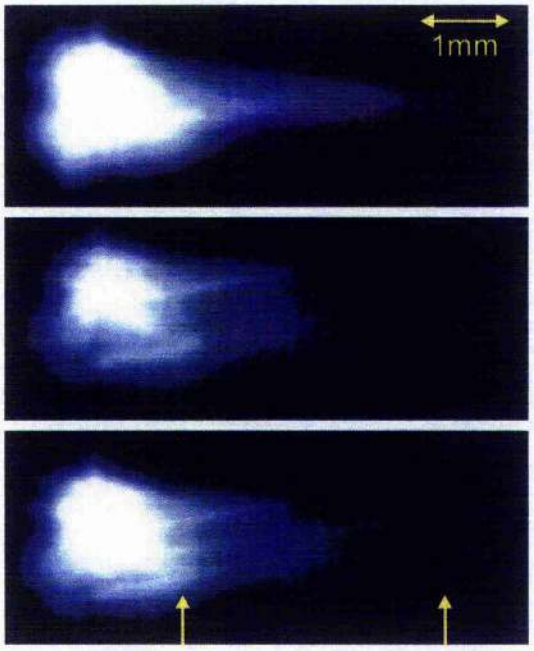

Figure 6.21: Images of the enhanced guiding of LVIS with an obstructed LG guide beam. Figure (a) is the LVIS, (b) is the introduction of the guide beam and (c) the insertion of the obstruction into the guide. Intensity profiles taken along the oblique guide over the distance indicated by the arrows are given in figure 6.22.

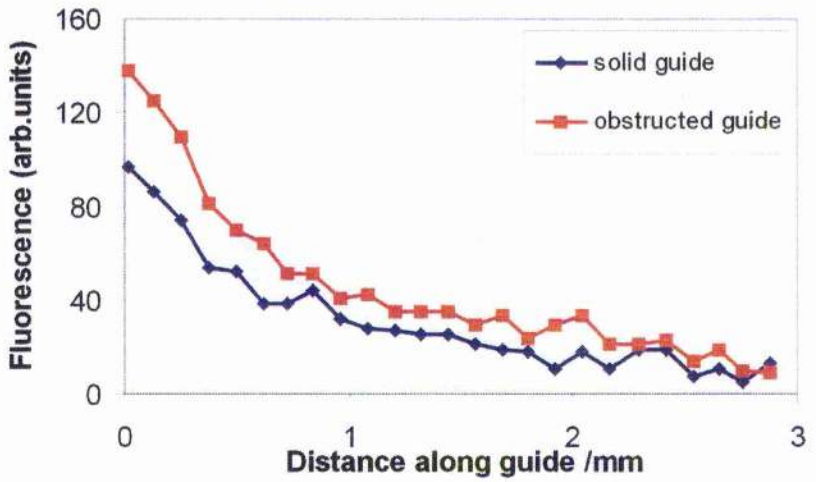

Figure 6.22: A comparison showing the enhancement of atom fluorescence along the oblique guide. The profile is taken along the guides as indicated in figure 6.21.

the TEM_{00} beam a beam can be produced that has one side of the ring very narrow and the other much thicker, this would make it easier for atoms to penetrate into the guide and provide a more intense potential at the back wall to contain the atoms, however, this technique will result in a guide beam that propagates with a constant asymmetry to it, this means the atoms will always see a lower potential on the near side of the guide and a permanent position from which the atoms can escape. Subsequently this idea was not used because the obstruction produced a more uniform beam which had the potential to diffractively fill and offer a circularly symmetric, two-dimensional guide beam away from LVIS.

The obstructed beam was incident on the MOT at an angle of 8^{o} with a detuning of 5GHz, once the guide beam was aligned the obstruction was inserted into the LG beam. Images of the resulting guides with and without the obstruction were taken. Figure 6.21 shows the guiding observed with a complete LG beam and with the obstructed beam, a comparison of the enhancement of fluorescence (between the arrows) along the guide is given in figure 6.22. The insertion of the guide considerably increases the coupling efficiency into the guide. The atomic flux within the LG beam is about 50% higher with the obstruction inserted measured about 2mm along the length of the oblique guide. In this experiment we have a "horse-shoe" shaped guide beam where one quadrant of the beam is in the shadow of the obstruction, this makes it possible for the atoms enter the guide beam. Although the gap in the ring starts to close up due to diffraction effects there can still be some loss of atoms along the guide as they can leak out through the hole. Ideally

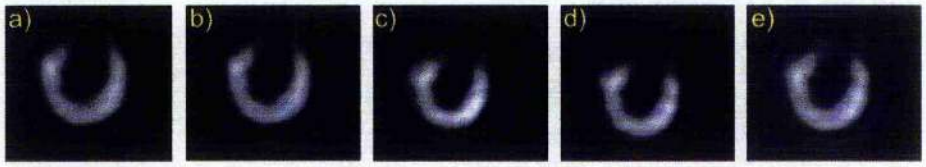

Figure 6.23: Propagation of the obstruction in the LG beam. The figures (a) to (e) show the obstructed beam at -10cm, -5cm, 0cm, +5cm and +10cm from the focus. This is well in excess of the guiding distance.

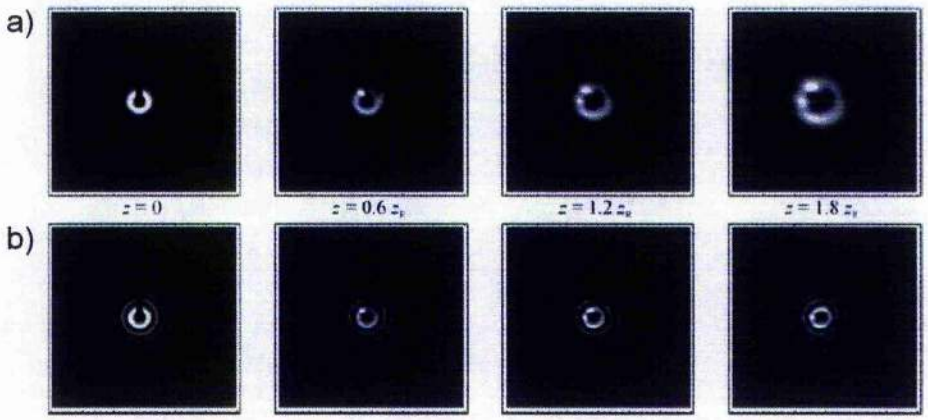

Figure 6.24: Simulated intensity cross-section of hollow beams with a rectangular obstruction of width 50μm. (a) shows an LG beam and (b) a Bessel beam, both have an azimuthal index l =3 and a peak radius of 150μm. The plots are shown in terms of Rayleigh range z_R from the intersection point.

we would like to find that the hole completely closes up on either side of the intersection with LVIS, in this way any atoms captured by the LG beam will continue along a true two dimensional guide. Experimentally we found that the gap does not close for more than the Rayleigh range of the LG beam, the gap in the LG beam propagates for several centimetres (see figure 6.23). This is well beyond the guiding distance involved in these experiments, therefore beyond the overlap with LVIS the guided atoms are not completely confined by a closed hollow guide. This behaviour of an obstructed beam was

confirmed by computer simulations by David McGloin using a standard Fourier transform beam propagation algorithm, figure 6.24. Here a rectangular obstruction of 50μm is placed in a beam with a peak radius of 150μm; the shadow takes more than 1 Rayleigh range, z_R, to fill in. Clearly this is not ideal method for creating a hole with which to permit the atomic flux.

One possible solution to the problem of closing the guide potentials could be the use of other hollow light beams such as the Bessel beam that can reform faster after an obstruction [10]. Simulation of the obstruction of a J_3 Bessel beam with a central ring of equal diameter to the LG beam used is given in figure 6.24b. The Bessel beam reforms around the obstruction after ~$0.6z_R$ and is almost uniform after $1.8z_R$. Another property of the Bessel beam is its non-diffracting nature, this combined with the self-reconstructing nature means a guide beam could be produced that will fill in around an obstruction and provide a constant dipole potential along the propagation distance of the guide.

This method of beam splitting is a technique which can also be used for velocity selection; only the atoms with the lowest longitudinal velocities in LVIS will be deflected by the guide beam leaving the faster atoms to continue through the guide beam. By carefully controlling the dipole potential of the guide atoms with velocities lower than an arbitrary threshold value could be removed from a cold atomic beam.

6.5 Far-off Resonance Guide

Co-linear guiding of LVIS using a red-detuned TEM_{00} beam has also been performed. This work was led by John Livesey and will be detailed in greater detail in his thesis, so only a brief description will be given here.

A Nd:YAG laser (wavelength 1064nm) was used as a far-off resonant guide and supplied up to 10W of power. The large detuning of the laser allowed a dichroic mirror to be used and the beam aligned to be exactly co-linear with LVIS. The beam waist of the guide beam was varied from 100μm to 500μm, with the majority of data taken at the larger end of this range to ensure good overlap with LVIS. From a 500μm waist beam we calculate a maximum potential of 13μK, well below that of the LG beams described earlier. The enhancement in flux observed with this guide beam is <10%, however, a brief surge (~160ms) in flux is observed when the guide is initially turned on, this effect had been noted by Houde *et al* [6] but was not investigated further.

To investigate the transient response a shutter with a rise time <1ms was used to introduce the guide beam. The guide does not couple the atoms out of the MOT (the detuning of the beam ensures that any scattering events are negligible), but enhances the flux by way of a non-adiabatic momentum kick due to the energy variation. The LVIS response was recorded and the surge and decay rates were calculated, a graph showing the increase in flux observed is given in figure 6.25. A surge in guided flux of up to 25% is observed ~160ms after the introduction of the guide, following which the

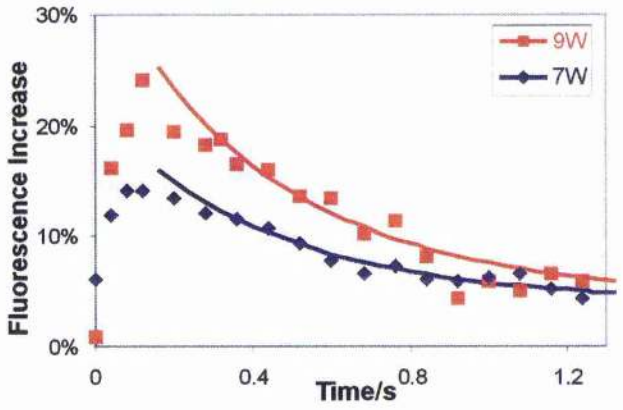

Figure 6.25: Transient response due to a far-off resonant guide beam for two guide powers. A non-adiabatic kick is given to the atomic flux leading to an increase in flux for 160ms which then decays down to a steady state value. The solid line is an exponential fit of the decay with τ=0.45s.

increase decays in an exponential fashion. The characteristic decay time is found to be 0.45s. This decay rate can be comparable with the loading time of the MOT, thus by slowly chopping the guide beam close to the decay rate of the transient it should be possible to operate the guide in a pulsed operation and obtain a substantially higher guided flux.

6.6 Summary

We have demonstrated guiding of a cold atomic beam along co-propagating collinear and oblique LG beams. The use of a collinear guide has been shown to increase the guided flux along the entire length of LVIS, further examination of the effects of power and detuning was made and the results showed good agreement with those of Xu *et al* [2]. Coupling into oblique

hollow guides introduces complications to an experimental arrangement. Initial experiments coupling into an oblique guide showed very little coupling, the majority of atoms either passed straight through the guide or were deflected around the walls of the beam. By imaging a hole in the side of the guide beam inside the trap an access point for the atoms is created and an enhancement of the guided flux was observed. Our method for producing the hole in the guide beam relies on diffractive filling to close the gap, however, this takes a significant distance to achieve and during this time the atoms are not truly confined within a two-dimensional guide. The use of a Bessel beam in this geometry is suggested to offer advantages due to the reconstructing nature of the beam closing the hole within a much shorter distance.

Bibliography

[1] L. Pruvost, D. Marescaux, O. Houde and H. T. Duong, "*Guiding and cooling of cold atoms in a dipole guide*," Opt. Commun. **166** 199 (1999)

[2] X. Xu, K. Kim, W. Jhe, and N. Kwon, "*Efficient optical guiding of trapped cold atoms by a hollow laser beam*," Phys. Rev.A. **63** 063401 (2001)

[3] T. L. Gustavson, P Bouyer and M. A. Kasevich, "*Precision Rotation Measurements with an Atom Interferometer Gyroscope*," Phys. Rev. Lett. **78** 2046 (1997)

[4] Z. T. Lu, K. L. Corwin, M. J. Renn, M. H. Anderson, E. A. Cornell and C. E. Wieman, "*Low-Velocity Intense Source of Atoms from a Magneto-optical Trap*," Phys. Rev. Lett. **77** 3331 (1994)

[5] J. Arlt, T. Hitomi and K. Dholakia, "*Atom guiding along Laguerre-Gaussian and Bessel light beams*," Appl. Phys. B **71** 549 (2000)

[6] O. Houde, D. Kadio and L. Pruvost, "*Cold Atom Beam Splitter Realised with Two Crossing Dipole Guides*," Phys. Rev. Lett. **85** 5543 (2000)

[7] M. Kasevich and S. Chu, "*Atomic Interferometry Using Stimulated Raman Transitions*," Phys. Rev. Lett. **67** 181 (1991)

[8] M. Yan, J. Yin and Y. Zhu, "*Dark-hollow-beam guiding and splitting of a low-velocity atomic beam*," J. Opt. Soc. Am. B **17** 1817 (2000)

[9] I. Manek, Y. B. Ovchinnikov and R. Grimm, "*Generation of a hollow laser beam for atom trapping using an axicon*," Opt. Commun **147** 67 (1998).

[10] R. P. MacDonald, S. A. Boothroyd, T. Okamato, J. Chrostowski and B. A. Syrett, "*Interboard optical data distribution by Bessel beam shadowing*," Opt. Commun. **122** 169 (1996)

Chapter 7:

Hollow Beam Guiding of a Free-falling Atom Cloud

7.1 Introduction

The previous chapter used hollow beams to guide an atomic beam; however, due to experimental constraints with the trap geometry we were unable to probe the atomic beam further than 15mm away from the MOT centre. In order to improve optical access and permit guiding over greater distances a new trap was built. The improved optical access also made it simpler to launch probe beams to more accurately measure the atomic flux than possible with the CCD camera. A free-falling atom cloud from a MOT is used as the source of atoms for these experiments rather then LVIS. This means we no longer produce a CW atomic beam, however, the velocity of the atoms is much reduced in a free falling cloud (over a 5cm drop the atoms have

reached an average velocity of 30cm/s compared to the 14m/s produced in LVIS) so the guide beams can have a greater effect on the atomic ensemble.

Previous experiments in blue-detuned guiding of a free-falling atom cloud have used axicon [1] and fibre [2] generated hollow beams. In this chapter we study the guiding of a free falling MOT with hollow Laguerre-Gaussian and Bessel beams [3]. The Bessel beam is a non-diffracting beam which provides a constant guiding potential over its propagation length but does not maintain this profile into the far-field. The LG beam is a true free-space mode and can, therefore, be used for extended guiding, though the beam is subject to divergence. We observe the power limitations on the central feature of the Bessel beam severely limits its usefulness as a guide beam compared to an equivalent sized LG beam generated with the same overall power.

7.2. Experimental Setup

In this chapter we are comparing Laguerre-Gaussian and Bessel beams for use as a guide beam, as such the experimental conditions are the same for each guide beam. In this section we shall first describe the generation of the MOT, then the creation of a probe beam for detecting the atomic flux along the guide and finally look at the timing mechanism for releasing the MOT and inserting the guide beam.

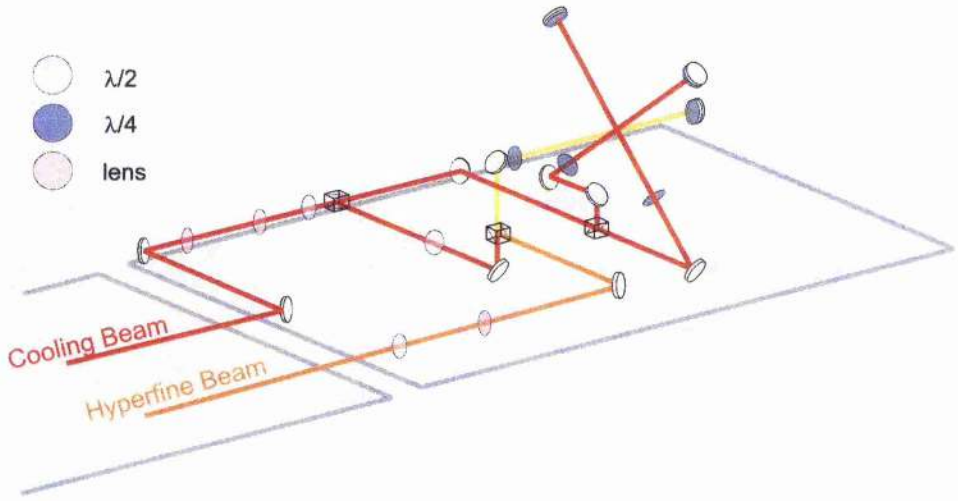

Figure 7.1: Experimental diagram of the MOT. The lasers used are the same as in figure 6.1.

7.2.1 Generation of a MOT

In order to make accurate measurements of the atomic flux the drum trap, described in section 4.4.3, was used. This provided more optical access for inserting probe beams and allows guiding of the atoms over a greater distance than the 10-way trap used in chapter 6. A MOT is formed in the centre of the trap using cooling beams, generated using the circularised diode injection locked to an ECDL, orientated at 45° to the vertical, a diagram of the experimental set up is given in figure 7.1. This leaves the top viewport clear so that the guide beam can co-propagate with a free falling atomic cloud in the direction of gravity. The hyperfine beam is provided by a second ECDL. The hyperfine is gently expanded using a f=100mm lens and is then combined with the horizontal cooling beam, to limit the amount of opto-mechanics which surrounds the trap, using a polarising beam splitting cube.

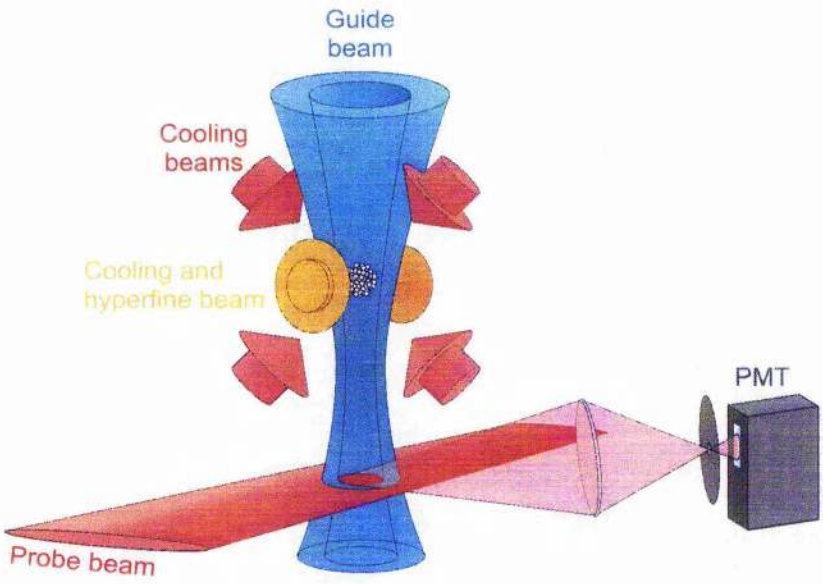

Figure 7.2: Experimental diagram for guiding of a free-falling atom cloud within a hollow beam. The guide beam propagates vertically down. This diagram illustrates the LG beam as a guide; however, the design is identical for the Bessel beam.

7.2.2 Detection of the Atoms

The general experimental set up for guiding is showing figure 7.2. Detection of the atoms is performed by two probe beams in order to take advantage of the optical access around the trap. The probe beam was a combination of light tuned to the $3S_{1/2}(F= 3) \rightarrow 3P_{3/2}(F'= 4)$ transition and the hyperfine beam at the $3S_{1/2}(F= 2) \rightarrow 3P_{3/2}(F'= 3)$ transition. Light from the cooling ECDL was separated off using a 70/30 beam splitter (70% to the trap); two AOMs, one providing a fixed 80MHz and the second an 80MHz ± 24MHz frequency change, were then used to shift the frequency of the probe beam light onto the transition (the cooling light is detuned by ~12MHz). This provided 1.5mW

of power which was then expanded using cylindrical lenses into a light sheet 1×5mm across. The probe beam was aligned perpendicular to the large viewport and could be used to probe up to 5cm from the centre of the MOT, however, due to the opto-mechanics required for the cooling beams probe access was restricted close to the MOT centre. For these short distances a second probe was incident onto the trap at 90° to the first beam through the small viewports which are free of cooling optics. The two probes could not be used to measure flux at different positions along the guide at the same time as the atoms would be heated up by absorption of the first probe. For fluorescence imaging the probe beams are retro-reflected after passing through a quarter wave plate, this provides an equal radiation pressure from both directions and limits the number of atoms pushed out of the probe beam. The fluorescence from the atoms was collected by an f=75mm lens placed ~100mm from the trap and focused onto a photomultiplier tube, PMT, (Hamamatsu, H7710-03). The signal from both probes was recorded to a digital oscilloscope (Tektronix, TDS 360). An absorption signal could be recorded by reducing the power in the probe beams below I_{sat} and replacing the retroreflecting mirror with a photodiode. In order to remove the noise detected from scattered light due to other sources in the lab a narrow band interference filter (75% transmission at 780nm) was placed in front of the detectors, this effectively removed the unwanted scattered light from other sources around the lab. However, scatter from the guide and cooling beams would pass the filter so care was also taken to physically shield the detectors from scatter light with cardboard tubes.

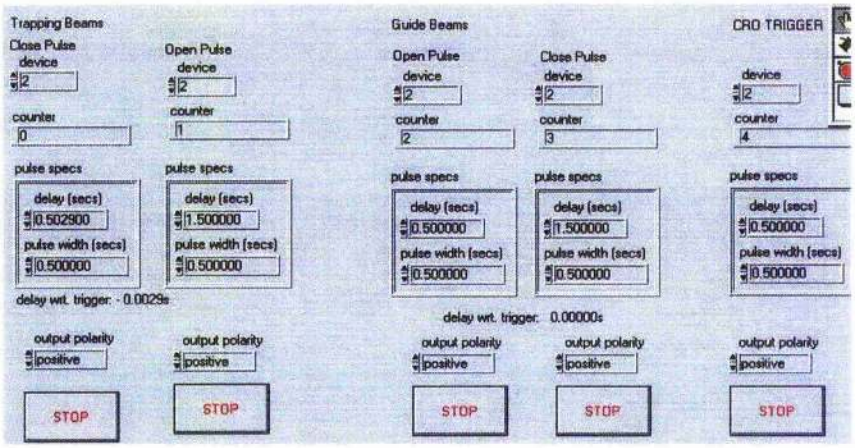

Figure 7.3: The front end of the LabVIEW timing program. Up to 8 pulses can be outputted using the connector board; the delay, pulse length and the sign of the pulse can all be individually set.

7.2.3 Experimental Timing

The guide beam is left turned off during the cloud build up so as not to distort the MOT, once the cooling beams are turned off and the atoms begin to free-fall the guide beam is turned on. The beams were turned on and off using mechanical shutters (Newport, 846HP), the timing of which were computer controlled using a LabVIEW program and a National Instruments PCI-6602 data acquisition card with a CB68LP connector block to provided up to eight output signals. The NI card contained a standard program for controlling the signals sent from the computer, this program was simply reproduced several times to provide on and off pulses for the trapping and guiding beams and to provide a trigger pulse to the oscilloscope to record the data, an example of the front end of the timing program is given in figure 7.3.

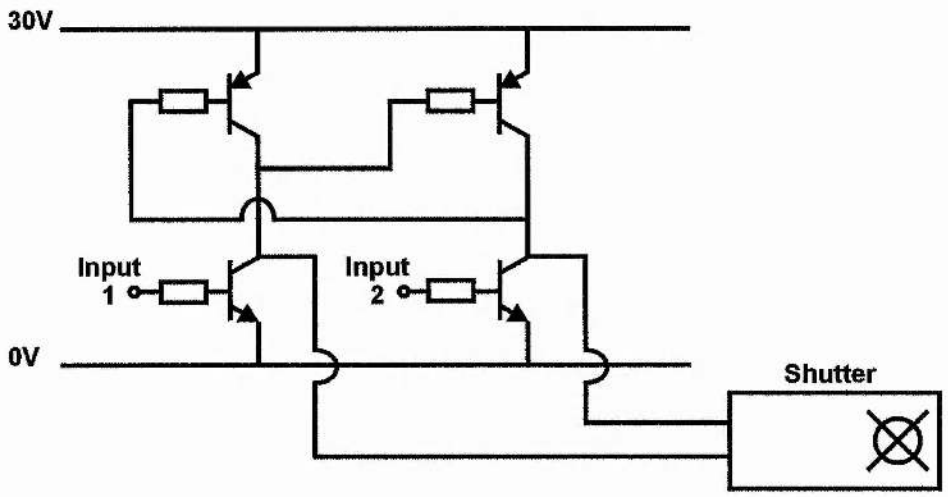

Figure 7.4: Amplifier circuit for the shutter signal.

The mechanical shutters open and close on positive and negative voltages, the speed of the shutter is dependent on the voltage applied; the computer supplied a maximum voltage of only 5V, which did not provide a sufficiently short closing time, and can only output a positive voltage. Instead the shutters were powered from an external power supply, the signal was sent to the shutter through a "see-saw" circuit which could be controlled by the computer. A circuit diagram of the "see-saw" is given in figure 7.4; this provided controlled pulses with positive or negative voltages. It is important to note that the shutters are not designed to run continuously from such high voltages and care needs to be taken to ensure the control pulses sent to the shutters are only a few seconds long. On more than one occasion a continuous signal was sent to the shutters, this was only noticed after a few minutes when the internal circuits in the shutter had melted and we began to smell the smoke; this was not a good thing and I do not recommend repeating this particular part of our experiments. However, when the shutters are run

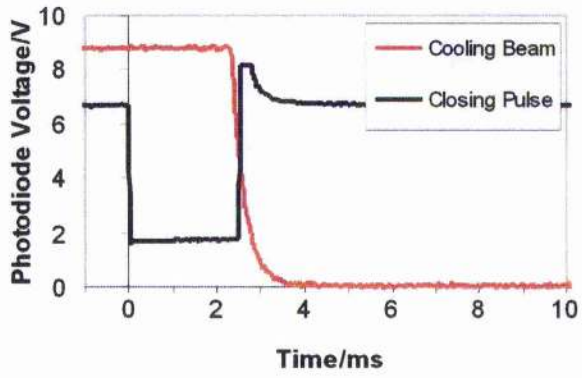

Figure 7.5: Fall time of the Shutter with a 30V close pulse. The shutter closes within 1ms, the delay shown here between the closing pulse (a negative pulse for closing the shutters) and the shutter actually closing can be corrected in the LabVIEW program.

correctly a 30V signal pulse results in a close time of ~1ms. Once the shutters were in place a photodiode was positioned after the shutter, a graph showing the extinction of the cooling beam is given in figure 7.5. The time that the shutter closed at was compared to the trigger of the oscilloscope and any delay between the beam being turned of and the trigger pulse was corrected for by placing extra delay components to the LabVIEW program. The full experimental sequence for the timing of the guide beam was such that concurrently with the cooling beams being extinguished the guide beam was turned on. After 5s the cooling beams were turned on and the guide off to allow the MOT to reform, figure 7.6 shows the timing sequence.

A second, cheaper, shutter system was considered for controlling the beams. These were based on an audio speaker [4], the cone of the speaker is removed and a thin sheet of metal is attached to the electromagnet to be used

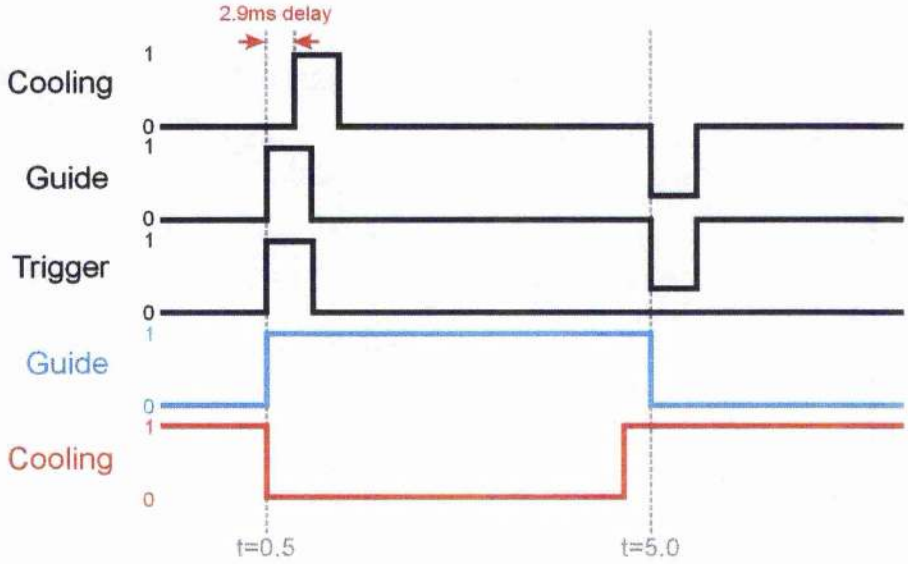

Figure 7.6: The timing sequence used for the guiding of a free-falling MOT. The black lines show the activation pulses, the pulses are 0.5s in duration. The red and blue indicate guide and cooling beams. The guide beam is turned on when MOT is dropped.

as the beam block, a strip of metal is attached over the speaker to stop the electromagnet leaving its housing and permit a larger range of motion for the shutter, a photograph of one of these shutters is shown in figure 7.7. When a voltage is sent to the speaker the electromagnet moves in and out, this opens and closes the shutter. This shutter can provide fast closing times, <2ms, but it was found that the delay between signal sent and the device responding varied by several ms, so it was unsuitable for our experiments. Figure 7.8 shows the closing speed of the shutter, the two pulses shown are generated from identical 10ms triggering pulses and demonstrate the inconsistent response time.

Figure 7.7: A digital photograph of a speaker shutter.

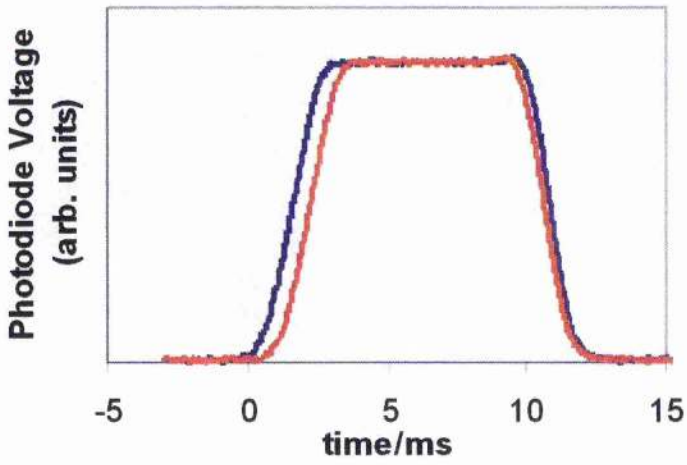

Figure 7.8: The response time of the speaker shutter. The 10ms control pulse is sent at t=0s.

7.3 Laguerre-Gaussian Guiding

The LG^1_0 beam was used to guide the atoms distances up to 5cm. The guide was focused to a beam waist of 600μm. The power of the guide was varied from 200mW to 500mW and the detuning of the laser was set between 2GHz and 10GHz. Graphs showing the recorded flux of different detuning of the 500mW guide at distances of 11mm and 50mm are given in figures 7.9 and 7.10 respectively. A Gaussian profile is fitted to the experimental data to give an approximate value of the total flux.

The guided flux is observed to arrive earlier than the free falling cloud with the higher detuning guides showing a profile tending more towards that of the free-falling atom cloud. The acceleration of the atoms occurs because they are not completely confined in the dark region of the LG beam, the atoms have a transverse velocity and can move within the beam. Atoms with a high enough energy can escape the guide beam, lower velocity atoms will only penetrate a certain distance into the beam before they are repelled back into the centre. The atoms continue to oscillate between the walls for the duration of the guide. This oscillation results in the atoms spending a percentage of the guide time within the walls of the LG beam. This leads to a radiation pressure effect pushing the atoms along the beam and reducing the time taken to reach the probe beam. The radiation pressure is greatest near to the atomic transition and it is the lowest detunings that display the greatest decrease in guide time and therefore the undergo the greatest radiation pressure force. The total flux when using a low detuned guide is higher than

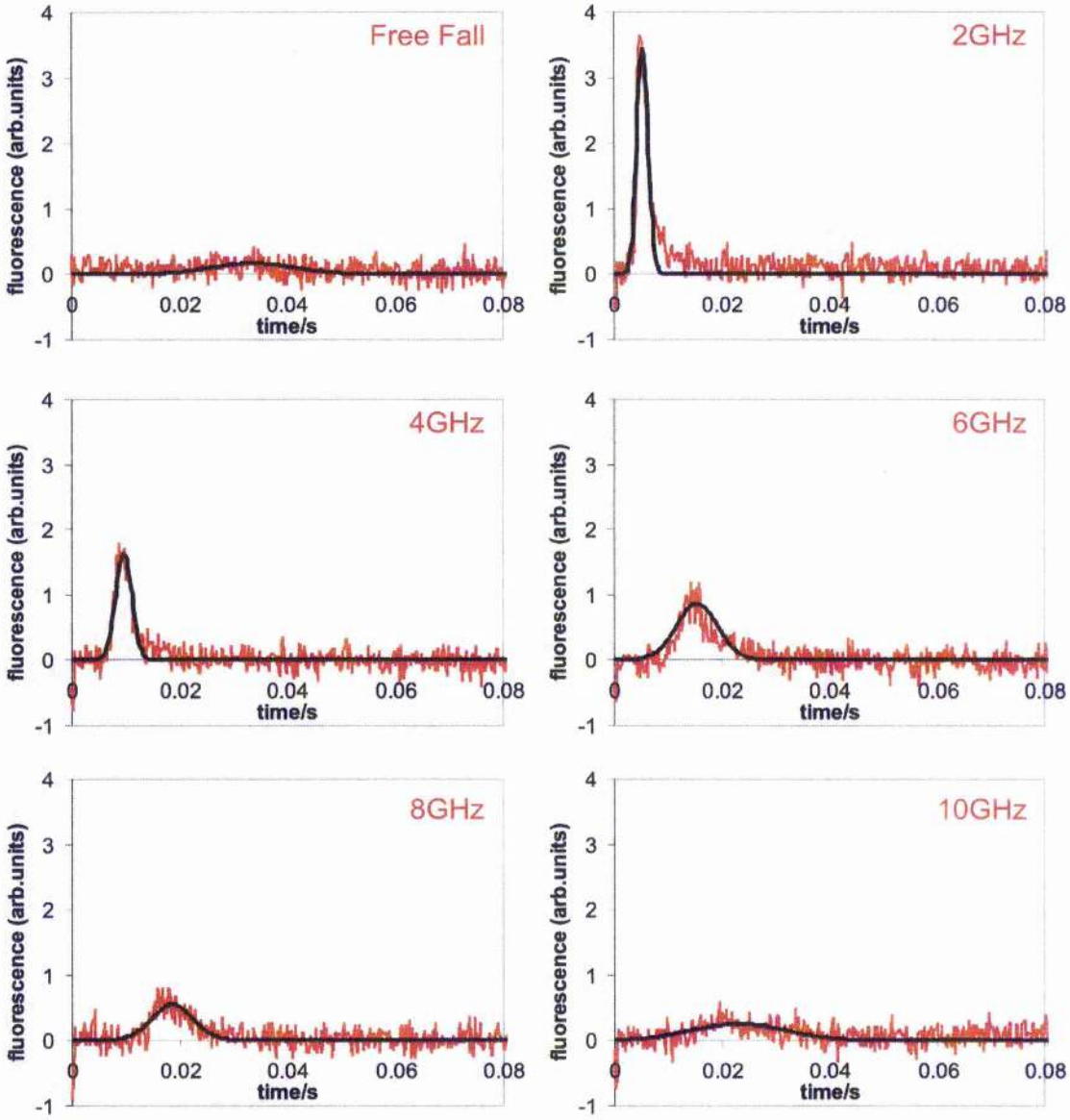

Figure 7.9: Atomic flux of falling atoms within an LG^{1}_{0} guide over 11mm. The black line is a Gaussian approximation.

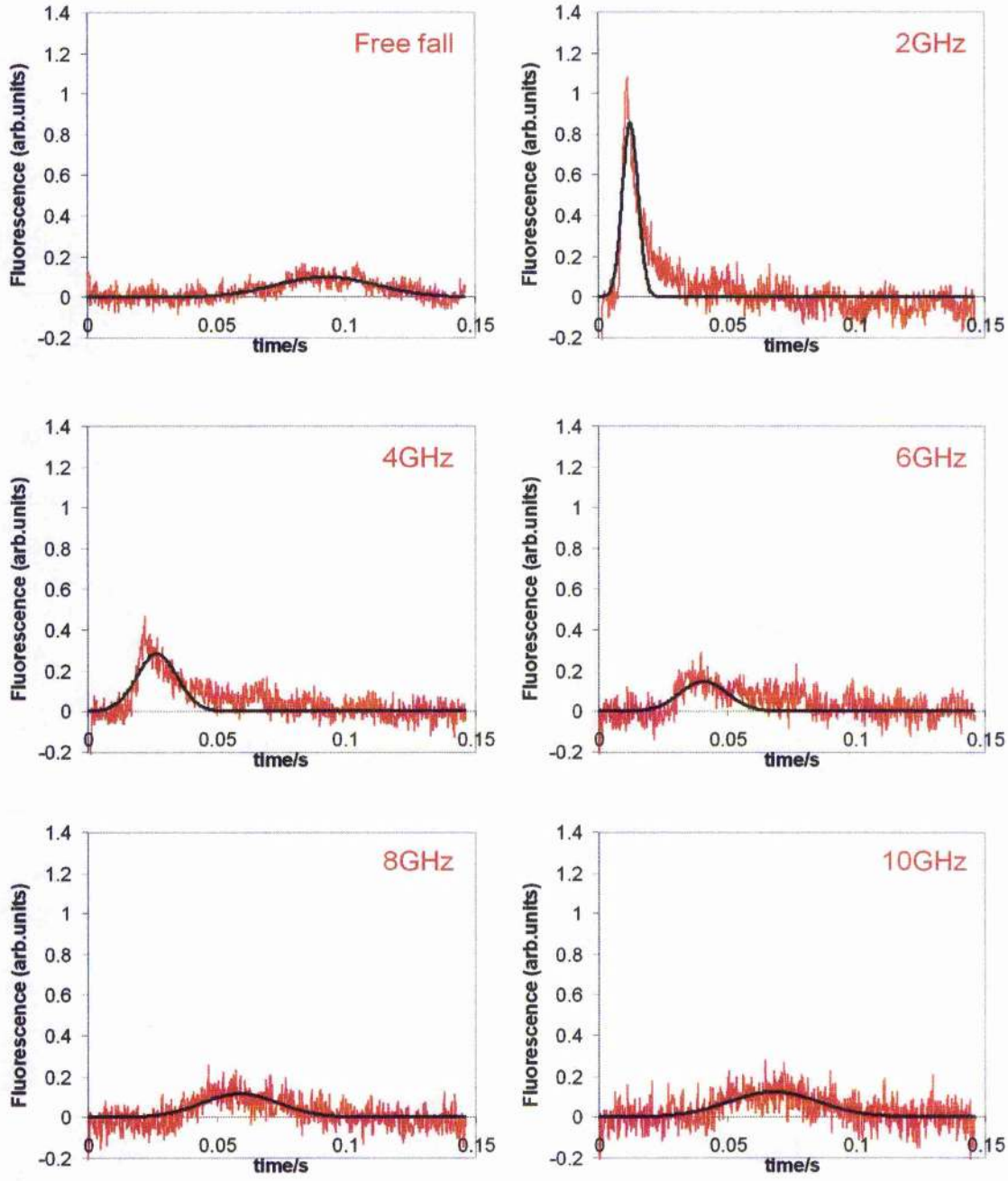

Figure 7.10: Atomic flux of falling atoms within an LG^1_0 guide over 50mm. The black line is a Gaussian approximation.

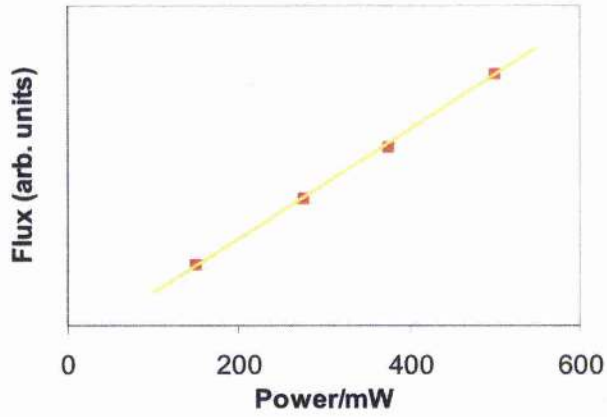

Figure 7.11: Graph showing the effect of increasing guide power for a 6GHz detuned LG^1_0 beam, measured at 11mm.The solid line is a best fit plot.

that of a free-falling cloud, for a 2GHz guide, with a power of 500mW, the increase in flux after 50mm is 40% (the increase is over 240% for a 10mm guide distance) which falls to 10% at 10GHz. This increase is due to a combination of the increase dipole potential, the 2GHz guide has a potential wall of 14mK whereas the 10GHz guide has a potential of 3mK, and the radiation pressure reducing the amount of time the atom is in the guide for and thus the amount of time with which to escape the beam. Reducing the power in the guide leads to a smaller increase in flux because of the corresponding reduction in dipole potential. A graph of power against flux for a 6GHz guide beam is shown in figure 7.11. There is a linear dependence observed because the dipole force is directly proportional to the intensity of the guide beam, as seen in equation 6.1.

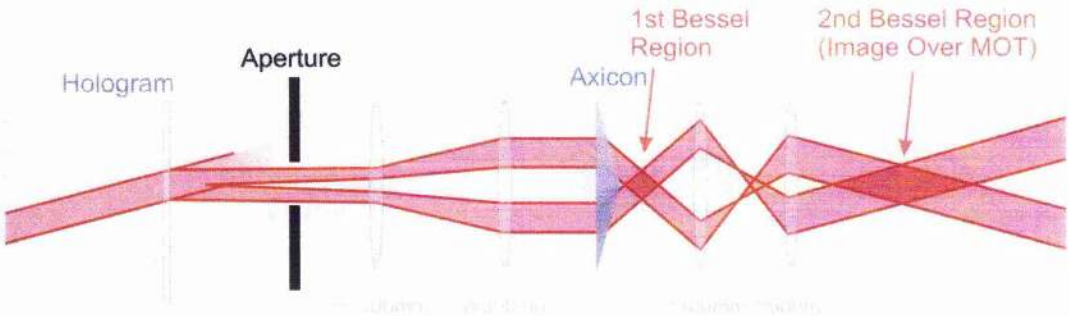

Figure 7.12: Schematic diagram of the generation of a high order Bessel beam. Please note the vast liberties taken with scale, for proper imaging of the Bessel beam the last two lenses have to be f_1+f_2 apart, i.e. 700mm.

7.4 Bessel Beam Guiding

The experimental set up is the same as described for LG beam guiding of a falling cloud. The Bessel beam is formed by illuminating a 0.3° axicon with the LG^1_0 beam used above, a diagram of the generation of the Bessel beam is given in figure 7.12. The Bessel beam is passed through a telescope to match the central ring size with that of the previous LG beam. This provides up to 400mW at trap centre, but due to the nature of the Bessel beam [5] all of this power is not used in the central ring, which is to be used for guiding, but distributed over all the concentric rings of light. By examining the Bessel beam with a CCD camera 12 concentric rings were seen, this implies the total power in the guide ring is a maximum of $1/12^{th}$ the total power, ~33mW.

The Bessel beam was used to guide the falling cloud up to 10mm using detunings of 2 to 10GHz. A graph showing the flux measured at 10mm is given in figure 7.13. There is a marked difference between the results seen

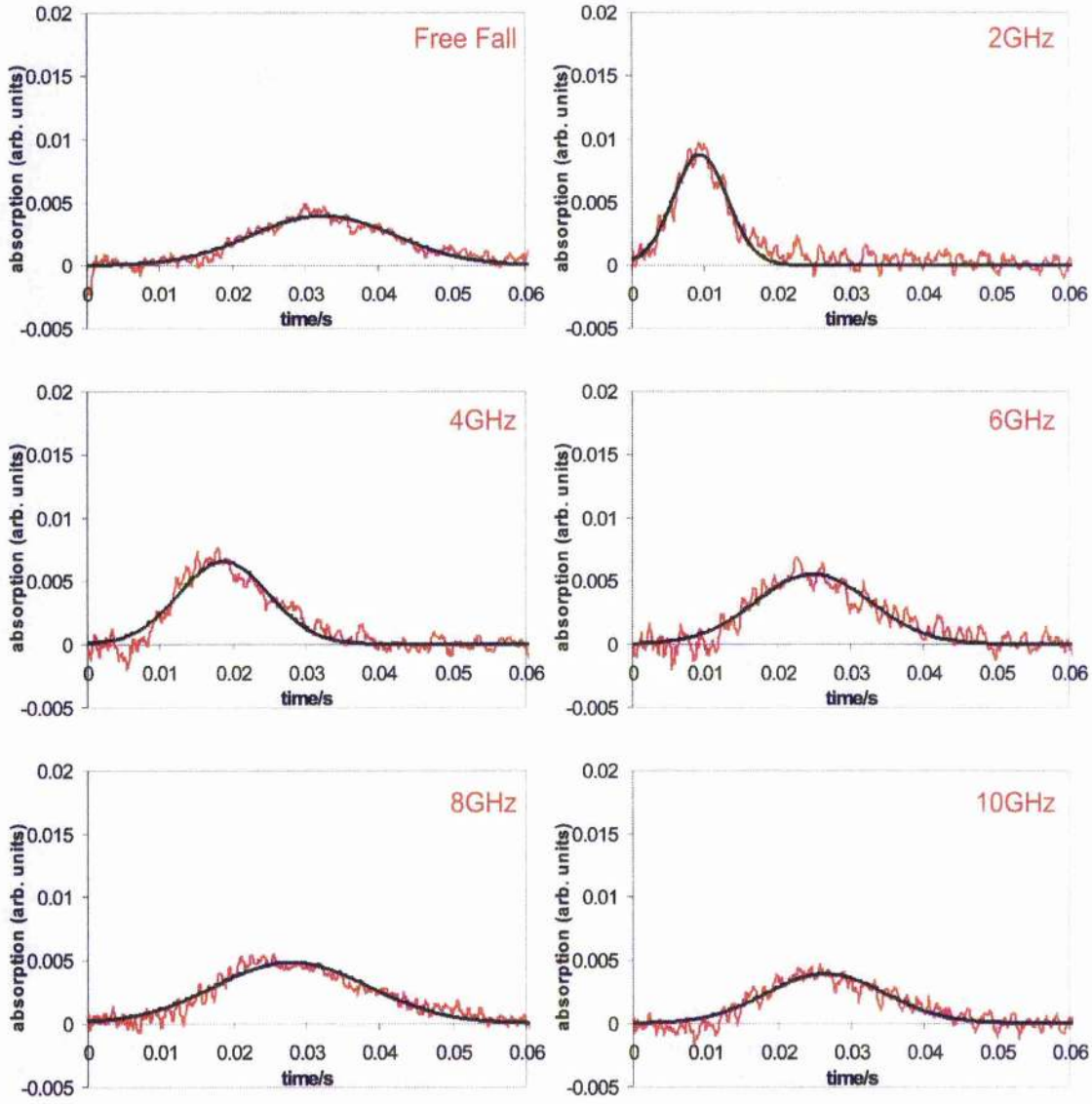

Figure 7.13: Atomic flux of falling atoms within a J_1 Bessel beam over 10mm.

The black line is a Gaussian approximation.

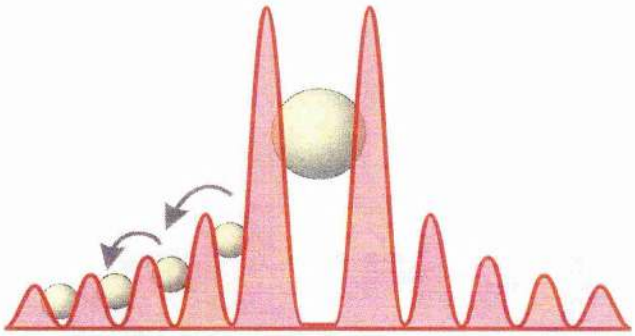

Figure 7.14: Diagram of atoms pushed out of the Bessel beam. Once the atoms are outside of the central ring the dipole potential is no longer equal on opposite sides of the atom, the inner rings have higher intensities and a greater repulsion for the atoms, thus the net force on the atom is away from the centre of the beam.

here with those of the LG beam at a similar distance (figure 7.9), we still see a reduction of guide time due to radiation pressure from the guide beam but the increase in total flux is significantly reduced with the guide beam present. In fact with the guide beam at a detuning of 2GHz there is a reduction of 20% in the total number of atoms detected was observed. This is because despite the steeper potential of the Bessel beam there is still some penetration into the guide walls this leads to the heating effects at detunings close to resonance allowing the atoms to escape the guide. The shape of the Bessel beam may assist in repelling the atoms away. Although the Bessel beam is a series of concentric rings as the radius of the rings increase there is a reduction in the intensity, the difference in intensity between two rings results in a net repulsive force outwards. This makes it unlikely that once atoms have escaped the central ring that they will be contained between two outer rings because the intensity imbalance has the effect of continually accelerating the atoms further from the centre of the beam, as illustrated in figure 7.14. At

higher guide detunings there is a small increase in the atomic flux, at 8GHz this is ~30%, however because of the limitations in power this is a much smaller increase than found when using the LG beam.

7.5 Summary

These experiments demonstrate an LG beam can be used to increase the atomic flux when is used to guide a cloud of falling atoms. However, when a Bessel beam is used, because the distribution of power in the beam the central ring has a much lower intensity than necessary to effectively guide the atoms. The profile of the Bessel beam actually assists atoms outside of the central ring to completely escape and we can observe a reduction in flux when using these beams with guide beam tuned close to resonance.

It is also not clear from these results how much the increase in flux is due to the dipole potential of the guide beam confining the atoms during the fall and how much is due to the reduced travel time leaving less opportunity for atoms to escape. The use of higher index beams may help to understand this; higher order beams have narrower rings of light with higher dipole potentials [6], increasing the azimuthal index of an LG guide should reduce the distance into the guide wall the atoms can penetrate and thus reduce the radiation pressure components. The comparison of different order LG beams is explored in the next chapter.

It is also worthwhile noting that there is no hyperfine beam propagating with the falling atoms, the hyperfine is only present within the probe beams, this permits atoms to fall out of the cooling cycles during the guiding time leading to a change in apparent detuning and a change to the atomic flux.

Bibliography

[1] Y, Song, D. Milan and W. T. Hill III, "*Long, narrow all-light atom guide*," Opt. Lett. **24** 1805 (1999)

[2] X. Xu, K. Kim, W. Jhe and N. Kwon, "*Efficient optical guiding of trapped atoms by a hollow laser beam*," Phys. Rev. A. **63** 063401 (2001)

[3] J. Arlt and K. Dholakia, "*Generation of high-order Bessel beams by use of an axicon*," Opt. Commun. **177** 297 (2000)

[4] K. Singer, S. Jochim, M. Mudrich, A. Mosk and M. Weidemüller, "*Low-cost mechanical shutter for light beams*," Rev. Sci. Instrum. **73** 4402 (2002)

[5] J. Durnin, "*Exact solutions for nondiffracting beams. I. The scalar theory*," J, Opt, Soc. Am. A. **4** 651 (1987)

[6] J. Arlt, T. Hitomi and K. Dholakia, "*Atom Guiding along Laguerre-Gaussian and Bessel light beams*," Appl. Phys. B. **71** 549 (2000)

Chapter 8:

Dynamically Reconfigurable Optical Potentials for Guiding Atoms

8.1 Introduction

This chapter describes the use of a spatial light modulator to generate the optical dipole potentials for guiding a cloud of cold atoms. The ease by which the SLM can be reconfigured allows rapid alteration of the optical parameters in the trap with minimal extra alignment. In the next section we experimentally demonstrate the use of SLM to create Laguerre-Gaussian beams of azimuthal index from l=1 to l=15 (beams with l>15 have been generated but with the

hologram specifications used higher indices start to display interference effects from neighbouring diffracted modes making comparisons with these beam less valid) and compare the guiding properties of the different beams. In the second part of this chapter we detail the generation of non-trivial beam shapes, in order to build atomic beam splitters and interferometers, using the SLM and our preliminary experiments with such beams.

8.2 Comparison of Different Order Laguerre-Gaussian Guide Beams

The spatial light modulator can be used to quickly change the parameters of the Laguerre-Gaussian guide beam. Previous experiments with LG beams have been limited to the use of l=1 beams [1]. Here we use the SLM to compare the guiding properties of different azimuthal index guides from l=1 to l=20 (because of the interference effects most data were recorded below l=15). First the beam waist is kept constant, allowing the LG beam to expand with increasing index, second the ring size of the LG beams are matched. By matching the ring size the peak intensity, I_l, around the guide varies as [2]:

$$I_l \propto \frac{l^{(l+1)}}{l!} e^{-l} \tag{8.1}$$

Using Stirling's approximation for $l!$ this reduces to a $l^{1/2}$ proportionality. Thus, increasing the azimuthal index not only increases guide intensity but also the steepness, since higher index beams have a narrower profile. This will

reduce atomic penetration into the guide walls and associated radiation pressure and heating effects so that the profile of the guided cloud becomes closer to that of a naturally free-falling atomic cloud.

8.2.1 Generation of the MOT

The drum trap is used for the MOT to provide longer guiding distances and greater optical access for probing the atomic beams. The main cooling laser for the MOT was the TA-100 tapered amplifier diode laser system supplying up to 400mW at 780nm. The cooling beams were expanded to 1.5cm beams and incident of the trapping region horizontally and at 45° to the vertical in order to leave the top viewport clear for the vertical guide beam, a diagram of the MOT set up is given if figure 8.1. The hyperfine beam is provided by an ECDL and is aligned to co-propagate with the guide beam using a polarising beam splitting cube. When the cooling beams are extinguished the hyperfine beam remains on to propagate with the falling atoms. This ensures that the atoms will be continuously repumped back into the F= 3 ground state and the detuning of the guide laser will remain constant. While this is not of such great concern when using a high power guide beam detuned far from resonance, when using low power hollow guides the detuning is significantly reduced to only a few GHz, if an atom falls into the wrong ground state within a guide detuned by only 2GHz the effect of the guide can change from a repulsive blue-detuned guide to the red-detuned regime. Thus at low guide detunings it is important to maintain the ground state of the guided atoms.

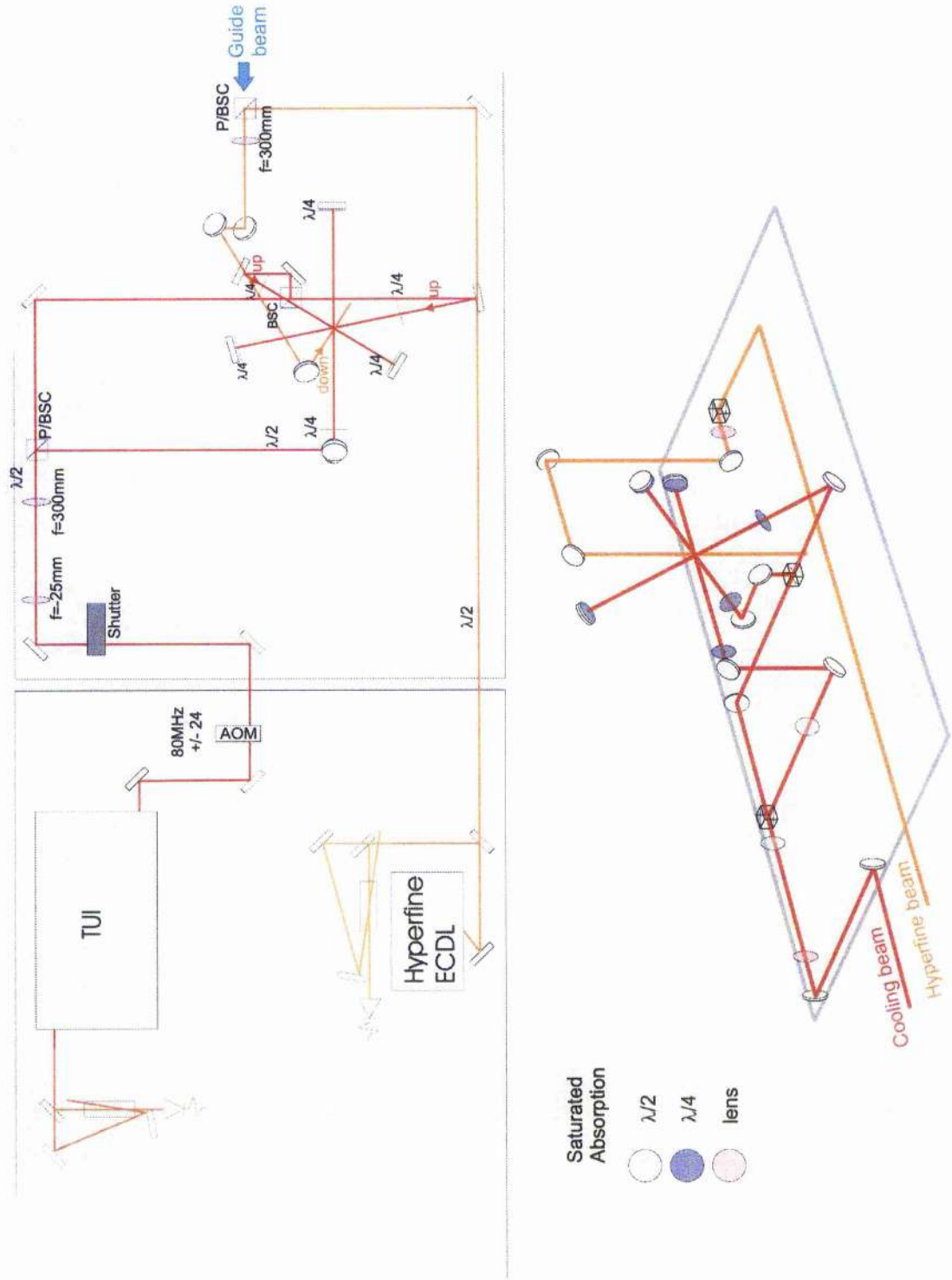

Figure 8.1: Experimental diagram of the MOT.

8.2.2 SLM Generation of Laguerre-Gaussian Beams

The LG beams were generated from a Ti:Sapphire laser incident on the SLM as described in chapter 5, with the LabView program used to control the SLM parameters. The number of grating lines, *N*, displayed on the SLM was seen in chapter 5 to heavily influence the efficiency of the SLM; a larger number of lines rapidly reduced the power in the first order since the quality of the blaze is reduced (the SLM is only 768 pixels across, increasing the number of grating lines leads to greater steps across the blaze). A value of N=70, was chosen for these experiments as it was the smallest value for N which did not display interference between the first and second diffracted orders for an l =15 beam. This resulted in a conversion efficiency into the first order of ~50%, and giving ~350mW of guide light in the trap centre.

The LG beam was put through a telescope arrangement of lenses to provide different beam waists within the trap. An f=300mm lens was used to image the beam from a focal point inside the trap, lenses with focal lengths of f=150mm, 200mm and 400mm were placed on flip mounts at their focal distance from the 300mm lens image point. By selecting only a single lens the LG beam is focused down to three different waists at this image point which in turn provides different beam sizes inside the trap. The beams waists inside the trap were approximately 450μm, 700μm and 950μm for the150mm, 200mm and 400mm focal length lenses respectively. The experimental set up of the guide beam is given in figure 8.2. The Rayleigh range of the guide beams are ~30cm, well beyond the guiding distance so the guides can be

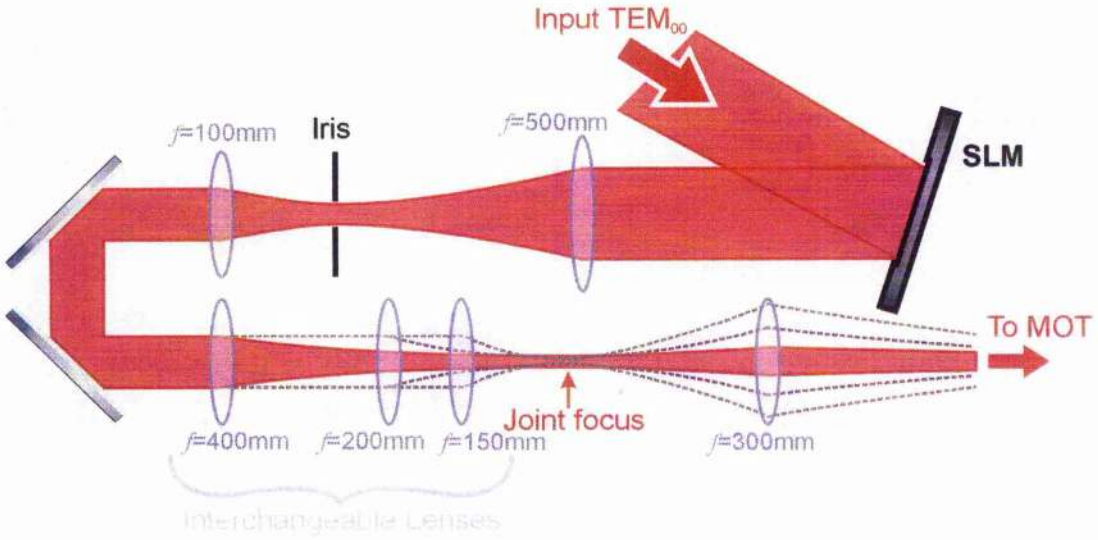

Figure 8.2: Schematic diagram of the spatial light modulator generation of Laguerre-Gaussian beams. By switching between the three interchangeable lenses we can image three different beam waists inside the trap.

approximated as simple non-diffracting tubes of light. Once the guide beam was initially aligned the index of the LG beam could be changed without any further modification required to the experimental set up emphasising the versatility of the SLM in this experiment.

8.2.3 Guiding with a Fixed Beam Waist

Once the cloud has been formed in the MOT the cooling beams are turned off (the hyperfine beam remains on) allowing the atoms to fall under gravity. The guide beam co-propagated vertically with the falling cloud and was turned on once the cooling beams were extinguished; an experimental diagram is given in figure 8.3. The timing of the beams is controlled by a LabView program as described in the previous chapter.

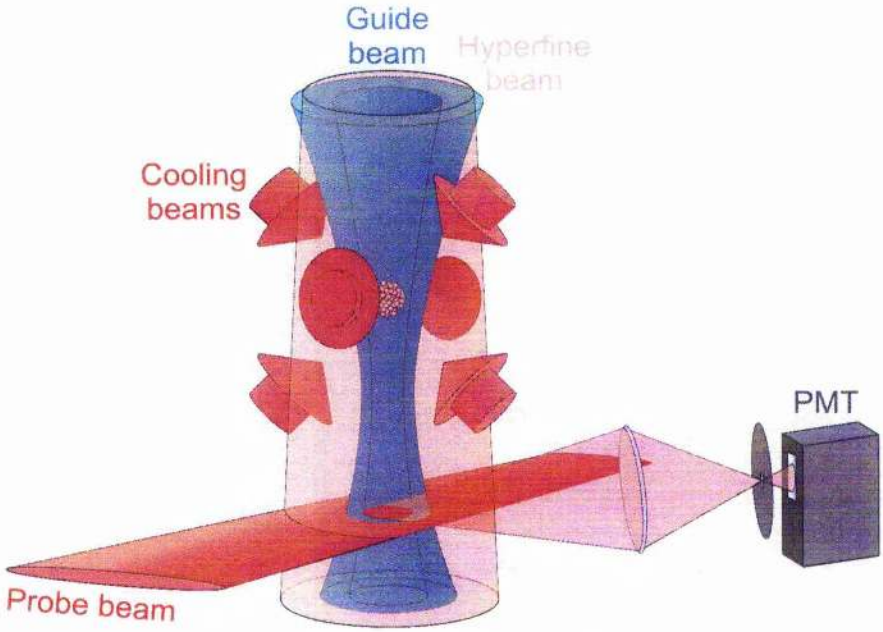

Figure 8.3: Schematic diagram of the experimental LG guiding of a falling atom cloud.

A probe beam consisting of a sheet of light (1×5mm) tuned to the cooling transition (F= 3→F'= 4) of the atoms intercepts the falling cloud at distance up to 50mm below the trap region. The probe beam is generated using a second stabilised ECDL, providing up to 4mW of power at trap centre. The fluorescence from the atoms as they fall through the probe beam is measured using a photomultiplier tube (PMT) and recorded onto a digital oscilloscope.

First we keep the telescope lens constant so as to compare the effect of increasing azimuthal index with a constant beam waist. This has the effect of increasing the ring sizes (the ring size is the peak to peak diameter of the annulus, this is a separate measurement to the beam waist) with increased azimuthal index, as described by equation 5.3, and a corresponding reduction in the optical dipole potential; an l =10 beam will have a ring radius ~3 times

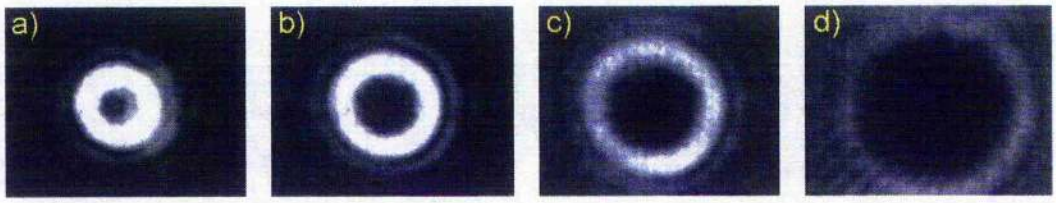

Figure 8.4: Images of the Laguerre-Gaussian beam produced. (a) to (d) show LG beams of azimuthal indices l=2, 5, 10 and 20 respectively, these are all formed with the same beam waist. Note the interference pattern (from an adjacent order) on the left side of the l=20 beam.

that of an l=1 beam and suffers an equivalent reduction in dipole force, for 2GHz detuned guiding an l=1 beam of waist 700μm has a dipole potential of 7.6mK and an l=10 has a potential of only 2.6mK. Figure 8.4 shows the profiles LG beams of l=2, 5, 10 and 20, the interference of the adjacent mode is clearly observed in the l=20 beam as a feathering around the left hand side of the profile.

Data were taken at detunings up to 10GHz from resonance, though statistically the data at detunings up to 5GHz offer the least variance due to the relatively low fluxes recorded. Due to the low signal to noise ratio of the recorded signals the data was put through a filtering program based on moving Gaussian average to remove the high frequency noise, essentially this acted as a low-pass filter. The width of the Gaussian function used was 1ms for the low index and low detuning guides but was increased to 5ms for the free-falling cloud data since the profile becomes closer to a Gaussian. Figure 8.5 shows the data acquired as we increase the azimuthal index for a guide distance of ~30mm at a constant detuning of 2GHz. For low azimuthal indices

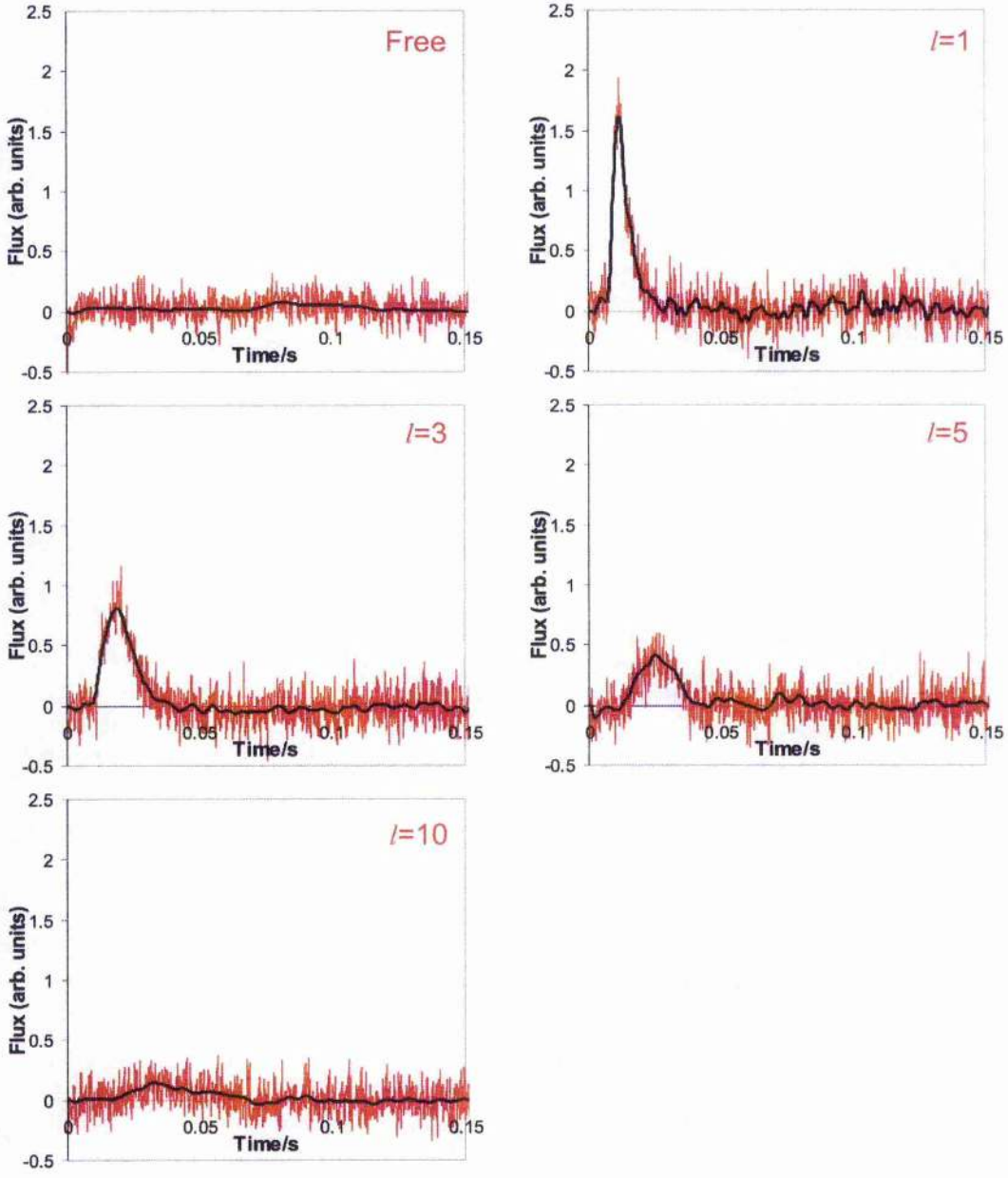

Figure 8.5: Increasing the azimuthal index of a Laguerre-Gaussian guide. The guide beam was detuned by 2GHz, and the atomic flux measured at 30mm below trap centre. The black line shows the results of filtering; the widths of the Gaussian functions were 5ms, 1ms, 2ms, 2ms and 3ms for the free-falling cloud and the l=1, l=3, l=5 and l=10 guide beams respectively. The guide efficiencies are given in figure 8.6.

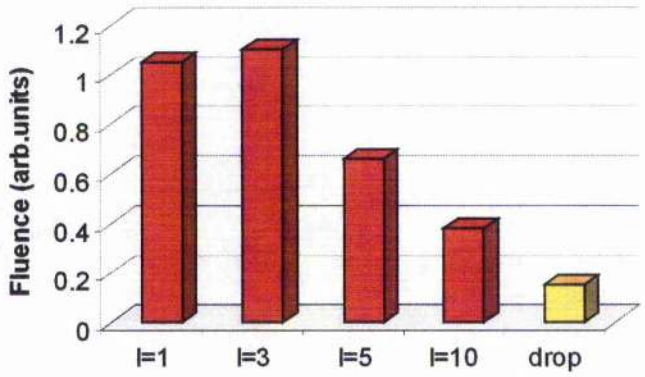

Figure 8.6: Total flux measured for different azimuthal index guides. The l =3 beam shows the greatest increase since it was the best matched to the size of the MOT. Data taken from figure 8.5.

we find that the cloud arrives much earlier than the free falling atom cloud (this agrees with the data in chapter 7), this is due to the radiation pressure imparted to the atoms as they penetrate into the shallow walls of the guide. As the index is increased the guide beam becomes larger and thus interacts less with the cloud, the reduction in intensity due to a larger area then leads to a reduced radiation pressure effect when the atoms do interact with the beam. These effects combine to reduce the total radiation pressure force encountered by the atoms and results in a more natural guiding of the atoms as apposed to the pushing observed in low index guiding. The time of flight of the higher index guided clouds increases with azimuthal index, however, the reduction in dipole potential due to the increase in beam size means there is a reduction in the overall flux measured. The data in figure 8.6 shows the total flux measured for increasing azimuthal index. We observe a maximum increase in the atom flux of 800%, for the low index guides, over a free falling cloud without the guide present. The data presented here shows this value to

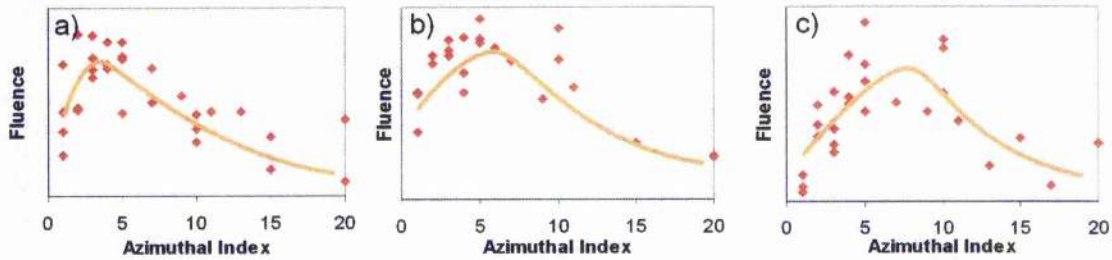

Figure 8.7: Total flux values for varying azimuthal indices. The flux measurements are taken at 30mm with a 2GHz guide beam with a beam waist of 950μm (a), 700μm (b) and 450μm (c). The solid line is not a calculated fit and is meant only as a guide.

occur are l=3 as opposed to l=1, which you might expect to result in the greatest flux measurement because of the larger radiation pressure can push more atoms through the probe before they can diffuse out of the probe region, however, the l=3 guide beam has a ring size that better matches the cloud dimensions and, therefore, more atoms are caught within the guide beam. As we alter the beam waist we see the azimuthal index for maximum flux increase change accordingly, see figure 8.7.

Simply increasing the detuning of the guide also has the effect of reducing the radiation pressure of the beam and thus increasing the total guide time towards that of a free falling atomic cloud, figure 8.8 shows the effect of guide detuning with an l=1 guide beam and beam waist of 700μm. A 10GHz, l=1 guide shows ~1/3 the total flux of the 2GHz guide (the potential of the guide is 5.6mK at 2GHz which falls to 1.1mK at 10GHz). Detuning the guide beam 10GHz is seen to increase the guide time to approximately half that of a free falling atom cloud, this is a greater effect than seen when solely increasing the

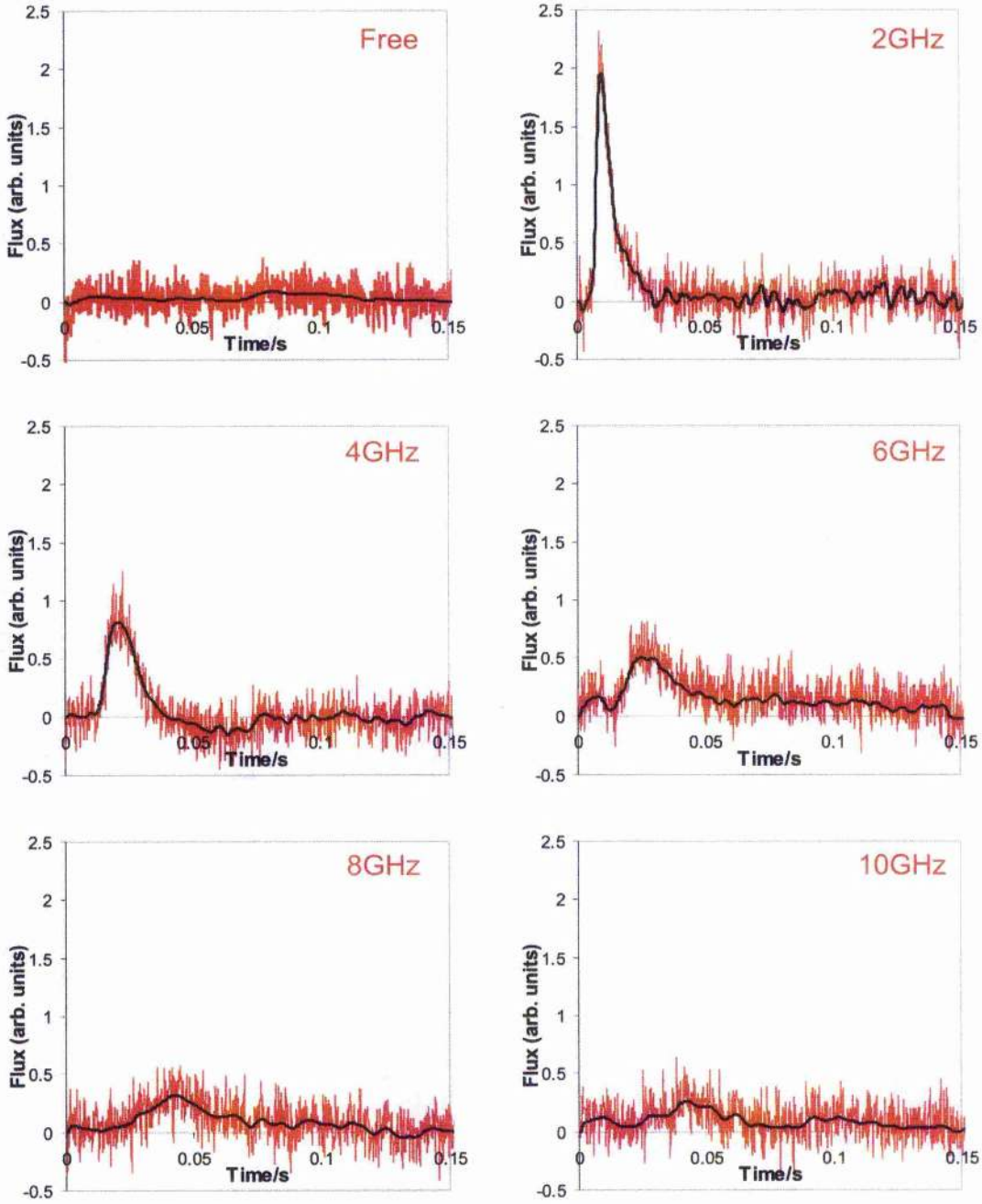

Figure 8.8: Increasing the detuning of a LG^1_0 guide beam. The guide beam has a beam waist of 700μm. The black line is the filtered data, the Gaussian widths are 5ms, 1ms, 2ms, 2ms 3ms and 3ms for the free-falling cloud and the 2GHz, 4GHz, 6GHz, 8GHz, and 10GHz guide beams respectively. The guide efficiencies for these data are given in figure 8.9

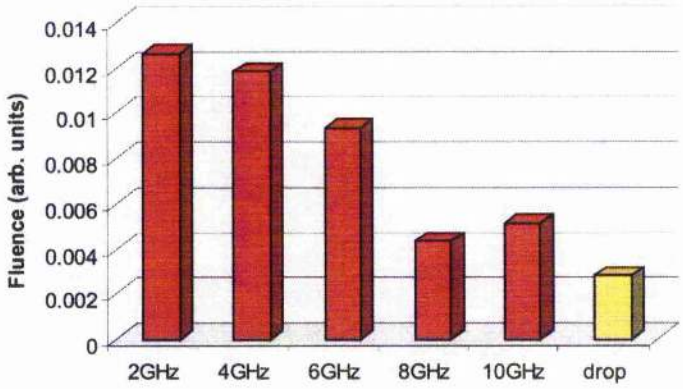

Figure 8.9: Total flux measured for different detunings of a LG^1_0 guide beam. Data taken from figure 8.8.

index of the guide to l=10. Figure 8.9 give the relative efficiencies of the guides.

The main disadvantage of a significant radiation pressure component is the associated heating of the atoms. Calculation of the spontaneous scattering rate shows that for low azimuthal indices the cloud will incur a temperature increase of approximately 10μK during the guiding time. Whilst this is only ~10% of the temperature of the MOT cloud used in these experiments this magnitude of temperature increase would be highly detrimental to guiding clouds from an optical molasses or Bose-Einstein condensate within such a low index LG beam. This heating effect falls dramatically with higher index guides because of the steeper gradient in the guide walls reducing penetration into areas of high intensity [2], and this has been seen in the above experimental results as a factor of the increased guide time.

The time of flight of the free-falling cloud was observed to be longer than expected for the probe distances used; the peak signal for a cloud detected 3cm below the MOT was recorded at ~90ms. The low signals detected made analysis difficult, however the fall time was consistently measured within ~5ms of this time. This falling time corresponds to a probe distance of 4cm, which was a significant enough discrepancy to indicate that it was not due to a simple misalignment of the probe beam. The magnetic field coils remained on throughout the experiment so their effect on the falling atoms was considered. The force on an atom in a magnetic field, B, is given in equation 2.6, expanding the magnetic moment of the atoms this equation becomes:

$$F = g_F \mu_B M_F \nabla B \tag{8.2}$$

where

$$g_F = \frac{F(F+1) + J(J+1) - I(I+1)}{2F(F+1)} g_J \tag{8.3}$$

g_J is the Landé g-factor, μ_B is the Bohr magnetron, M_F is the hyperfine state of the atoms, I is the nuclear spin and J and F are the total angular momenta of the fine and hyperfine states respectively. With a magnetic field gradient of 10G/cm this produces a force ~0.2 of gravity multiplied by the M_F level. Thus with the atom in the correct hyperfine state the magnetic coils could account for the measured reduction in the acceleration of the atoms. However, the use of a linearly polarised hyperfine beam, which produces no optical pumping of the atomic energy levels (see section 2.3.4), implies a distribution into all hyperfine states. Since the exact nature of the M_F states is unknown further investigation is required to account for the increased time of flight.

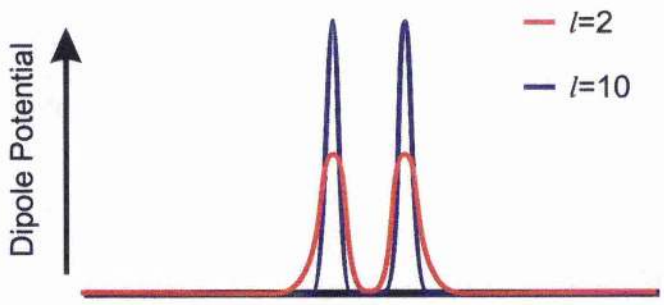

Figure 8.10: Increasing the azimuthal index with a fixed ring size.

Comparison between the different index LG beams is not clear with these experimental results because the fixed waist size means the guide sizes vary. Thus it is not clear whether higher order LG beams seem to offer a more natural guide, as opposed to a pushed cloud, because the reduction in penetration into the guide walls reduces the radiation pressure component or whether what we are seeing is simply a result of the reduction in intensity leading to a lower radiation pressure effect. For a more direct comparison of the effect of index on guiding characteristics the ring size of the guides need to be matched. Figure 8.10 shows the dipole potential of two LG beams with matched ring size, the higher index beam shows a steeper and higher dipole potential. In this thesis the ring size is taken to be the diameter of the annulus measured between the positions of peak intensity, the beams illustrated in figure 8.10 have the same ring size, but the beam waists are different.

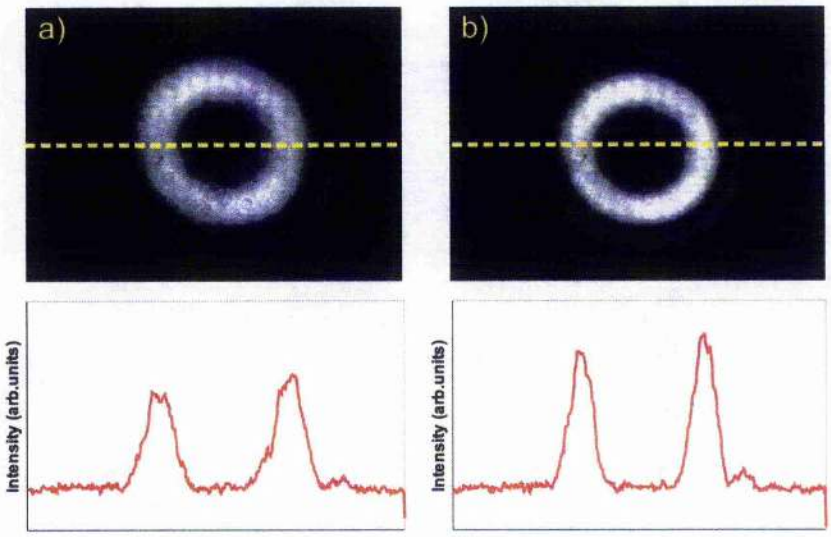

Figure 8.11: Comparison of the intensities of different azimuthal index Laguerre-Gaussian beams. The intensity plots are taken along the lines shown, an l=5 (b) LG beam displays a narrower ring size and higher peak intensity than an l=2 beam (a).

8.2.4 Guiding with Matched Ring Size

In order to form a more direct demonstration of the beam index on the guiding characteristic the previous experiment was repeated with beam waists which were adjusted to give the same ring size to different index beams. Two ring sizes were chosen for study; the larger size had a ring diameter (taken from the radial point of highest intensity) of 2.2mm, this gave a guide that was just larger than the diameter of the MOT cloud. The second size was 1.5mm; this size was slightly smaller that the cloud diameter and the guide beam slightly clips and deforms the edges of the cloud. Images of the ring matched guides are given in figure 8.11, profiles taken across the beams show the narrowing of the ring and increase in intensity. The ring sizes were matched by

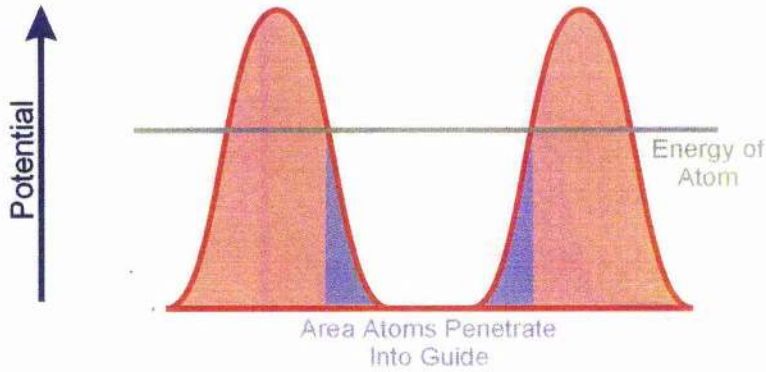

Figure 8.12: Schematic diagram of the distance the atoms penetrate into the blue-detuned guide. As the index of the LG beam is increased the potential walls become steeper and relative area that the atom is within the beam is reduced.

increasing the azimuthal index of the guide beam and exchanging one of the lenses within the telescope arrangement; the restrictions in the telescope arrangement only permitted the matching of three different LG beams. For the 2.2mm ring size the LG beams used were l=3, 5 and 12 and for 1.5mm guiding the indices were l=1, 2, 7. As an approximate indication of the difference in the atom-guide interaction we can expect the volume that an atom of temperature 100μK can penetrate into the guide beam was calculated, see figure 8.12. For an atom in an l=3 beam 19% of the volume in which the atom can move is within the walls of the guide beam, if we increase the index of the LG beam to l=12 because the potential walls of the guide are steeper this amount is reduced to 7%. This implies a significant reduction in the interaction with the intense walls of the LG beam as therefore an increase in the guide time should be observed together with the associated reduction in the heating. It may also be that when the guide is turned on atoms at the edge of the MOT start inside the walls of the guide and therefore

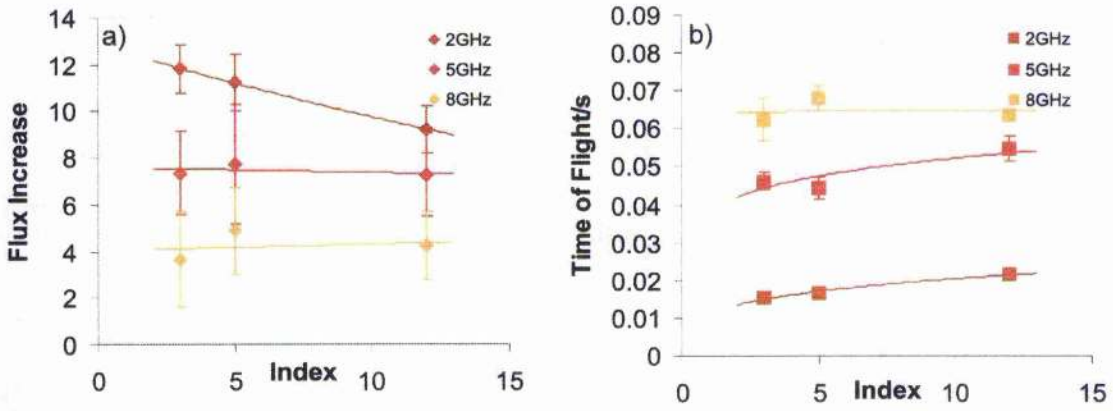

Figure 8.13: Increasing azimuthal index Laguerre-Gaussian beams with a matched ring size of 2.2mm (slightly larger than the diameter of the MOT). (a) shows the efficiency of the guide, the time taken to fall 30mm is shown in (b). The solid lines are shown purely to guide the eye.

gain significantly more energy. Increasing l widens the dark region and provides a steeper potential so fewer atoms can gain energy by starting within the soft wall of the guide.

Data were taken for detunings up to 10GHz from resonance, though, as before, for detunings above 5GHz there is a significant variance in the recorded results due to the poor signal-noise ratio detected. Figure 8.13 shows the results of guiding with the 2.2mm diameter guide over 3cm. The dipole potentials of the different azimuthal indices, for a 2GHz guide beam, are 2.5mK, 3.6mK and 5.7mK for l=3, 5 and 12 respectively. Figure 8.14 shows the equivalent data for the 1.5mm ring size. Here the dipole potentials far a 2GHz guide are 4.0mK, 5.6mK and 7.4mK for l=1, 2 and 7. This increase in potential is accompanied by a slight increase in the initial capture

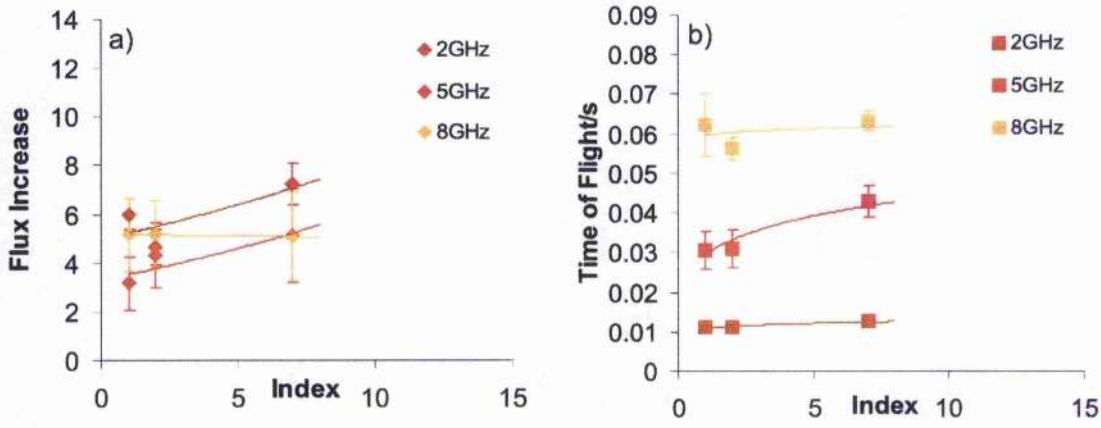

Figure 8.14: Increasing azimuthal index Laguerre-Gaussian beams with a matched ring size of 1.5mm (slightly smaller than the diameter of the MOT). (a) shows the efficiency of the guide, the time taken to fall 30mm is shown in (b). The solid lines are shown purely to guide the eye.

area; this is more significant in the 1.5mm guide as the beam is only slightly smaller than the cloud.

At low detunings we observe a dramatic radiation pressure push [3]. This is more significant in the 1.5mm guide because the guide does clip the edge of the cloud, however, the effect is still large for the 2.2mm guide, where the atoms should all be contained within the dark region of the beam. With the 2.2mm guide at 2GHz detuning we observe a slight fall in the recorded atom flux with increasing azimuthal index. The radiation pressure push acts to enhance the efficiency of the guiding because the atoms are accelerated towards the probe beam, increasing the order of the LG beam leads to a reduction of the radiation pressure and hence a slightly smaller signal. The increase in dipole force in these guides is not sufficient to result in a greater

measured flux because of the dominance of the radiation pressure at these low detunings.

Increasing the detuning of the guide to 5GHz shows a clear reduction in the radiation pressure as seen by the longer guide time (up to approximately half that of a free-falling cloud). The increase in guide time compared to that of the 2GHz guide implies a significant reduction of the heating associated with the scatter from the guide walls. At this point there is very little change in the efficiency of the guide with increasing index, but there is still an increase in guide time towards that of a free-falling atom cloud. We are approaching a regime of pure guiding and still observe and enhancement of 700% to the efficiency of the atom transfer. This trend is followed in the 8GHz detuned guide, the guide time becomes even closer to that of a free-falling cloud and there is an approximate constant guiding efficiency of 400%.

The decrease in atomic flux with increased index is not seen with the 1.5mm guide because the guide beam is smaller than the cloud diameter and, therefore, some atoms are lost to heating effects before they can be guided (or pushed) towards the probe. The small increase in guide area obtained with the higher index beams and the reduction in initial heating provides an adequate increase in atoms within the guide to more than compensate for the reduction in radiation pressure.

The time-of-flight profile of the dropped cloud is seen to change with detuning and azimuthal index, as illustrated in Figure 8.15 for the 2.2mm beam, implying a reduction in the radiation pressure push. The roughly Gaussian

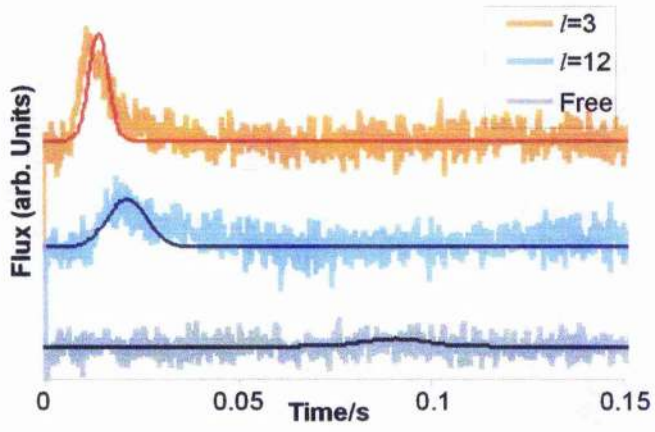

Figure 8.15: Time of flight profiles for guided and free falling clouds. The guide beam is 2.2mm in diameter and detuned 2GHz from resonance. In the time domain the acceleration of the cloud by the guide distorts the roughly Gaussian profile of the atom cloud. The darker lines show a Gaussian approximation to the data.

distribution of the unguided cloud is compressed and distorted by acceleration under radiation pressure, causing a proportionally higher flux for the early part of the signal. These results, illustrating the acceleration of the falling cloud by radiation pressure from a co-propagating beam, reinforce those of Song *et al* [4], who observed deceleration and levitation of falling atoms when using a counter-propagating hollow guide beam of low detuning.

8.3 Guiding Along Tailored Optical Potentials

The effect of the SLM need not be a simple propagating beam, patterns can be built up that can be observed at a focal plane. In this section we have generated simple beam splitters and interferometers that can be imaged

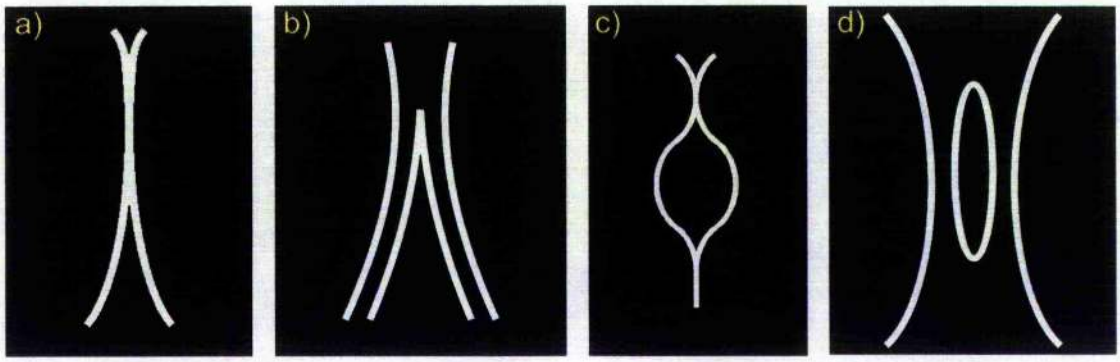

Figure 8.16: Original beam splitter designs for the SLM. (a) and (c) are red-detuned guides for a beam splitter and Mach-Zehnder interferometer respectively, (b) and (d) show the blue-detuned patterns. The hologram produced for (a) is given in figure 8.17.

inside a MOT to guide the atoms. This is in contrast to work performed by Birkl *et al* [5] and Houde *et al* [6] which rely on separate crossed beams to form a beam splitter. A preliminary experiment using the red-detuned guides with moderate values of detuning was performed, however, the low efficiency of the tailored beam shapes meant no guiding along the potentials was observed.

8.3.1 Generation of Optical Beam Splitters and Interferometers

Optical beam splitters were designed based on simple "Y" and loop shapes, these patterns were drawn in black and white, indicating zero and high intensity respectively, using a standard draw package. These patterns are given in figure 8.16. These images were then inputted into an IDL program which, using an iterative technique, generates the hologram necessary to

Figure 8.17: Hologram designed to image the red-detuned Y-splitter beam shown in 8.16(a).

produce a beam of that shape, one of these holograms is shown in figure 8.17. The flow chart of the iteration method is given in section 5.2.1. The beam shapes made by this method are transverse to the beam propagation and are seen at the focus of the beam, this allows us to exploit diffractive filling to "close" the pattern away from the focus of the beam, in this way the walls of the blue detuned guides (figure 8.16 (b) and (d)) can be filled in around the focus and therefore create a three-dimensional optical potential. The orientation of the pattern across the beam also leads to a change in alignment to the previous guiding experiments, instead of propagating the guide beam in the direction of the atoms the guide beam is aligned perpendicular to the direction of the atoms allowing the atoms to fall through the shaped potential across the guide beam (see figure 8.18).

The Ti:sapphire laser was used to illuminate the SLM, initially the beam was expanded using a f=-38mm and f=630mm telescope to produce a beam 50mm in diameter in order to fill the active area of the SLM, which is 2cm by 2cm. However, the optics placed after the SLM for imaging inside the trap

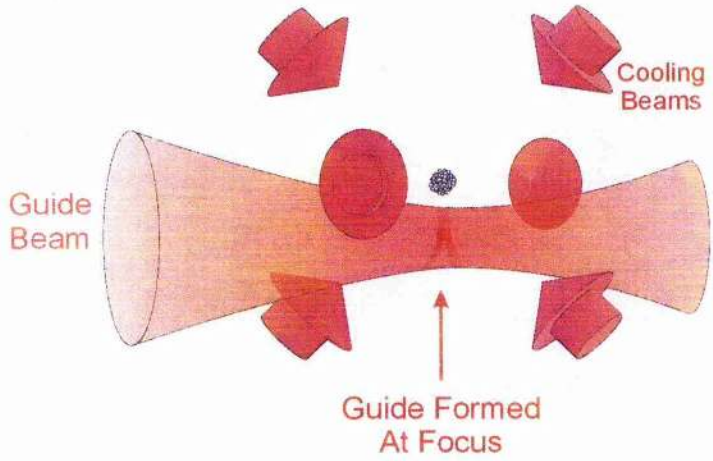

Figure 8.18: Schematic diagram for guiding along the SLM generated beam splitter potentials. The atoms fall through the image formed at the focus of the beam.

had only 1inch diameters, this meant the edges of the beam were clipped as the beam propagated. For this reason the size of the hologram projected onto the SLM was reduced to 384x384 pixels, half the size of the active area (this is achieved during the creation of the hologram, not by simply reducing the size of the 768x768 holograms). The smaller hologram meant the incident beam did not need to be expanded as much so the second lens of the telescope was replaced with an f=400mm lens, this still resulted in a beam which overfilled the hologram so as to present flat wave fronts to the SLM.

Examples of the guide beams produced are given in figure 8.19, as well as the desired image there are weaker, diffracted orders seen spreading out from the zeroth order beam and vertical reflections about the centre line (these unwanted images can not be seen without completely saturating the CCD camera with the zeroth order pattern). These reflected orders are a feature of the SLM, and can be moved away from the desired image by applying an

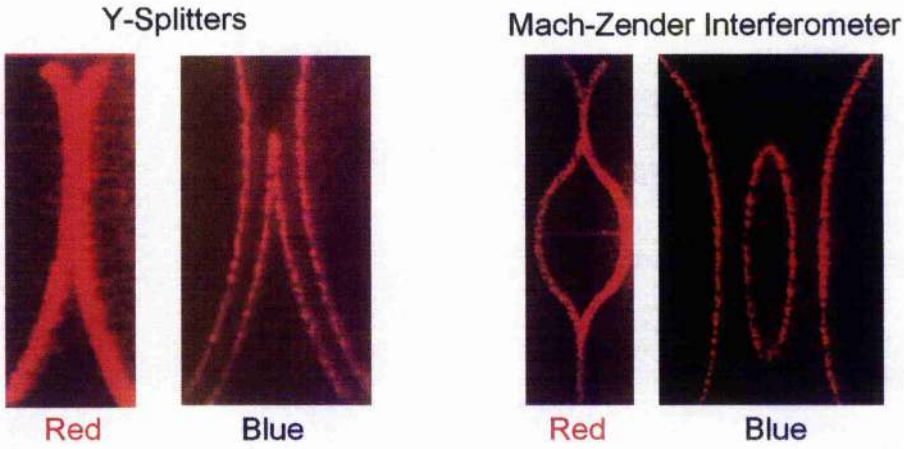

Figure 8.19: Images of the beam splitters patterns produced. These are the images of the patterns in figure 8.16.

offset (blaze) to the hologram but they cannot be completely removed. The exact size of the final image is dependant on the imaging lens used, the design of the hologram incorporates the Fourier transform through a specified lens. Our holograms were designed to produce the desired image after a 160mm focal length lens as this was the shortest distance to the MOT region that could be reached outside of the vacuum system. Imaging after an f=160mm produced a Y-splitter ~4mm long. The propagation of the Y-splitter hologram though the focus of an f=160mm lens is shown in figure 8.20, we observe a combination of two separate beam profiles propagating along the beam. The hologram generated guide pattern itself propagates through the focus to expand to twice the original size after ~3mm, on top of this there is a second light field which focuses to a bright spot at the centre of the pattern, this is the normal reflection off the front of the SLM which has not passed through the liquid crystals. Away from the focus the un-modulated reflection quickly dominates over the faster decomposing guiding pattern as shown in

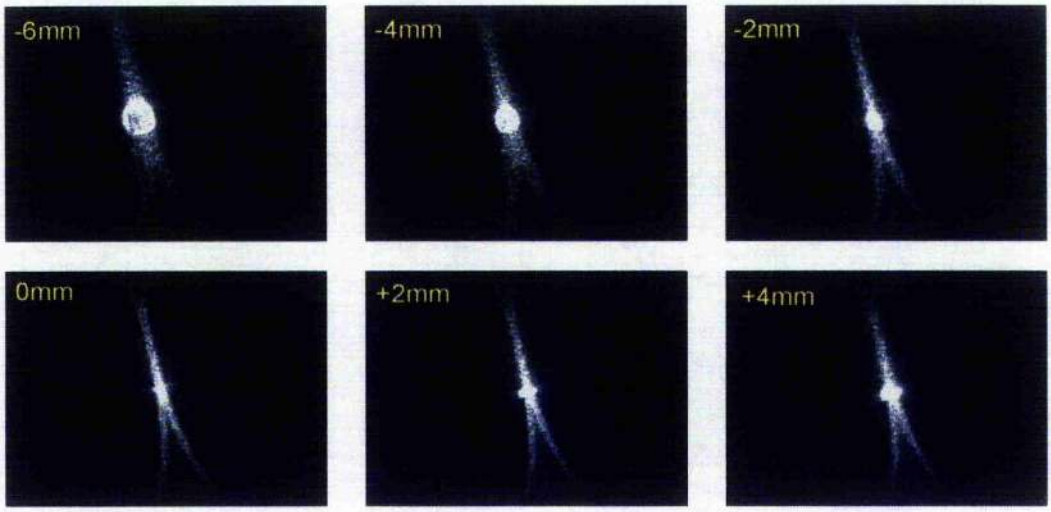

Figure 8.20: Propagation of the Y-splitter pattern through the focus of a lens. The inset number is the distance from the focus of the lens. The bright spot is from the un-modulated normal reflection from the SLM.

Figure 8.21: 3D profile of the Y-splitter pattern. The normal reflection clearly dominates the pattern away from the focus.

figure 8.21. The bright normal reflection could aid the guiding by slowing the atoms before the split in the dipole potential, making it less likely that the atoms will pass straight through the guide beam. The efficiency of these beams is found to be only ~20% of the total power incident of the SLM, though it should also be noted that <30% of the total power is reflected from the phase encoded area of the SLM given an efficiency of the hologram itself

of ~60%. Thus we have a beam with a total power of ~150mW with which to guide the atoms.

8.3.2 Guiding Along a "Y"-shaped Beam Splitter

The "Y"-splitter holographic pattern was tested first as this was simpler of the two designs. The red-detuned guide would prove to be easier to implement as it would not require diffractive filling to create a three-dimensional trap unlike the blue-detuned design. Recent experiments reported by Wolschrijn and co-workers [7] demonstrated guiding along beams red-detuned by only a few tens of GHz from resonance, over distances of 6mm using only 85mW. This gives an intensity of ~9W/cm^2 at the focus. Using 150mW in our Y-splitter guide beam we can achieve intensities in the order of 1.5W/cm^2, thus we should be able to observe some guiding using detunings around 40GHz (this is a detuning that can be set simply by rotating the thin etalon until two mode hops have been observed, see section 4.3.1 for detail on the Ti:Sapphire laser).

Imaging the Cloud

For these experiments a shadow imaging technique was used to probe the atom cloud, the use of a narrow probe beam to induce fluorescence was unsuitable due to the small distances guided and the lack of access close to the MOT centre. A weak probe beam (intensity ~0.2I_{sat}) tuned to the

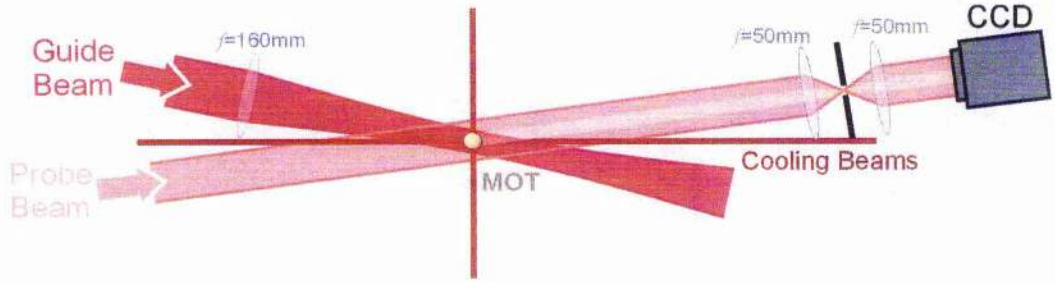

Figure 8.22: Schematic diagram of the setup of the guide and probe beams. The MOT is formed just above the guide, atoms are detected by absorption of a weak probe beam by a CCD camera.

F= 3→F'= 4 transition was expanded and passed through the atom cloud, absorption of the beam by the atoms would result in a shadow in the beam which can then be observed on a CCD camera, two confocal 50mm focal length lenses imaging through an aperture were used to block out scattered light from other sources (owing to the alignment of the cooling, guide and probe beams there was a significant scatter from the glass viewport of the trap which had to be removed). A diagram of the experimental set up is given in figure 8.22. The guide beam and probe beams had to be aligned to overlap as much as possible so that the image seen on the CCD is along the propagation direction of the guide beam and no blurring out of the image is seen from looking side onto the guide. Polarising optics could be used to achieve a viewing angle along the direction of the guide beam itself; however, none of these were available at the time of our experiments.

An acousto-optic modulator (AOM) was used to control the probe beam; in order to probe the cloud without any appreciable motion of the atoms the probe was pulsed such that it was only on for 50μs, the pulse length and

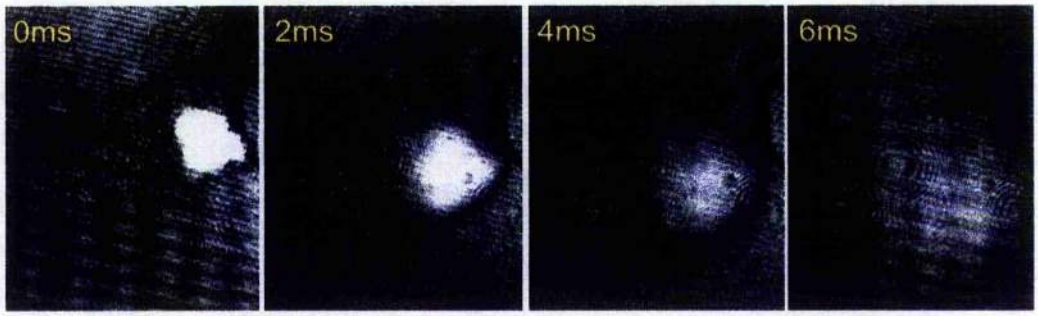

Figure 8.23: Absorption image of a free-falling atomic cloud.

timing of the triggering pulse to the AOM was controlled from the same LabView program as the trapping beams. The shadow image was recorded on S-VHS video from the CCD camera. The trapping beams are extinguished with a mechanical shutter, then after a specified delay the AOM is turned on for 50μs, approximately 500ms after this the cooling beams are opened, and the cloud is allowed to build up (the guide beam remained on throughout the experiment, since it was positioned below the cloud it did not interfere with the build up time of the MOT), the sequence repeats every six seconds so that many runs could be performed in a row without resetting the trap. Using this sequence many data points were collected in a single run, the video is then captured digitally and the frames of interest can then be found six seconds apart. It was found that due to the very short time the probe beam is incident on the CCD camera we lose up to 50% of the data to a black screen, it was presumed that these probe images are lost in between the fields taken by the CCD, the exact number of lost frames was seen to vary with the total time taken for the probe cycle. Once the data are captured images of the cloud are analysed by subtracting the experimental image from the image obtained

of the guide beam without the cloud present. Images of the cloud as it falls over 6ms are shown in figure 8.23.

Guiding Along an Optical Beam Splitter

The guide beam was focused into the trap using a 160mm lens mounted onto an X-Y-Z-translation stage to ensure the guide is focused properly at the MOT (moving the focus by a couple of mm has been shown to make the normal reflection dominate the optical potential, see figure 8.21). Accurate focusing of the guide beam was achieved by turning the SLM off and allowing it to act like a mirror, the beam will now focus down to a spot after the 160mm lens, with the power in the beam reduced the final lens is moved to look for the ablation of the cloud due to heating effects, where the shadow in the MOT is most sharply defined is the focus of the lens. With the correct position of the final lens the SLM is turned on, the bright spot seen in the middle of the pattern can be used to confirm the alignment of the beam. The guide beam is then moved down so the bright spot and split of the guide is just below the cloud, this allows the atomic ensemble to fall through the beam splitter.

Data were taken with the probe beam flashed up to 20ms after the cloud has been dropped, with the guide beam detuned by 20GHz, 40GHz and 200GHz. The 20ms guide time allows the atoms to fall ~1mm, this is not the full length of the guide, however, it is far enough for the atoms to pass through the split of the guide beam. The atomic cloud is seen to fall and expand, but no increase in the signal was observed along the position of the guide beam. At

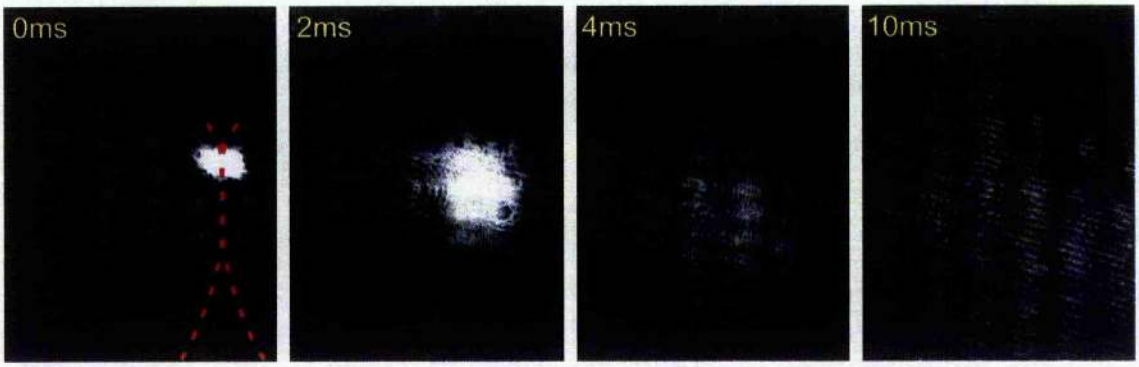

Figure 8.24: Absorption image of an atom cloud falling through the Y splitter. No increase of flux of intensity is observed along the guide beam, the path of the guide is indicated by the dashed line.

10ms the image of the cloud had expanded far enough to pass the split in the guide (although the centre of mass of the cloud has only just reached this point), see figure 8.24, however, after this time the signal had degraded so that a clear shadow image could not be seen.

Since no increase in signal could be observed along the path of the guide beam attempts were made to generate guides with higher efficiencies. The main loss of power comes from overfilling the SLM in order to present flat wave fronts. The size of the illuminating beam was reduced, by replacing the second lens of the telescope with a 150mm focal length lens, so that all of the power was centred on the encoded area of the SLM, this resulted in the loss of some of the information at he corners of the hologram but the effect on the final image was negligible, see figure 8.25. This had the immediate effect of increasing the efficiency of the generation to 60% (the bright spot at the centre of this contains about 20% of the power in the pattern).It should be noted that this efficiency is equal to the effective efficiency, taken from the

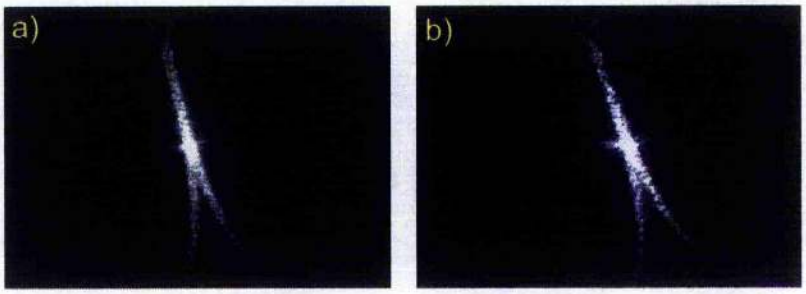

Figure 8.25: Comparison of Y-splitter patterns. The image formed with the enlarged beam is given in (a), the pattern generated using a Gaussian beam (b) shows very little difference in quality.

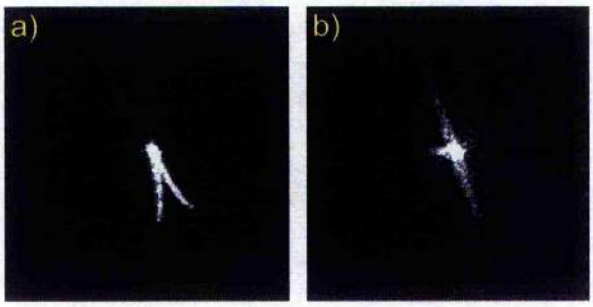

Figure 8.26: Replacement guiding patterns generated. The reflection caused by the SLM can be seen in the V-splitter pattern (a).

light incident on the encoded area of the SLM, observed when illuminated by the expanded beam.

Other guide beams were also designed to try and improve the efficiency of the hologram; an even simpler beam splitter was made as a "V" shape, the apex of the V was positioned in the centre of the hologram to coincide with the focus of the normal spot, and a simple line guide, examples of these guides are given in figure 8.26. The "V" guide displayed a clear reflection in the horizontal axis, this allowed us to aperture this element and improve our estimation of the efficiency of the hologram; approximately 15% of the total

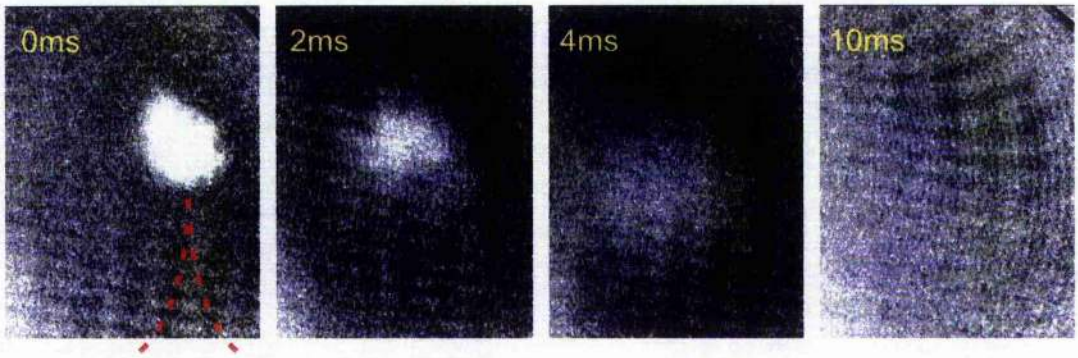

Figure 8.27: Guiding along the V-splitter pattern. No enhancement of the flux is observed along the path of the beam, indicated by the dashed line.

power in the guide is found in this reflected order reducing the overall efficiency of the hologram to ~50%. This is an increase in the total power of the guide by a factor of nearly three times over the initial experiment.

These new beam shapes were aligned with the cloud as before, once the guide is in position the SLM can be used to switch between any of the guides without the need for further alignment. Guiding was attempted as earlier with the guide detuned by 20GHz, 40GHz and 200GHz. Data captured still did not show any sign of increased flux along the guide beam, see figure 8.27.

From these results it is clear that we need to improve the sensitivity of the detection of the atoms and improve the quality of the guide beams. The quality of the guides could be improved by measuring the incident beam shape and then accounting for the Gaussian profile in the generation of the hologram. It is also seen that the images produced by the SLM are noticeably pixelated, this may be due to the nature of the SLM itself and a way to reduce such artefacts in the beam could be to increase the number of pixels used in

the generation of the beam. Since only half the active area of the SLM was used for these experiments illuminating the whole SLM and subsequently reducing the size of the beam to fit the optics may effect a reduction to this pixelisation. Increasing the sensitivity of detection could be improved by the used of cooled CCD cameras, however, these are expensive pieces of equipment and such an outlay of money should not be required since other groups [4] use standard CCD's for similar imaging methods. A more parallel viewing method, guide and probe beams separated by polarising optics as mentioned earlier, would help to remove blurring out of the absorption and also make detection clearer.

8.4 Summary

We have demonstrated the versatility of the SLM for creating optical potentials for guiding cold atoms. Laguerre-Gaussian beams have been generated with high efficiency and have been utilised for guiding a free falling MOT cloud, the SLM permits rapid change of the guide parameters without the need for further beam alignment leading to a comparison of various high-order Laguerre-Gaussian beams with azimuthal indices from 1 to 15. Our experiments confirm that for a given ring radius beams of higher aimuthal index offer larger potential barriers and lower radiation pressure effects than low index beams, yielding comparable fluxes with a smaller radiation pressure push. The SLM has also been used to produce optical patterns, not normally possible using traditional laser beams, for the generation of simple beam

splitters and interferometers. While guiding with these potentials has not yet been demonstrated the use of the SLM in this way opens the door for creating custom designed circuits along which atoms can be guided.

The quality of the LG beams produced by the SLM was seen to be as high as the static holograms in our possession with no pixelisation observed due the nature of the SLM. The iteratively generated beam splitters did, however, display significant pixelisation in the image plane, which may have contributed to the lack of guiding results

Bibliography

[1] M. Schiffer, M. Rauner, S. Kuppens, M. Zinner, K, Sengstock and W. Ertmer, "*Guiding, focusing and cooling of atoms in a strong optical potential*," Appl. Phys. B. **67** 705 (1998)

[2] J. Arlt, T. Hitomi and K Dholakia, "*Atom guiding along Laguerre-Gaussian and Bessel light beams*," Appl. Phys. B. **71** 2089 (2001)

[3] X. Xu, V. G. Minogin, K. Lee, Y. Wang and W. Jhe, "*Guiding cold atoms in a hollow laser beam*," Phys. Rev. A. **60** 4796 (1999)

[4] Y. Song, D. Milam and W.T.Hill, "*Long, narrow all-light atom guide*," Opt. Lett. **24** 1805 (1999)

[5] R. Dumke, T. Müther, M. Volk, W. Ertmer and G. Birkl, "*Interferometer-Type Structures for Guided Atoms*," Phys. Rev. Lett **89** 220402 (2002)

[6] O. Houde, D. Kadio and L. Pruvost, "*Cold Atom Beam Splitter Realised with Two Crossing Dipole Guides*," Phys. Rev. Lett. **85** 5543 (2000)

[7] B. T. Wolschrijn, R. A. Cornelussen, R. J. C. Spreeuw and H. B. van Linden van den Heuvall, "*Guiding of cold atoms by a red detuned laser beam of moderate power*," New J. Phys. **4** 69.1 (2002)

Chapter 9:

Summary and Outlook

9.1 Review of Thesis

The aims of this thesis have been to investigate the use of low power blue-detuned hollow beams as an alternative to a normal Gaussian beam for the guiding of cold atoms. To this end we have demonstrated guiding of an atomic beam along co-propagating and oblique Laguerre-Gaussian guides and have used high-order LG beams and Bessel beams to guide a dropped atom cloud.

Before any experiment can be performed a source of atoms must be obtained. During this thesis we have designed and built three separate MOTs from scratch in order to exploit different possible guiding geometries and these traps have each been tested and characterised. The first trap built was

the glass trap; two chambers linked by a small aperture so that atoms could be guided from a trapping chamber into a "clean" chamber. Ultimately this trap was rejected because the aperture prevented the formation of a stable atomic beam. A second trap was then built around a standard ten-way cross UHV piece; four unused viewports allowed optical access ~1cm around MOT centre. This trap was used successfully for the generation and guiding of LVIS. The drum trap was built to increase the optical access around the MOT and permit extended guiding of a dropped MOT. Atoms were detected up to 5cm from the MOT and the large viewports of the trap allowed several routes for probing the atomic flux.

Several different laser systems have been maintained during this research in order to trap and guide the atoms. The majority of the trapping was implemented by home-made extended cavity diodes lasers, stabilisation to the correct frequency was performed by locking electronics built in-house which we then tested and calibrated for our experimental requirements. Two commercial laser systems have also been used during these experiments, the tuning characteristics of the Ti:Sapphire laser, as our guide beam source, in particular were carefully characterised to enable accurate detuning of the guide from the atomic transitions. The later guiding experiments involving a dropped MOT required precision timing of the various laser beams as the experiment is, by its design, a pulsed operation. Accordingly we have developed computerised timing circuits and shutter switches in order to achieve sub-ms control over the different beams used.

We have experimentally studied the guiding of LVIS along co-propagating and oblique LG beams. In the collinear geometry we observe enhancement of up to 120% of the guided flux. The increase of guide power is seen to have a linear effect on the measured flux, decreasing the detuning of the laser increases the flux up to a point where the heating effects of a near resonant beam become significant at which point the flux is seen to drop off rapidly. Oblique guiding initially resulted in few atoms coupled into the guide, most atoms are deflected by or pass straight though the guide. This highlights some important considerations for developing elements based on hollow light beams. A novel experiment imaging an obstruction in the LG beam was performed allowing the atom to enter the guide more easily, enhancing the flux coupled into the guide

Guiding of atoms dropped from a MOT has also been studied. A comparison of LG and Bessel beam guiding was carried out. It was found that the structure of the Bessel beam hinders its use as a guide owing to the distribution of power across the beam. Limited guiding was observed for distances up to ~1cm. However, guiding with an LG beam of the same total power produced an increase in flux two orders of magnitude higher than the Bessel beam for the same guiding distance. The use of high order LG beams as guide beam has also been investigated, high order beams generate narrower profile beams for a given ring size increasing the intensity and trap steepness of the guide and thus reducing interactions with the atoms. A spatial light modulator was used generate the beam holograms and allowed rapid changes of the guide parameters with no further alignment of the guide

optics. The quality of SLM generated LG beams were seen be just as good as the static holograms in our possession. The SLM generated LG beams have been demonstrated to increase the atomic flux by up to a factor of 12. The use of high order beams has been shown to be just as effective as low order beams with a marked reduction in the associated radiation pressure force and heating effects. This use of the SLM has successfully demonstrated their use as a versatile tool for creating novel optical potentials with high efficiencies. The use of the SLM means we are no longer restricted in the number of holograms available, tailored optical potentials were also generated to produce beam splitter and interferometer patterns for guiding atoms.

9.2 Future Work

The next step in this research will be the development of an optical molasses to reduce the temperature of the atoms down to ~10μK, this will increase the effectiveness of our optical guides.

The use of the Bessel beam still remains an interesting proposition owing to its non-diffracting nature. Guiding of a molasses cooled atom cloud will hopefully help overcome the power limitations of the beam and allow guiding over greater distances. In order to properly utilise the nature of the Bessel beam it would be of interest to reduce the diameter of the guide. Our preliminary experiment compared beams with a ring size of ~1mm, at this size

the LG beam is relatively non-diffracting over several centimetres. Reducing the guide size to a few μm severely limits the use of Gaussian beams due to diffraction whereas the Bessel beam can propagate with a constant guiding potential over tens of centimetres. Such an experiment will require optics to be placed very close to the MOT region to create beams of the necessary size and will therefore require further refinement of the trap design. One solution would be placing a secondary trapping region (a glass cube) on the top of the drum trap, thus the MOT could be formed closer to the necessary optics and atoms could be guided through the entire height of the drum trap.

The optical beam splitter and interferometer patterns also warrant further investigation. Here again the use of optical molasses will improve the effectiveness of the guide beams. Improvements in the detection could be performed by viewing the atoms co-linear with the guide beam. The use of a smaller trapping volume, as described above, may also be of benefit allowing the tighter focusing of the beams resulting in higher dipole potentials. In addition further refinements to the hologram to remove the grainy profile of the beam and account for the curved wavefronts of the illuminating beam will hopefully generate a smoother guide potential and improve the efficiency of the guide. These beams need not be confined to guiding in the centre of the vacuum; the pattern could be focused above an evanescent wave mirror trap to provide similar potentials to those of the magnetic atom chips. The use of external holograms could provide for different guiding parameters with a single experiment and the lack of current carrying wires could allow CW operation and remove the break up associated with magnetic guiding of BEC.

Finally the SLM has proved a versatile tool for creating optical potentials and its continued use should be a priority. Their ability to create different holograms yields a vast simplification of experimental procedures. Optimisation of the hologram design to account for input beam shape should produce some increase in efficiency, and improvements in technology will soon provide higher resolution devices which are fast enough to manipulate the optical potentials whilst atoms are being guided leading to a new generation of optically manipulated atomic beam experiments.

Reason notwithstanding, the universe continued unabated.

The Hitchhikers Guide to the Galaxy